

The Role of Physico-chemical Properties and Test Environment on Biological Effects of Copper and Silver Nanoparticles

ALEKSANDR KÄKINEN

TALLINN UNIVERSITY OF TECHNOLOGY
Faculty of Chemical and Materials Technology
Laboratory of Inorganic Materials

NATIONAL INSTITUTE OF CHEMICAL PHYSICS AND BIOPHYSICS
Laboratory of Environmental Toxicology

This dissertation was accepted for the defence of the degree of Doctor of Philosophy in Chemical and Materials Technology on May 20, 2014.

Supervisors: Dr. Anne Kahru, Laboratory of Environmental Toxicology,
National Institute of Chemical Physics and Biophysics,
Estonia

Dr. Rein Kuusik, Laboratory of Inorganic Materials,
Tallinn University of Technology, Estonia

Opponents: Dr. Anita Jemec, Biotechnical faculty,
University of Ljubljana, Slovenia

Dr. Vambola Kisand, Faculty of Science and Technology,
Institute of Physics, University of Tartu, Estonia

Defence of the thesis: May 20, 2014 Tallinn University of Technology,
Ehitajate tee 5, Tallinn

Declaration:

Hereby I declare that this doctoral thesis, my original investigation and achievement, submitted for the doctoral degree at Tallinn University of Technology has not been submitted for any academic degree.

Aleksandr Käkinen



European Union
European Social Fund



Investing in your future

Copyright: Aleksandr Käkinen, 2014
ISSN 1406-4774
ISBN 978-9949-23-611-4 (publication)
ISBN 978-9949-23-612-1 (PDF)

KEEMIA JA KEEMIATEHNIKA G35

**Vase ja hõbeda nanoosakeste
füüsikalis-keemiliste omaduste ja
testikeskkonna mõju nende bioloogilisele toimele**

ALEKSANDR KÄKINEN

TABLE OF CONTENTS

LIST OF ORIGINAL PUBLICATIONS	7
INTRODUCTION	11
1. LITERATURE REVIEW	13
1.1. Properties and unfavorable effects of synthetic nanoparticles	13
1.1.1. Nanosilver	14
1.1.2. Nano CuO.....	14
1.2. Toxicity evaluation of nanoparticles	15
1.2.1. Role of test media in modulation of the toxicity of nanoparticles	15
1.2.2. Dissolution analysis of metal nanoparticles	16
1.2.3. Toxicological profiling of nanoparticles using bacterial biosensors	17
1.3. Interaction between nanoparticles and biomolecules	17
1.3.1. Protein corona	17
1.3.2. Nanoparticle-enzyme interaction and effect on enzymatic activity	18
AIMS OF THE STUDY	19
2. MATERIALS AND METHODS.....	20
2.1. Complexing potential of ecotoxicological and microbiological test media.....	20
2.2. Nanoparticles	23
2.2.1. Preparation of stock suspensions of nanoparticles and metal ions.....	23
2.2.2. Physico-chemical characterization of nanoparticles	23
2.3. Determination of free metal ion concentration and dissolution of nanoparticles.....	24
2.3.1. Ion-Selective Electrode	24
2.3.2. Atomic absorption spectroscopy and inductively coupled plasma mass spectrometry.....	25
2.4. Bacterial biosensors.....	25
2.5. Interaction of silver nanoparticles with firefly luciferase. Effect on enzymatic activity.....	29
3. RESULTS AND DISCUSSION	31
3.1. Characterisation of nanoparticles	31
3.2. Binding potential of ecotoxicological and microbiological test media	32
3.2.1. Response of Cu-Ion Selective Electrode on CuSO ₄ and nano-CuO in different test media.....	32
3.1.2. Response of bacterial Cu-Biosensor on CuSO ₄ and nano-CuO in different test media.....	34
3.3. Investigation of antimicrobial properties and toxicity mechanisms of nanoparticles.....	35
3.4. Interaction of nanoparticles with firefly luciferase. Effect on enzymatic activity	40
CONCLUSIONS	43

REFERENCES	44
ACKNOWLEDGEMENTS.....	52
ABSTRACT.....	53
KOKKUVÕTE	55
PUBLICATION I.....	57
PUBLICATION II	85
PUBLICATION III.....	99
PUBLICATION IV	121
<i>CURRICULUM VITAE</i>	137
ELULOOKIRJELDUS	140
DISSERTATIONS DEFENDED AT TALLINN UNIVERSITY OF TECHNOLOGY ON <i>CHEMISTRY AND CHEMICAL ENGINEERING</i>	143

LIST OF ORIGINAL PUBLICATIONS

MAIN PUBLICATIONS

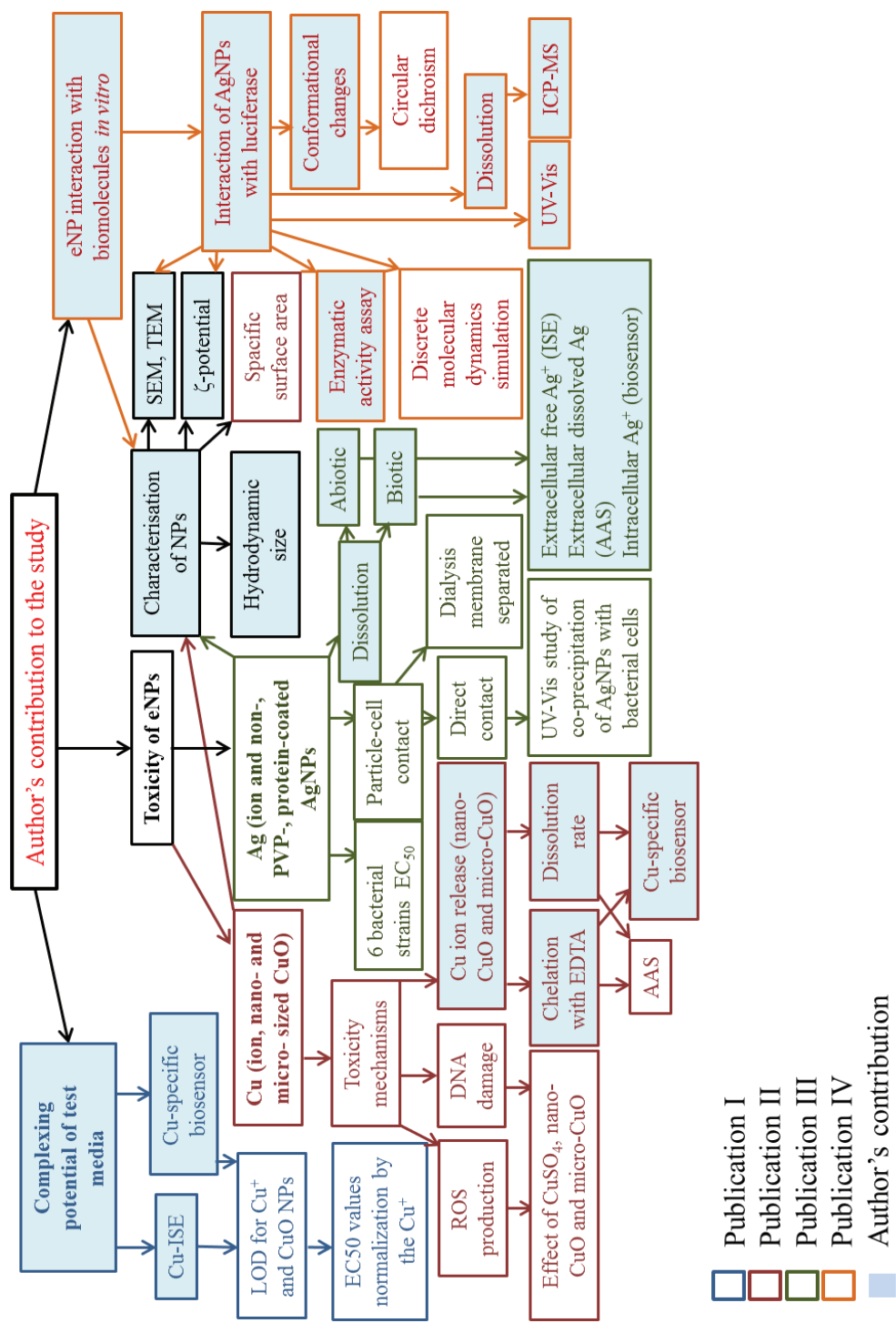
- I** **Käkinen A**, Bondarenko O, Ivask A, Kahru A (**2011**). The effect of composition of different ecotoxicological test media on free and bioavailable copper from CuSO₄ and CuO nanoparticles: comparative evidence from a Cu-selective electrode and a Cu-biosensor. *Sensors*, 11(11), 10502 – 10521
- II** Bondarenko O, Ivask A, **Käkinen A**, Kahru A (**2012**). Sub-toxic effects of CuO nanoparticles on bacteria: kinetics, role of Cu ions and possible mechanisms of action. *Environmental Pollution* 169, 81 – 89
- III** Bondarenko O, Ivask A, **Käkinen A**, Kurvet I, Kahru A (**2013**). Particle-cell contact enhances antibacterial activity of silver nanoparticles. *PLoS ONE*, 8(5), e64060
- IV** **Käkinen A**, Ding F, Chen P, Mortimer M, Kahru A and Ke PC (**2013**). Interaction of firefly luciferase and silver nanoparticles and its impact on enzyme activity. *Nanotechnology*, 24(34):345101

AUTHORS CONTRIBUTION TO THE PUBLICATIONS

- I** Aleksandr Käkinen participated in the study design, performed experiments with copper ion-selective electrode and a part of the assays with *Pseudomonas fluorescens* OS8::KnCueRPcopAlux Cu-biosensor, participated in the interpretation of data and in the preparation of the manuscript.
- II** Aleksandr Käkinen participated in the study design, performed nanoparticles hydrodynamic size measurements, participated in copper oxide dissolution experiments, in the interpretation of data and in the preparation of the manuscript.
- III** Aleksandr Käkinen participated in the study design, performed the nanoparticles characterisation, participated in the interpretation of the data and preparation of the manuscript.
- IV** Aleksandr Käkinen participated in the planning of the experiments, performed the experiments and participated in the interpretation of the data and preparation of the manuscript.

Graphical representation of the study and author's contribution to the publications are presented in Fig. 1.

Figure 1. Graphical representation of author's contribution to the publications



OTHER PUBLICATIONS IN PEER-REVIEWED JOURNALS

- Klauson D, Budarnaja O, Stepanova K, Krichevskaya M, Dedova T, **Käkinen A**, Preis S (2014). Selective performance of sol-gel synthesised titanium dioxide photocatalysts in aqueous oxidation of various-type organic pollutants. *Kinetics and Catalysis*, 55(1), 47 - 55.
- Radic S, Geitner N. K, Podila R, **Käkinen A**, Chen P, Ke PC, Ding F (2013). Competitive binding of natural amphiphiles with graphene derivatives. *Scientific Reports*, 3, 2273.
- Klauson D, Pilnik-Sudareva J, Pronina N, Budarnaja O, Krichevskaya M, **Käkinen A**, Juganson K, Preis S (2013). Aqueous photocatalytic oxidation of prednisolone. *Central European Journal of Chemistry*, 11(10), 1620 - 1633.
- Blinova I, Niskanen J, Kajankari P, Kanarbik L, **Käkinen A**, Tenhu H, Penttinen OP, Kahru A (2013). Toxicity of two types of silver nanoparticles to aquatic crustaceans *Daphnia magna* and *Thamnocephalus platyurus*. *Environmental Science and Pollution Research*, 20(5), 3456 - 3463.
- Blinova I, Bityukova L, Kasemets K, Ivask A, **Käkinen A**, Kurvet I, Bondarenko O, Kanarbik L, Sihtmäe M, Aruoja V, Schvede H, Kahru A (2012). Environmental hazard of oil shale combustion fly ash. *Journal of Hazardous Materials*, 229, 230, 192 - 200.

INTRODUCTION

Production of man-made nanoparticles (NPs) is continuously increasing and they are already used in thousands of industrial and household products. The growing production increases the possibility of release of the NPs into the environment. Nanoscience has undergone rapid development, but still relatively little is known on the interaction of NPs with living systems. The knowledge of nanoparticles' behavior in the environment and characterization of their biological effects is needed for the environmental risk assessment.

Biological effects of NPs are usually examined in aqueous environments in the presence of various components that support survival and/or growth of the test organisms or cells. Various standardized *in vitro* toxicity assays are used with different composition of test media depending on the test organism and type of assay. Generally, biological environment, e.g. test medium, contains various organic (lipids, proteins, sugars *etc.*) and inorganic (salts, minerals *etc.*) components. Once NPs encounter the biological matter, they start to interact with it. Adsorption of biomolecules onto NPs surface is a well-established phenomenon. Thus, the physico-chemical properties of NPs may significantly change in the biological environment. Coating with biomolecules can change the stability of NP's suspension, increase of the dissolution rate of metal-based NPs, or modulate the interaction of NPs with cells. It is widely accepted that the formed bio-corona is what the cell actually "sees" during interaction with NPs. In turn, the structure of the adsorbed biomaterial may change leading to loss of biological activity. Moreover, the ion release and the formation of reactive oxygen species (ROS) are the main mechanisms of toxic effect of metal-containing NPs. Thus, studying interaction of NPs with the surrounding environment, including adsorption of biomolecules, is crucial for understanding how exposure to nanoparticles affects the biological responses of cells and organisms.

The main objective of this study was to obtain new scientific knowledge on interaction of NPs with organisms, biomolecules and test environment and how these interactions modify the toxic effects of NPs.

The focus was set on the role of test environment and cell-NP contact on resulting biological effects using nano-CuO and nanosilver as model compounds and bacteria as model test organisms.

ABBREVIATIONS

AAS	atomic absorption spectroscopy
AFW	artificial freshwater
ASTM	American Society for Testing and Materials
ATP	adenosine triphosphate
BSA	bovine serum albumin
CAS	unique number given to chemicals by the Chemical Abstracts Service
(Cu-)ISE	(Cu-)Ion Selective Electrode
DI	deionized water
D _h	hydrodynamic diameter
DLS	dynamic light scattering
DMD	discrete molecular dynamic
DNA	deoxyribonucleic acid
EC ₅₀	the median effective concentration of the toxicant that induces a designated effect in 50% of the test organisms after a specific exposure time
EDTA	ethylenediaminetetraacetic acid
FBS	fetal bovine serum
FTIR	Fourier transform infrared spectroscopy
HMM	heavy metal MOPS medium
ICP-MS	inductively coupled plasma mass spectrometry
ISO	International Organization for Standardization
kDa	kilodalton
LB	Luria-Bertani medium
LOD	limit of determination
MOPS	3-(N-morpholino)propanesulfonic acid
NP(s)	nanoparticle(s)
OD	optical density
OECD	Organization for Economic Cooperation and Development
PL	photoluminescence
PVP	polyvinylpyrrolidone
ROS	reactive oxygen species
SEM	scanning electron microscopy
SPR	surface plasmon resonance
TEM	transmission electron microscopy
UV-Vis	ultraviolet–visible

1. LITERATURE REVIEW

1.1. Properties and unfavorable effects of synthetic nanoparticles

According to the recent review issued by the European Commission [1] nano-material is defined as "a natural, incidental or manufactured material containing particles, in an unbound state or as an aggregate or as an agglomerate and where, for 50% or more of the particles in the number size distribution, one or more external dimensions is in the size range 1 - 100 nm. In specific cases and where warranted by concerns for the environment, health, safety or competitiveness the number size distribution threshold of 50% may be replaced by a threshold between 1 and 50 %". In scientific literature nanoparticles (NPs) are usually defined as particles with at least one dimension between 1 and 100 nm.

Annual production of metal-based NPs exceeds 20 000 tons and continues to increase (Fig. 2). Thus the question of NPs risk assessment is highly relevant.

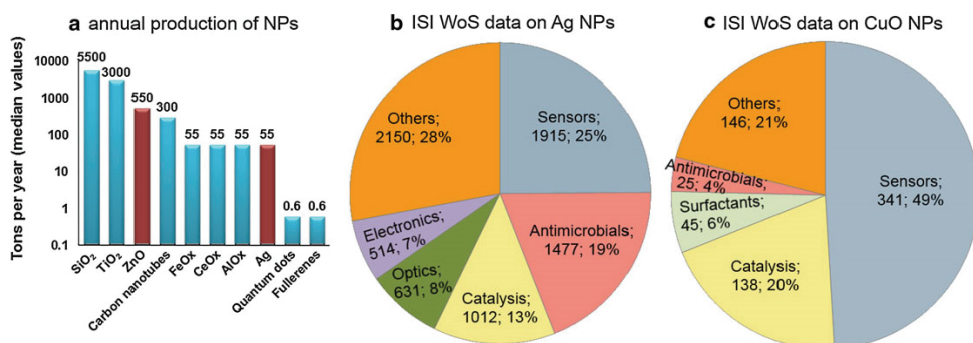


Figure 2. (a) Annual production of nanoparticles (NPs) and application of (b) Ag and (c) CuO NPs. Modified from Bondarenko et al., 2013 [2].

The main reason of different properties of NPs compared to their micro-scale counterparts is the particle size. With decreasing size, the number of atoms on particle external surface increases, leading to significant increase in specific surface area (surface area of a material per unit mass [3]) and thus, increased reactivity [4, 5].

High reactivity significantly enhances interaction of NPs with surrounding environment (binding of gases, organic molecules including proteins, DNA, cell membranes) [6]. This interaction may lead to changes in the properties of vital biomolecules, membrane damage, increased dissolution of NPs and formation of reactive oxygen species (ROS). ROS are small active derivatives of molecular oxygen, e.g., hydroxyl radical ($\bullet\text{OH}$), hydrogen peroxide (H_2O_2) and superoxide anion (O_2^-). It is important to note that ROS are natural by-products of normal oxygen metabolism, but in excessive amounts cause cellular oxidative stress [7]. The formation of ROS [8] and dissolution (ion release) [9, 10] may be the main explanation of toxic effect of metal-containing NPs. In addition, binding of biomolecules, most often proteins,

to NPs surface leads to protein corona formation, which it turn plays an important role in uptake of NPs by various cells and organisms and other biological effects. In the case of metal-containing NPs ROS can be caused by released toxic metal ions triggering ROS inducing redox reactions and/or in case of all types of NPs ROS can be directly induced on NPs surface by interaction of molecular oxygen with NPs.

In order to understand toxicity mechanisms of NPs the processes that take place on bio-nano interface are very important. For example, for different organisms the toxicology may be unpredictably varying: a bacterial, prokaryotic cell has no endocytosis, thus they are *a priori* protected against NPs entry, whereas most eukaryotic cells can internalize NPs relatively easily [11]. In addition to the organism, test environment also affects on the test results. Organic and inorganic components of test media can lead to aggregation, or increased stability and dissolution of NPs. Thus, nanoparticle toxicity studies require careful planning to take into consideration various factors that may interfere with the results [12].

1.1.1. Nanosilver

Silver nanoparticles (AgNPs) have long been known for their antibacterial properties. Protein-stabilized nanosized Ag particles have been used for medical purposes already since the late 19th century [13, 14]. Nowadays, AgNPs are widely used in over 300 consumer products [15] as broad-spectrum antimicrobials in cosmetics, clothing, detergents, electronics, water purification systems, dietary supplements and medical equipment [16, 17]. According to recent evaluation, annual production of silver nanoparticles is tens of tons [18]. There is a significant risk of environmental pollution mainly *via* industrial waste and sewage treatment plants [19-21], as well as due to silver leaching from the nanosilver-containing consumer products.

The toxicity of AgNPs is widely studied [2]. Despite numerous publications, the antimicrobial mechanism of AgNPs is still under debate. In general, the mechanism of AgNPs toxicity is similar to that of silver ions [22] and is supposedly dictated by Ag-ion release [23, 24]: released Ag-ions from AgNPs may enter the cell and bind to SH-groups of proteins and may generate ROS [25, 26]. However, in some studies the silver nanoparticles were reported to be more toxic than predicted from released Ag ions [22, 27-31]. The latter can be explained by the contact of Ag nanoparticles with the cell membrane that results in membrane damage and consequently, higher uptake of Ag ions. In addition, several studies have shown that antimicrobial effect of AgNPs is correlated to the particle size: smaller particles induce higher toxic effects [9, 32], probably due higher binding affinity to the cell membrane [33] and subsequent higher ion release. In addition, the binding of vital molecules (e.g., enzymes) to AgNPs may irreversibly reduce the activity of these biomolecules.

1.1.2. Nano CuO

Historically, copper has been widely used in metallurgy, agriculture and household products such as cookware. Biocidal properties of copper compounds have been

used for centuries in antifouling agents. In recent time, as a result of nanotechnology development, nanosized copper oxide (CuO NPs) has become widely used in various applications, such as electronics (semiconductors, computer chips), heat transfer nanofluids due their excellent thermophysical properties [34] and as antimicrobial agent in textiles, hospital equipment, as wood preservation and antifouling paint due to its toxic properties [35].

At low concentrations copper is a micronutrient for microorganisms, plants and animals, but above physiological level it can cause adverse effects. The toxicological studies have shown the toxicity of CuO NPs to aquatic organisms such as algae [36], crustaceans [37], fish [38], bacteria [26] as well as mammalian cells *in vitro* [39, 40]. In addition, the ability of CuO NPs to induce oxidative stress and DNA damage has been demonstrated [39]. Moreover, the exposure to CuO NPs may lead to accumulation of copper in the animal tissues [41]. For example, upon exposure to Cu NPs, accumulation of copper in the isopod *Porcellio scaber* has been demonstrated, due to the liberation of Cu ions inside the digestive tract of isopods.

1.2. Toxicity evaluation of nanoparticles

1.2.1. Role of test media in modulation of the toxicity of nanoparticles

Dissolution of metal-containing NPs (release of free ions) may be one of the main mechanisms underlying their toxicity [42]. It is widely accepted that bioavailability (the fraction of a chemical or NPs that is available for certain organism/cells) and subsequently, the toxic effects of metals, depend on their speciation. Thus, metal speciation in different environmental matrices (natural waters, soils, sediments) has received remarkable attention [42]. In toxicology, for most of the standardized *in vitro* toxicity assays the composition of the test media to be used is defined by the Organisation for Economic Co-operation and Development (OECD), the International Organization for Standardization (ISO), the American Society for Testing and Materials (ASTM) norms and varies depending on the test organism and type of the assay. Moreover, every standard laboratory toxicological assay needs to be performed in specific conditions, e.g., temperature, time *etc.*, which all may influence the chemical speciation and consequently, the test results [43]. In order to provide the ecologically and physiologically relevant conditions for a given test organism/cell, test media usually contain organic and inorganic components – ligands, that form complexes with the metal ions. The solubility of NPs as well as stability of suspensions depends on their interactions with compounds of test environment (proteins, amino acids, natural organic matter, humic substances *etc.*). For instance, organic compounds may coat and disperse NPs (Fig. 3). NPs may become remarkably unstable and sediment in mineral media. In contrast, the components of the complex organic rich test media are able to disperse NPs and prevent their sedimentation [2].

Hence, the knowledge on the potential impact of test media on toxicity outcome is necessary to evaluate the test results and compare the data between different toxicological assays, test species (organisms and cells) and various laboratories.

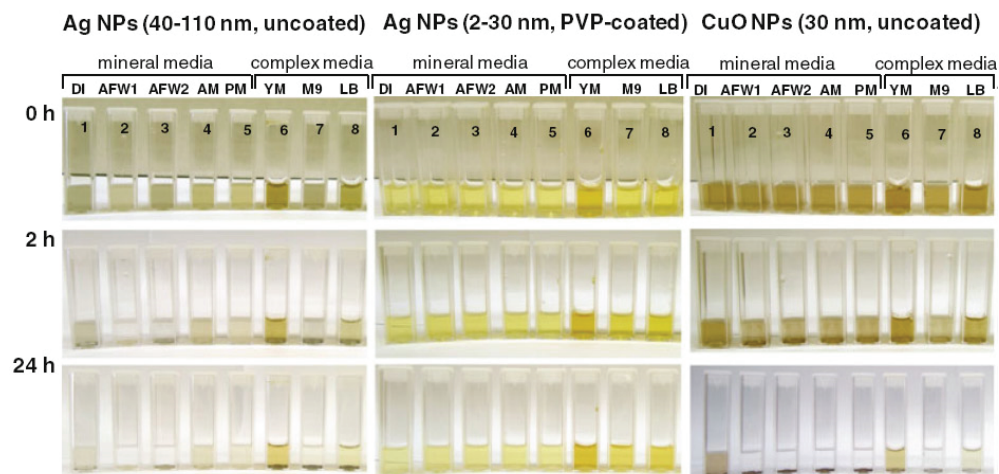


Figure 3. Illustration of NPs stability suspended in various test environments: uncoated Ag (50 mg/L), PVP-coated Ag (50 mg/L) and uncoated CuO (50 mg/L) nanoparticles after 0, 2 and 24 hours of incubation in (1) deionized water; (2) artificial freshwater (AFW) for the tests with *Daphnia* sp. (OECD 202); (3) AFW for *Thamnocephalus* sp.; (4) algal growth medium (OECD 201); (5) protozoan mineral test medium (Osterhout's); (6) yeast extract peptone dextrose medium; (7) bacterial M9 medium supplemented with 0.1 % glucose and 0.5 % amino acids; (8) bacterial LB medium containing tryptone and yeast extract. Detailed composition of test media presented in Table 1. Modified from Bondarenko et al., 2013 [2].

1.2.2. Dissolution analysis of metal nanoparticles

Solubilisation is a critical step in order to understand and predict harmful effects of metal-based NPs. One of the most widely applied techniques to determine free ionic forms of dissolved metal is the ion-selective electrode (ISE) [44, 45]. Although, remarkably high sensitivities of some electrodes have been reported (up to 10^{-11} M [8]), the ISE have also some limitations: the non-target ions (Cl, Br, Fe, sulfides, organics *etc.*) may interfere with the results and measurement accuracy is sensitive to ionic strength of the solution [46, 47]. Analogously, dissolution of metal-based NPs can be analysed by dialysis [48], ultracentrifugation [40], or ultrafiltration [49] and subsequent total metal analysis of supernatant or filtrates by atomic absorption spectroscopy (AAS) or inductively coupled plasma mass spectrometry (ICP-MS). These approaches are usually suitable, but the separation of small (< 10 nm) NPs can be challenging and the filter material may also adsorb certain amount of metals [50].

One has to stress, however, that the bioavailable fraction of metal is more informative than the total dissolved metal fraction for the interpretation of the results

of bioassays. Bioavailable fraction of a chemical is the fraction available to a certain organism. For example, metal in test solution may exist in the form of soluble metal complexes [51], which may be not bioavailable to the cells and thus will not induce toxic effect. Therefore, although the concentration of total dissolved metal may be high, the actual bioavailable concentration of metal that causes biological effects may be remarkably lower. There are several biological tools that can be used for the analysis of bioavailable metals. For example microbial biosensors [52, 53] allow specific detection of bioavailable metals through a highly sensitive biorecognition process followed by induction of a measurable signal, e.g., bioluminescence [54]. These metal-specific recombinant bacteria have been applied for the analysis of bioavailable metals in soils, sediments [55, 56], as well as in metal-containing NPs [37, 57]. The above described biosensors contain a promoter that selectively senses metal ions and activates a reporter gene, which initiates the synthesis of luciferase and production of light (bioluminescence). Produced light is proportional to the intracellular concentration of the tested metal ion.

1.2.3. Toxicological profiling of nanoparticles using bacterial biosensors

As discussed above (section 1.1), reactive oxygen species (ROS) can form on the surface of NPs. ROS may result in significant damage to cell structures [58]. Usually fluorescent dyes are used to detect ROS in biological samples [59-61]. Fluorescent dyes increase their fluorescence after intracellular oxidation. In case of metal-based NPs, released ions can quench the fluorescence of the dyes [59], making certain methods not suitable for the detection of ROS induced by metal-based NPs. Another method for the detection of ROS is using stress-induced whole-cell biosensors. Similarly to metal-specific biosensors, these genetically modified (recombinant) bacteria react to the presence of ROS by producing bioluminescence [62-64].

In addition to ROS inducible strain, a single-stranded DNA damage-inducible strain was used in the current study to investigate DNA damaging potential of NPs.

1.3. Interaction between nanoparticles and biomolecules

1.3.1. Protein corona

Protein corona is the protein adsorption layer that forms on the surface of NPs and plays an important role in their interaction with living matter. It is a dynamic phenomenon that can change over time, where initially adsorbed abundant proteins are replaced by proteins with higher affinity for the nanostructure (Vroman's effect) [65]. During interaction with NPs, in addition to the potential to change colloidal stability of NPs and increase dissolution of metal-based NPs, proteins undergo structural rearrangement, leading to changes in secondary structure up to protein unfolding and, as a consequence, changes in biological response [66]. Protein corona's structure and composition depends on both, the physicochemical properties of the NPs, such as composition, size, shape, surface charge, functionalization and the

nature of the protein and the environment. Also, time is an important factor in the concent of formation of the protein corona.

Knowledge on the protein adsorption on nanomaterial surfaces is highly needed in many research fields such as drug delivery [67-70], tissue regeneration [71-73], biosensing [74-77], nanotoxicology [4] and others.

1.3.2. Nanoparticle-enzyme interaction and effect on enzymatic activity

Enzymes regulate life processes in all living cells [78] and changes in enzymatic activity may adversely affect physiological processes. Certain chemicals, e.g. heavy metals and nanoparticles, can effectively bind biomolecules, including enzymes [79, 80]. This binding may cause inhibition effect on enzymatic activity due to conformational changes of enzyme's secondary as well as tertiary structure [66]. Metal ions can be bound to enzyme's active cite, blocking enterance of the substrate into active pocket and reduce enzymatic activity. The reduction in enzymatic activity may be also due to the binding to NPs. Also, the geometry of the active site of the enzyme can be changed. In addition, allosterical effects may take place upon chemical-enzyme interaction. For example, heavy metals have high affinity for the sulfhydryl ($-SH$) groups in the cysteine residues of the protein structure [79].

AIMS OF THE STUDY

Although engineered nanoparticles (NPs) are already used in a large variety of consumer products and the production of some types of nanomaterials is already on the industrial scale, the knowledge on potential harmful effects and mechanisms of toxic action of NPs is still scarce.

The main objective of this study was to obtain new scientific knowledge on interaction of NPs with organisms, biomolecules and test environment and how these interactions modify the toxic effects of NPs. The focus was set on nano-CuO and nanosilver due to their high toxicity and biocidal use. The main aim was to clarify the role of the test environment and cell-NP contact (using bacteria, – the primary target organisms of various biocidal compounds) in the toxicity on NPs. In addition, the effect of enzyme-silver NPs interaction on enzymatic activity was investigated.

This was approached through the following specific aims:

1. to select and refine the suite of the laboratory methods for physico-chemical characterization of nanoparticles relevant for ecotoxicological analysis: hydrodynamic size, ζ -potential and solubilisation.
2. to reveal the effect of complexing potential of test media in ecotoxicological studies of copper and CuO particles.
3. to evaluate the role of CuO solubilisation in toxicological effects of CuO NPs combining chemical methods and a suite of bioluminescent *Escherichia coli*-based sensor bacteria.
4. to elucidate the importance of contact between bacteria and NPs on solubility-driven toxic effects of nanosilver.
5. to determine the mechanisms of interaction between enzymes and nanosilver using firefly luciferase as a model.

2. MATERIALS AND METHODS

2.1. Complexing potential of ecotoxicological and microbiological test media

The test media used for toxicity assays are standardized, depend on the test organism and may influence the test results [43]. Therefore the study of test media effect on results is necessary to correctly understand toxicological studies.

In order to investigate the complexing potential of test media a series of standard ecotoxicological and microbiological media were analysed (Table 1). The media selection for the analysis was based on ecotoxicological and microbiological assays (Publication I): 2% NaCl (used for Microtox toxicity test with bioluminescent bacteria *Vibrio fischeri*), algal medium (used for the toxicity testing with algae *Pseudokirchneriella subcapitata* according to OECD 201), two artificial freshwaters (used for tests with crustaceans *Daphnia magna* according to OECD 202 and with *Thamnocephalus platyurus*). Malt extract (ME) and YPD (Yeast Peptone Dextrose medium) are used for the cultivation of yeasts. Luria-Bertani (LB) medium is an undefined rich medium that supports the growth of variety of bacteria. The M9 medium has been used in studies for toxicity evaluation of metals and organic chemicals to *Escherichia coli* [81] and for the analysis of bioavailable metals using metal-inducible bioluminescent bacterial sensors [54, 82]. HMM medium has been specifically suggested for the analysis of heavy metals due to its minimal metal-complexing capability [83]. M9 and HMM media were supplemented by 0.5 % Cas-amino acids (AA). Also 0.9% NaCl and its Cas-amino acid (AA) supplemented versions were tested as 0.1% AA amended 0.9% NaCl has been applied earlier to study the bioavailability and toxicity of metal-containing NPs [26, 37, 84].

Table 1. Toxicological and microbiological test media. Modified from Table 1 of Publication I.

Designation of the media (traditional test organism for this medium)	Content per L	pH
Ecotoxicological test media		
Osterhout's medium (protozoan <i>Tetrahymena</i> sp.)	104 mg NaCl, 8.5 mg MgCl ₂ , 4 mg MgSO ₄ , 2.3 mg KCl, 1 mg CaCl ₂	5.2
Artificial freshwater 1 (AFW1) (crustacean <i>Daphnia</i> sp.)	294 mg CaCl ₂ ·2H ₂ O, 123.25 mg MgSO ₄ ·7H ₂ O, 64.75 mg NaHCO ₃ , 5.75 mg KCl	7.8
Artificial freshwater 2 (AFW2) (crustacean <i>Thamnocephalus</i> sp.)	60 mg CaSO ₄ ·2H ₂ O, 123 mg MgSO ₄ ·7H ₂ O, 96 mg NaHCO ₃ , 4 mg KCl	7.8
Algal medium (algae <i>Pseudokirchneriella subcapitata</i>)	15 mg NH ₄ Cl, 12 mg MgCl ₂ ·6H ₂ O, 18 mg CaCl ₂ ·2H ₂ O, 15 mg MgSO ₄ ·7H ₂ O, 1.6 mg KH ₂ PO ₄ , 50 mg NaHCO ₃ , 0.1 mg Na ₂ EDTA·2H ₂ O, 0.08 mg FeCl ₃ ·6H ₂ O, 0.185 mg H ₃ BO ₃ , 0.415 mg MnCl ₂ ·4H ₂ O, 3·10 ⁻³ mg ZnCl ₂ , 1.5·10 ⁻³ mg, CoCl ₂ ·6H ₂ O, 7·10 ⁻³ mg Na ₂ MoO ₄ ·2H ₂ O, 10 ⁻⁵ mg CuCl ₂ ·2H ₂ O	8.3
Microbiological test media		
Malt extract (ME) (yeast <i>Saccharomyces cerevisiae</i>)	11 g maltose, 8 g carbohydrates, 1 g proteins	5.2
Yeast extract peptone dextrose (YPD) (yeast <i>Saccharomyces cerevisiae</i>)	20 g Bacto peptone, 10 g yeast extract, 20 g glucose	6.7
M9 (bacteria e.g., <i>Escherichia coli</i>)	6 g Na ₂ HPO ₄ , 3 g KH ₂ PO ₄ , 0.5 g NaCl, 1 g NH ₄ Cl, 0.25 g MgSO ₄ ·7H ₂ O, 0.01 g CaCl ₂	7.0

Table 1. Toxicological and microbiological test media. Continues.

Designation of the media	Content per L	pH
M9+0.5%AA (bacteria e.g., <i>Escherichia coli</i>)	6 g Na ₂ HPO ₄ , 3 g KH ₂ PO ₄ , 0.5 g NaCl, 1 g NH ₄ Cl, 0.25 g MgSO ₄ ·7H ₂ O, 0.01 g CaCl ₂ , 5 g Cas-amino acids, 1 g glucose	7.0
LB (bacteria e.g., <i>Escherichia coli</i>)	10 g tryptone, 5 g yeast extract, 5 g NaCl	7.0
Heavy metal MOPS medium (HMM) (bacteria e.g., <i>Escherichia coli</i>)	8.4 g MOPS, 0.22 g glycerol-2-phosphate, 3.7 g KCl, 0.54 g NH ₄ Cl, 0.06 g MgSO ₄ , 0.162 mg FeCl ₃	7.2
HMM+0.5%AA (bacteria e.g., <i>Escherichia coli</i>)	8.4 g MOPS, 0.22 g glycerol-2-phosphate, 3.7 g KCl, 0.54 g NH ₄ Cl, 0.06 g MgSO ₄ , 0.162 mg FeCl ₃ , 5 g Cas-amino acids, 4 g glucose	7.2
2% NaCl (marine bacteria e.g., <i>Vibrio fischeri</i>)	20 g NaCl	4.4
Supplemented 0.9% saline		
0.9% NaCl	9 g NaCl	5.8
0.9% NaCl+0.01%AA	9 g NaCl, 1 g glucose, 0.1 g Cas-amino acids	6.1
0.9% NaCl+0.05%AA	9 g NaCl, 1 g glucose, 0.5 g Cas-amino acids	6.3
0.9% NaCl+0.1%AA	9 g NaCl, 1 g glucose, 1 g Cas-amino acids	6.2
0.9% NaCl+0.5%AA	9 g NaCl, 1 g glucose, 5 g Cas-amino acids	6.2

2.2. Nanoparticles

2.2.1. Preparation of stock suspensions of nanoparticles and metal ions

Metal ions and micro-sized particles were used in parallel to metallic NPs to study the effects of dissolution and size, respectively (Publication II). Stock solutions of soluble metal salts ($\text{CuSO}_4 \cdot 7\text{H}_2\text{O}$, AgNO_3) and nanoparticles of CuO, uncoated AgNPs, protein coated colloidal Ag (collargol, Col-AgNPs), polyvinylpyrrolidone-coated Ag (PVP-AgNPs) and micro-particles of CuO were prepared in deionized (DI) water. Particle solutions were homogenized using ultrasonic probe (Branson 450). For the tests, stock solutions were diluted in DI water (Publication I, II and IV) or in the respective test media (Publications I and III). All chemicals and particles were purchased, except PVP-AgNPs, that were synthesized in the laboratory of Prof. Heikki Tenhu (University of Helsinki, Finland) as described in [85] (Table 2).

Table 2. Soluble metal salts and particles.

Nanoparticles	Purchased from	Coating
nano-CuO	Sigma-Aldrich	uncoated
micro-CuO	Alfa Aesar	uncoated
citrate-AgNPs	NanoComposix	citrate
PVP-AgNPs	synthesized as described in [85]	polyvinyl-pyrrolidone (71%)
Col-AgNPs	Laboratorios Argenos S. L.	casein (30%)
AgNPs	Sigma-Aldrich	uncoated
Salts	Purchased from	
$\text{CuSO}_4 \cdot 7\text{H}_2\text{O}$	Alfa Aesar	
AgNO_3	J.T.Backer; Sigma-Aldrich	

2.2.2. Physico-chemical characterization of nanoparticles

Transmission (TEM; SUMY-SELMi, EM-125 (Publication III), Hitachi H7600 (Publication IV)) and scanning (SEM; JSM-8404 (Publication II)) electron microscopy imaging were used to determine average primary size of particles (Publications II, III and IV) and to visualise NP-protein interaction and protein corona formation (Publications IV). As reported previously, compared to bulk analogues, NPs display larger specific surface area that leads to increased reactivity and thus, also enhanced bactericidal properties [4]. Specific surface area measurements (SSA, Sorptometer Kelvin 1042) of the powders of micro (primary size $> 1 \mu\text{m}$) and nano sized particles were performed in Tallinn University of Technology (Estonia).

The hydrodynamic diameters (D_h) of nanoparticles in suspensions (DI water and in test media) were measured using dynamic light scattering (DLS; Malvern Zetasizer Nano-ZS (Malvern Instruments)) (Publications II, III and IV). UV-Vis absorption spectra of NPs in DI water, buffer solution or medium were obtained using a spectrophotometer (Thermo Multiscan Spectrum (Thermo Electron) (Publi-

cation II), Thermo Multiskan Spectrum (Thermo Electron Corporation) (Publication III) and Cary 300 Bio (Varian) (Publication IV)). ζ -potential measurements were applied to characterise nanoparticles in solution (using Malvern Zetasizer Nano-ZS (Malvern Instruments)) (Publications II, III and IV) (Fig. 4).

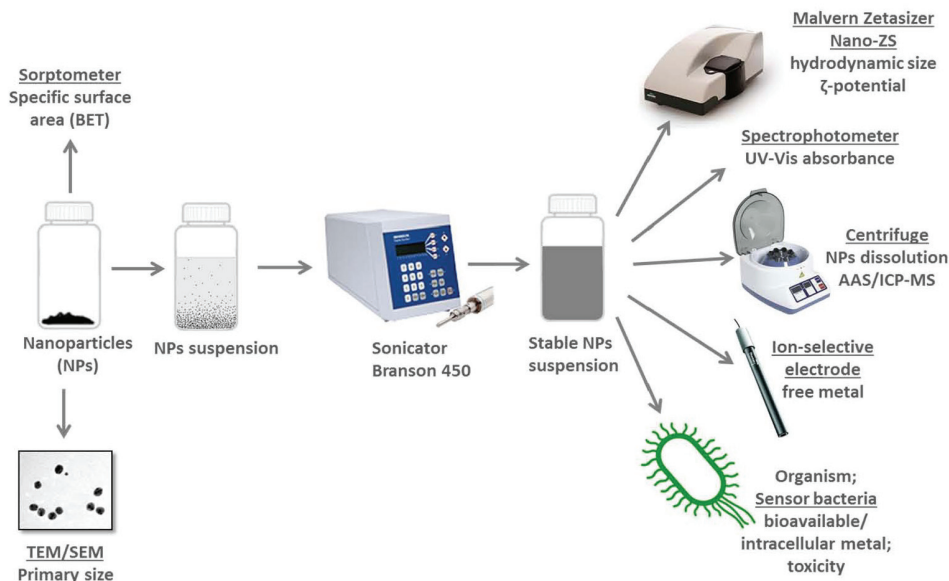


Figure 4. Schematic representation of nanoparticle stock suspension preparation and characterisation.

2.3. Determination of free metal ion concentration and dissolution of nanoparticles

2.3.1. Ion-Selective Electrode

Copper ion selective electrode (Cu-ISE; Orion Research) was applied to study the free ionic form of copper in different environmental conditions (Publication I). CuSO_4 and CuO NPs dilutions were performed in appropriate medium and incubated for 2 h at 30 °C prior to measurement. Free Cu was calculated using following equation:

$$\text{Free Cu (\%)} = \frac{\text{Cu ISE}_{\text{LOD}} \text{ in test media}}{\text{Cu ISE}_{\text{LOD}} \text{ in DI water}} \times 100 \quad (1)$$

The limit of detection (LOD) of the Cu-ISE in each test media was calculated as recommended for ion-selective electrodes by International Union of Pure and Applied Chemistry (IUPAC) [86]. Briefly, $\log(10)$ of the added Cu was plotted against the electrode potential and the crossing point between the linear increase of the

electrode potential and the line representing the electrode background potential was designated as the limit of detection ($\text{Cu-ISE}_{\text{LOD}}$) (Figure S1 of Publication I). In addition to test media complexing potential investigation, the Cu-ISE was used to determine dissolution rate of the CuO nanoparticles.

2.3.2. Atomic absorption spectroscopy and inductively coupled plasma mass spectrometry

Soluble fraction of metals was determined using atomic absorption spectroscopy (AAS) (Publication II and III) and inductively coupled plasma mass spectrometry (ICP-MS) (Publication IV). The samples were centrifuged to remove insoluble fraction and particle-free-supernatant was analysed.

2.4. Bacterial biosensors

Three types of bioluminescent bacterial sensors were used: (i) metal-inducible bacteria were used to quantify bioavailable metal (Fig. 5); (ii) stress-inducible biosensors were used to detect specific stress response of bacteria to toxic metals; (iii) recombinant constitutively luminescent control strains (Table 3). All the biosensor strains used in this study were new and were constructed in the Laboratory of Environmental Toxicology, National Institute of Chemical Physics and Biophysics, Estonia. ROS-inducible and single-stranded DNA (ssDNA) damage-inducible strains were constructed by Dr. Olesja Bondarenko (Publication II) and the rest of the sensors by Dr. Angela Ivask [54].

Before testing all bioluminescent test bacteria were pre-grown overnight in Luria-Bertani (LB) medium [87] (Publications I-III). The overnight culture was diluted 1:50 with fresh LB medium and grown until OD_{600} of ~ 0.6 . Cell pellet was washed twice in respective medium. For that bacteria were centrifuged at $5000 \times g$ for 10 min and resuspended in fresh medium. Prior to the test the bacteria were diluted to $\text{OD}_{600} = 0.1$ ($\sim 10^6$ bacterial cells/ml). 100 μL of chemical was pipetted onto white polypropylene 96-well microplate, 100 μL of bacterial suspension was added to each well and plates were incubated at 30°C . Bioluminescence was measured using microplate luminometer (Orion II, Berthold Detection Systems GmbH).

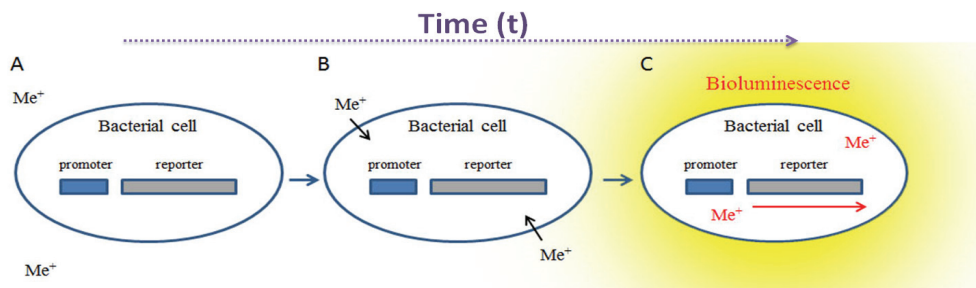


Figure 5. Schematic representation of the induction of metal-specific bioluminescent bacteria: (A) sensor bacteria with metal contaminated sample; (B) heavy metal entering the bacterial cell; (c) metal-specific element sensing intracellular metal ions and activating reporter element which initiates bioluminescence (light production).

Table 3. Luminescent bacterial strains used in the study.

Strain	Description	Publication
Metal-ion-specific luminescent biosensors		
<i>Pseudomonas fluorescens</i> OS8::CueRPcopAlux	Cu-inducible strain	I and II
<i>Escherichia coli</i> MC1061 (pSLcueR/pDNPPcopAlux)	Cu-inducible strain; Ag-inducible strain	II and III
Stress-inducible recombinant luminescent strains		
<i>E. coli</i> K12::katGlux	ROS-inducible strain	II
<i>E. coli</i> MC1061 (pDEWrecAlux)	ssDNA damage-inducible strain	II
Constitutively luminescent bacteria		
<i>E. coli</i> K12::lux	Control strain for <i>E. coli</i> K12::katGlux	II
<i>E. coli</i> MC1061 (pDEWlux)	Control strain for <i>E. coli</i> MC1061 (pDEWrecAlux)	II
<i>E. coli</i> MC1061 (pSLlux)	Control strain for <i>E. coli</i> MC1061 (pSLcueR/pDNPPcopAlux)	II
<i>P. fluorescens</i> OS8::lux	Control strain for <i>P. fluorescens</i> OS8::KncueRPcopAlux Growth inhibition assay	II and III
<i>E. coli</i> MC1061	Growth inhibition assay	III
<i>P. putida</i> KT2440	Growth inhibition assay	III
<i>P. aeruginosa</i> DS10-129	Growth inhibition assay	III
<i>Bacillus subtilis</i> BR151	Growth inhibition assay	III
<i>Staphylococcus aureus</i> RN2440	Growth inhibition assay	III

For the determination of the soluble fraction of CuO NPs (Publication I and II) and AgNPs (Publication III) we used two biosensor strains: *E. coli* MC1061(pSLcueR/pDNPcopAlux) and *P. fluorescens* OS8::KncueRPcopAlux. ROS-generation potential of chemicals and NPs was analysed by *E. coli* K12::katGlux and *E. coli* MC1061 (pDEWrecAlux) was used as ssDNA damage-inducible strain.

The biosensors were first calibrated with respective soluble heavy metal salts, assuming 100% bioavailability of the metal ion, and then nano- or micro-sized particles were analyzed. The concentration of dissolved ions was quantified by comparing the sub-toxic linear part of concentration-response curves of biosensors to particles and to the respective metal ions. A schematic representation of biosensor response to soluble metal salt and nominal concentrations of nano- and micro-sized particles is presented on Fig. 5. Fold induction of bacterial sensor bioluminescence was calculated as follows:

$$\text{Fold induction of bioluminescence} = \frac{CL_s}{SL_s} \cdot CF, \quad (2)$$

where SL_s was the luminescence of the biosensor strain after exposure to chemicals or particles, CL_s - the luminescence of the same strain in control solution and CF was the correction factor. CF was calculated using:

$$CF = \frac{CL_c}{SL_c}, \quad (3)$$

where CL_c was the luminescence of the control strain in a chemical-free control solution and SL_c was the luminescence of that strain after its exposure to chemical or particle.

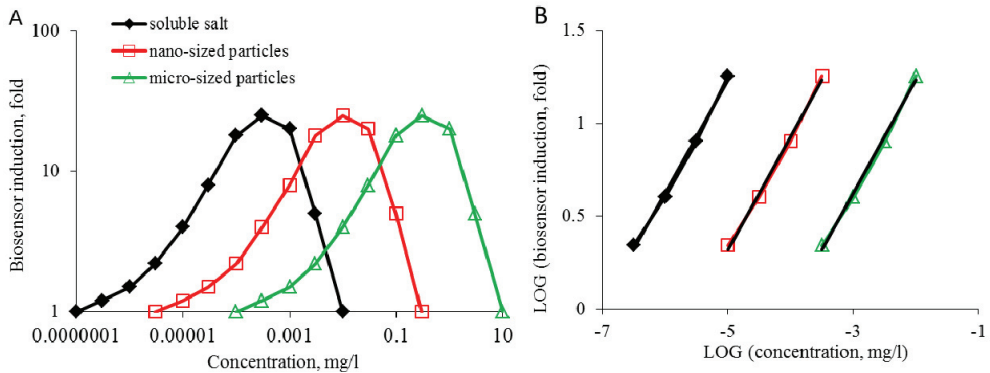


Figure 6. (A) a schematic representation of bacterial biosensor response to soluble heavy metal salt (metal ions) (◆), nano-sized (◻) and micro-sized (△) metal-containing particles; (B) log-log regressions of the sub-toxic linear part of the nominal concentration response curves.

Increase of bioluminescence upon incubation of biosensor with nano and micro-sized particles confirms the presence of ion release and bacterial internalization of soluble ions from particles (Fig. 6A). The dissolution of particles was quantified by linear regression from concentration-response curves, i.e. by comparing the response of biosensor to appropriate metal soluble salt and to particles (Fig. 6B). Using this approach, dissolution of CuO and Ag NPs was calculated in publications II and III, respectively.

2.5. Interaction of silver nanoparticles with firefly luciferase. Effect on enzymatic activity

The effect of nanoparticles on enzymatic activity was investigated using a firefly *Photinus pyralis* luciferase as a model enzyme. This enzyme has a wide use as a reporter in a variety of *in vitro* bioassays. Luciferase is a 62 kDa enzyme comprising of 550 amino acid residues and catalyzes the production of light by converting chemical energy into photoenergy. Specifically, this process involves the oxidation of luciferin - the heterocyclic substrate of the enzyme, in the presence of Mg-ATP and molecular oxygen into oxyluciferin (Fig. 7) [88].

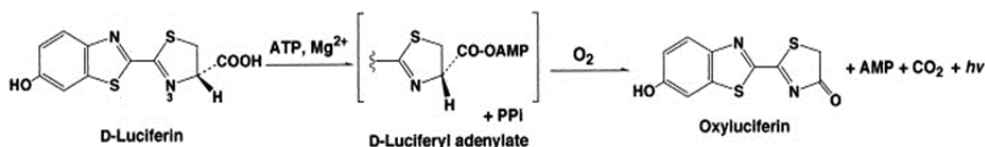


Figure 7. Mechanism of firefly luciferase catalyzed bioluminescence [89].

The reaction releases a photon of light (*hν*) when electronically excited state oxyluciferin returns to the ground state. The produced light intensity is proportional to the amount of functional enzyme. Thus luciferase is a suitable model for the investigation of enzymatic activity by direct measurement of bioluminescence. In the current study the effect of silver nanoparticles (Biopure, 20 nm, citrate coated) on luciferase (QuantiLum Recombinant Firefly Luciferase, Promega) activity was investigated (Publication IV).

Surface plasmon resonance (SPR) of pure AgNPs and AgNPs pre-incubated with enzyme was measured using UV-Vis spectroscopy. TEM imaging allowed visualization of adsorbed layer of protein on NP surface. The study was performed also with soluble silver salt to investigate the impact of Ag-ions. Circular dichroism spectroscopy was used to determine changes in protein secondary structure due to binding on nanoparticles. Since modification of NPs surface can have an effect on ion release, dissolution of NPs over time was studied: luciferase and AgNPs were incubated at room temperature for 0, 2, 4, 8, 24, 48 and 72 h, centrifuged and particle-free supernatants were analysed.

The Luciferase Assay System (Promega) was used to determine the effect of AgNPs on luciferase activity. Luciferase was pre-incubated with different concen-

trations of AgNPs or AgNO₃ for 2 h at room temperature prior to the measurement. A pre-incubated Ag–luciferase mixture of 20 µl was added to 100 µl of the Luciferase Assay System and the signal was recorded with a luminometer (Turner BioSystem 20/20n). The luciferase activity assay was also performed in the presence of Na⁺ or Au³⁺ to determine the specificity of the observed inhibition by Ag-ions. The rapid kinetic measurements of the luciferase in the time scale of seconds were performed on microplate luminometer.

3. RESULTS AND DISCUSSION

3.1. Characterisation of nanoparticles

In this study we analysed CuO and Ag NPs which are currently widely used in consumer products and in various industrial applications. Altogether four types of AgNPs were studied: uncoated and coated with protein and PVP were used for antibacterial activity study (Publication III) and citrate-coated AgNPs were used for the enzyme activity study (Publication IV). In parallel to nanosized CuO particles, the chemically identical micro-sized analogue was analysed to investigate effect of size on antimicrobial properties of CuO (Publication II). Respective soluble salts were used in parallel as (ionic)controls (Table 2).

The electron microscopic imaging was used to investigate surface morphology and primary size of nanoparticles (Fig. 8).

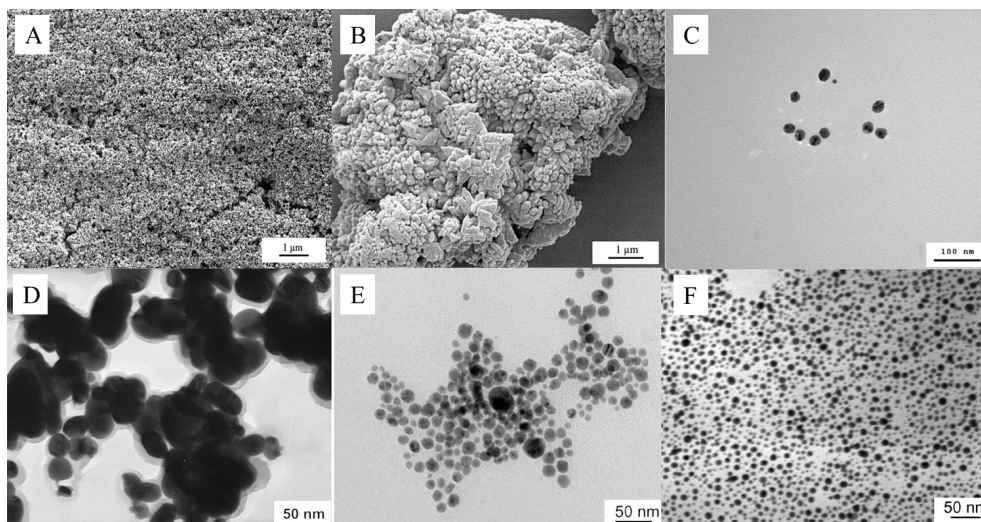


Figure 8. Scanning electron microscopy (SEM) images of (A) nano-sized CuO particles, (B) micro-sized CuO particles, transmission electron microscopy (TEM) images of (C) citrate-coated AgNPs, (D) uncoated AgNPs, (E) protein-coated AgNPs and (F) PVP-coated AgNPs. Modified from Publication III and IV.

Based on electron microscopic images, the primary size of nanoparticles (Table 4) was less than 100 nm, coinciding with the information provided by the manufacturers. Hydrodynamic sizes (D_h) of CuO and Ag NPs, measured by dynamic light scattering (DLS), were larger than the primary size observed by microscopic imaging. The difference in the primary and hydrodynamic sizes is a well-known phenomenon and can be explained by different measurement principles of these two techniques. A dry powder of nanoparticles is used for primary size measurement, whereas hydrodynamic size (DLS) measurements are performed in aqueous solu-

tion by measuring the Brownian motion of NPs [90]. Since NPs tend to agglomerate in aqueous environment, frequently D_h measures size of the clusters, aggregates/agglomerates of nanoparticles. Particles tend to agglomerate even more in solution containing inorganic salts and organic components [2] (see also Fig. 2).

Table 4. Primary and hydrodynamic sizes of studied nanoparticles.

Nanoparticles	Hydrodynamic size (D_h)		
	Primary size, nm	in deionised water (DI), nm ***	D_h in test medium, nm ***
nano-CuO	30 *	190	385 (HMM + 0.1% AA)
micro-CuO	>1000	n.a.	n.a.
citrate-AgNPs	20 **	26	26 (TRIS-acetate)
PVP-AgNPs	8-11 **	122	139 (NaCl-free LB)
Col-AgNPs	5-30 **	44	53 (NaCl-free LB)
AgNPs	30-100 **	89	269 (NaCl-free LB)

AA- amino acids; n.a. - not analysed; * - measured by scanning electron microscopy; ** - measured by transmission electron microscopy; *** - D_h measured by dynamic light scattering.

Table 4 presents the hydrodynamic size (D_h) of nanoparticles in deionised (DI) water and different test media. Most of the nanoparticles had bigger D_h in test media, than in DI water. For example, average primary size of nano-CuO was 30 nm, in DI water size (D_h) increased to 190 nm and in test media was 385 nm.

3.2. Binding potential of ecotoxicological and microbiological test media

As discussed previously, the physico-chemical properties of NPs can be modified upon interaction with components of the test medium. To study that, a comparative study of CuSO_4 and nano-CuO was performed using an ion-selective electrode and a bacterial biosensor (Publication I).

3.2.1. Response of Cu-Ion Selective Electrode on CuSO_4 and nano-CuO in different test media

As mentioned above (see section 1.2.1), the composition of test medium can change the speciation of metal ions, lead to binding of free ions, or influence nanoparticle dissolution. All that has an effect on bioavailable fraction of metals, i.e., on toxicity. The effect of test medium composition should be studied and may be considered as one of the important factors in interpreting the results of toxicity tests.

Seventeen standard ecotoxicological and microbiological test media were analysed for the speciation and bioavailability of copper and copper nanoparticles (Table 1). The copper ion-selective electrode (Cu-ISE) was used to identify free metal ions and *Pseudomonas fluorescens* OS8::KnCueR_PcopAlux bacterial biosensor was used to measure bioavailable copper. Speciation analysis of CuSO_4 in 17 selected

test media showed that most of the test media contained ligands complexing the Cu ions and thus, reduced the amount of free Cu. The amount of free Cu was highest in mineral media. Despite the absence of organics that are strong binding agents of metals, mineral media may contain chelating agents, as EDTA, that is a well-known trace metal chelator [91], or phosphates, which have been demonstrated to form strong metal-phosphate complexes, that often precipitate [92]. The amount of free Cu was remarkably lower in organics-rich media. In addition, response of Cu-ISE to CuSO₄ in organics-containing media was generally in correlation with organics content of the media. This was clearly evident in the case of 0.9% NaCl supplemented with amino acids (AA), where the gradual addition of AA was accompanied by a respective increase of the electrode limit of detection (ISE_{LOD}).

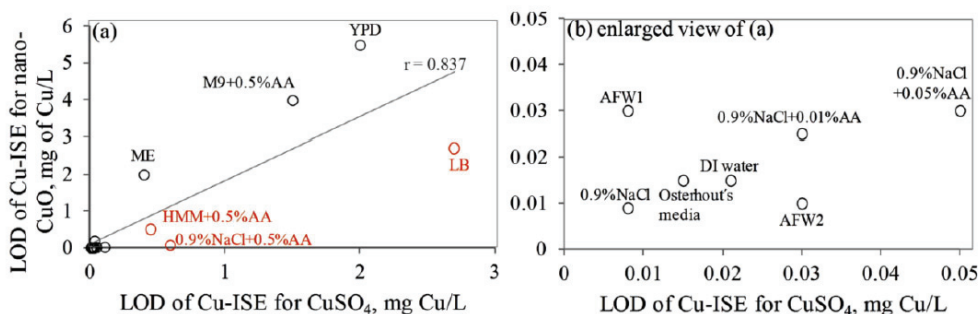


Figure 9. Correlation between Cu-ISE_{LOD} in CuSO₄ and in nano-CuO suspensions prepared in different ecotoxicological and microbiological media. The names of test media correspond to Table 1; (b) is enlarged view of (a). Symbols in brown color indicate media where the concentration of free ions in nano-CuO suspensions was lower than could be predicted from what was observed in case of CuSO₄. Taken from Fig. 4 of Publication I.

In the case of CuO nanoparticles, the Cu-ISE limits of detection in test media were almost identical. This indicates that at these low concentrations all Cu from CuO NPs was likely dissolved and present in the form of free ions. In general, there was a good correlation between the free Cu ions in CuSO₄ and in CuO NPs-spiked test media, but there were several exceptions (Fig. 9). Notably, in some media more free Cu was detected in CuO NPs suspensions than could be predicted from the results of CuSO₄. Therefore, based on experiments it can be suggested that differently from CuSO₄, in case of CuO NPs additional processes take place. These processes likely include agglomeration of nanoparticles, release of Cu ions from the CuO, and interaction of the released Cu ions with the media components.

Analogous results were observed in literature: in organics-containing ‘rich’ media the dissolution of CuO was indeed high if compared to that in water or in saline [61]. One reason for the enhanced dissolution may be the decrease in effective hydrodynamic size of the nanomaterials as a result of coating and stabilisation of the particle suspension with organic molecules. Indeed, in accordance with this hypothesis, our study confirmed decrease of hydrodynamic size of CuO NPs in suspension when Cas-amino acids were added to 0.9% NaCl.

3.1.2. Response of bacterial Cu-Biosensor on CuSO_4 and nano-CuO in different test media

In parallel to measurements made by Cu-ISE the Cu-sensor bacteria were used to quantify bioavailable fraction of copper to these bacteria. According to Rensing et al., 2003 [93] and Brandt et al., 2008 [94] the response of microbial biosensor cells may be due to soluble ionic forms of metals as well Cu - dissolved organic matter complexes (DOM) bioavailable to Cu-sensor bacteria. The LOD values of the bacterial biosensor and Cu-ISE in CuSO_4 spiked media were significantly correlated (Fig. 10). Analogously to the Cu-ISE, sensor bacteria results showed decrease of bioavailable Cu with increasing amount of organics in the media. Interestingly, for both, CuSO_4 and CuO NPs, the LOD of the Cu-biosensor was remarkably lower than that of Cu-ISE.

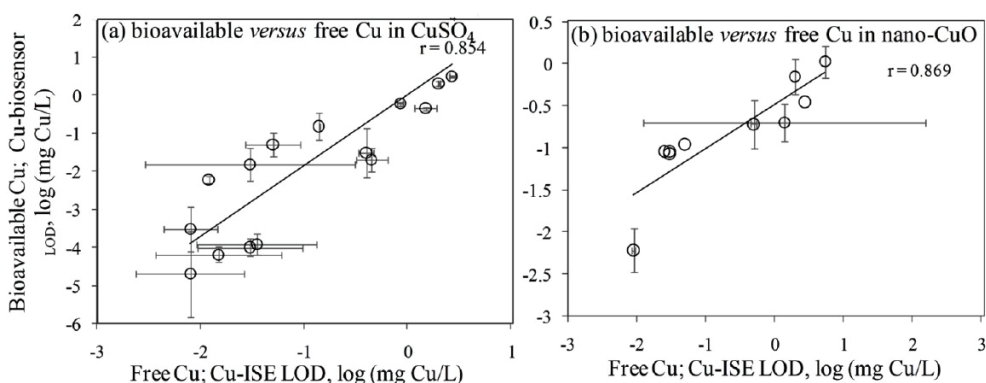


Figure 10. Correlation between limits of determination (LOD) of Cu-ISE (indicative of free Cu) and Cu-biosensor (indicative of bioavailable Cu) for CuSO_4 in different ecotoxicological and microbiological media. Data are plotted from Tables 2 and 3 in Publication I. (a) $\text{Cu-ISE}_{\text{LOD}}$ and $\text{Cu-biosensor}_{\text{LOD}}$ for CuSO_4 ; (b) $\text{Cu-ISE}_{\text{LOD}}$ and $\text{Cu-biosensor}_{\text{LOD}}$ for nano-CuO. Modified from Fig. 2 of Publication I.

The lower LOD suggests that bacterial cells were also able to access additional fractions of Cu in addition to the free ions detected by Cu-ISE. Thus, in case of particle-containing samples (including CuO NPs), more Cu may be bioavailable to living (e.g., microbial) cells than could be predicted based on only dissolved fraction of Cu.

Biosensor used in this study showed higher sensitivity for heavy metals than ion-selective electrode, and may be more relevant and informative method in environmental hazard analysis.

In addition, we screened the literature to collect the EC_{50} values (the concentration of test substance that causes studied adverse effect to 50% of the test organisms) for copper (determined using standard ecotoxicological test organisms, such as protozoa, crustaceans, algae, bacteria, yeasts) and normalized them for calculated

free Cu in the test media. After normalization, the difference in EC_{50} values decreased from 4 orders of magnitude to 1.8. Toxicity tests, from which the EC_{50} values were obtained, were performed in the same media that were used for Cu speciation and bioavailability analysis. Thus, the free ion concentration may be considered as relatively suitable parameter for copper toxicity prediction.

3.3. Investigation of antimicrobial properties and toxicity mechanisms of nanoparticles

Despite of increasing number of nanotoxicological studies, the toxicological mechanisms of NPs are not yet fully understood [54]. We investigated the toxic effect of CuO NPs and AgNPs using bacteria as test organisms. For the study of CuO toxicity mechanisms (Publication II) ROS (*E. coli* K12::katGlux) and DNA damage (*E. coli* MC1061(pDEWrecAlux)) biosensors were constructed, which were sensing reactive oxygen species or DNA damage, respectively. The construction of biosensors is described in Publication II and was performed by Dr. Olesja Bondarenko. *E. coli* MC1061 (pSLcueR/pDNPcopAlux) bacteria were used as metal ion-specific biosensors.

Upon incubation of sensor bacteria with copper compounds a time-dependent response was observed. *E. coli* Cu-ion biosensor was induced already after 0.5 h of exposure to all three Cu compounds (CuSO₄, nano- and micro-CuO particles), induction of hydrogen peroxide inducible (ROS) biosensor started only after 5 h and the induction of DNA damage biosensor after 8 h of exposure (Fig. 11).

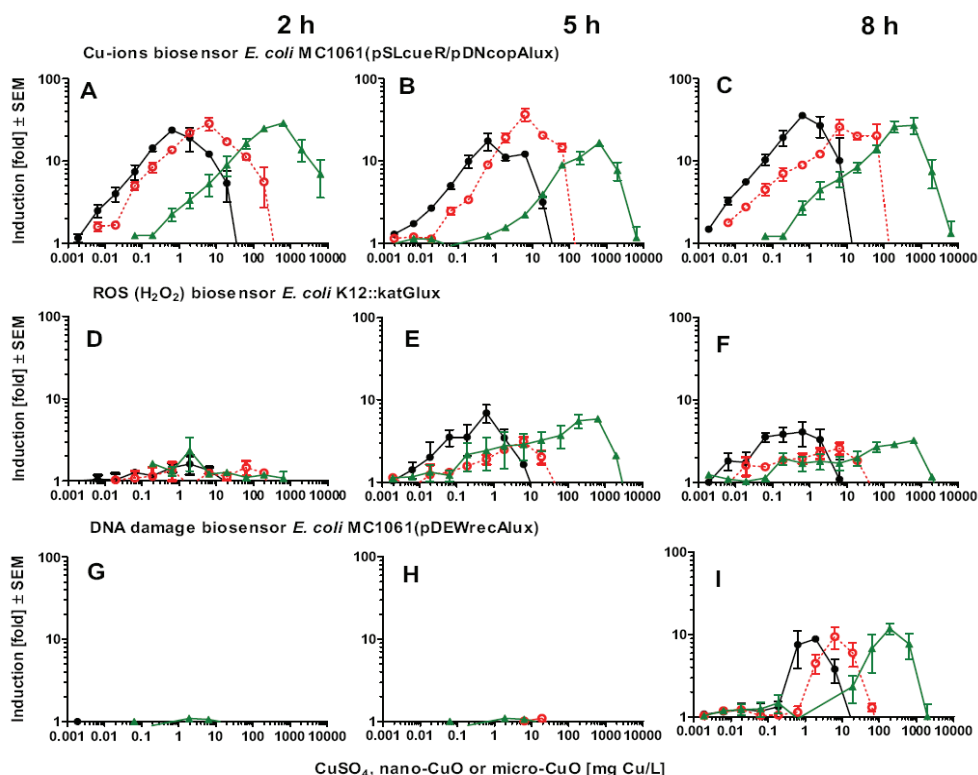
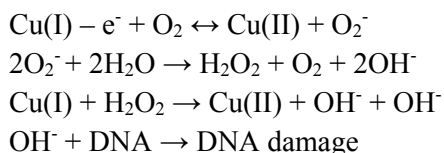


Figure 11. Time-course response of *Escherichia coli* based bioluminescent sensors to different Cu formulations. (A-C) Induction of ion-specific biosensor *E. coli* MC1061(pSLcueR/pDNPcopAlux); (D-F) ROS biosensor *E. coli* K12::katGlux and (G-I) DNA damage biosensor *E. coli* MC1061(pDEWrecAlux) by CuSO₄ (•), nano-CuO (○) and micro-CuO (▲) for 2 (left panels), 5 (middle panels), and 8 (right panels) hours. Concentrations are presented on Cu basis (mg Cu/L). Mean of 3 individual experiments ± standard error of the mean is shown. Taken from Fig. 2 of Publication II. Reprinted with the permission of Elsevier.

Since copper ion biosensor is responding to soluble metal fraction [54] and the response patterns of ROS and DNA damage biosensors were very similar to Cu ion biosensor, we assumed, that Cu ions, solubilized from CuO particles, triggered the ROS and DNA damage responses. The particle dissolution study showed around 10% solubility of nano-sized CuO and 0.1% of micro-sized CuO. Investigation of metal ion concentration which corresponds to sensors maximum induction at appropriate concentration of particles showed presence of equal amounts of soluble Cu and confirmed that ROS and DNA damage detected by the biosensors were indeed triggered by dissolved Cu. It is worth noting that at least part of dissolved Cu was not bioavailable to sensor bacteria. The fraction of dissolved Cu determined by AAS was significantly higher than the fraction of free Cu ions that entered the bacterial cells and caused the observed effects.

In addition, we investigated the effect of metal chelating agent (ethylenediaminetetraacetic acid, EDTA) to the biosensors' response to different Cu formulations. The addition of EDTA abolished the response of biosensors to copper. This additionally confirmed that the observed ROS and DNA damage in bacterial cells were indeed caused by dissolved Cu ions and not by particles themselves.

According to the literature the accumulation of intracellular ROS after prolonged exposure to low sub-toxic concentrations of Cu formulations may be explained by Cu ion compartmentalization in the bacterial cell and Cu chemistry [8]. The ROS can be produced during Cu(I) oxidation to Cu(II) in the following Cu recycling redox system [95]:



The reason of response delay between ion-specific, ROS and DNA damage biosensors may be due to solubilisation of copper derivatives. Metal ions are directly detectable by ion-specific biosensors, whereas ROS and DNA damage biosensors are responding to ion initiated processes in the bacterial cell. There may be a cascade of events, which explain the time dependence phenomenon: the internalised Cu ions are mainly stored in the periplasm (a space bordered by the inner membrane and the outer membrane in Gram-negative bacteria [96]), where they first induce the production of superoxide anions [8]. Superoxide anions diffuse into the cytosol, where they activate superoxide dismutase (catalyzes the dismutation of superoxide (O_2^-) into oxygen and hydrogen peroxide) gene – inducing the ROS biosensor. Intracellular and other superoxide dismutases convert superoxide into H_2O_2 that triggers the activation of catalase (catalyzes the decomposition of hydrogen peroxide). Finally, cytosolic H_2O_2 induces Fe-dependent production of hydroxyl radicals *via* the Fenton reaction [97], which leads to unspecific oxidation of various biomolecules including DNA, which activates ssDNA inducible gene – finally inducing DNA damage biosensor.

Notably, we observed similar results in antibacterial study of silver nanoparticles with different surface modification (Publication III). The effects of non-coated (AgNPs), protein (casein) coated (collargol; Col-AgNPs) and PVP-coated Ag (PVP-AgNPs) nanoparticles to six bacterial strains (Gram-negative *Escherichia coli*, *Pseudomonas fluorescens*, *P. putida*, *P. aeruginosa* and Gram-positive *Bacillus subtilis* and *Staphylococcus aureus*) were demonstrated (Fig. 12). We observed, that the toxicity of AgNO_3 to these bacteria varied only slightly (the 4-h EC_{50} varied only 4-fold (Table 5)). But the toxicity of AgNPs to various bacterial strains differed remarkably (up to 130-fold), followed the order PVP-AgNPs > Col-AgNPs > AgNPs (Fig. 12), showing a clear positive correlation with their dissolution rates, but not their size.

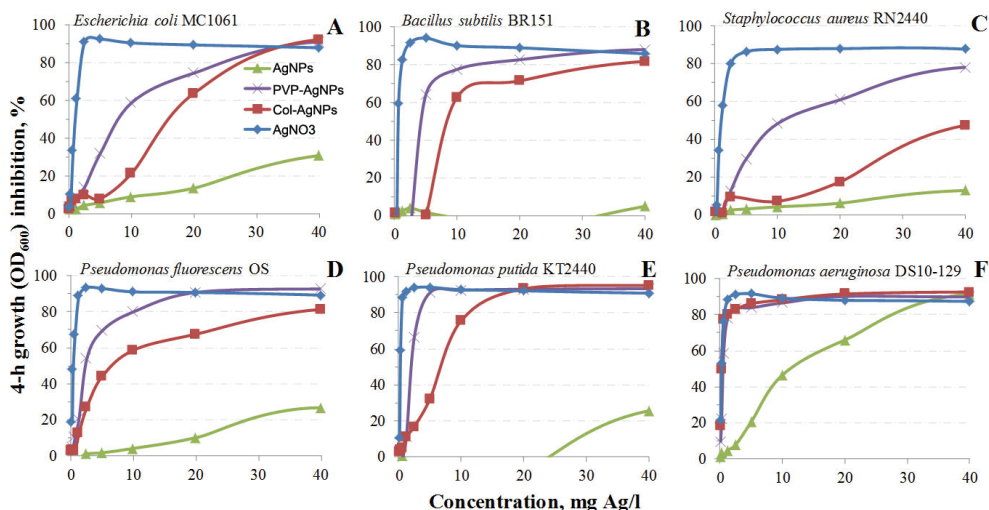


Figure 12. Growth inhibition of bacterial strains by silver nanoparticles. Growth inhibition of (A) *Escherichia coli*, (B) *Bacillus subtilis*, (C) *Staphylococcus aureus*, (D) *Pseudomonas fluorescens*, (E) *Pseudomonas putida* and (F) *Pseudomonas aeruginosa* by (▲) uncoated Ag nanoparticles (AgNPs), (×) PVP-coated AgNPs (PVP-AgNPs), (■) protein-coated AgNPs (Col-AgNPs), and (◆) AgNO₃ after 4-h incubation in half-strength NaCl-free LB medium at 30°C. The representative figures from three biological replicates are shown. Modified from Fig. 5S of Publication III supplementary information.

Table 5. 4-h EC₅₀ values (half effective concentration) for different silver formulations to bacteria (AgNO₃, PVP-coated (PVP-AgNPs) and protein-coated (Col-AgNPs). EC₅₀ values are calculated from dose-response curves presented in Fig. 12.

Bacterial strain	4-h EC ₅₀ , mg Ag/l		
	AgNO ₃	Col-AgNPs	PVP-AgNPs
<i>Escherichia coli</i>	0.8	18.7	8.9
<i>Bacillus subtilis</i>	0.5	15.6	5.2
<i>Staphylococcus aureus</i>	1.2	46.1	16.1
<i>Pseudomonas fluorescens</i>	0.4	11.2	2.6
<i>P. putida</i>	0.3	6.2	2.2
<i>P. aeruginosa</i>	0.35	0.35	0.59

The toxicity of AgNPs was not caused only by Ag ions present in the solution, but each bacterial strain had different influence on NPs dissolution *via* bacterial exudates (organic acids, peptides, biosurfactants) and the cellular uptake of Ag ions *via* cell-NP interaction was different in different bacterial strains. It is generally acknowledged that Ag⁺ ions interact with -SH groups of bacteria membrane-bound enzymes and other proteins, uncoupling the respiratory chain [98, 99] and disrupting bacterial cell membranes [100].

The biotic and abiotic (in the presence and absence of microorganisms, respectively) AgNPs dissolution study (AAS and Ag-ISE) (Fig. 13) revealed that all

AgNPs derivatives were not dissolved more in the presence of bacteria than in abiotic conditions. But in the case of cell-NPs interaction the extracellular Ag^+ concentration detectable by biosensor was about 3 times higher than was internalized when the biosensor was exposed to ultracentrifuged supernatants of AgNPs.

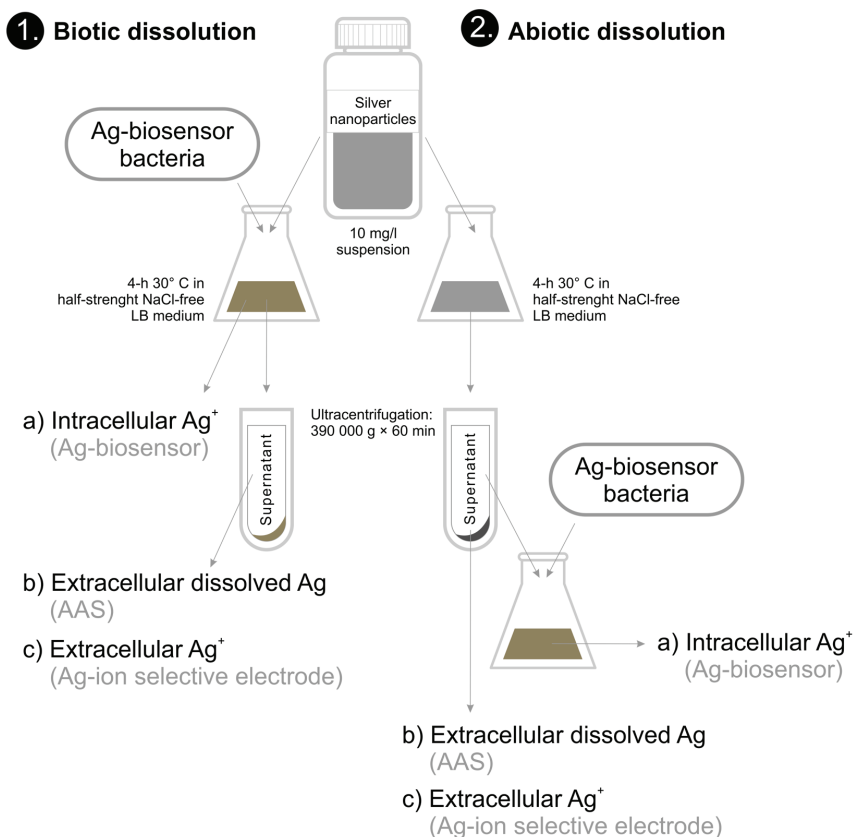


Figure 13. Schematic representation of the experiment to study dissolution of AgNPs. Intracellular Ag ions, extracellular dissolved Ag and extracellular Ag ions were quantified in biotic (left) as well abiotic (right) conditions. Ag-biosensor *E. coli* MC1061(pSLcueR/pDNPCopAlux) was exposed either to the 10 mg/l suspensions of AgNPs (biotic dissolution) or to the supernatants obtained after ultracentrifugation (390 000 g×60 min) of the respective AgNPs' suspensions (abiotic dissolution). Intracellular Ag ions were quantified as a function of increase of bioluminescence Ag-biosensor *E. coli* MC1061(pSLcueR/pDNPCopAlux), extracellular dissolved Ag was measured by atomic absorption spectroscopy (AAS) and extracellular Ag ions by ion-selective electrode (Ag-ISE). Taken from Fig. 4 of Publication III.

In addition, co-precipitation experiment of six bacteria with Col-AgNPs by UV-Vis spectra measurements of centrifuged supernatants was performed. We observed, that *P. aeruginosa* cells had higher affinity to AgNPs than the other tested

bacterial strains. As *P. aeruginosa* has also pathogenic strains, the high biocidal efficiency of Collargol towards these bacteria may have practical application.

These results reveal the importance of direct contact of AgNPs with bacterial cells and demonstrate that the extracellular concentration of Ag ions in the test medium may underestimate the effective intracellular concentrations and hence, antibacterial potency of Ag ions from AgNPs.

Our data is in good correlation with other publications, where it has been shown, that AgNPs are more toxic to bacterial cells than dissolved silver released from these NPs [28, 101, 102].

3.4. Interaction of nanoparticles with firefly luciferase. Effect on enzymatic activity

Nanosilver is widely used in consumer products, mostly due to its antimicrobial properties. The wide use of nanosilver products increases the probability of exposure not only to the targeted organisms (bacteria, fungi) but also to other organisms in surface water ecosystems, wastewater treatment plant microbial communities as well as humans [2]. These organisms have something in common – they all contain enzymes in their cells – proteins that catalyze complex and specific biochemical reactions in high speed at ambient or body temperatures [103]. To study the impact of silver nanoparticles to enzymes we chose firefly luciferase as a model as the activity of this enzyme is easily measurable by recording its light output. Also, firefly luciferase is often used as a bioreporter and for the evaluation of cellular viability *via* ATP analysis. For the latter the interference of nanoparticles with the enzyme activity is undesirable as it could lead to false interpretations.

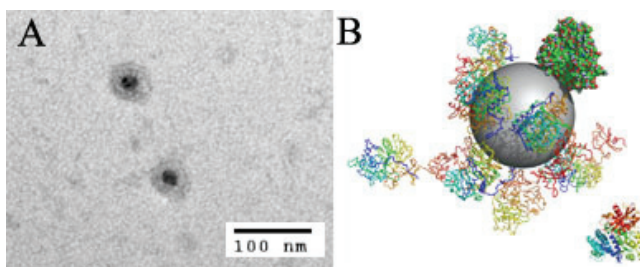


Figure 14. (A) TEM image of AgNPs–luciferase corona. Black dots are 20 nm AgNPs and dark grey cloud around particles is luciferase corona with average thickness of 20 nm; (B) discrete molecular dynamics (DMD) simulation of AgNP–luciferase corona. These images showed the binding of the enzyme with the AgNPs and revealed multilayer protein coating of the nanoparticles. Modified from Fig. 1 and Fig. 5 of Publication IV.

We showed that 20 nm citrate-coated AgNPs dose-dependently inhibited the enzymatic activity of firefly luciferase. The inhibition mechanism was examined by characterizing the physicochemical properties and biophysical interactions of the enzyme and the AgNPs and quantification of the silver-ions released from the

AgNPs. We showed that mixing of the enzyme and AgNPs induced an increase in ζ -potential triggered a red-shift of 44 nm in the absorbance peak of the AgNPs, and rendered a ‘luciferase protein corona’ of 20 nm in thickness on the nanoparticle surfaces (Fig. 14A). However, the secondary structure of the luciferase was only marginally affected upon formation of the corona, as verified by circular dichroism spectroscopy and multiscale discrete molecular dynamics simulations (Fig. 14B).

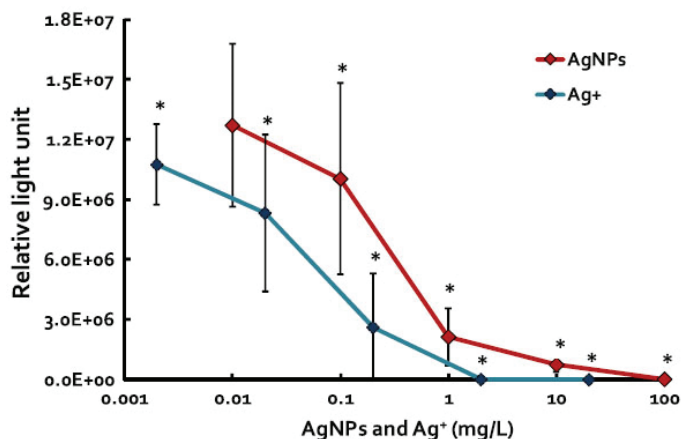


Figure 15. Inhibition of luciferase activity by AgNPs and Ag⁺. Taken from Fig. 3 of Publication IV. Reprinted with the permission of IOP Publishing.

By comparing the enzymatic inhibitory patterns of AgNPs and Ag-ions we showed that the inhibition was primarily due to the release of silver ions from AgNPs (Fig. 15). Interestingly, silver ions showed the dose-dependent inhibition of luciferase already in sub-second contact time at sub-ppm level (Fig. 16). The high affinity of silver ions towards Cys residues and N-groups may be the primary cause of the inhibition.

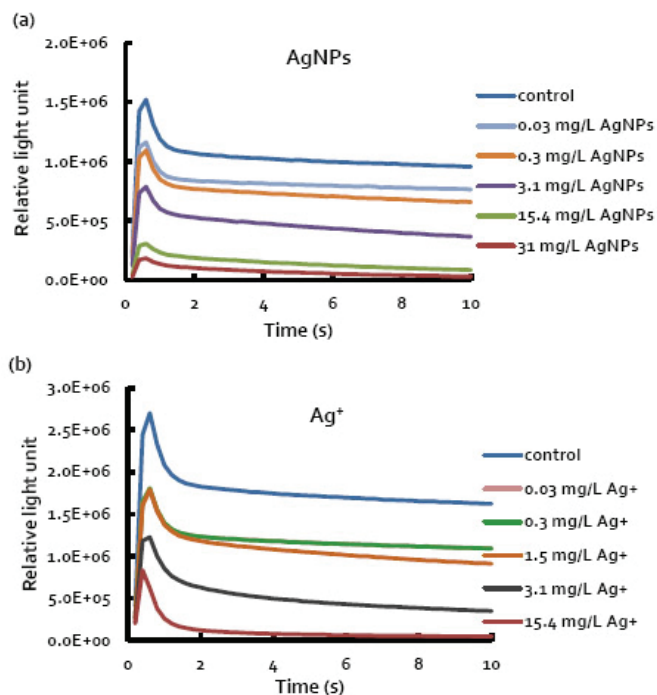


Figure 16. Rapid kinetics of luciferase bioluminescence: effects of (a) AgNPs and (b) Ag⁺ on enzyme activity. The kinetics showed rapid initial flashes at 0.6 s and concentration-dependent inhibition of the luminescence already within the first 1-10 s of incubation with AgNPs or Ag⁺. Modified from Fig. 3S of Publication IV supplementary information.

CONCLUSIONS

- The CuO nanoparticles (NPs) and 4 different types of AgNPs were physico-chemically characterized by measuring ζ -potential, primary and hydrodynamic size. The dissolution of NPs was tested to evaluate the role of metal ions in NPs toxicity (Publications I, II, III, IV)
- The speciation of the metal ions (using Cu ions as example) in different ecotoxicological and microbiological test media (Publication I) was analyzed using ion-selective electrode (ISE) and metal-specific sensor bacteria (biosensor). We observed enhanced dissolution in organics-rich media due to increased dispersion of CuO NPs and complexing of dissolved Cu^{2+} by organics present in the medium. In general, mineral media showed significantly more free and bioavailable copper than organics-containing media. In general, there was a good correlation between data obtained by Cu-ISE and Cu-biosensor. Interestingly, Cu-biosensor used in this study showed higher sensitivity than Cu-selective electrode. In environmental hazard analysis sensor bacteria may prove more environmentally relevant and informative technique than conventional chemical methods. The observed remarkable difference in sensitivity of various aquatic organisms towards copper may be largely explained by the different speciation of copper in the respective test media.
- The Cu ion-specific biosensor in combination with chemical analysis of Cu ion revealed that dissolution (Cu^{2+}) of CuO particles was the key factor triggering the ROS and DNA damage responses in bacteria (Publication II).
- The direct contact between the bacterial cell and AgNPs enhanced the toxic effect of nanosilver (Publication III). Namely, cell-NPs contact increased the cellular uptake of particle-associated Ag ions. In addition, bacterial strain-specific bioavailability of Ag^+ liberated from AgNPs was observed.
- AgNPs dose-dependently inhibited the activity of luciferase – an enzyme often used as a reporter in various biological assays (Publication IV). This inhibition effect was largely caused by released silver ions and not by the physical adsorption onto AgNPs, as the induced conformational changes in protein secondary structure exerted only a minor effect on enzyme function.

REFERENCES

1. European Commission (2013) Communication from the Commission to the European Parliament, the Council and the European Economic and Social Committee. Second Regulatory Review on Nanomaterials Brussels, 3.10.2012, COM(2012) 572 final.
2. Bondarenko O, Juganson K, Ivask A, Kasemets K, Mortimer M, et al. (2013) Toxicity of Ag, CuO and ZnO nanoparticles to selected environmentally relevant test organisms and mammalian cells in vitro: a critical review. *Archives of Toxicology* 84: 1181 - 1200.
3. IUPAC Compendium of Chemical Terminology 2nd Edition (1997).
4. Nel A, Xia T, Mädler L, Li N (2006) Toxic potential of materials at the nanolevel. *Science* 311: 622-627.
5. Warheit DB (2008) How meaningful are the results of nanotoxicity studies in the absence of adequate material characterization? *Toxicol Sci* 101: 183–185.
6. Xia T, Kovochich M, Brant J, Hotze M, Sempf J, et al. (2006) Comparison of the abilities of ambient and manufactured nanoparticles to induce cellular toxicity according to an oxidative stress paradigm. *Nano Letters* 6: 1794-1807.
7. Fridovich I, Freeman B (1986) Antioxidant defenses in the lung. *Annu Rev Physiol* 48: 693-702.
8. Hoshino N, Kimura T, Yamaji A, Ando T (1999) Damage to the cytoplasmic membrane of *Escherichia coli* by catechin-copper (II) complexes. *Free Radic Biol Med* 27: 1245-1250.
9. Choi O, Hu Z (2008) Size dependent and reactive oxygen species related nanosilver toxicity to nitrifying bacteria. *Environ Sci Technol* 42: 4583-4588.
10. Puzyn T, Rasulev B, Gajewicz A, Hu X, Dasari TP, et al. (2011) Using nano-QSAR to predict the cytotoxicity of metal oxide nanoparticles. *Nat Nano* 6: 175-178.
11. Arvizo RR, Bhattacharyya S, Kudgus RA, Giri K, Bhattacharya R, et al. (2012) Intrinsic therapeutic applications of noble metal nanoparticles: past, present and future. *Chem Soc Rev* 41: 2943-2970.
12. Handy R, Cornelis G, Fernandes T, Tsyusko O, Decho A, et al. (2012) Ecotoxicity test methods for engineered nanomaterials: Practical experiences and recommendations from the bench. *Environ Toxicol Chem* 31: 15-31.
13. Fung MC, Bowen D (1996) Silver products for medical indications: risk-benefit assessment. *J Toxicol Clin Toxicol* 34: 119–126.

14. Nowack B, Krug HF, Height M (2011) 120 Years of nanosilver history: implications for policy makers. *Environ Sci Technol* 45: 1177–1183.
15. The Project on Emerging Nanotechnologies <http://www.nanotechproject.org/> (23.04.2014).
16. Marambio-Jones C, Hoek E (2010) A review of the antibacterial effects of silver nanomaterials and potential implications for human health and the environment. *J Nanopart Res* 12: 1531–1551.
17. Cerkez I, Kocer HB, Worley SD, Broughton RM, Huang TS (2012) Multifunctional cotton fabric: Antimicrobial and durable press. *J Appl Polym Sci* 124: 4230–4238.
18. Kahru A, Ivask A (2013) Mapping the dawn of nanoecotoxicological research. *Acc Chem Res* 46: 823–833.
19. Cleveland D, Long SE, Pennington PL, Cooper E, Fulton MH, et al. (2012) Pilot estuarine mesocosm study on the environmental fate of silver nanomaterials leached from consumer products. *Sci Total Environ* 421–422: 267–272.
20. Mueller NC, Nowack B (2008) Exposure modeling of engineered nanoparticles in the environment. *Environ Sci Technol* 42: 4447–4453.
21. Wijnhoven SWP, Peijnenburg WJGM, Herberts CA, Hagens WI, Oomen AG, et al. (2009) Nano-silver – a review of available data and knowledge gaps in human and environmental risk assessment. *Nanotoxicology* 3: 109–138.
22. Pal S, Tak YK, Song JM (2007) Does the antibacterial activity of silver nanoparticles depend on the shape of the nanoparticle? A study of the gram-negative bacterium *Escherichia coli*. *Appl Environ Microbiol* 73: 1712–1720.
23. Lok CN, Ho CM, Chen R, He QY, Yu WY, et al. (2007) Silver nanoparticles: partial oxidation and antibacterial activities. *J Biol Inorg Chem* 12: 527–534.
24. Xiu ZM, Zhang QB, Puppala HL, Colvin VL, Alvarez PJJ (2012) Negligible particle-specific antibacterial activity of silver nanoparticles. *Nano Letters* 12: 4271–4275.
25. Hwang ET, Lee JH, Chae Y, Kim YS, Kim BC, et al. (2008) Analysis of the toxic mode of action of silver nanoparticles using stress-specific bioluminescent bacteria. *Small* 4: 746–750.
26. Ivask A, Bondarenko O, Jephthina N, Kahru A (2010) Profiling of the reactive oxygen species-related ecotoxicity of CuO, ZnO, TiO₂, silver and fullerene nanoparticles using a set of recombinant luminescent *Escherichia coli* strains: differentiating the impact of particles and solubilised metals. *Anal Bioanal Chem* 398: 701–716.

27. Lok CN, Ho CM, Chen R, He QY, Yu WY, et al. (2006) Proteomic analysis of the mode of antibacterial action of silver nanoparticles. *J Proteome Res* 5: 916–924.
28. Jin X, Li M, Wang J, Marambio-Jones C, Peng F, et al. (2010) High-throughput screening of silver nanoparticle stability and bacterial inactivation in aquatic media: influence of specific ions. *Environ Sci Technol* 44: 7321–7328.
29. Gunawan C, Teoh W, Marquis C, Lifia J, Amal R (2009) Reversible antimicrobial photoswitching in nanosilver. *Small* 5: 341–344.
30. McQuillan JS, Infante GH, Stokes E, Shaw AM (2012) Silver nanoparticle enhanced silver ion stress response in *Escherichia coli* K12. *Nanotoxicology* 6: 857–866.
31. Ivask A, George S, Bondarenko O, Kahru A (2012). Metal-containing nanoantimicrobials: differentiating the impact of solubilized metals and particles. In: *Nano-antimicrobials- Progress and Prospects*, Cioffi N RM, Editor. Springer. pp. 253–290.
32. Panacek A, Kvitek R, Prucek M, Kolar R, Vecerova N, et al. (2006) Silver colloid nanoparticles: synthesis, characterization, and their antibacterial activity. *J Phys Chem B* 110: 16248–16253.
33. Morones JR, Elechiguerra JL, Camacho A, Holt K, Kouri JB, et al. (2005) The bactericidal effect of silver nanoparticles. *Nanotechnology* 16: 2346–2353.
34. Ebrahimnia-Bajestan E, Niazmand H, Duangthongsuk W, Wongwises S (2011) Numerical investigation of effective parameters in convective heat transfer of nanofluids flowing under a laminar flow regime. *Int J Heat Mass Transfer* 54: 4376–4388.
35. Gabbay J, Borkow G, Mishal J, Magen E, Zatcoff RS, et al. (2006) Copper oxide impregnated textiles with potent biocidal activities. *J Ind Text* 35: 323–335.
36. Aruoja V, Dubourguier HC, Kasemets K, Kahru A (2009) Toxicity of nanoparticles of CuO, ZnO and TiO₂ to microalgae *Pseudokirchneriella subcapitata*. *Sci Total Environ Sci Technol* 407: 1461 - 1468.
37. Heinlaan M, Ivask A, Blinova I, Dubourguier HC, Kahru A (2008) Toxicity of nanosized and bulk ZnO, CuO and TiO₂ to bacteria *Vibrio fischeri* and crustaceans *Daphnia magna* and *Thamnocephalus platyurus*. *Chemosphere* 71: 1308–1316.
38. Griffitt RJ, Weil R, Hyndman KA, Denslow ND, Powers K, et al. (2007) Exposure to copper nanoparticles causes gill injury and acute lethality to zebrafish (*Danio rerio*). *Environ Sci Technol* 41: 8178–8186.

39. Karlsson HL, Cronholm P, Gustafsson J, L Ml (2008) Copper oxide nanoparticles are highly toxic: a comparison between metal oxide nanoparticles and carbon nanotubes. *Chem Res Toxicol* 21: 1726-1732.
40. Midander K, Cronholm P, Karlsson HL, Elihn K, Möller L, et al. (2009) Surface characteristics, copper release, and toxicity of nano- and micrometersized copper and copper(II) oxide particles: a cross-disciplinary study. *Small* 5: 389-399.
41. Golobič M, Jemec A, Drobne D, Romih T, Kasemets K, et al. (2012) Upon exposure to Cu nanoparticles, accumulation of copper in the isopod *Porcellio scaber* is due to the dissolved Cu ions inside the digestive tract. *Environ Sci Technol* 46: 12112-12119.
42. Kahru A, Dubourguier HC (2010) From ecotoxicology to nanoecotoxicology. *Toxicology* 269: 105-119.
43. Witters HE (1998) Chemical speciation dynamics and toxicity assessment in aquatic systems. *Ecotoxicol Environ Safety* 41: 90-95.
44. Bakker E, Pretsch E (2002) The new wave of ion-selective electrodes. *Anal Chem* 74: 420A-426A.
45. Pesavento M, Alberti G, Biesuz R (2009) Analytical methods for determination of free metal ion concentration, labile species fraction and metal complexation capacity of environmental waters: A review. *Anal Chim Acta* 631: 129-141.
46. Dybko A (2001) Errors in chemical sensor measurements. *Sensors* 1: 29-37.
47. Dimeski G, Badrick T, John AS (2010) Ion Selective Electrodes (ISEs) and interferences—A review. *Clin Chim Acta* 411: 309-317.
48. Rice RH, Vidrio EA, Kumfer BM, Qin Q, Willits NH, et al. (2009) Generation of oxidant response to copper and iron nanoparticles and salts: Stimulation by ascorbate. *Chem Biol Interact* 181: 359-365.
49. Lyven B, Hasselöv M, Turner DR, Haraldsson C, Andersson K (2003) Competition between iron- and carbon-based colloidal carriers for trace metals in a freshwater assessed using flow fieldflow fractionation coupled to ICPMS. *Geochim Cosmochim Acta* 67: 3791–3802.
50. Handy RD, von der Kammer F, Lead JR, Hasselöv M, Owen R, et al. (2008) The ecotoxicology and chemistry of manufactured nanoparticles. *Ecotoxicology* 17: 287-314.
51. Cuppett JD, Susan E, Duncan SE, Dietrich AM (2006) Evaluation of copper speciation and water quality factors that affect aqueous copper tasting response. *Chem. Senses* 31: 689– 697.

52. Harms H, Wells M, Meer J (2006) Whole-cell living biosensors—Are they ready for environmental application? *Appl Microbiol Biotechnol* 70: 273-280.
53. Yagi K (2007) Applications of whole-cell bacterial sensors in biotechnology and environmental science. *Appl Microbiol Biotechnol* 73: 1251-1258.
54. Ivask A, Rolova T, Kahru A (2009) A suite of recombinant luminescent bacterial strains for the quantification of bioavailable heavy metals and toxicity testing. *BMC Biotechnol* 9: 41.
55. Ivask A, Francois M, Kahru A, Dubourguier H, Virta M, et al. (2004) Recombinant luminescent bacterial sensors for the measurement of bioavailability of cadmium and lead in soils polluted by metal smelters. *Chemosphere* 55: 147-156.
56. Kahru A, Ivask A, Kasemets K, Pollumaa L, Kurvet I, et al. (2005) Biotests and biosensors in ecotoxicological risk assessment of field soils polluted with zinc, lead and cadmium. *Environ Toxicol Chem* 24: 2973-2982.
57. Mortimer M, Kasemets K, Kahru A (2010) Toxicity of ZnO and CuO nanoparticles to ciliated protozoa *Tetrahymena thermophila*. *Toxicology* 269: 182-189.
58. Devasagayam TPA, Tilak JC, Bloor KK, Sane Ketaki S, Ghaskadbi SS, et al. (2004) Free radicals and antioxidants in human health: current status and future prospects. *Journal of Association of Physicians of India (JAPI)* 52: 796.
59. Invitrogen <http://probes.invitrogen.com/media/pis/mp36103.pdf> (2006).
60. Karlsson HL, Cronholm P, Gustafsson J, Möller L (2008) Copper oxide nanoparticles are highly toxic: a comparison between metal oxide nanoparticles and carbon nanotubes. *Chem Res Toxicol* 21: 1726-1732.
61. Gunawan C, Teoh WY, Marguis CP, Amal R (2011) Cytotoxic origin of copper(II) oxide nanoparticles: Comparative studies with micron-sized particles, leachate, and metal salts. *ACS Nano* 27: 7214-7225.
62. Hassan HM, Fridovich I (1977) Enzymatic defences against the toxicity of oxygen and of streptonigrin in *Escherichia coli*. *J Bacteriol* 129: 1574-1583.
63. Greenberg JT, Monach P, Chou JH, Josephy PD, Dimple B (1990) Positive control of a global antioxidant defense regulon activated by superoxide-generating agents in *Escherichia coli*. *PNAS* 87: 6181-6185.
64. Christman MF, Morgan RW, Jacobson FS, Ames BN (1985) Positive control of a regulon for defenses against oxidative stress and some heat-shock proteins in *Salmonella typhimurium*. *Cell* 41: 753-762.
65. Vroman L, Adams AL, Fischer GC, Munoz PC (1980) Interaction of high molecular-weight kininogen, factor-Xii, and fibrinogen in plasma at interfaces. *Blood* 55: 156-159.

66. Rahman M, Laurent S, Tawil N, Yahia L, Mahmoudi M, Protein-Nanoparticle Interactions. The Bio-Nano Interface. Series: Springer Series in Biophysics, Vol. 15. (2013).
67. Horcajada P, Chalati T, Serre C, Gillet B, C S, et al. (2010) Porous metal–organic-framework nanoscale carriers as a potential platform for drug delivery and imaging. *Nature Mater* 9: 172–178.
68. Goldberg M, Langer R, Jia X (2007) Nanostructured materials for applications in drug delivery and tissue engineering. *J Biomater Sci Polym Ed* 18: 241–268.
69. Duncan R (2006) Polymer conjugates as anticancer nanomedicines. *Nat Rev Cancer* 6: 688-701.
70. Vicent MJ, Duncan R (2006) Polymer conjugates: nanosized medicines for treating cancer. *Trends in Biotechnology* 24: 39-47.
71. Stevens MM, George JH (2005) Exploring and engineering the cell surface interface. *Science* 310: 1135-1138.
72. Ferreira L, Karp JM, Nobre L, Langer R (2008) New opportunities: the use of nanotechnologies to manipulate and track stem cells. *Cell Stem Cell* 3: 136-146.
73. Langer R, Tirrell DA (2004) Designing materials for biology and medicine. *Nature* 428: 487-492.
74. Patolsky F, Zheng G, Hayden O, Lakadamyali M, Zhuang X, et al. (2004) Electrical detection of single viruses. *Proceedings of the National Academy of Sciences of the United States of America* 101: 14017-14022.
75. Zheng G, Patolsky F, Cui Y, Wang WU, Lieber CM (2005) Multiplexed electrical detection of cancer markers with nanowire sensor arrays. *Nat Biotech* 23: 1294-1301.
76. Ferrari M (2005) Cancer nanotechnology: opportunities and challenges. *Nat Rev Cancer* 5: 161-171.
77. Farokhzad OC, Langer R (2006) Nanomedicine: Developing smarter therapeutic and diagnostic modalities. *Adv Drug Deiver Rev* 58: 1456-1459.
78. Smith AL, Oxford dictionary of biochemistry and molecular biology. (1997), Oxford: Oxford University Press.
79. Louie AY, Meade TJ (1999) Metal complexes as enzyme inhibitors. *Chemical Reviews* 99: 2711-2734.
80. Li WR, Xie XB, Shi QS, Zeng HY, Ou-Yang YS, et al. (2010) Antibacterial activity and mechanism of silver nanoparticles on *Escherichia coli*. *Appl Microbiol Biotechnol* 85: 1115-1122.

81. Kurvet I, Ivask A, Bondarenko O, Sihtmäe M, Kahru A (2011) *LuxCDABE*—Transformed constitutively bioluminescent *Escherichia coli* for toxicity screening: Comparison with naturally luminous *Vibrio fischeri*. *Sensors* 11: 7865-7878.
82. Hakkila K, Green T, Leskinen P, Ivask A, Marks R, et al. (2004) Detection of bioavailable heavy metals in EILATox-oregon samples using whole-cell luminescent bacterial sensors in suspension or immobilized onto fibre-optic tips. *J Appl Toxicol* 24: 333-342.
83. LaRossa R, Smulski D, Van Dyk T (1995) Interaction of lead nitrate and cadmium chloride with *Escherichia coli* K-12 and *Salmonella typhimurium* global regulatory mutants. *J Ind Microbiol* 14: 252-258.
84. Blinova I, Ivask A, Heinlaan M, Mortimer M, Kahru A (2010) Ecotoxicity of nanoparticles of CuO and ZnO in natural water. *Environ Pollut* 158: 41-47.
85. Blinova I, Niskanen J, Kajankari P, Kanarbik L, Kakinen A, et al. (2012) Toxicity of two types of silver nanoparticles to aquatic crustaceans *Daphnia magna* and *Thamnocephalus platyurus*. *Environ Sci Pollut Res Int* 20: 4293.
86. Buck PB, Lindner E (1994) Recommendations for nomenclature of ion-selective electrodes. *Pure Appl Chem* 66: 2527-2536.
87. Sambrook J, Fritsch EF, Maniatis T, *Molecular Cloning: A Laboratory Manual*, 2nd ed. (1989), NY, USA: Cold Spring Harbor Laboratory Press: Plainview.
88. Conti E, Franks NP, Brick P (1996) Crystal structure of firefly luciferase throws light on a superfamily of adenylate-forming enzymes. *Structure* 4: 287-298.
89. Baldwin TO (1996) Firefly luciferase: the structure is known, but the mystery remains. *Structure* 4: 223-228.
90. Kumar A, Pandey AK, Singh SS, Shanker R, Dhawan A (2011) A flow cytometric method to assess nanoparticle uptake in bacteria. *Cytometry A* 79: 707-712.
91. Hart JR, Ethylenediaminetetraacetic acid and related chelating agents. *Ullmann's encyclopedia of industrial chemistry*. (2005), Germany: Wiley-VCH: Weinheim.
92. Hughes MN, Poole RK (1991) Metal speciation and microbial growth—the hard (and soft) facts. *J General Microbiol* 137: 725-734.
93. Rensing C, Maier M (2003) Issues underlying use of biosensors to measure metal bioavailability. *Ecotoxicol Environ Safety* 56: 140-147.
94. Brandt KK, Holm PE, Nybroe O (2008) Evidence for copper-dissolved organic matter complexes and transiently increased copper bioavailability in

- manure-amended soils as determined by bioluminescent bacterial sensors. *Environ Sci Technol* 42: 3102-3108.
95. Macomber L, Rensing C, Imlay JA (2007) Intracellular copper does not catalyze the formation of oxidative DNA damage in *Escherichia coli*. *J Bacteriol* 189: 1616-1626.
 96. Outten FW, Huffman DL, Hale JA, O'Halloran TV (2001) The independent *cue* and *cus* systems confer copper tolerance during aerobic and anaerobic growth in *Escherichia coli*. *J Biol Chem* 276: 30670-30677.
 97. Imlay JA, Chin SM, Linn S (1988) Toxic DNA damage by hydrogen peroxide through the Fenton reaction *in vivo* and *in vitro*. *Science* 240: 640-642.
 98. Bragg PD, Rainnie DJ (1974) The effect of silver ions on the respiratory chains of *Escherichia coli*. *Can J Microbiol* 20: 883-889.
 99. Holt KB, Bard AJ (2005) Interaction of silver (I) ions with the respiratory chain of *Escherichia coli*: an electrochemical and scanning electrochemical microscopy study of the antimicrobial mechanism of micromolar Ag⁺. *Biochemistry* 44: 13214-13223.
 100. Feng QL, Wu J, Chen GQ, Cui FZ, Kim TN, et al. (2000) A mechanistic study of the antibacterial effect of silver ions on *Escherichia coli* and *Staphylococcus aureus*. *J Biomed Mater Res* 52: 662-668.
 101. Fabrega J, Fawcett SR, Renshaw JC, Lead JR (2009) Silver nanoparticle impact on bacterial growth: effect of pH, concentration, and organic matter. *Environ Sci Technol* 43: 7285-7290.
 102. Sotiriou GA, Pratsinis SE (2010) Antibacterial activity of nanosilver ions and particles. *Environ Sci Technol* 44: 5649-5654.
 103. Nanosilver dims firefly's light
<http://nanotechweb.org/cws/article/lab/54643> (09.04.2014).

ACKNOWLEDGEMENTS

This study was carried out in the Laboratory of Environmental Toxicology of National Institute of Chemical Physics and Biophysics, Tallinn, Estonia and supported by Laboratory of Inorganic Materials of Tallinn University of Technology, Tallinn, Estonia. The luciferase activity inhibition study was mainly carried out in Clemson University, SC, USA, in Nano-Biophysics and Soft Matter Laboratory (group leader Prof. Pu Chun Ke).

The work was financially supported by the Estonian Ministry of Science and Education (targeted funding projects SF0690063s08, SF0222601Bs03 and IUT23-5), Estonian Science Foundation (grants No. 6974, 7686, 8066, 8561 and 9347), the Centre for Academic Mobility - Archimedes Foundation, European Social Fund, EU FP7 Project NanoValid (grant agreement No 263147) and NSF grant no. CBET-1232724. This work was also supported by the graduate school "Functional Materials and Technologies" funded by European Social Fund under project 1.2.0401.09-0079.

I sincerely thank my supervisor Dr. Anne Kahru for guidance, support and encouragement, for her time and knowledge invested to my development and for the opportunity to be a member of her research group.

I would like to express my gratitude to my supervisor Prof. Rein Kuusik for his support during my studies in TUT.

I genuinely thank Prof. Pu Chun Ke for his help, knowledge, advices and collaboration. Thank for hosting my stay and leading the practical work in his research team in Clemson University.

I thank all my colleagues from the Laboratory of Environmental Toxicology (NICPB) for willingness to help, assistance, advice, discussions and enjoyable atmosphere. I would like to thank Olesja Bondarenko for guidance, for her help and constant kindness.

I also would like to thank my parents, brothers and friends for their support.

ABSTRACT

Engineered nanoparticles (NPs) have become more and more used in consumer products, e.g. in cosmetics, disinfectants, in medicine, engineering etc. The growing production increases the possibility of release of NPs into the environment. Recently nanoscience has undergone rapid development, but relatively little is known on the interaction of nanomaterials with living systems. Therefore, the studies on effects of engineered NPs on biota and vital biomolecules are crucial for the hazard evaluation of nanosized materials.

In this Thesis we performed toxicological evaluation of copper oxide and silver nanoparticles. Specifically, physico-chemical properties of NPs (hydrodynamic size, ζ -potential and solubilisation), role of test medium composition on metal speciation (including complexing of metal ions) and particle dissolution were studied. Also, the mechanism of harmful effects of NPs upon the direct contact with microorganisms – bacteria – and biologically essential molecules – enzymes – were investigated.

The speciation and bioavailability of copper ions and copper oxide (CuO) NPs were investigated in seventeen standard ecotoxicological and microbiological test media using comparative study applying ion-selective electrode (ISE) and ion-specific sensor bacteria. Complexing of copper ions by organic compounds of media was observed and there was a good correlation between physico-chemical (ISE) and biological methods (Cu-biosensors) while biosensors were even more sensitive than Cu-ISE and thus may prove more useful in environmental hazard analysis.

The dissolution of CuO NPs and its potential to induce ROS production and DNA damage were analyzed using *Escherichia coli* based biosensors. According to the results obtained, CuO NPs toxicity mechanisms were primarily triggered by released Cu ions.

We also assessed the role of direct contact between bacterial cell and silver nanoparticles (AgNPs) in Ag toxicity. Incubation of 6 bacterial strains with silver showed similar toxicity for AgNO₃ but response on AgNPs differed remarkably between strains. We analyzed antibacterial efficiency of AgNPs with different surface functionalization - non-coated, protein- and PVP-coated AgNPs and observed clear positive correlation with their dissolution rates. Bioavailability of Ag ions liberated from AgNPs was strain-specific and may be explained by different cellular uptake and inequality of extracellular dissolution.

The investigation of citrate-coated silver NPs interaction with enzyme luciferase established dose-dependent inhibition of firefly luciferase activity. Although luciferase readily bound to AgNPs through electrostatic interactions, *van der Waals* forces, dynamic exchanges with the citrate, as well as hydrogen bonding to render a protein corona as evidenced by our physicochemical characterizations and state-of-the-art DMD computer simulations, little conformational changes in the enzyme resulted from such direct interactions. Instead, AgNPs readily released silver ions that dose-dependently inhibited the enzymatic activity. The released silver ions

could readily react with the cysteine residues and N-groups of the enzyme to alter the physic-chemical environment of their neighboring catalytic site and subsequently impair the enzymatic activity.

KOKKUVÕTE

Süntetilised nanoosakesed leiavad tänapäeval üha rohkem kasutust tarbekaupades, näiteks kosmeetikas, desinfitseerimisvahendites; neile on leitud rakendusi meditsiinis, masinaehituses jne. Nanoteadus areneb kiiresti ja nanoosakesi toodetakse juba tööstuslikes mahtudes. Kasvav tootmine suurendab nanomaterjalide keskkonda sattumise võimalust, kuid suhteliselt vähe on teada nanoosakeste mõjust elukeskkonnale.

Antud doktoritöös uuriti vaskoksiidi ja hõbeda nanoosakeste toksilisuse mehhanisme. Hinnati nanoosakeste füüsikalisi-keemilisi omadusi (hüdrodünaamiline suurus, ζ -potentsiaal ja lahustuvus) ja katsekeskkonna mõju metallidele (sealhulgas kompleksseerumisele). Samuti uuriti nanoosakeste koostoimeid mikroorganismidega ja bioloogiliselt oluliste molekulidega – ensüümidega.

Uuriti vase soola ja vase nanoosakeste spetsiatsiooni ja biosaadavust seitsmeteistkümmes erinevas ökotoksikoloogilises ning mikrobioloogilises testlahuses, kasutadesioon-selektiivset elektroodi (ISE) ja ioon-spetsiifilisi sensorbaktereid (Cubiosensor). Näidati, et testlahuste orgaanilised komponendid kompleksseeriti vaseioonide poolt ning saadi hea korrelatsioon füüsikalisi-keemilise (ISE) ja bioloogilise (biosensor) meetodi vahel.

Uuriti CuO lahustuvust ja võimet tekitada reaktiivseid hapnikuühendeid (i.k. ROS) ning DNA kahjustusi, kasutades spetsiaalseid sensorbaktereid. Testid põhinesid *Escherichia coli* bakterirakkudel, mis olid geneetiliselt modifitseeritud tootma luminescentsentsvalgust vastusena metalliioonile, vesinikperoksiidile või DNA kahjustustele. Leiti, et CuO nanoosakeste toksilisus on peamiselt tingitud lahustunud ioonidest.

Lisaks täheldati, et Ag nanoosakeste kontakt bakterirakkudega võib põhjustada nanohõbeda suuremat lahustuvust ja kõrgemat toksilisust. Kuue bakteritüve inkubeerimine eritüübiliste hõbedaühenditega näitas võrreldavat tundlikkust AgNO₃-le, kuid vastus Ag nanoosakestele erines tüvede lõikes märkimisväärselt. Analüüsiti erinevalt funktsionaliseeritud Ag nanoosakeste (katmata, valgu- ja PVP-ga kaetud Ag nanoosakesed) antibakteriaalset mõju ja täheldati selget positiivset seost osakeste lahustuvusega. Ag nanoosakestest vabanenud hõbedaioonide biosaadavus oli tüvespetsiifiline ja võib olla seletatav nanoosakeste erineva rakuvälise lahustuvuse ja vabanenud ioonide rakku sisenemisega.

Uurides tsitraadiga kaetud Ag nanoosakeste interaktsioone ensüümiga lutsiferaas leiti, et ensüümi aktiivsus inhibeeritakse sõltuvalt lahustunud metalliiooni kontsentratsioonist. Kuigi lutsiferaas seondus kergesti Ag nanoosakestega elektrostaatiliselt vastasmõju tõttu, *van der Waals*'i jõudude tõttu, reaktsioonide tõttu valgu vesiniksidemete ning tsitraadiga, ei põhjustanud see ensüümi sekundaarstruktuuris selliseid muutusi, mis mõjutaksid ensüümi aktiivsust. Seevastu lahustunud hõbedaioonid võivad kergesti reageerida ensüümi tsüsteiinijääkidega ja N-rühmadega ning ensüümi aktiivsust inhibeerida.

PUBLICATION I

Käkinen A, Bondarenko O, Ivask A, Kahru A (2011). The effect of composition of different ecotoxicological test media on free and bioavailable copper from CuSO₄ and CuO nanoparticles: comparative evidence from a Cu-selective electrode and a Cu-biosensor. *Sensors*, 11(11), 10502 – 10521

Article

The Effect of Composition of Different Ecotoxicological Test Media on Free and Bioavailable Copper from CuSO₄ and CuO Nanoparticles: Comparative Evidence from a Cu-Selective Electrode and a Cu-Biosensor

Aleksandr Käkinen ^{1,2,†}, Olesja Bondarenko ^{1,3,†}, Angela Ivask ^{1,*} and Anne Kahru ^{1,*}

¹ Laboratory of Molecular Genetics, National Institute of Chemical Physics and Biophysics, Akadeemia tee 23, Tallinn 12618, Estonia; E-Mails: aleksandr.kakinen@kbfi.ee (A.K.); olesja.bondarenko@kbfi.ee (O.B.)

² Department of Chemical and Materials Technology, Tallinn University of Technology, Ehitajate tee 5, Tallinn 19086, Estonia

³ Department of Gene Technology, Tallinn University of Technology, Ehitajate tee 5, Tallinn 19086, Estonia

* Authors to whom correspondence should be addressed; E-Mails: angela.ivask@kbfi.ee (A.I.); anne.kahru@kbfi.ee (A.K.); Tel.: +372-6-398-382 (A.I.); +372-6-398-373 (A.K.); Fax: +372-6-398-382 (A.I.); +372-6-398-382 (A.K.).

† These authors contributed equally to this work.

Received: 20 September 2011; in revised form: 20 October 2011 / Accepted: 31 October 2011 / Published: 3 November 2011

Abstract: The analysis of (bio)available copper in complex environmental settings, including biological test media, is a challenging task. In this study, we demonstrated the potential of a recombinant *Pseudomonas fluorescens*-based biosensor for bioavailability analysis of CuSO₄ and CuO nanoparticles (nano-CuO) in seventeen different ecotoxicological and microbiological test media. In parallel, free Cu in these test media was analysed using Cu-ion selective electrode (Cu-ISE). In the case of CuSO₄, both free and bioavailable Cu decreased greatly with increasing concentration of organics and phosphates in the tested media. A good correlation between free and bioavailable Cu was observed ($r = 0.854$, $p < 0.01$) indicating that the free Cu content in biological test media may be a reasonably good predictor for the toxicity of CuSO₄. As a proof, it was demonstrated that when eleven EC₅₀ values for CuSO₄ from different organisms in different test media were normalized

for the free Cu in these media, the difference in these EC_{50} values was decreased from 4 to 1.8 orders of magnitude. Thus, toxicity of $CuSO_4$ to these organisms was attributed to the properties of the test media rather than to inherent differences in sensitivity between the test organisms. Differently from $CuSO_4$, the amount of free and bioavailable Cu in nano-CuO spiked media was not significantly correlated with the concentration of organics in the test media. Thus, the speciation of nano-CuO in toxicological test systems was not only determined by the complexation of Cu ions but also by differential dissolution of nano-CuO in different test conditions leading to a new speciation equilibrium. In addition, a substantial fraction of nano-CuO that was not detectable by Cu-ISE (*i.e.*, not present as free Cu-ions) was bioavailable to Cu-biosensor bacteria. Thus, in environmental hazard analysis of (nano) particulate materials, biosensor analysis may be more informative than other analytical techniques. Our results demonstrate that bacterial Cu-biosensors either in combination with other analytical/speciation techniques or on their own, may serve as a rapid (eco)toxicological screening method.

Keywords: copper-containing nanoparticles; bacteria; bioluminescent bioreporter; ion-selective electrode; speciation; toxicity; complexation

1. Introduction

Copper is a microelement necessary for various vital functions, but at the same time one of the most toxic heavy metals for aquatic organisms (e.g., crustaceans, algae, bacteria [1]), acting adversely already at sub-ppm concentrations. Indeed, soluble copper salts have been extensively used as pesticides. During the past decade, copper-containing nanoparticles are also increasingly appearing in various applications, elevating the risk of their environmental release upon usage or disposal of the respective products.

It is widely accepted that bioavailability and subsequently, the toxic effects of heavy metals, depend on their speciation. Thus, metal speciation in different environmental matrices (natural waters, soils, sediments) has received remarkable attention [2] and the corresponding information is considered crucial for proper (environmental) risk analysis. Although metal speciation is usually the main concern in environmental matrices, every standard laboratory toxicological assay needs to be performed in certain specific conditions, e.g., test media and temperature, which may influence the metal speciation and consequently, the test results [3]. In toxicity testing, the test medium has to support e.g., viability, growth or reproduction of the test organisms. Although for most of the standardized toxicity assays the media used are described by OECD, ISO, ASTM norms, it may vary depending on the test organism and type of the test. However, for an (eco)toxicological test to result in environmentally relevant and accurate prediction of metal toxicity, the estimation of metal complexing potential of the test media is of vital importance [4]. Currently, the theme of differential heavy metal complexing potential of toxicological test media has received a new impulse in the context of rapidly increasing nano(eco)toxicological data and their interpretation. It has been suggested that the vast knowledge and experience obtained from metal toxicity and speciation studies may also be applicable to

metal-containing nanomaterials. This is mainly derived from emerging experimental data which indicate that dissolution of metal-containing nanomaterials may be one of the main issues underlying their toxicity [5].

Despite the importance of heavy metal speciation in interpretation of the results of toxicological assays, the available techniques to determine metal speciation and bioavailability are relatively limited. One of the most robust and probably the most widely applied techniques for speciation analysis is the ion-selective electrode (ISE) [6,7]. Unfortunately, ISEs that have the capacity of detecting free ions only exist for limited types of metal ions [7]. Furthermore, although extremely high sensitivity of some electrodes has been reported (up to 10^{-11} M [8]), the detection limits of ISEs are generally too high (e.g., in case of Cu-ISE usually 10^{-6} M, *i.e.*, 63.5 µg Cu/L) to be applied for environmental samples. In addition, interference of ISEs with metal-organics complexes and non-target inorganic ions (Cl, Br, Fe, *etc.*) has been discussed [9,10]. Despite all these drawbacks, so far no other speciation technique has been able to outcompete ISEs. Often, the practical metal speciation measurements by ISEs have been accompanied by theoretical speciation modeling, most often performed using the Visual MINTEQ equilibrium model [11]. The results from chemical equilibrium models may be complemented with involve information about competitive binding of metals to organic ligands on biological surfaces in more complex models like Free Ion Activity Model or Biological Ligand Model and used to describe metal bioavailability [12]. On the other hand, there has been a considerable effort in developing simple bioassays that may be used for direct assessment of heavy metal bioavailability. An example of such bioassays are microbial biosensors [13,14], which allow specific detection of bioavailable metals through a highly sensitive biorecognition process followed by induction of a measurable signal, e.g., bioluminescence [15]. These metal-specific microbial biosensors have been applied for the analysis of bioavailable metals in soils, sediments, [16,17] and metal-containing nanomaterials [18,19].

In this study, we performed a comprehensive comparison between free and bioavailable copper (applied as CuSO₄ and nano-CuO) determined using a Cu ion-selective electrode (Cu-ISE) and a Cu-specific bacterial biosensor. Seventeen different standard ecotoxicological and microbiological test media were analysed with the aim to: (i) determine the complexing potential of these media for CuSO₄ and nano-CuO and (ii) compare the responses of the Cu-biosensor and Cu-ISE. In parallel, Cu speciation was calculated using the Visual MINTEQ equilibrium model. The results for Cu speciation in the selected test media were used to calculate the amount of free ions at reported experimentally determined toxicity values (E(I)C₅₀) for different aquatic test organisms.

2. Experimental Section

2.1. Test Chemicals and Their Preparation for the Analysis with the Cu-ISE and Bacterial Cu-Biosensor

CuSO₄·5H₂O (analytical grade) was purchased from Riedel-de-Haën. 63.5 g Cu/L stock solution was prepared in deionised (DI) water and stored in the dark at room temperature. CuSO₄·5H₂O was added to the test media as 100-fold concentrated stock solution in water.

Nano-CuO (advertised particle size 30 nm) was purchased from Sigma-Aldrich. The primary size of nano-CuO was confirmed to be 31 ± 12.8 nm in an earlier study by Blinova *et al.* [20]. TEM and SEM images of nano-CuO preparation are shown elsewhere [20,21]. 63.5 g Cu/L stock suspension on

nano-CuO was made in DI water; the suspension was sonicated for 30 min as described earlier [18]. Hydrodynamic diameter of nano-CuO in DI water (measured from 20 mg/L suspension using Zetasizer Nano-ZS; Malvern Instruments, UK) was 195 ± 2 nm. Nano-CuO was added to the test media as 100-fold concentrated stock suspension in water. Hydrodynamic size of nano-CuO in final media was measured as in case of DI water; average hydrodynamic diameter and Pdi (polydispersity index) were calculated from three parallel measurements.

2.2. Test Media

The list of standard ecotoxicological and microbiological media used in this study is presented in Table 1. All mineral salts used for preparation of the media were of analytical grade. Cas-aminoacids (AA) (casein hydrolysate), Tryptone, Yeast extract and Malt extract were from LabM (Lancashire, UK), Peptone was from Difco Laboratories (Beckton Dickinson, MD, USA). The test media were prepared by dissolving the desired amount of ingredients in DI water, autoclaved (121 °C for 15 min) or filter-sterilized (0.1 µm filter pore size, Minisart) and stored at room temperature.

Concentration of Cu in the test media was also determined by AAS-graphite furnace method according to the standard procedures (EVS-EN ISO/IEC 17025:2005) in a certified laboratory of the Institute of Chemistry, Tallinn University of Technology (Estonia). Additionally, pH (Orion PerpHect ROSS) and conductivity (EcoScan CON 5 conductometer; Eutech Instruments, Singapore) of the test media were measured. Conductivity of DI water was measured to be 0.0003 mS/cm.

2.3. Analysis of Free Cu Using a Cu Ion-Selective Electrode

A copper ion-selective electrode 96–29 ionplus (Orion Research, Thermo Scientific, MA, USA) was used. Before measurement, the electrode was thoroughly washed with DI water, then with 0.025 M H₂SO₄, followed by polishing of the sensor surface with Al₂O₃ polishing strip. Electrode was calibrated daily using 10^{-8} M (6.4×10^{-4} mg Cu/L)– 10^{-1} M (6,350 mg Cu/L) CuSO₄·5H₂O dilutions in DI water. Prior measurement, the ionic strength of all solutions was adjusted by supplementing the sample with 0.1 M NaNO₃. Ionic strength of the test solution was adjusted because of its importance in the response of ISE as shown by Sauvé *et al.* [22]. Appropriate dilutions of CuSO₄ and nano-CuO were prepared in 5 mL of test media and the measurements were conducted in 30 mL polypropylene tubes. Dilutions of nano-CuO were allowed equilibrate for 2 h at 30 °C before the measurement. The limit of detection (LOD) of Cu-ISE in each test media was calculated as recommended for ion-selective electrodes by IUPAC [23]. Briefly, log(10) of the added Cu was plotted against the electrode potential and the crossing point between the linear increase of the electrode potential and the line representing the electrode background potential was designated as the limit of detection (Cu-ISE_{LOD}) (Figure S1). The LODs and respective standard deviations were calculated from three independent measurements. Free Cu was calculated using the following equation:

$$\text{Free Cu(\%)} = \frac{\text{Cu ISE}_{\text{LOD}} \text{ in test media}}{\text{Cu ISE}_{\text{LOD}} \text{ in DI water}} \times 100 \quad (1)$$

Table 1. Toxicological and microbiological test media used in this study.

Designation of the media (traditional test organism for this medium)	Content per L	pH	Conductivity, mS/cm	Cu, mg/L ^a	Reference
ECOTOXICOLOGICAL TEST MEDIA					
Osterhout's medium (protozoan <i>Tetrahymena</i> sp.)	104 mg NaCl, 8.5 mg MgCl ₂ , 4 mg MgSO ₄ , 2.3 mg KCl, 1 mg CaCl ₂	5.2	0.29	<detection	[24]
Artificial freshwater 1 (AFW1) (crustacean <i>Daphnia</i> sp.)	294 mg CaCl ₂ ·2H ₂ O, 123.25 mg MgSO ₄ ·7H ₂ O, 64.75 mg NaHCO ₃ , 5.75 mg KCl	7.8	0.64	<detection	OECD 202
Artificial freshwater 2 (AFW2) (crustacean <i>Thamnocephalus</i> sp.)	60 mg CaSO ₄ ·2H ₂ O, 123 mg MgSO ₄ ·7H ₂ O, 96 mg NaHCO ₃ , 4 mg KCl	7.8	0.24	<detection	[25]
Algal medium (algae <i>Pseudokirchneriella subcapitata</i>)	15 mg NH ₄ Cl, 12 mg MgCl ₂ ·6H ₂ O, 18 mg CaCl ₂ ·2H ₂ O, 15 mg MgSO ₄ ·7H ₂ O, 1.6 mg KH ₂ PO ₄ , 50 mg NaHCO ₃ , 0.1 mg Na ₂ EDTA·2H ₂ O, 0.08 mg FeCl ₃ ·6H ₂ O, 0.185 mg H ₃ BO ₃ , 0.415 mg MnCl ₂ ·4H ₂ O, 3×10^{-3} mg ZnCl ₂ , 1.5×10^{-3} mg CoCl ₂ ·6H ₂ O, 7×10^{-3} mg Na ₂ MoO ₄ ·2H ₂ O, 10^{-5} mg CuCl ₂ ·2H ₂ O	8.3	0.05	<detection	OECD 201
MICROBIOLOGICAL TEST MEDIA					
Malt extract (ME) (yeasts <i>Saccharomyces cerevisiae</i>)	11 g maltose, 8 g carbohydrates, 1 g proteins	5.2	0.82	0.0076	Lab M, UK
Yeast extract peptone dextrose (YPD) (yeasts <i>Saccharomyces cerevisiae</i>)	20 g Bacto peptone, 10 g yeast extract, 20 g glucose	6.7	3.39	0.0089	[26]
M9 ^b (bacteria e.g., <i>Escherichia coli</i>)	6 g Na ₂ HPO ₄ , 3 g KH ₂ PO ₄ , 0.5 g NaCl, 1 g NH ₄ Cl, 0.25 g MgSO ₄ ·7H ₂ O, 0.01 g CaCl ₂	7.0	8.43	<detection	[26]
M9 + 0.5%AA (bacteria e.g., <i>Escherichia coli</i>)	6 g Na ₂ HPO ₄ , 3 g KH ₂ PO ₄ , 0.5 g NaCl, 1 g NH ₄ Cl, 0.25 g MgSO ₄ ·7H ₂ O, 0.01 g CaCl ₂ , 5 g Cas-amino acids, 1 g glucose	7.0	9.92	0.0056	see previous
LB (bacteria e.g., <i>Escherichia coli</i>)	10 g tryptone, 5 g yeast extract, 5 g NaCl	7.0	19.55	0.0195	[26]

Table 1. Cont.

Designation of the media (traditional test organism for this medium)	Content per L	pH	Conductivity, mS/cm	Cu, mg/L ^a	Reference
Heavy metal MOPS medium (HMM)^b (bacteria e.g., <i>Escherichia coli</i>)	8.4 g MOPS, 0.22 g glycerol-2-phosphate, 3.7 g KCl, 0.54 g NH ₄ Cl, 0.06 g MgSO ₄ , 0.162 mg FeCl ₃	7.2	8.9	<detection	[27]
HMM + 0.5%AA (bacteria e.g., <i>Escherichia coli</i>)	8.4 g MOPS, 0.22 g glycerol-2-phosphate, 3.7 g KCl, 0.54 g NH ₄ Cl, 0.06 g MgSO ₄ , 0.162 mg FeCl ₃ , 5 g Cas-amino acids, 4 g glucose	7.2	8.9	0.0021	see previous
2% NaCl (marine bacteria e.g., <i>Vibrio fischeri</i>)	20 g NaCl	4.4	>20	n.a.	
supplemented 0.9% NaCl	SUPPLEMENTED 0.9% SALINE				
0.9% NaCl	9 g NaCl	5.8	16.6	n.a.	
0.9% NaCl + 0.01%AA	9 g NaCl, 1 g glucose, 0.1 g Cas-amino acids	6.1	16.8	n.a.	
0.9% NaCl + 0.05%AA	9 g NaCl, 1 g glucose, 0.5 g Cas-amino acids	6.3	17.0	n.a.	
0.9% NaCl + 0.1%AA	9 g NaCl, 1 g glucose, 1 g Cas-amino acids	6.2	17.2	0.0042	
0.9% NaCl + 0.5%AA	9 g NaCl, 1 g glucose, 5 g Cas-amino acids	6.2	18.8	0.0069	

^a concentration of Cu in the test media measured by AAS (limit of determination 0.002 mg/L). All values <0.02 mg/L were designated as <detection; ^b included to the analysis mineral controls for M9 + 0.5%AA and HMM + 0.5%AA; AA—amino acids; n.a.—not analysed.

In addition, the Cu-ISE results were used to calculate free Cu at EC₅₀ of different organisms for CuSO₄ and nano-CuO. The EC₅₀ values were obtained from earlier published studies (except that of *S. cerevisiae* in YPD media that was personal communication from Dr. K. Kasemets, NICPB, Estonia). Experimental EC₅₀ values were obtained in exactly the same media (composition of the media was verified) that were used for Cu speciation analysis in this study (Table 1). To calculate the amount of free Cu at EC₅₀ values for CuSO₄ or nano-CuO in different media, the potential of Cu-ISE at EC₅₀ concentrations in these media was measured and compared to CuSO₄ or nano-CuO concentrations that induced similar electrode potential in DI water (Figure S2). The respective concentration in DI water was considered as the concentration of free Cu at this EC₅₀ value.

2.4. Calculation of Free Ion Concentration Using Visual MINTEQ

Chemical equilibrium model Visual MINTEQ 2.51 [28] was used to calculate Cu ion speciation in CuSO₄ solutions prepared in different mineral media. Due to the lack of respective equilibrium models, no calculations were performed for complex organics-containing media. For mineral media, respective pH, concentrations of all main cations and anions were used as input; temperature was set to 23 °C. The sum of free and hydrated Cu ions was considered as the gross free Cu in the test media.

2.5. Analysis of Bioavailable Cu Using a Cu-Biosensor Bacterium

The Gram-negative Cu-sensing *Pseudomonas fluorescens* OS8::KnCueRPCopAlux, in which bioluminescence is specifically induced by bioavailable Cu ions [15], was used to measure bioavailable Cu. Sensor bacteria were pre-grown overnight on a shaker (200 rpm, 30 °C) in 3 mL of LB medium (Table 1) supplemented with 100 µg/L of kanamycin. 20 mL of fresh LB was inoculated with 1/50 diluted overnight culture, and bacteria were grown until mid-exponential phase (OD₆₀₀ of 0.6), and cells were separated by centrifugation at 5,000 ×g for 10 min. Cell pellet was washed twice with 20 mL of appropriate test medium and further diluted with the same medium until OD₆₀₀ ~ 0.1 (approximately 10⁶ bacterial cells/mL). 100 µL of CuSO₄ or nano-CuO dilution or medium only (blank medium control) was pipetted onto white polypropylene 96-well microplate (Greiner Bio-one, Germany); 100 µL of bacterial suspension was added to each well and plates were incubated at 30 °C for 2 h. Bioluminescence was measured using Orion II luminometer (Berthold Detection Systems, Germany) and response of sensor bacteria to copper compounds was calculated as follows:

$$\text{Induction (fold)} = \frac{\text{Bioluminescence in Cu containing sample}}{\text{Bioluminescence in blank medium}} \quad (2)$$

Two parallel experiments were included per individual assay and three independent individual assays were performed. Due to the different potency of the cells to induce bioluminescence in ‘nutritionally’ different media absolute induction values in these media differed. Thus, the induction of the bacterial biosensor was expressed as %, where maximum induction value was considered as 100 and induction in blank medium as 1. Limit of the detection (LOD) of the Cu-biosensors was set at 20% induction (Figure S3).

3. Results and Discussion

3.1. Comparative Response of the Cu Ion Selective Electrode (Cu-ISE) and the Bacterial Cu-Biosensor to CuSO₄ in Standard Ecotoxicological and Microbiological Media

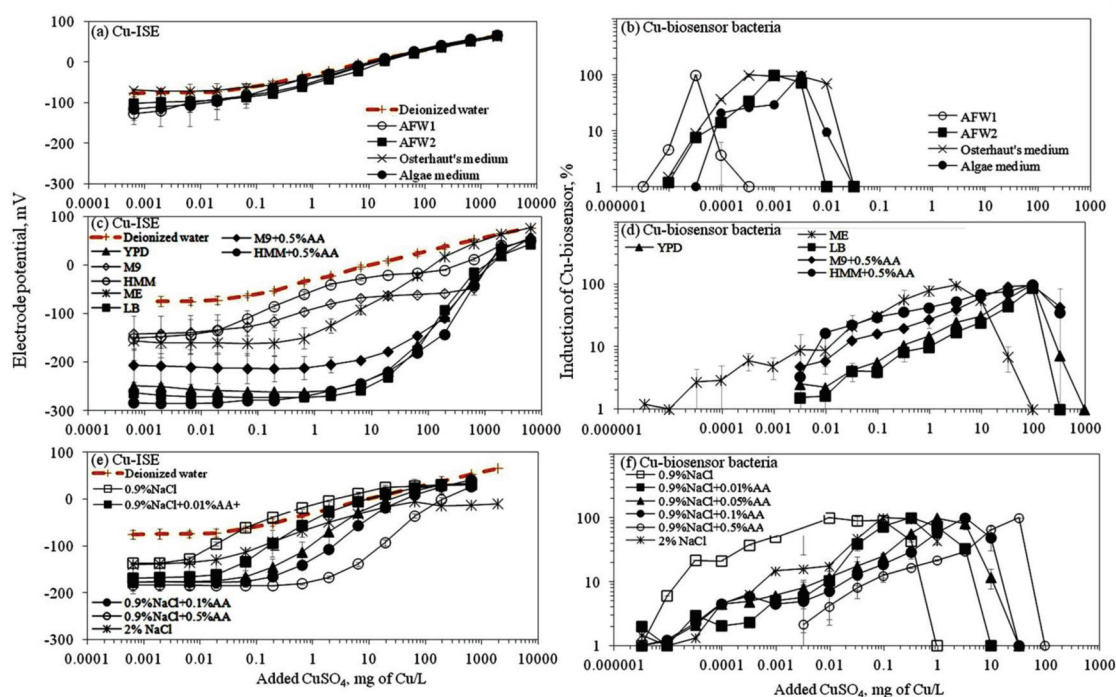
In this study, we analysed the speciation (free ion content) and bioavailability of copper in seventeen different media. The media selection included various standard ecotoxicological test media: 2% NaCl (used for Microtox toxicity test with bioluminescent bacteria *Vibrio fischeri*), algal medium (used for the toxicity testing with *Pseudokirchneriella subcapitata* according to OECD 201), two artificial freshwaters (used for tests with crustaceans *Daphnia magna* according to OECD 202 and with *Thamnocephalus platyurus*). In addition, common media used for cultivation of microorganisms were included: LB medium (an undefined rich medium that supports the growth of variety of bacteria), malt extract (ME) and YPD (Yeast Peptone Dextrose medium) both used for the cultivation of yeasts (Table 1). Also, M9 and HMM media that were supplemented with 0.5% Cas-amino acids (AA) were studied. The M9 medium has been used in our previous studies for toxicity evaluation of metals and organic chemicals to *Escherichia coli* [29] and for the analysis of bioavailable metals using metal-inducible bioluminescent bacterial sensors [15,30]. HMM medium has been specifically suggested for the analysis of heavy metals due to its minimal metal-complexing capability [27]. Also 0.9% NaCl and its Cas-amino acid (AA) supplemented versions were tested as 0.1% AA amended 0.9% NaCl has been applied by us earlier to study the bioavailability and toxicity of CuO nanomaterials [18,20,21]. Cu speciation and complexing potential of these different laboratory test media were studied using two methods: (i) a Cu-ISE that responds to free Cu ions and (ii) a Cu-specific bacterial biosensor that responds to bioavailable Cu.

3.1.1. Response of Cu-ISE to CuSO₄: Measurement of Free Cu

Ion selective electrodes (ISEs) have been relatively widely applied to study the speciation of e.g., certain heavy metals in different environmental conditions [31] and the corresponding standard protocols have been developed [22]. Thus, speciation analysis using ISEs may be considered as a well established method. Response of ISEs has been considered to indicate the content of free ions of the studied elements and has been often correlated with bioavailability and toxicity of these elements [32,33]. Speciation analysis of CuSO₄ in seventeen selected laboratory test media showed that most of the media contained ligands capable of complexing the Cu ions and thus, reduced the amount of free Cu (see calibration curves in Figure 1). As expected, the limit of detection of the Cu-ISE (Cu-ISE_{LOD}) (Table 2) was lowest in test media with no or low organics content. Overall, the order of Cu-ISE_{LOD} for CuSO₄ in different tested media was: 0.9% NaCl \cong AFW1 < 2% NaCl < Osterhout's medium \cong HMM < AFW2 \cong 0.9% NaCl + 0.01%AA < algal medium < M9 \cong 0.9% NaCl + 0.05%AA < 0.9% NaCl+0.1%AA < malt extract < HMM + 0.5%AA < 0.9% NaCl + 0.5%AA < M9 + 0.5%AA < YPD < LB. Interestingly, in some mineral media—Osterhout's medium, AFW1, HMM, 0.9% and 2% NaCl—the LOD of Cu-ISE was lower than that in DI water (considered to contain 100% free Cu ions) (Figure 1, Table 2). As discussed by Lanza [34], this may be due to the presence of interfering ions like Cl[−] in these media. Indeed, the difference in electrode potential leading to abnormally low LOD values was observed only at low Cu concentrations; at higher Cu concentrations the difference

between the electrode potential in DI water and these media disappeared (Figure 1(a)). However, the media showing very low Cu-ISE_{LOD} values—Osterhout's medium, AFW1, HMM, 0.9% NaCl and 2% NaCl—contained the highest amount of free Cu ions also according to Visual MINTEQ equilibrium model (Figure S4). At the same time, the amount of free Cu was remarkably lower in other mineral media—algal medium, AFW2 and M9 mineral media—in which the prevalent Cu species were Cu-EDTA, CuCO₃ and CuHPO₄, respectively (Figure S4). The prevalence of these species could be expected. Indeed, EDTA (in algal medium) is a well-known trace metal chelator [35] and phosphates have been demonstrated to form strong metal-phosphate complexes that often precipitate [36]. Yet, phosphate-containing media like M9 or phosphate-buffered saline (PBS) are often used for toxicological tests as: (i) phosphates have a good buffering capacity and (ii) are required for several physiological functions of living cells. However, when phosphates were substituted with morpholinepropane sulfonic acid (MOPS) for buffering capacity and organic phosphate (β -glycerophosphate) to serve as physiological phosphate supply in HMM media as suggested by [37,38], the fraction of free Cu was significantly increased compared to phosphate-containing media (Table 2, Figure 1).

Figure 1. Response of Cu-ISE (left panels) and Cu-biosensor *Pseudomonas fluorescens* OS8::KnCueRPCopAlux (right panels) to CuSO₄ in different ecotoxicological and microbiological media. (a,b) 'poor' mineral media; (c,d) organics-containing media (LB, ME, YPD) and mineral media (M9, HMM) supplemented with 0.5% of Cas-amino acids; (e,f) 0.9% NaCl with various concentrations of Cas-amino acids (AA). Numeric values of respective LODs are presented in Table 2.



Response of Cu-ISE to CuSO₄ in organics-containing media (Figure 1(c)) was generally in correlation with organics content of the media. This was clearly evident in the case of 0.9% NaCl where the gradual addition of AA was accompanied by a respective increase of the Cu-ISE_{LOD}. Addition of 0.5% (wt) of AA to 0.9% NaCl increased the Cu-ISE_{LOD} by 87-fold (Table 2). Analogously, the addition of 0.5% AA to M9 and HMM mineral media increased the LOD of the Cu-ISE about 30-fold. Indeed, complexation of Cu by organic ligands and formation of relatively strong complexes in ‘rich’ media is a known phenomenon [36,39]. The following step in the current study was to compare the results from Cu-ISE with the response of bacterial Cu-biosensor in the same test media.

Table 2. Limit of detection (LOD) of the Cu-ion selective electrode (Cu-ISE) (indicative of free Cu ions) and *Pseudomonas fluorescens* OS8::KnCueR_{PCo}AluX Cu-biosensor (indicative of bioavailable Cu) for CuSO₄ in selected ecotoxicological and microbiological media. Average of three replicates ± standard deviation is shown. Data calculated from Figure 1.

Designation of the medium ^a	Cu-ISE _{LOD} , mg/L	Free Cu ²⁺ (mg/L) at Cu-ISE _{LOD} ^b	Cu-biosensor _{LOD} , mg/L	Free Cu ²⁺ (mg/L) at Cu-biosensor _{LOD} ^a
Deionized (DI) water ^c	0.021 ± 0.005	0.021 ^c	n.a	n.a.
Osterhout's medium	0.015 ± 0.005	0.017	0.000065 ± 0.000003	0.00006
AFW1	0.008 ± 0.002	0.0016	0.00002 ± 0.000005	0.000005
AFW2	0.03 ± 0.01	0.0054	0.0001 ± 0.000006	0.000012
Algal medium	0.035 ± 0.014	0.003	0.00012 ± 0.000009	0.000003
Malt extraxt (ME)	0.4 ± 0.07	n.a.	0.03 ± 0.013	n.a.
YPD	2.0 ± 0.07	n.a.	2 ± 0.37	n.a.
M9 + 0.5%AA	1.5 ± 1.09	n.a.	0.35 ± 0.041	n.a.
M9	0.05	0.0018	n.a.	n.a.
LB	2.7 ± 0.17	n.a.	3.1 ± 0.21	n.a.
HMM + 0.5%AA	0.45 ± 0.2	n.a.	0.02 ± 0.0036	n.a.
HMM	0.015	0.0053	n.a.	n.a.
2% NaCl	0.012	0.0086	0.006 ± 0.00025	0.0043
0.9% NaCl	0.008 ± 0.001	0.006	0.0003 ± 0.00005	0.0046
0.9% NaCl + 0.01%AA	0.03 ± 0.02	n.a.	0.015 ± 0.0036	n.a.
0.9% NaCl + 0.05%AA	0.05 ± 0.01	n.a.	0.05 ± 0.012	n.a.
0.9% NaCl + 0.1%AA	0.14 ± 0.001	n.a.	0.15 ± 0.066	n.a.
0.9% NaCl + 0.5%AA	0.71 ± 0.3	n.a.	0.6 ± 0.12	n.a.

^a chemical composition is shown in Table 1; ^b Free Cu at Cu-ISE_{LOD} in test media was calculated using the Visual MINTEQ chemical equilibrium model (see also Figure S3); ^c 100% free ions were assumed in deionized water; n.a.—not analysed.

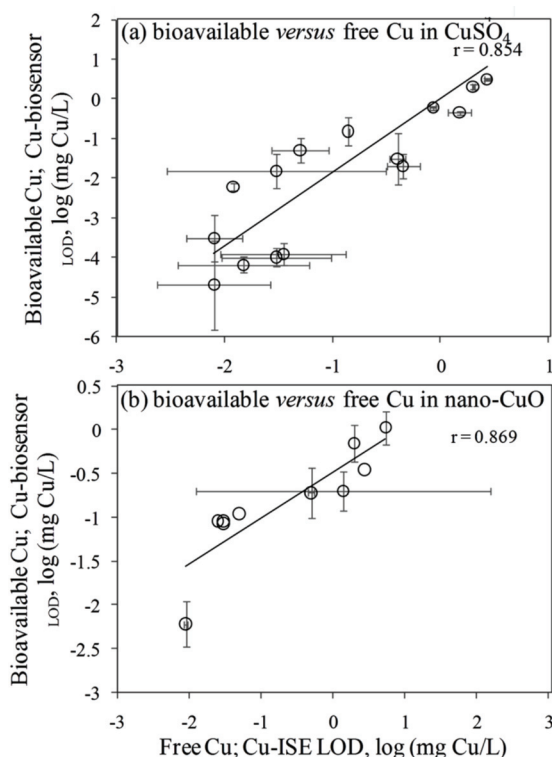
3.1.2. Response of Bacterial Cu-Biosensor to CuSO₄: Measurement of Bioavailable Cu

Contrary to Cu-ISE, which is a well established method for metal speciation analysis, bacterial metal-specific biosensors are currently largely in their developmental stage. Indeed, despite their more than 20-year history, they have not been widely applied yet for real environmental analysis [13]. Most likely, the development of these bacterial sensor cells has been inhibited by the ongoing dispute about the actual fraction of the metal that is triggering their biological/analytical response and thus, by

difficulties in interpreting the obtained results. According to [40] the response of microbial biosensor cells may be exclusively due to the soluble ionic forms of metals. However, recently Brandt *et al.* reported that in addition to free Cu, Cu-DOM (dissolved organic matter) complexes were also bioavailable to Cu sensor bacteria [41]. Due to the current uncertainty in the interpretation of biosensor results for environmental risk assessment, this technique suffers also from the lack of comprehensive validation and standardization of the method. By parallel analysis of Cu speciation in similar samples, the current study aims to draw correlations between the response of bacterial Cu-biosensor and Cu-ISE.

Before discussing the response of the bacterial biosensor to CuSO_4 in different media, one must note that being a live bacterial cell, this recombinant biosensor is not ‘operating’ at extremely low ionic strength solutions (e.g., DI water). The latter usually results in a relative poor bioluminescent response of sensor bacteria to copper if analysed in low organics-containing media: the bioluminescence in live bacteria consumes considerable amounts of cellular energy [42] and in extremely low nutrient conditions the energy level may be insufficient. Due to different levels of bioluminescence produced by the biosensor cells in different media, we present the induction of the Cu-biosensor bacteria as percentage of the maximal induction (see Section 2.5).

Figure 2. Correlation between limits of determination (LOD) of Cu-ISE (indicative of free Cu) and Cu-biosensor (indicative of bioavailable Cu) for CuSO_4 in different ectotoxicological and microbiological media. Data are plotted from Tables 2 and 3. **(a)** $\text{Cu-ISE}_{\text{LOD}}$ and $\text{Cu-biosensor}_{\text{LOD}}$ for CuSO_4 ; **(b)** $\text{Cu-ISE}_{\text{LOD}}$ and $\text{Cu-biosensor}_{\text{LOD}}$ for nano-CuO.



In general, the LOD values of the *P. fluorescens* OS8::KnCueRPCopAlux bacterial biosensor and Cu-ISE in CuSO₄ spiked media were significantly correlated: the corresponding *r* value was 0.854 (Figure 2(a,b)) indicating that the bacterial sensor, at least in the media tested herein, responded mainly to free species of copper. Analogously to the Cu-ISE results, decrease of bioavailable Cu with increasing amount of organics in the media, was observed (see Cu-biosensor_{LOD} values in Table 2). The effect of media composition on Cu toxicity to bioluminescent bacterial cells and its relation with free Cu in these media has been demonstrated also by some other authors. For example, [33] showed that the bioluminescent response of bacteria was correlated with the free Cu in a set of soil pore waters. Also, [43] found a good correlation between free Cu measured by Cu-ISE and bacterial response in few samples analysed by them. Respectively, decrease in Cu toxicity with increasing dissolved organic carbon levels has also been shown by Apte *et al.* [44]. Our study showed that in addition to excellent correlation between free Cu ions and bioavailable Cu, the Cu-biosensor bacteria responded generally to remarkably lower CuSO₄ levels than did Cu-ISE. Thus, bacterial biosensors used in the current study can be considered more sensitive warning systems for heavy metal-caused potential environmental hazard than the free metal ion measurement.

Table 3. Limit of detection (LOD) of Cu-ISE (indicative of free Cu ions) and *Pseudomonas fluorescens* OS8::KnCueRPCopAlux Cu-biosensor (indicative of bioavailable Cu) for nano-CuO in selected ecotoxicological and microbiological media. Hydrodynamic diameter (*D_h*) of the nano-CuO suspension in respective test medium is shown for comparison.

Designation of the medium ^a	<i>D_h</i> ^b ± SD (Pdi) ^b	Cu-ISE _{LOD} , mg/L	Cu-biosensor _{LOD} , mg/L
Deionized (DI) water	195 ± 2 (0.2)	0.015 ± 0.003	n.a.
Malt extract (ME)	391 ± 17 (0.2)	2	0.7 ± 0.2
YPD	1,644 ± 54 (0.4)	5.5	1.05 ± 0.2
M9 + 0.5%AA	525 ± 30 (0.2)	2.8	0.35 ± 0.04
LB	690 ± 21 (0.2)	1.4 ± 0.064	0.20 ± 0.06
HMM + 0.5%AA	786 ± 31 (0.2)	0.5	0.19 ± 0.05
0.9% NaCl	1,113 ± 31 (0.2)	0.009 ± 0.009	0.006 ± 0.0006
0.9% NaCl + 0.01%AA	952 ± 29 (0.2)	0.025 ± 0.0006	0.09 ± 0.025
0.9% NaCl + 0.05%AA	694 ± 33 (0.2)	0.03 ± 0.0005	0.085 ± 0.019
0.9% NaCl + 0.1%AA	504 ± 31 (0.2)	0.03 ± 0.0002	0.09 ± 0.013
0.9% NaCl + 0.5%AA	428 ± 35 (0.2)	0.05 ± 0.001	0.11 ± 0.03

^a chemical composition of the media is presented in Table 1; ^b Pdi—polydispersity index; measurement by Malvern Zetasizer Nano-ZS; n.a.—not analysed.

3.2. Comparative Response of Cu-Ion Selective Electrode and Bacterial Cu-Biosensor to Nano-CuO

There is a general belief that a fraction of toxicity of metal-containing nanomaterials may result from dissolved metal ions [45]. The release of Cu ions from CuO nanoparticles was reported as the main case of CuO toxicity for the crustaceans *Thamnocephalus platyurus*, the bacteria *Vibrio fischeri* [18] and *Escherichia coli* [21], the algae *Pseudokirchneriella subcapitata* [46] and the nematodes *Caenorhabditis elegans* [47]. Recently, Puzyn *et al.* [48] have developed a quantitative structure-activity relationship (QSAR) model for metal containing NPs using the formation of metal ions as a single

predictor for their toxicity. Therefore, we decided to use a Cu-ISE and bacterial Cu-biosensor in parallel, to study the speciation of Cu in suspensions of CuO nanoparticles. Due to the poor bioluminescent response of Cu-biosensor bacteria in mineral media (Osterhout's medium, AFW1, AFW2, algal medium, 2% NaCl and 0.9% NaCl; the induction of bioluminescence in these media was only about 10% of that in organics-containing media; data not shown) discussed above, we did not include these media in speciation analysis of nano-CuO.

Interestingly, the limits of detection of Cu-ISE to CuSO₄ (0.021 ± 0.005 mg Cu/L (Table 2)) and nano-CuO (0.015 ± 0.003 mg Cu/L (Table 3)) were almost identical. This indicates that at these low concentrations all Cu from nano-CuO was likely dissolved and present in the form of free ion. Analogously to CuSO₄, the fraction of free Cu ions decreased when nano-CuO was introduced to various laboratory test media (Figure 3). Although there was generally a good correlation between the free Cu ions in CuSO₄ and in nano-CuO-spiked test media ($r = 0.837$; Figure 4) there were several exceptions. Specifically, in LB medium, HMM and 0.9% NaCl supplemented with 0.5%AA the concentration of free Cu in CuSO₄ was not the best predictor for the free Cu concentration in suspensions of nano-CuO. Notably, more free Cu was detected in nano-CuO suspensions than could be predicted from the results of CuSO₄ (Figure 4, the 'outlier'-media are marked with brown color). Therefore, we suggest that differently from CuSO₄, where the only process affecting the Cu speciation was interaction of Cu ions with media components, additional processes take place in case of nano-CuO. These processes likely include agglomeration of nanoparticles, release of Cu ions from the CuO, and finally, interaction of the released Cu ions with the media components. Unfortunately, dissolution and speciation of dissolved metals from metal-containing nanomaterials has not been studied in a systematic manner. Only a recent report by Gunawan *et al.* [49] demonstrated differential dissolution of CuO nanoparticles in different media. Their results showed that in organics-containing 'rich' media the dissolution of CuO was indeed high if compared to that in water or in saline solution. Similar observation has been done for nano ZnO in a study by Li *et al.* [50] where the authors suggested that the affinity of Zn for ligands present in these media was responsible for dissolution of ZnO. Organic ligand-enhanced dissolution due to the presence of proteins and organic substances in the test media has been observed also in other studies concerning CdSe, iron oxides, aluminium oxides and aluminium oxyhydroxides [51]. One reason for the enhanced dissolution may be the decrease in effective hydrodynamic size of the nanomaterials as a result from coating of the particles with organic molecules. This may lead to stabilization of the nanomaterials aggregates and increased dissolution. Thus, in our experiments differential dissolution of nano-CuO due to media components and differential speciation of dissolved Cu in the media is a very likely scenario. Behaviour of nano-CuO in 0.9% NaCl amended with different amounts of amino acids is a relevant example. Differently from CuSO₄ in case of which the fraction of free Cu decreased with increasing amino acid content, very similar Cu-ISE_{LOD} as well as Cu-biosensor_{LOD} values for nano-CuO were obtained (Table 3). Thus, it could be supposed that with increasing amino acid content in the medium, the dissolution of Cu from nano-Cu increased. In accordance with the hypothesis about organic ligand-induced decrease in effective hydrodynamic diameter of the nanomaterials, we observed that the Dh of nano-CuO decreased when Cas-aminoacids were added to saline (Table 3).

Overall, there was a good correlation between LODs of Cu-ISE and Cu-biosensor bacteria for nano-CuO ($r = 0.869$; Figure 2). However, in most of the tested media, the LOD of the Cu-biosensor

was remarkably up to 5-fold lower than that of Cu-ISE (Figure 2; Table 3). This interesting observation suggests that in nano-CuO suspensions, bacterial cells were also able to access fractions of Cu other than just the free ion form detected by Cu-ISE. This finding is similar to our previous reports showing partial bioavailability of particulate matter bound Cu in soil and sediment samples [52]. Thus, we propose that in case of particle-containing samples (including Cu-containing nanomaterials), more Cu may be bioavailable to living (e.g., microbial) cells than could be predicted based on only dissolved fraction of Cu.

Figure 3. Response of Cu ion-selective electrode (Cu-ISE; left panels) and *Pseudomonas fluorescens* OS8::KnCueR_PcopAlux Cu-biosensor (right panels) to nano-CuO in different ecotoxicological and microbiological media. (a,b) organics-containing media; (c,d) 0.9% NaCl with various concentrations of Cas-amino acids (AA).

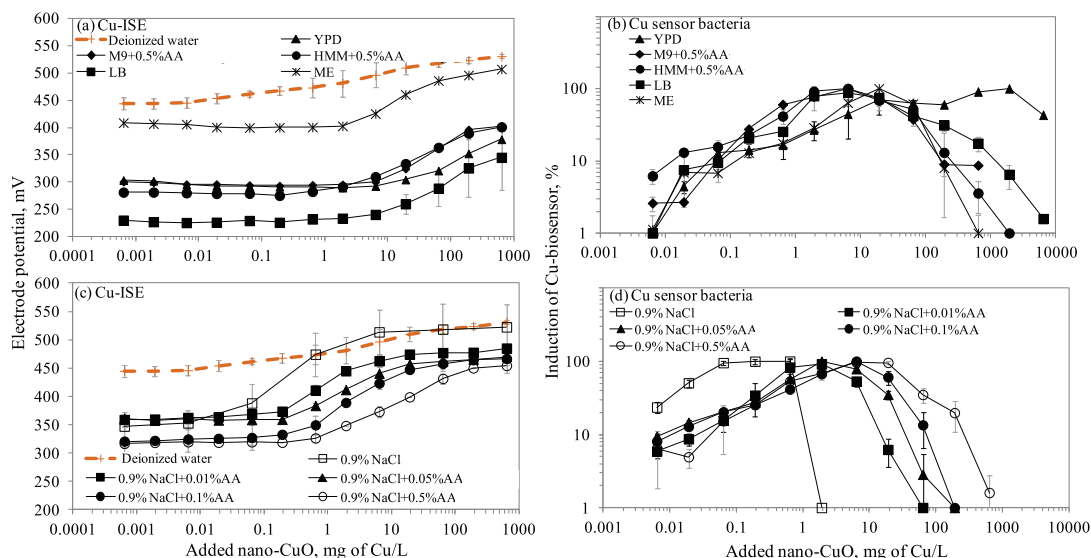
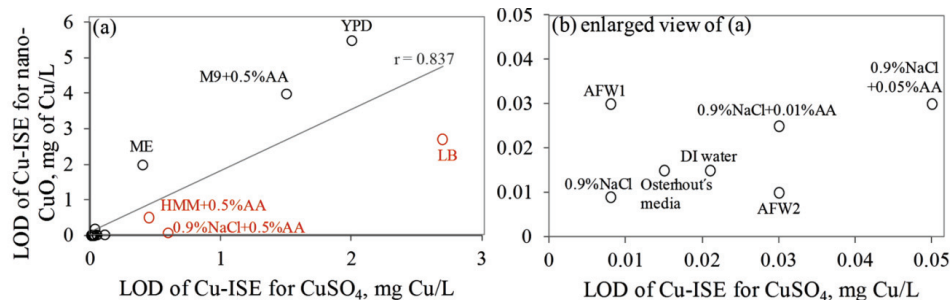


Figure 4. Correlation between Cu-ISE_{LOD} in CuSO₄ and in nano-CuO suspensions prepared in different ecotoxicological and microbiological media. The names of test media correspond to Table 1; (b) is enlarged view of (a). Symbols in brown color indicate those media where the concentration of free ions in nano-CuO suspensions was lower than could be predicted from what was observed in case of CuSO₄.



3.3. Toxicity of CuSO₄ and Nano-CuO to Different (Eco)toxicological Model Organisms: Normalization to Free and Bioavailable Ions

Usually, the difference in toxicity of copper to several freshwater and saltwater organisms varies remarkably, ranging from 0.005 to 10 mg/L [53]. When a certain organism group is considered, the variation is smaller, but still considerable; in a recent review [5] acute toxicity data (48–96 h LC₅₀) of Cu²⁺ for fish from the literature were compared. Thirteen EC₅₀ values for zebrafish, rainbow trout, trout, common carp, gibel carp and mullet were included; these values ranged for almost two orders of magnitudes from 0.03 till 1.4 mg/L, the median value being 0.21 mg/L. According to [53], this variability may be due to the species differences but also due to differential speciation of copper in different test environments (media) used to perform these toxicity assays.

Table 4. Toxicity (EC₅₀ value) of CuSO₄ and nano-CuO to different organisms in their conventional test or cultivation media. Free Cu at EC₅₀-s was calculated according to Cu-ISE.

Media	Test organism	EC ₅₀ mg Cu/L	free Cu at EC ₅₀ , mg Cu/L
Test compound: CuSO₄			
Osterhout's medium	<i>Tetrahymena thermophila</i>	1.6 ^a	1.1
AFW1	<i>Daphnia magna</i>	0.07 ^b	0.49
AFW2	<i>Thamnocephalus platyurus</i>	0.044 ^b	0.1
Algal medium	<i>Pseudokirchneriella subcapitata</i>	0.02 ^c	0.15
Malt extract (ME)	<i>Saccharomyces cerevisiae</i>	11.4 ^d	1.97
YPD	<i>Saccharomyces. cerevisiae</i>	368 ^e	6.4
2% NaCl	<i>Vibrio fisheri</i>	0.64 ^f	1.88
M9 + 0.5%AA	<i>Escherichia coli</i>	83.5 ^g	0.97
0.9% NaCl	<i>Escherichia coli</i>	1.22 ^g	2.66
0.9% NaCl + 0.1%AA	<i>Escherichia coli</i>	3.84 ^h	0.19
Test compound: nano-CuO			
Malt extract (ME)	<i>Saccharomyces cerevisiae</i>	16.6 ^d	11.1
0.9% NaCl + 0.1%AA	<i>Escherichia coli</i>	40.4 ^h	90.2

^a [19]; 24-h mortality test; ^b [18]; 48-h mortality test; ^c [46]; 72-h growth inhibition test; ^d [54]; 8-h growth inhibition test; ^e K. Kasemets, personal communication; 8-h growth inhibition test; ^f [18]; 30-min bioluminescence inhibition test; ^g [29]; 30-min bioluminescence inhibition assay with recombinant *E. coli*; ^h [21]; 30-min bioluminescence inhibition test; AA—Cas-amino acids.

Here, we collected ‘in house’ toxicity data (EC₅₀ values) for CuSO₄ and nano-CuO which were determined using standard ecotoxicological test organisms (protozoa, crustaceans, algae, bacteria) and yeasts (Table 4). All these toxicity tests were performed in the same media that were used for Cu speciation and bioavailability analysis in the current study. The collected EC₅₀ values of these organisms towards CuSO₄ differed by 4 orders of magnitude (from 0.02 to 368 mg/L, Table 4). Using data from Cu-ISE, we calculated the amount of free Cu ions at each of the EC₅₀ values. When we normalized the CuSO₄ EC₅₀ values for free Cu in the test media, the difference in EC₅₀ values comprised just 1.8 orders of magnitude. Thus, in case of CuSO₄, the free ion concentration may be considered as relatively suitable parameter for toxicity prediction, as also earlier demonstrated by

Apte *et al.* [44]. To our surprise, a good agreement between the EC_{50} values and free Cu content was observed in our experiments, even though they were conducted with different organisms of substantially different biological complexity (ranging from bacteria to algae and crustaceans). This brings us to the conclusion that the apparently big differences observed in toxicity of $CuSO_4$ towards these organisms could be attributed to the properties of the testing media rather than to inherent differences in sensitivity between the test organisms. Unfortunately, we were unable to calculate the bioavailable Cu corresponding to respective EC_{50} values using the Cu-biosensor bacteria as all the EC_{50} values for $CuSO_4$ exhibited already strong toxic effects towards the Cu-biosensor (Figure 1). However, as the working principle of biosensor bacteria is to respond to subtoxic amounts of heavy metals, high toxicity of EC_{50} concentrations of Cu compounds to sensor bacteria was anticipated.

4. Conclusions

In this study, we used a Cu ion-selective electrode (Cu-ISE) and a bacterial Cu-biosensor in parallel, to analyze the speciation of $CuSO_4$ and nano-CuO in seventeen selected laboratory test media. In case of $CuSO_4$, both the ISE and sensor bacteria showed that organics-containing media contained lower free and bioavailable copper than did mineral media. However, in case of nano-CuO the ‘complexing’ effect was not so evident. It could be assumed that upon dispersion of nano-CuO in organics-containing media two simultaneous processes take place: (i) enhanced dissolution of copper due to the increased dispersion of CuO and (ii) complexing of dissolved Cu by organics present in the medium. Overall, the free Cu measured with the Cu-ISE and bioavailable Cu measured by the Cu-biosensor correlated well. Interestingly, in nano-CuO suspensions, more bioavailable Cu (bacterial sensor assay) than free Cu (ISE) was detected. Thus, we suggest that bacterial biosensors were able to access additional fraction of nano CuO that was not dissolved and detectable by Cu-ISE. Hence, in the environmental hazard analysis of metal-containing (nano) particulate materials, biosensor analysis may be more informative than other respective analytical techniques. We also demonstrated that the remarkable difference in sensitivity of various aquatic organisms towards copper may be largely explained by the differential speciation of this metal in the test media used. Therefore, although very different aquatic organisms were compared (bacteria, algae, yeasts, crustaceans, protozoa) the concentrations of free copper harmful to these organisms were quite similar. This suggests that there seems to be no big inherent differences in sensitivity towards copper between different types of organisms. Moreover, the effect of composition of the test media should be considered as one of the most important factors in interpreting the results of toxicity tests.

Acknowledgements

This work was financially supported by the Estonian Ministry of Science and Education (targeted funding project SF0690063s08), Estonian Science Foundation (grants No. 6974, 7686, 8066 and 8561), EMP45, Centre for Academic Mobility, Archimedes Foundation and European Social Fund and EU FP7 Project NanoValid (grant agreement No 263147) We thank Kaja Kasemets for providing the *S. cerevisiae* toxicity data and Irina Blinova for inspiring discussions. We thank Rein Kuusik from Department of Chemical and Materials Technology, Tallinn University of Technology for his advice.

References

1. Borgmann, U.; Ralph, K.M. Complexation and toxicity of copper and the free metal bioassay technique. *Water Res.* **1983**, *17*, 1697-1703.
2. Ehlers, L.J.; Luthy, R.G. Contaminant bioavailability in soil and sediment. *Environ. Sci. Technol.* **2003**, *37*, 295A-302A.
3. Witters, H.E. Chemical speciation dynamics and toxicity assessment in aquatic systems. *Ecotoxicol. Environ. Safety* **1998**, *41*, 90-95.
4. Batley, G.E.; Apte, S.C.; Stauber, J. Acceptability of aquatic toxicity data for the derivation of water quality guidelines for metals. *Mar. Freshw. Res.* **1999**, *50*, 729-738.
5. Kahru, A.; Dubourguier, H.-C. From ecotoxicology to nanoecotoxicology. *Toxicology* **2010**, *269*, 105-119.
6. Bakker, E.; Pretsch, E. The new wave of ion-selective electrodes. *Anal. Chem.* **2002**, *74*, 420A-426A.
7. Pesavento, M.; Alberti, G.; Biesuz, R. Analytical methods for determination of free metal ion concentration, labile species fraction and metal complexation capacity of environmental waters: A review. *Anal. Chim. Acta* **2009**, *631*, 129-141.
8. Bakker, E.; Pretsch, E. Potentiometric sensors for trace-level analysis. *Trends Anal. Chem.* **2005**, *24*, 199-207.
9. Dybko, A. Errors in chemical sensor measurements. *Sensors* **2001**, *1*, 29-37.
10. Dimeski, G.; Badrick, T.; John, A.S. Ion Selective Electrodes (ISEs) and interferences—A review. *Clin. Chim. Acta* **2010**, *411*, 309-317.
11. Unsworth, E.R.; Warnken, K.W.; Zhang, H.; Davison, W.; Black, F.; Buffle, J.; Cao, J.; Cleven, R.; Galceran, J.; Gunkel, P.; *et al.* Model predictions of metal speciation in freshwaters compared to measurements by *in situ* techniques. *Environ. Sci. Technol.* **2006**, *40*, 1942-1949.
12. Worms, I.; Simon, D.F.; Hassler, C.S.; Wilkinson, K.J. Bioavailability of trace metals to aquatic microorganisms: Importance of chemical, biological and physical processes on biouptake. *Biochimie* **2006**, *88*, 1721-1731.
13. Harms, H.; Wells, M.; Meer, J. Whole-cell living biosensors—Are they ready for environmental application? *Appl. Microbiol. Biotechnol.* **2006**, *70*, 273-280.
14. Yagi, K. Applications of whole-cell bacterial sensors in biotechnology and environmental science. *Appl. Microbiol. Biotechnol.* **2007**, *73*, 1251-1258.
15. Ivask, A.; Rolova, T.; Kahru, A. A suite of recombinant luminescent bacterial strains for the quantification of bioavailable heavy metals and toxicity testing. *BMC Biotechnol.* **2009**, doi: 10.1186/1472-6750-9-41.
16. Ivask, A.; Francois, M.; Kahru, A.; Dubourguier, H.; Virta, M.; Douay, F. Recombinant luminescent bacterial sensors for the measurement of bioavailability of cadmium and lead in soils polluted by metal smelters. *Chemosphere* **2004**, *55*, 147-156.
17. Kahru, A.; Ivask, A.; Kasemets, K.; Pollumaa, L.; Kurvet, I.; Francois, M.; Dubourguier, H. Biotests and biosensors in ecotoxicological risk assessment of field soils polluted with zinc, lead and cadmium. *Environ. Toxicol. Chem.* **2005**, *24*, 2973-2982.

18. Heinlaan, M.; Ivask, A.; Blinova, I.; Dubourguier, H.; Kahru, A. Toxicity of nanosized and bulk ZnO, CuO and TiO₂ to bacteria *Vibrio fischeri* and crustaceans *Daphnia magna* and *Thamnocephalus platyurus*. *Chemosphere* **2008**, *71*, 1308-1316.
19. Mortimer, M.; Kasemets, K.; Kahru, A. Toxicity of ZnO and CuO nanoparticles to ciliated protozoa *Tetrahymena thermophila*. *Toxicology* **2010**, *269*, 182-189.
20. Blinova, I.; Ivask, A.; Heinlaan, M.; Mortimer, M.; Kahru, A. Ecotoxicity of nanoparticles of CuO and ZnO in natural water. *Environ. Pollut.* **2010**, *158*, 41-47.
21. Ivask, A.; Bondarenko, O.; Jephthina, N.; Kahru, A. Profiling of the reactive oxygen species-related ecotoxicity of CuO, ZnO, TiO₂, silver and fullerene nanoparticles using a set of recombinant luminescent *Escherichia coli* strains: Differentiating the impact of particles and solubilised metals. *Anal. Bioanal. Chem.* **2010**, *398*, 701-716.
22. Sauvé, S.; McBride, M.B.; Hendershot, W.H. Ion-selective electrode measurements of copper(II) activity in contaminated soils. *Arch. Environ. Contam. Toxicol.* **1995**, *29*, 373-379.
23. Buck, P.B.; Lindner, E. Recommendations for nomenclature of ion-selective electrodes. *Pure Appl. Chem.* **1994**, *66*, 2527-2536.
24. Gorovsky, M.A.; Yao, M.C.; Keevert, J.B.; Pleger, G.L. Isolation of micro- and macronuclei of *Tetrahymena pyriformis*. *Meth. Cell. Biol.* **1975**, *9*, 311-327.
25. *Standard Methods for Examination of Water and Wastewater*; Available online: <http://www.umass.edu/tei/mwwp/acrobat/sm9222DMFT.PDF> (accessed on 20 September 2011).
26. Sambrook, J.; Fritsch, E.F.; Maniatis, T. *Molecular Cloning: A Laboratory Manual*, 2nd ed.; Cold Spring Harbor Laboratory Press: Plainview, NY, USA, 1989.
27. LaRossa, R.; Smulski, D.; Van Dyk, T. Interaction of lead nitrate and cadmium chloride with *Escherichia coli* K-12 and *Salmonella typhimurium* global regulatory mutants. *J. Ind. Microbiol.* **1995**, *14*, 252-258.
28. Gustafsson, J. *Visual Minteq v2.51*; KTH: Stockholm, Sweden, 2008.
29. Kurvet, I.; Ivask, A.; Bondarenko, O.; Sihtmäe, M.; Kahru, A. *LuxCDABE*—Transformed constitutively bioluminescent *escherichia coli* for toxicity screening: Comparison with naturally luminous *Vibrio fischeri*. *Sensors* **2011**, *11*, 7865-7878.
30. Hakkila, K.; Green, T.; Leskinen, P.; Ivask, A.; Marks, R.; Virta, M. Detection of bioavailable heavy metals in EILATox-oregon samples using whole-cell luminescent bacterial sensors in suspension or immobilized onto fibre-optic tips. *J. Appl. Toxicol.* **2004**, *24*, 333-342.
31. De Marco, R.; Clarke, G.; Pejic, B. Ion-selective electrode potentiometry in environmental analysis. *Electroanalysis* **2007**, *19*, 1987-2001.
32. Sauvé, S.; McBride, M.B.; Norvell, W.A.; Hendershot, W.H. Copper solubility and speciation of *in situ* contaminated soils: Effects of copper level, pH and organic matter. *Water Air Soil Pollut.* **1997**, *100*, 133-149.
33. Vulkan, R.; Zhao, F.-J.; Barbosa-Jefferson, V.; Preston, S.; Paton, G.I.; Tipping, E.; McGrath, S.P. Copper speciation and impacts on bacterial biosensors in the pore water of copper-contaminated soils. *Environ. Sci. Technol.* **2000**, *34*, 5115-5121.
34. Lanza, P. The behaviour of copper(II)-selective electrodes in chloride-containing solutions. *Anal. Chim. Acta* **1979**, *105*, 53-65.

35. Hart, J.R. *Ethylenediaminetetraacetic Acid and Related Chelating Agents*. Ullmann's Encyclopedia of Industrial Chemistry; Wiley-VCH: Weinheim, Germany, 2005.
36. Hughes, M.N.; Poole, R.K. Metal speciation and microbial growth—the hard (and soft) facts. *J. General Microbiol.* **1991**, *137*, 725-734.
37. Tauriainen, S.; Karp, M.; Chang, W.; Virta, M. Luminescent bacterial sensor for cadmium and lead. *Biosens. Bioelectron.* **1998**, *13*, 931-938.
38. Corbisier, P.; van der Lelie, D.; Borremans, B.; Provoost, A.; de Lorenzo, V.; Brown, N.L.; Lloyd, J.R.; Hobman, J.L.; Csöregi, E.; Johansson, G.; *et al.* Whole cell- and protein-based biosensors for the detection of bioavailable heavy metals in environmental samples. *Anal. Chim. Acta* **1999**, *387*, 235-244.
39. Borgmann, U.; Ralph, K.M. Complexation and toxicity of copper and the free metal bioassay technique. *Water Res.* **1983**, *17*, 1697-1703.
40. Rensing, C.; Maier, M. Issues underlying use of biosensors to measure metal bioavailability. *Ecotoxicol. Environ. Safety* **2003**, *56*, 140-147.
41. Brandt, K.K.; Holm, P.E.; Nybroe, O. Evidence for copper-dissolved organic matter complexes and transiently increased copper bioavailability in manure-amended soils as determined by bioluminescent bacterial sensors. *Environ. Sci. Technol.* **2008**, *42*, 3102-3108.
42. Wilson, T.; Hastings, J.W. Bioluminescence. *Annu. Rev.* **1998**, *14*, 197-230.
43. Karlén, C.; Odnevall Wallinder, I.; Heijerick, D.; Leygraf, C. Runoff rates, chemical speciation and bioavailability of copper released from naturally patinated copper. *Environ. Pollut.* **2002**, *120*, 691-700.
44. Apte, S.C.; Batley, G.E.; Bowles, K.C.; Brown, P.L.; Creighton, N.; Hales, L.T.; Hyne, R.V.; Julli, M.; Mearkitch, S.J.; Pablo, F.; *et al.* Comparison of copper speciation measurements with the toxic responses of three sensitive freshwater organisms. *CSIRO Publishing* **2005**, *2*, 320-330.
45. Kahru, A.; Dubourgier, H.; Blinova, I.; Ivask, A.; Kasemets, K. Biotests and biosensors for ecotoxicology of metal oxide nanoparticles: A minireview. *Sensors* **2008**, *8*, 5153-5170.
46. Aruoja, V.; Dubourgier, H.-C.; Kasemets, K.; Kahru, A. Toxicity of nanoparticles of CuO, ZnO and TiO₂ to microalgae *Pseudokirchneriella subcapitata*. *Sci. Total Environ.* **2009**, *407*, 1461-1468.
47. Wang, D.Y.; Xing, X.J. Assessment of locomotion behavior defects induced by acute toxicity from heavy metal exposure in nematode *Caenorhabditis elegans*. *J. Environ. Sci.* **2008**, *20*, 1132-1137.
48. Puzyn, T.; Rasulev, B.; Gajewicz, A.; Hu, X.; Dasari, T.P.; Michalkova, A.; Hwang, H.-M.; Toropov, A.; Leszczynska, D.; Leszczynski, J. Using nano-QSAR to predict the cytotoxicity of metal oxide nanoparticles. *Nat. Nano* **2011**, *6*, 175-178.
49. Gunawan, C.; Teoh, W.Y.; Marguis, C.P.; Amal, R. Cytotoxic origin of copper(II) oxide nanoparticles: Comparative studies with micron-sized particles, leachate, and metal salts. *ACS Nano* **2011**, *27*, 7214-7225.
50. Li, M.; Zhu, L.; Lin, D. Toxicity of ZnO nanoparticles to *Escherichia coli*: Mechanism and the influence of medium components. *Environ. Sci. Technol.* **2011**, *45*, 1977-1983.
51. Xia, T.; Kovochich, M.; Liong, M.; Mädler, L.; Gilbert, B.; Shi, H.; Yeh, J.I.; Zink, J.I.; Nel, A.E. Comparison of the mechanism of toxicity of zinc oxide and cerium oxide nanoparticles based on dissolution and oxidative stress properties. *ACS Nano* **2008**, *2*, 2121-2134.

52. Peltola, P.; Ivask, A.; Astrom, M.; Virta, M. Lead and Cu in contaminated urban soils: Extraction with chemical reagents and bioluminescent bacteria and yeast. *Sci. Total. Environ.* **2005**, *350*, 194-203.
53. Riedel, G.F. *Copper*; Elsevier: Amsterdam, The Netherlands, 2008.
54. Kasemets, K.; Ivask, A.; Dubourguier, H.-C.; Kahru, A. Toxicity of nanoparticles of ZnO, CuO and TiO₂ to yeast *Saccharomyces cerevisiae*. *Toxicol. Vitro* **2009**, *23*, 1116-1122.

© 2011 by the authors; licensee MDPI, Basel, Switzerland. This article is an open access article distributed under the terms and conditions of the Creative Commons Attribution license (<http://creativecommons.org/licenses/by/3.0/>).

Supplementary Information

Aleksandr Käkinen^{1,2,†}, Olesja Bondarenko^{1,3,†}, Angela Ivask^{1,*} and Anne Kahru^{1,*}

¹ Laboratory of Molecular Genetics, National Institute of Chemical Physics and Biophysics, Akadeemia tee 23, Tallinn 12618, Estonia; E-Mails: aleksandr.kakinen@kbfi.ee (A.K.); olesja.bondarenko@kbfi.ee (O.B.)

² Department of Chemical and Materials Technology, Tallinn University of Technology, Ehitajate tee 5, Tallinn 19086, Estonia

³ Department of Gene Technology, Tallinn University of Technology, Ehitajate tee 5, Tallinn 19086, Estonia

* Authors to whom correspondence should be addressed; E-Mails: angela.ivask@kbfi.ee (A.I.); anne.kahru@kbfi.ee (A.K.); Tel.: +372-6-398-382 (A.I.); +372-6-398-373 (A.K.); Fax: +372-6-398-382 (A.I.); +372-6-398-382 (A.K.).

† These authors equally contributed to this work.

Received: 20 September 2011; in revised form: 20 October 2011 / Accepted: 31 October 2011 / Published: 3 November 2011

Figure S1. Example for the calculation of limit of detection (LOD) of Cu-ion selective electrode, as recommended for ion-selective electrodes by IUPAC [1]. Log(10) of the added Cu was plotted against the electrode potential and the crossing point between the linear segment of the electrode potential (diagonal dotted grey line) and the line representing background potential of the electrode (horizontal dotted grey line) was sought. The concentration of added Cu at which the two lines were crossing (vertical dotted grey line) was designated as the limit of detection (Cu-ISE_{LOD}). In the current example, LOD of Cu-ISE is 0.021 mg Cu/L = 3.2×10^{-7} M. Prior measurement, the ionic strength of all solutions was adjusted by adding 5 M NaNO₃ in a ratio 1:50 (NaNO₃:sample).

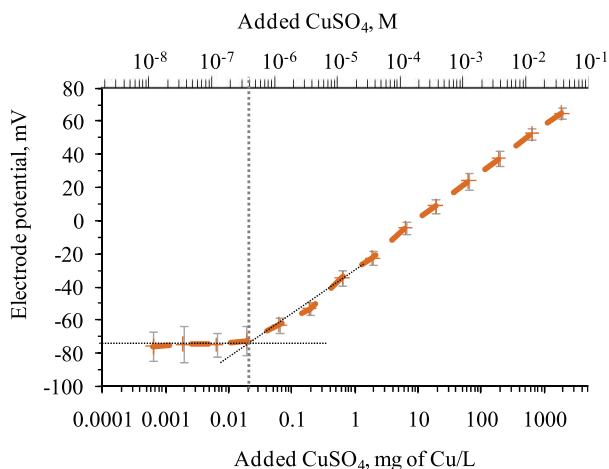


Figure S2. Example for the calculation of free Cu at a certain CuSO_4 concentration in a specific media (Malt extract (ME) as an example). Normalized electrode potentials for DI water (100% of added Cu assumed in free form) and for the given medium (ME) as a function of added Cu are plotted. Then, the electrode potential at desired concentration (11.4 mg of added Cu/L in this case) in the medium is read (1) and the Cu concentration corresponding to that electrode potential in DI water is found (2). This Cu concentration in DI water (1.97 mg/L in this case) is considered as the free Cu concentration in this media at the given (11.4 mg of added Cu/L) concentration.

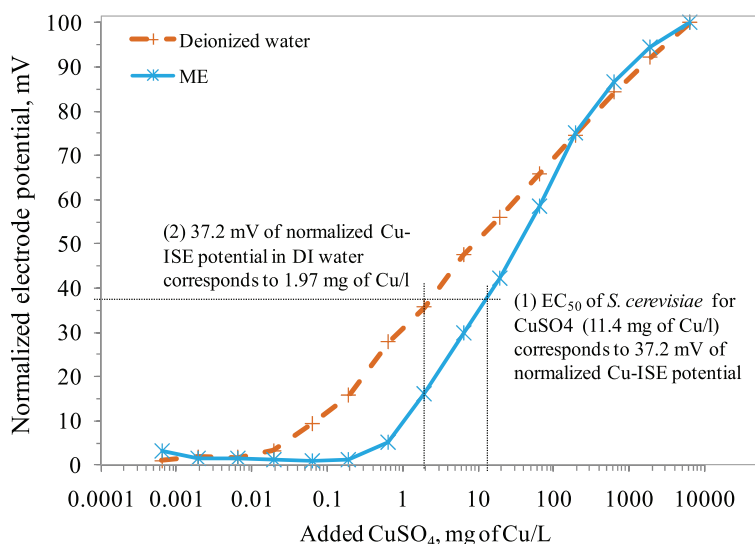


Figure S3. Example for the calculation of limit of detection (LOD) of Cu-biosensor bacteria *Pseudomonas fluorescens* OS8::KnCueR_PcopAlux in HMM media supplemented with 0.5% Cas-aminoacids (Table 1). **(a)** representation of fold induction of Cu sensor bacteria with increasing Cu concentrations (dose-response curve); in our earlier studies [2,3], concentration of added metals resulting in 2-fold induction of a bacterial sensor (marked with dashed lines) was considered significant induction of the sensor over the background signal and thus, suggested as LOD. **(b)** representation of the same data as % induction of the bacterial sensor; in this plot, concentration of added metals resulting in 20% induction of the bacterial sensor of maximal induction potential of the sensor in the current test conditions (marked with dashed lines) was considered as LOD. This normalization was performed because the fold induction of the bacterial sensor varied along with the nutrient profile in different media studied. For panel (a) the LOD is 0.13 mg/L; for panel (b) the LOD is 0.2 mg/L.

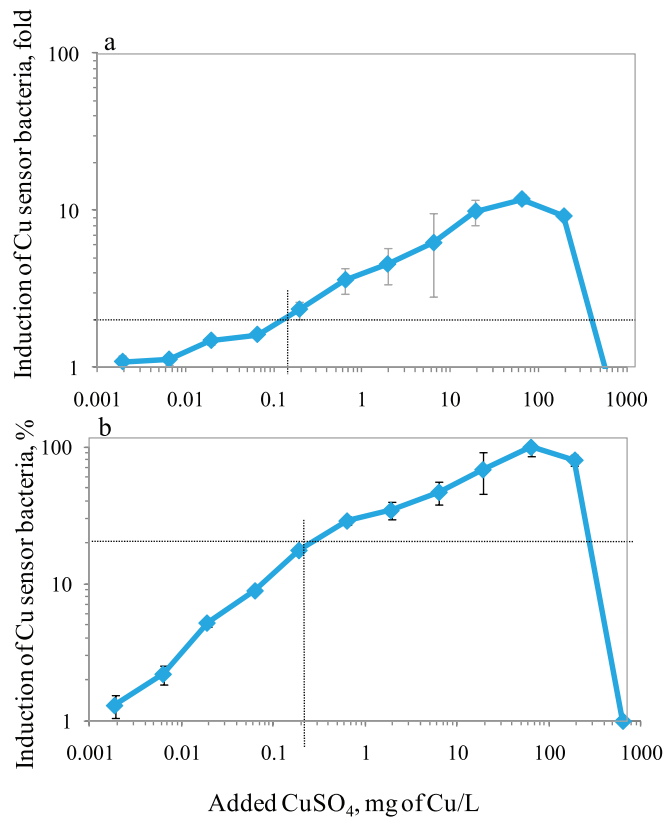
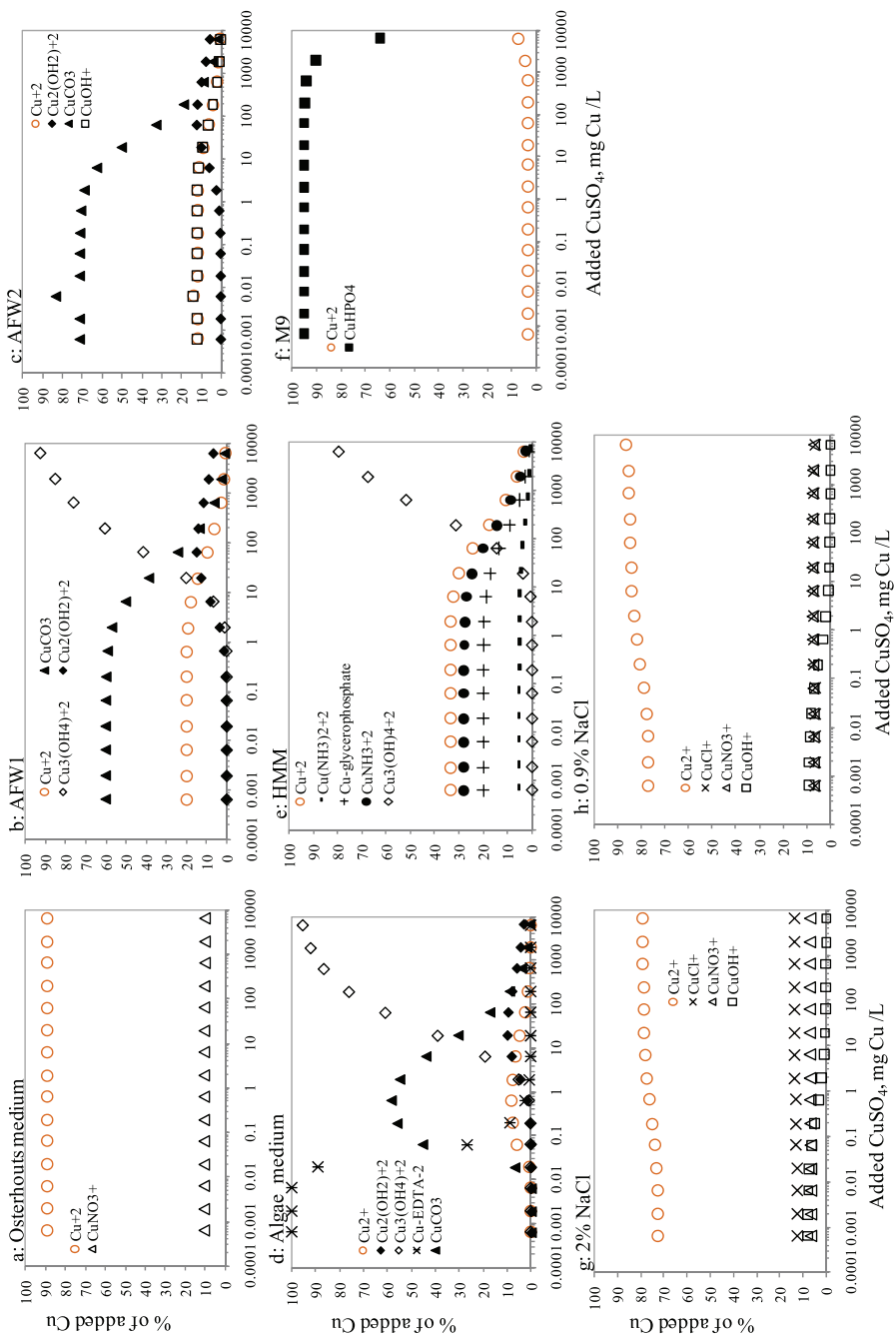


Figure S4. Speciation of Cu (added to respective media as CuSO_4) in different test media containing mainly mineral salts or very low levels of organic components (glucose and β -glycerophosphate). Only main species (constituting at least 5% of the total Cu species over the concentration range tested) are indicated. AFW1—Artificial freshwater 1; AFW2—Artificial freshwater 2; HMM—Heavy metal MOPS medium, M9 (see the content of these media in Table 1). Chemical equilibrium model Visual MINTEQ 2.51 [4] was used for the calculations.



References

1. Buck, P.B.; Lindner, E. Recommendations for nomenclature of ion-selective electrodes. *Pure Appl. Chem.* **1994**, *66*, 2527-2536.
2. Hakkila, K.; Green, T.; Leskinen, P.; Ivask, A.; Marks, R.; Virta, M. Detection of bioavailable heavy metals in EILATox-oregon samples using whole-cell luminescent bacterial sensors in suspension or immobilized onto fibre-optic tips. *J. Appl. Toxicol.* **2004**, *24*, 333-342.
3. Ivask, A.; Rolova, T.; Kahru, A. A suite of recombinant luminescent bacterial strains for the quantification of bioavailable heavy metals and toxicity testing. *BMC Biotechnol.* **2009**, *9*, 41.
4. Gustafsson, J. *Visual Minteq v2.51*; The Royal Institute of Technology (KTH): Stockholm, Sweden, 2008.

© 2011 by the authors; licensee MDPI, Basel, Switzerland. This article is an open access article distributed under the terms and conditions of the Creative Commons Attribution license (<http://creativecommons.org/licenses/by/3.0/>).

PUBLICATION II

Bondarenko O, Ivask A, **Käkinen A**, Kahru A (2012). Sub-toxic effects of CuO nanoparticles on bacteria: kinetics, role of Cu ions and possible mechanisms of action. *Environmental Pollution* 169, 81 – 89



Sub-toxic effects of CuO nanoparticles on bacteria: Kinetics, role of Cu ions and possible mechanisms of action

Olesja Bondarenko^{a,b,*}, Angela Ivask^a, Aleksandr Käkinen^{a,c}, Anne Kahru^{a,*}

^aLaboratory of Molecular Genetics, National Institute of Chemical Physics and Biophysics, Akadeemia tee 23, Tallinn 12618, Estonia

^bDepartment of Gene Technology, Tallinn University of Technology, Akadeemia tee 15, Tallinn 12618, Estonia

^cDepartment of Chemical and Materials Technology, Tallinn University of Technology, Ehitajate tee 5, Tallinn 19086, Estonia

ARTICLE INFO

Article history:

Received 21 March 2012

Received in revised form

25 April 2012

Accepted 8 May 2012

Keywords:

Escherichia coli biosensor
Copper oxide nanoparticles
Toxicity mechanisms
Reactive oxygen species
DNA damage

ABSTRACT

The sub-toxic effects of CuO nanoparticles (nano-CuO) were evaluated using three recombinant luminescent *Escherichia coli* bacteria responding specifically to (i) reactive oxygen species (ROS), (ii) single-stranded DNA breaks and (iii) bioavailable Cu ions. Using these sensors we showed that nano-CuO induces the formation of superoxide anions, hydrogen peroxide and single-stranded DNA already at very low sub-toxic levels (0.1 mg Cu/L). The maximal sub-toxic response of all biosensors to nominal concentrations of nano-CuO, micro-CuO (size control) and CuSO₄ (solubility control) occurred at ~6, ~600 and ~0.6 mg Cu/L, respectively. According to the chemical analysis all the latter concentrations yielded ~0.6 mg of soluble Cu/L, indicating that dissolution of CuO particles was the key factor triggering the ROS and DNA damage responses in bacteria. Cu-ions chelation studies also showed that CuO particles were not involved in these stress responses. The solubilization results were confirmed by *Pseudomonas fluorescens* Cu-ion sensor.

© 2012 Elsevier Ltd. All rights reserved.

1. Introduction

The biocidal properties of copper are widely acknowledged and various copper compounds have been used as antifoulants for centuries (Thomas and Brooks, 2010). With the development of nanotechnology, copper has been increasingly used in the form of nanoparticles (NPs, particles with at least one dimension between 1 and 100 nm) and applied in e.g., antimicrobial textiles, hospital equipment, wood preservation and antifouling paints (Gabbay et al., 2006). Compared to bulk analogues, NPs display larger specific surface area that leads to increased reactivity and thus, also enhanced bactericidal properties (Nel et al., 2006). For example, the effectiveness of CuO NPs (generally at concentrations between 10 and 100 mg/L) towards a wide range of Gram-positive and Gram-negative bacteria including *Bacillus subtilis*, *Pseudomonas aeruginosa*, *Escherichia coli* and *Staphylococcus aureus* has been reported (Ren et al., 2009; Baek and An, 2011). However, purposeful use of CuO NPs due to their antimicrobial properties calls extra attention from the environmental protection viewpoint. Unlike antibiotics that have specific targets in bacterial cells for their toxic action,

copper containing NPs are also toxic to other organisms that may be exposed to these NPs via co-exposure or various waste streams. For example, nano-CuO has been shown to be toxic to crustaceans *Daphnia magna* and *Thamnocephalus platyurus* and algae *Pseudokirchneriella subcapitata* already at remarkably low concentrations (EC₅₀ 3.2, 0.18 and <1 mg/L, respectively) (Heinlaan et al., 2008; Aruoja et al., 2009) and thus, should be classified as 'very toxic' to aquatic organisms (European Chemicals Bureau, 2006). High ecotoxicity of CuO NPs has been considered as a serious limitation for their implementation in new applications (Ebrahimnia-Bajestan et al., 2011) and prior mechanistic toxicological characterization of this material is needed (Fahmy and Cormier, 2009; Kahru and Dubourguier, 2010). Therefore, in the current study, we focused on toxicological profiling of CuO NPs. Based on the current literature, at least part of toxic effects of nano-CuO is attributed to the release of Cu ions (Ruparelia et al., 2008; Wu et al., 2010). Cu ions may be involved in recycling redox reactions between Cu²⁺ and Cu⁺, which generate reactive oxygen species (ROS) on the surface of bacterial cells (Hoshino et al., 1999). However, according to some studies, the fraction of Cu dissolved from nano-CuO is too low to explain all the cytotoxic effects of nano-CuO (Griffitt et al., 2007; Heinlaan et al., 2008; Karlsson et al., 2008). These studies suggest that particles themselves may generate additional ROS and the investigation of the relationship between the cellular responses to

* Corresponding authors.

E-mail addresses: olesja.bondarenko@kbfi.ee (O. Bondarenko), anne.kahru@kbfi.ee (A. Kahru).

sub-toxic concentrations of nano-CuO and the oxidative stress endpoints has been proposed (Fahmy and Cormier, 2009).

We have recently demonstrated that nano-CuO was more toxic to superoxide dismutase-deficient *Escherichia coli* than to the wild-type bacteria and this effect was apparently mediated by superoxide anions (Ivask et al., 2010). In the current study we expanded our investigation by constructing two new stress-specific luminescent bacterial biosensors that respond to hydrogen peroxide (a ROS) and single-stranded DNA breaks. We used these biosensors in parallel with two Cu-ion specific biosensors to reveal the nature of sub-toxic effects of nano-CuO in bacterial cells. The used sensor bacteria are based on promoters of *Escherichia coli* genes which are involved in sensing and detoxification of ROS, DNA damage or Cu and are activated upon respective stress. In biosensor strains, these promoters are genetically coupled to bioluminescence-encoding genes (*luxCDABE* genes from *Photobacterium luminescens*) and thus, the sub-toxic stress condition may be measured by increased bacterial bioluminescence. Such an approach allows the detection of specific perturbations already at sub-toxic concentrations (Hwang et al., 2008; Gou et al., 2010) and is orders of magnitudes more sensitive compared to the common viability endpoints (L(E) C50 values). All biosensors were exposed to nano-CuO but also micro-CuO (size control) and CuSO₄ (solubility control) from sub-toxic (sub-ppb, i.e., below µg/L) till toxic concentrations (1000 ppm, i.e., mg/L). Comparison of the responses of the stress-specific bacteria with that of Cu ions-sensing bacteria and chemical analysis/chelation of dissolved Cu allowed us to conclude that (i) nano-CuO induces the bacterial ROS and DNA damage defence systems already at very low sub-toxic levels and (ii) these early adverse effects of nano-CuO in *Escherichia coli* cells are triggered by dissolved Cu ions.

2. Materials and methods

2.1. Chemicals

Paraquat, mitomycin C (MMC) and 3,5-dichlorophenol (3,5-DCP) were purchased from Sigma–Aldrich, CuSO₄·7H₂O from Alfa Aesar, H₂O₂ from Merck and EDTA from Serva. All the chemicals were at least of analytical grade. All the stock solutions were prepared in sterile deionized water at the following concentrations:

paraquat at 40 g/L, MMC at 20 mg/L, H₂O₂ at 300 g/L, 3,5-DCP at 100 mg/L, CuSO₄·7H₂O at 63.5 g Cu/L and EDTA at 58.4 g/L. Deionized sterile water was used for dilutions of all chemicals throughout the study. CuO particles are characterized below.

2.2. Physico-chemical characterization of CuO particles

CuO nanoparticles (nano-CuO; primary particle size 30 nm (Blinova et al., 2010)) were from Sigma–Aldrich and micro-CuO from Alfa Aesar. The stock solutions of copper oxides (63.5 g Cu/L) were prepared in deionized water, sonicated in the ultrasonication bath for 30 min and stored in the dark at +4 °C. Before every use, the suspensions were vortexed. Deionized sterile water was used for CuO dilutions throughout the study. Scanning electron microscopy (SEM, JSM-8404) and determination of specific surface area (SSA, Sorptometer Kelvin 1042) of the powders of nano- and micro-CuO was performed in Tallinn University of Technology (Estonia). The hydrodynamic size (Dh) of nano-CuO (6.35 mg Cu/L) and micro-CuO (635 mg Cu/L) was measured in deionized water and biosensor test medium (heavy metal MOPS medium; see below) using dynamic light scattering (DLS) (Malvern Zetasizer Nano-ZS, Malvern Instruments). Visible wavelength absorption spectra (UV–Vis) of 63.5 mg Cu/L nano-CuO and 6350 mg Cu/L micro-CuO particles in deionized water were obtained using a Thermo Multiscan Spectrum (Thermo Electron).

2.3. Luminescent bacterial biosensors

Luminescent recombinant *E. coli* strains used in this study are listed in Table 1. The ROS-inducible strain *E. coli* K12::katGlux and DNA damage-inducible strain *E. coli* MC1061(pDEWrecAlux) were constructed as described in Supplementary data. The constitutively luminescent *E. coli* MC1061(pDEW201) was constructed by electroporating the plasmid pDEW201 into competent *E. coli* cells. *E. coli* K12::lux, MC1061(pSLcueR/pDNPCopAlux), MC1061(pSLlux), *Pseudomonas fluorescens* OS8::lux and *P. fluorescens* OS8::KncueRPCopAlux were constructed and described previously (Leedj  rv et al., 2006; Ivask et al., 2009, 2010).

2.4. Bacterial biosensor assay

Recombinant luminescent bacteria were pre-grown in 3 mL of Luria Bertani (LB) medium (Sambrook et al., 1989) supplemented with appropriate antibiotics (Table 1) overnight. Twenty millilitres of fresh medium was inoculated with 1/50 diluted overnight culture and bacteria were grown until mid-exponential phase (OD₆₀₀ of 0.6). All cultivations were performed on a shaker at 200 rpm, at 30 °C. The exponential phase culture was centrifuged at 5000× g for 10 min and washed twice with heavy metal MOPS medium (HMM) (8.4 g of MOPS, 0.22 g of glycerol-2-phosphate, 3.7 g of KCl, 0.54 g of NH₄Cl, 0.06 g of MgSO₄, and 0.162 mg of FeCl₃ per 1 L of MQ water; LaRossa et al., 1995) supplemented with 0.1% glucose and 0.1% cas-aminoacids (acid hydrolysate of casein, Lab M). For the bioluminescence induction assays, the test final OD₆₀₀ of bacterial culture in glucose and aminoacids-supplemented HMM media was 0.1 (~ 10⁶ bacterial cells per mL).

Table 1
Luminescent recombinant *Escherichia coli* and *Pseudomonas fluorescens* strains used in this study.

Strain	Designation	Description	Antibiotic concentration in medium (mg/L)	Reference
Stress-inducible recombinant luminescent strains				
<i>E. coli</i> K12::katGlux	ROS-inducible strain	Chromosomal insertion of <i>luxCDABE</i> genes under the control of <i>katG</i> (catalase-peroxidase) promoter	Kanamycin (30)	This study
<i>E. coli</i> MC1061 ^a (pDEWrecAlux)	ssDNA damage-inducible strain	<i>luxCDABE</i> genes under control of <i>recA</i> (recombinase A) promoter in a medium-copy number plasmid	Ampicillin (100)	This study
Metal-inducible recombinant luminescent strains				
<i>E. coli</i> MC1061 ^a (pSLcueR/pDNPCopAlux)	Cu-inducible strain	<i>luxCDABE</i> genes under control of <i>copA</i> (Cu/Ag-responsive) promoter in a medium-copy plasmid	Ampicillin (100) Tetracycline (10)	Ivask et al., 2009
<i>P. fluorescens</i> OS8::KncueRPCopAlux	Cu-inducible strain	Chromosomal insertion of <i>luxCDABE</i> genes under control of <i>copA</i> (Cu/Ag-responsive) promoter	Kanamycin (100)	Ivask et al., 2009
Recombinant constitutively luminescent (control) strains^b				
<i>E. coli</i> K12::lux	Control strain for <i>E. coli</i> K12::katGlux	Chromosomal insertion of <i>luxCDABE</i> genes	Kanamycin (30)	Ivask et al., 2010
<i>E. coli</i> MC1061 ^a (pDEWlux)	Control for <i>E. coli</i> MC1061 (pDEWrecAlux)	<i>luxCDABE</i> genes in a medium-copy plasmid pDEW201	Ampicillin (100)	This study
<i>E. coli</i> MC1061 ^a (pSLlux)	Control strain for <i>E. coli</i> MC1061 (pSLcueR/pDNPCopAlux)	<i>luxCDABE</i> genes in a medium-copy plasmid pSLlux	Ampicillin (100)	Leedj��rv et al., 2006
<i>P. fluorescens</i> OS8::lux	Control strain for <i>P. fluorescens</i> OS8::KncueRPCopAlux	Chromosomal insertion of <i>luxCDABE</i> genes	Kanamycin (100)	Ivask et al., 2009

^a Genotype: araD139 Δ(ara, leu)7697 ΔlacX74 galU galK hsdR2 strA mcrA mcrB1.
^b Used to take into account the quenching of bioluminescence by the turbid and coloured CuO samples.

ROS-generation potential of chemicals or CuO particles was analysed by *E. coli* K12::katGlux, DNA damaging potential by *E. coli* MC1061(pDEWrecAlux) and the liberation of Cu ions (dissolution) by *E. coli* MC1061(pSLcueR/pDNPcopAlux) and *Pseudomonas fluorescens* OS8::KncueR/pDNPcopAlux (Table 1). As CuO suspensions were turbid, potential quenching of bacterial bioluminescence was taken into account by parallel use of constitutively luminescent control bacteria, not inducible by the target chemical: *E. coli* K12::lux, *E. coli* MC1061(pDEW201), *E. coli* MC1061(pSLlux) and *P. fluorescens* OS8::lux, respectively (Table 1). One hundred microlitres of appropriate dilution of analysed chemicals or CuO particles in deionized water (or deionized water for the chemical-free control) was mixed with 100 μ L of bacterial suspension in aminoacid supplemented HMM medium on a 96-well microplate. In case of chelation experiments, EDTA in final concentration of 3 mM was added to CuSO₄ (0.635 mg Cu/L), nano-CuO (6.35 mg Cu/L), micro-CuO (635 mg Cu/L) (the concentrations were selected based on the highest sub-toxic response of biosensor towards respective Cu compounds) and chemical-free control. Bioluminescence was measured with Orion II plate luminometer (Berthold Detection Systems) every 10 min during the first hour of incubation and once per hour after that. Between measurements the plates were covered to avoid evaporation. All the measurements were performed in at least three independent experiments conducted on different days. Fold induction of bioluminescence of recombinant bacterial sensors was calculated as follows:

$$\text{Fold induction of bioluminescence} = \frac{\text{SLs}}{\text{CLs}} \times \text{CF},$$

where SLs was the luminescence of the sensor strain after exposure to chemical/particles, CLs was the luminescence of the same strain in control solution and CF was the correction factor. CF was calculated:

$$\text{CF} = \frac{\text{CLc}}{\text{SLc}},$$

where CLc was the luminescence of the constitutively luminescent strain in chemical-free control solution and SLc was the luminescence of that strain after exposure to chemical or particle. Limit of detection (LOD) of the sensor bacteria for the tested chemical was set to fold induction of bioluminescence = 2. In parallel to bioluminescence assay, the growth of biosensor bacteria was measured. The growth assay was carried out analogously to bioluminescence assay but in transparent 96-well microplates and the OD₆₀₀ (growth) was measured by Multiskan plate reader (Thermo Scientific). In parallel, the number of bacterial cells in the test was analysed by counting the colony forming units (CFU) before the test and after 5 and 8 h of incubation. CFU were counted after incubation of appropriate dilution of bacterial culture for 24 h on LB agar plates supplemented with appropriate antibiotics (Table 1).

2.5. Chemical analysis of dissolved Cu

Preparation of Cu formulations for the chemical analysis was identical to biosensor test procedure and was performed in three independent experiments. Briefly, suspension of Cu-biosensor bacteria (in cas-aminoacids supplemented HMM) was mixed 1:1 with CuSO₄ (0.635 mg Cu/L), nano-CuO (6.35 mg Cu/L) or micro-CuO (635 mg Cu/L) in 20 mL volume and ultracentrifuged at 30,000 g for 30 min. In order to determine the dissolved Cu in the beginning of the test and during the test, the samples were centrifuged immediately after mixing the bacteria with Cu compounds and also after 5 and 8 h of incubation. Supernatants were removed and analysed for soluble Cu by AAS-graphite furnace method in certified laboratory of Tallinn University of Technology, Estonia, using standard procedures EVS-EN ISO/IEC 17025:2005. Before the AAS analysis, the absence of nanoparticles in centrifuged CuO supernatants was analysed. For that, particle count rate function of Malvern Zetasizer Nano-ZS was used. As the particle count rate in centrifuged supernatants was similar to that in deionized water, it was concluded that no nanoparticles were present in nano-CuO supernatants after their centrifugation.

3. Results and discussion

3.1. Physico-chemical characterization of CuO particles

The manufacturer-advertised size of nano-CuO used in this study was 30 nm. No size range was available for purchased micro-CuO particles. The specific surface area (SSA) was 25.5 m²/g for nano-CuO and 0.64 m²/g for micro-CuO (Table 2). According to SEM images, nano-CuO contained mainly <100 nm particles and its structure was distinct from micro-CuO (Fig. S1A and B). The average hydrodynamic diameter (Dh) of nano-CuO suspension in deionised water ranged from 80 to 400 nm, with an average of 192.5 nm (Fig. S1C). In aminoacids-supplemented HMM medium the average particle size was increased till 385 nm (Table 2; Fig. S1D). This was likely caused by partial NPs agglomeration due to the mineral salts and aminoacids in HMM medium. However, by filtering the nano-CuO suspension in HMM media through 100 nm pore-sized filter and analysing the filtrate by DLS, we demonstrated that particles of <100 nm were still present (Table 2). The size distribution of micro-CuO was multimodal with the average Dh of 342.7 nm in deionized water and 617 nm in aminoacids-supplemented HMM medium (Table 2). A small fraction of nano-range particles was presented in micro-CuO suspension in deionized water (Fig. S1C) but not in its suspension in HMM medium (Table 2). The UV–Visible absorption spectra of nano-CuO (Fig. S1E) showed characteristic absorption peak at approximately 325 nm. No peak was observed in micro-CuO suspension as the particles settled very quickly. Thus, the nano-CuO used for further toxicological analysis was clearly distinct from micro-CuO.

3.2. Construction, characterization and calibration of sensor bacteria

E. coli K12::katGlux biosensor was constructed by fusing the promoter of *katG* (encoding catalase-peroxidase enzyme converting hydrogen peroxide to water) with bacterial bioluminescence-encoding genes – *luxCDABE* from *Photobacterium luminescens*. *KatG* gene is expressed in the presence of H₂O₂ in bacterial cell (Belkin et al., 1996) and thus, *E. coli* K12::katGlux biosensor was expected to be induced by this ROS. *E. coli* MC1061(pDEWrecAlux) biosensor was constructed by fusing the promoter of *recA* gene (part of bacterial SOS regulon) with *P. luminescens luxCDABE* genes. As *recA* is expressed in response to single-stranded lesions in DNA (Vollmer et al., 1997), this sensor was expected to respond to DNA damaging agents. In order to confirm the applicability and specificity of the newly constructed biosensors, their response to positive controls (H₂O₂; paraquat as a source of superoxide anions; mitomycin C (MMC) as a DNA damaging agent) and a negative control (3,5-dichlorophenol (3,5-DCP)) was measured.

Fig. 1A–C represent the dose-dependent change of bioluminescence in H₂O₂-inducible biosensor *E. coli* K12::katGlux after 2, 5 and 8-h exposure to target and non-target chemicals. Although the

Table 2
Characterization of CuO particles used in the current study.

Particle	Primary size, nm	Specific surface area, ^a m ² /g	Hydrodynamic size (average), ^b nm		
			Deionized water	HMM + 0.1% cas-aminoacids	
				Not filtered	After filtering (pore size 100 nm)
Nano-CuO	30	25.5	192.5	385	70.86
Micro-CuO	Not provided	0.64	342.7 ^c	617 ^c	Low count rate

^a Measured using BET (from Ivask et al., 2010).

^b Measured by dynamic light scattering (DLS).

^c Multimodal distribution, the average hydrodynamic size of all peaks is presented.

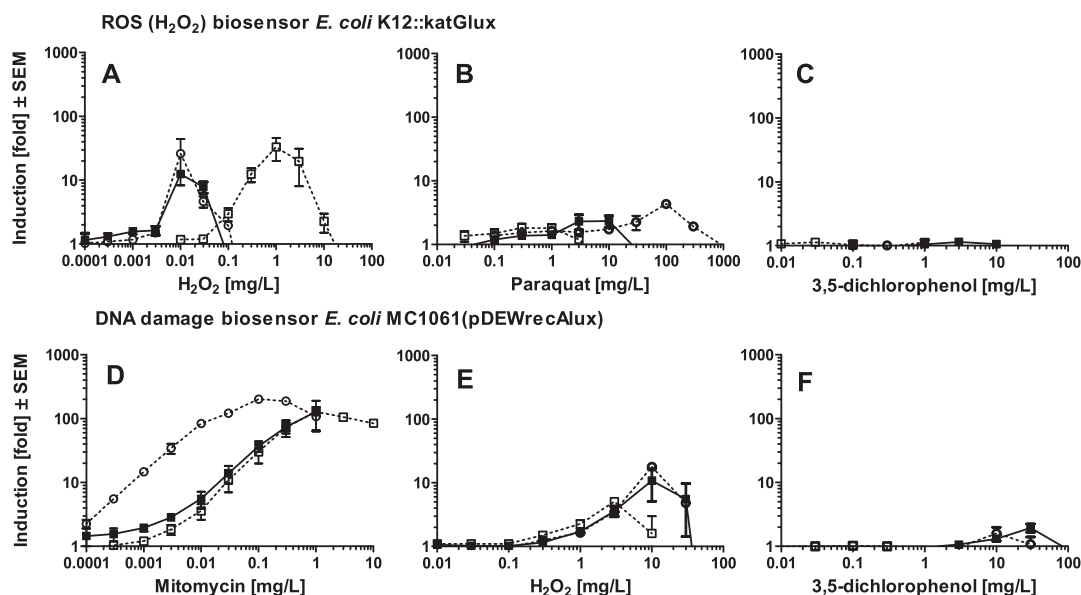


Fig. 1. Time-course response of the *Escherichia coli* based bioluminescent stress sensors to target and non-target chemicals. 2 h (□), 5 h (■) and 8 h (○) exposure time. A–C: induction of bioluminescence in ROS biosensor *E. coli* K12::katGlux by H_2O_2 (A), paraquat (B) and 3,5-dichlorophenol (C). D–F: induction of bioluminescence in DNA damage biosensor *E. coli* MC1061(pDEWrecAlux) by mitomycin C (D), H_2O_2 (E) and 3,5-dichlorophenol (F). Mean of 3 individual experiments \pm standard error of the mean is shown.

response of this biosensor to H_2O_2 was observed already after 10 min of exposure (data not shown), the LOD decreased with exposure time from 0.1 mg H_2O_2 /L at 2 h till 0.003 mg H_2O_2 /L at 5 and 8 h indicating that this biosensor was remarkably more sensitive to H_2O_2 after prolonged incubation (Fig. 1A). The 2-h LOD of *E. coli* K12::katGlux to H_2O_2 was comparable and even lower than that reported for *katG*-based biosensors previously (Belkin et al., 1996; Lee and Gu, 2003; Ahn et al., 2004). After 8 h of exposure, *E. coli* K12::katGlux was also slightly induced by paraquat, which may be considered as an indirect inducer of the *katG* gene (Fig. 1B). Paraquat produces mainly superoxide radicals, which may be further converted to H_2O_2 by intracellular superoxide dismutases. Expectedly, there was no induction of this biosensor by the negative control 3,5-DCP (Fig. 1C).

DNA damage biosensor *E. coli* MC1061(pDEWrecAlux) (Fig. 1D and F) was induced by mitomycin C (MMC) – a direct mutagen, which acts by covalent binding to DNA, and H_2O_2 – an indirect mutagen acting *via* oxidative damage of DNA. Induction of the sensor by MMC was already observed after 30 min of exposure (data not shown). The 2-h LOD of this biosensor to MMC was 0.01 mg/L (Fig. 1D), which was comparable to previously constructed *recA*-based biosensors (Vollmer et al., 1997; Davidov et al., 2000; Mitchell and Gu, 2004). With increasing exposure time (up to 8 h), sensitivity of DNA damage sensor to MMC increased. H_2O_2 induced the biosensor only at relatively high concentration (3 mg H_2O_2 /L) (Fig. 1E) and only after 1 h of incubation (Fig. 1E). Again, as expected, there was no induction of the sensor by negative control 3,5-DCP (Fig. 1F).

In summary, both constructed stress-specific biosensors were induced by direct and indirect inducers, whereas the response to the latter was weak and delayed. As most nanomaterials that need the toxicological characterization are probably weak inducers, the biosensor response to weak indirect inducers should be carefully evaluated.

3.3. ROS-generating and DNA-damaging potential and dissolution of CuO

Induction of ROS, DNA damage and dissolution of CuO nanoparticles at sub-toxic concentrations was analysed using biosensor bacteria *E. coli* K12::katGlux, *E. coli* MC1061(pDEWrecAlux) and *E. coli* MC1061 (pSLcuer/pDNpCopAlux), respectively. All the three biosensors were induced by all the studied Cu-formulations – nano and micro-sized CuO and CuSO₄ but showed differences in the response time (Fig. 2). While *E. coli* Cu-ion biosensor was already induced after 0.5 h of exposure to all three Cu formulations, induction of ROS biosensor started after 5 h and the induction of DNA damage biosensor started only after 8 h of exposure. Because such a long time was required for the induction of these biosensors, we assured that the growth of biosensors in Cu-supplemented samples didn't differ from the chemical free control samples. The enumeration of bacterial cells showed that the growth of bacteria in different samples was indeed comparable (data not shown).

The detailed response of biosensors to Cu formulations after 5 h (Cu ion and ROS biosensors) and 8 h (DNA damage biosensor) exposure is shown in Fig. 3. The dose–response pattern of ROS (Fig. 3D–F) and DNA damage-specific sensor bacteria (Fig. 3G–I) to different Cu formulations was similar to that of Cu ions biosensor (Fig. 3A–C). Particularly, the maximum bioluminescent response of all the three biosensors to soluble Cu salt was at 0.635 mg Cu/L (10^{-5} M), for nano-CuO at 6.35 mg Cu/L (10^{-4} M) and for micro-CuO at 635 mg Cu/L (10^{-2} M) (ratio of nominal concentrations 1:10:1000). As Cu ion biosensor is responding exclusively to Cu ions (Ivask et al., 2009) and the response pattern of ROS and DNA damage biosensors was very similar to that of Cu ion biosensor, we hypothesized that Cu ions solubilized from CuO particles triggered the ROS and DNA damage response.

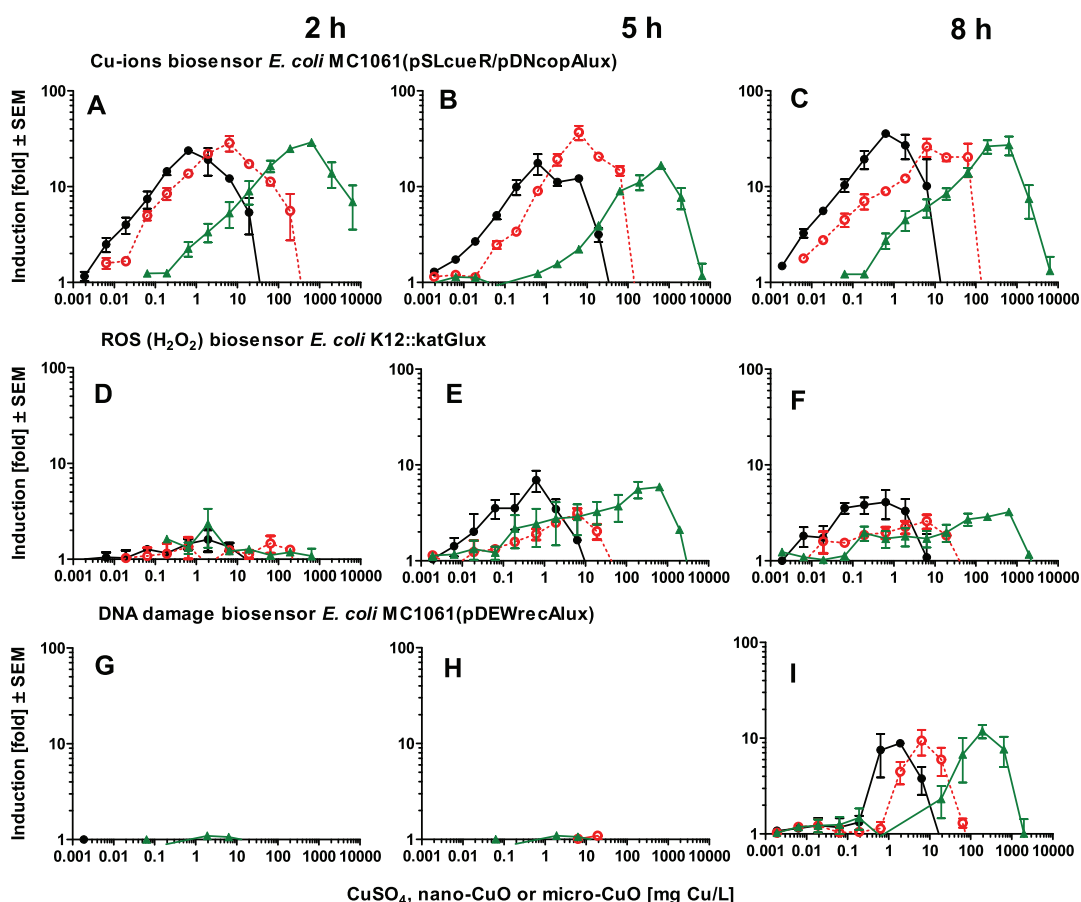


Fig. 2. Time-course response of *Escherichia coli* based bioluminescent sensors to different Cu formulations. Induction of *E. coli* MC1061(pSLcueR/pDNcopAlux) (A–C), ROS biosensor *E. coli* K12::katGlux (D–F) and DNA damage biosensor *E. coli* MC1061(pDEWrecAlux) (G–I) by CuSO₄ (●), nano-CuO (○) and micro-CuO (▲) for 2 (left panels), 5 (middle panels), and 8 (right panels) hours. Concentrations are presented on Cu basis (mg Cu/L). Mean of 3 individual experiments ± standard error of the mean is shown.

3.3.1. Chemical analysis of dissolved Cu

As Cu ions were 10-fold more potent inducers of biosensors compared to nano-CuO and 1000-fold more potent than micro-CuO, the solubility of nano-CuO could be around 10% and solubility of micro-CuO around 0.1%. To verify the results of biosensors, we measured the dissolved Cu at the concentrations where the sensors were equally (maximally) induced (0.635 mg Cu/L CuSO₄, 6.35 mg Cu/L nano-CuO and 635 mg Cu/L micro-CuO) by chemical analysis (AAS). We assumed that at chosen concentrations, Cu formulations should result in equal soluble Cu content if the biosensors responded exclusively to Cu ions. Indeed, in the beginning of the bioassay, 0.635 mg Cu/L CuSO₄, 6.35 mg Cu/L nano-CuO and 635 mg Cu/L micro-CuO all resulted in 0.635 mg of dissolved Cu/L (Fig. 4A). This confirmed that 10% of nano-CuO and 0.1% of micro-CuO were in the form of ionic Cu already at the beginning of the exposure and that ROS and DNA damage detected by the biosensors was indeed triggered by dissolved Cu.

As CuO particles may additionally dissolve during the test, we next determined by AAS the concentrations of soluble Cu in the biosensor test assay after 5-h and 8-h exposure. The analysis

showed that both nano-CuO and micro-CuO were additionally solubilized during the test and the concentration of soluble Cu in 6.35 mg Cu/L nano-CuO and 635 mg Cu/L micro-CuO increased from 0.6 till ~4 mg of soluble Cu/L (Fig. 4B). Based on CuSO₄ concentration–response curve (Fig. 2B, E and I) 4 mg of soluble Cu/L should already inhibit the bioluminescence of the biosensors. However, as such inhibition was not observed in case of 6.35 mg Cu/L nano-CuO and 635 mg Cu/L micro-CuO after 5-h exposure we suggest that at least part of dissolved Cu was not bioavailable to bacterial cells. It is important to note that the bioavailable fraction of Cu that is measured by bacterial sensors includes only free Cu ions (Rensing and Maier, 2003). On the other hand, dissolved Cu measured by AAS includes both, (i) free Cu ions and (ii) soluble Cu complexes (Cu ions complexed by components of the media or bacterial exudates). Thus, the fraction of dissolved Cu determined by AAS was significantly higher than the fraction of free Cu ions that entered the bacterial cells and caused toxic effects.

3.3.2. The role of Cu ions in biosensor response

To further differentiate between the role of dissolved copper and CuO particles in the response of the biosensors, we added

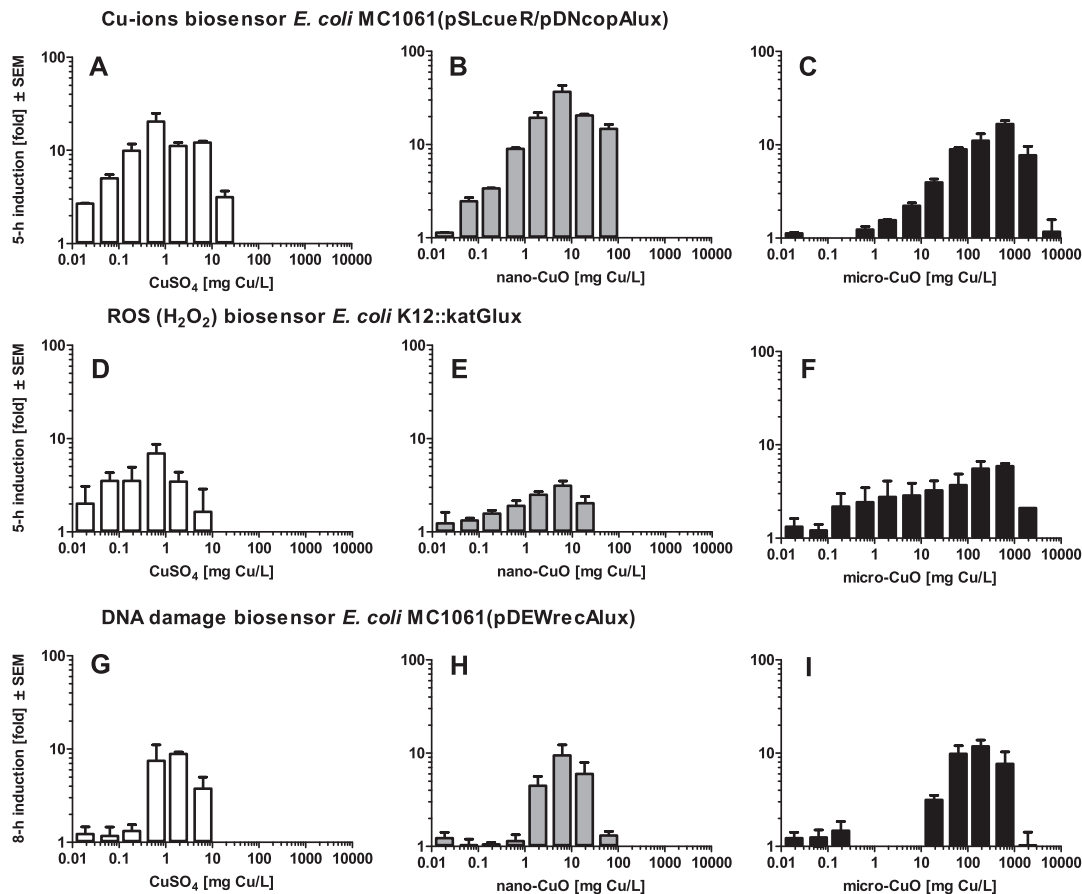


Fig. 3. Induction of bioluminescence in *Escherichia coli* based biosensors to different Cu formulations. Responses of Cu-ion biosensor *E. coli* MC1061(pSLcueR/pDNcopAlux) (A–C) and ROS biosensor *E. coli* K12::katGlux (D–F) after 5-h incubation and response of DNA damage biosensor *E. coli* MC1061(pDEWrecAlux) (G–I) after 8-h exposure to CuSO₄ (white bars), nano-CuO (grey bars) and micro-CuO (black bars). Mean of 3 individual experiments ± standard error of the mean is shown.

EDTA, a chelating agent that sequesters di- and trivalent metal ions (Iijima et al., 2007), to the Cu formulations and measured the response of biosensors. Three millimolar EDTA (the highest concentration that was not yet toxic to bacterial cells; data not

shown) – abolished the response of the biosensors (Fig. 5). This additionally confirmed that the observed ROS and DNA damage in bacterial cells were indeed caused by dissolved Cu ions and not by CuO particles themselves.

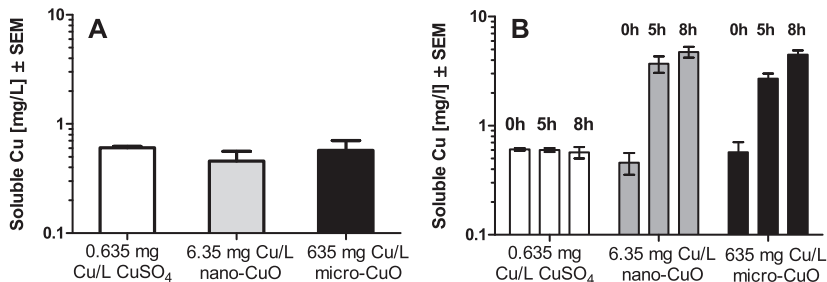


Fig. 4. Soluble Cu in the biosensor test media as determined by atomic absorption spectroscopy (AAS) after 0 (A) and 0–8 h (B) of exposure. AAS was performed from the particle-free supernatants (centrifugation at 30 000× g for 30 min) of CuSO₄ (white bars), nano-CuO (grey bars) and micro-CuO (black bars) at nominal concentrations of 0.635, 6.35 and 635 mg Cu/L, respectively. The concentrations yielding maximum response of the biosensors were chosen for the analysis.

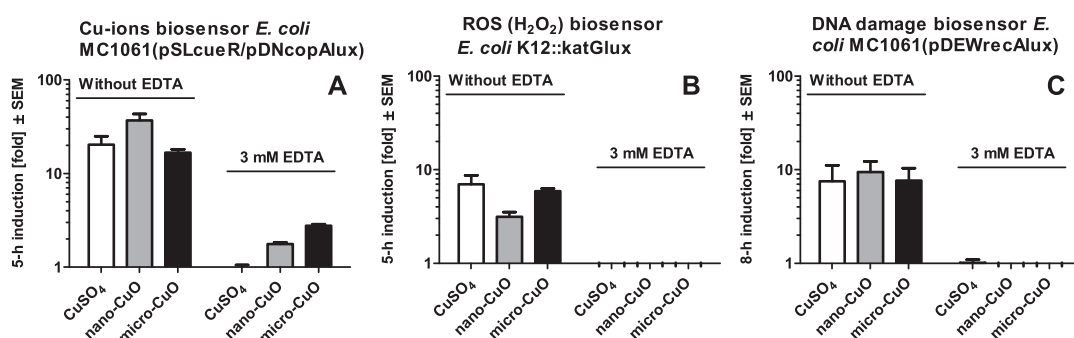


Fig. 5. Effect of addition of 3 mM EDTA on the induction of Cu ion-biosensor (A), ROS biosensor (B) and DNA damage biosensor (C) exposed to nano-CuO, micro-CuO and CuSO₄ at concentrations yielding maximum response of the sensors: 0.635 mg Cu/L (white bars); 6.35 mg Cu/L nano-CuO (grey bars) and micro-CuO (635 mg Cu/L; black bars).

3.3.3. Analysis of dissolved Cu using *Pseudomonas fluorescens*-based Cu-ion biosensor

E. coli is an important model in molecular biology with well described stress response mechanisms. However, when the potential release of nanoparticles to the environment is of concern, selection of a more environmentally relevant bacterium would be appropriate. *Pseudomonas* sp. is a species commonly present in soil. Therefore, we compared the responses of *E. coli* and *P. fluorescens* Cu-ion specific biosensors to different Cu formulations (Fig. 6). Similarly to *E. coli* (Fig. 3A–C), for the *P. fluorescens*-based Cu-biosensor the most potent inducer was CuSO₄, followed by nano-CuO and then micro-CuO. Despite of the fact that *P. fluorescens* Cu-biosensor was 30-times less sensitive to all Cu formulations than *E. coli* biosensor, it showed the same pattern of response with the maximum induction at 19.05 mg Cu/L in case of CuSO₄, 190.5 mg Cu/L in case of nano-CuO and ≥6350 mg Cu/L in case of micro-CuO. Thus, the solubility of nano-CuO predicted by *P. fluorescens* Cu-biosensor was similar to what was predicted by *E. coli* biosensor: 10% for nano-CuO and ≤0.3% for micro-CuO. The more accurate determination of dissolution of micro-CuO was not possible, since higher than 6350 mg Cu/L concentrations of micro-CuO were quenching around 95% of bioluminescence of *P. fluorescens* Cu-biosensor due to their black colour. This result confirms that solubility of CuO (both, nano and micro) determined with *E. coli* was also reproducible with the *P. fluorescens*-based Cu-ion biosensor and show that most probably also for other Gram-negative bacteria the ROS- and DNA-damaging effects of CuO nanoparticles are mediated by ionic Cu.

3.4. Possible mechanisms of action of CuO particles

Our results on Cu-ion dependent sub-toxic effects of CuO on *E. coli* and *P. fluorescens* are in good agreement with the data on general toxicity of nano-CuO to bacteria *Vibrio fischeri* (Heinlaan et al., 2008), *E. coli*, *Staphylococcus aureus* and *Listeria monocytogenes* (Cioffi et al., 2005). On the other hand, detection of hazardous properties of nano-CuO already at low sub-toxic level supplies new information for proactive approaches. The sensor bacteria applied in this study may be used for such an early warning purpose before the actual mortality and long term effects will appear. Additionally, the step-wise time-dependent activation of *E. coli* stress-inducible promoters (Fig. 2) offers a view into the bacterial defence systems involved in the response to nano-CuO exposure. Among all biosensors, the most rapid response to nano-CuO was observed with the Cu-ion biosensor *E. coli* MC1061(pSLcueR/pDNPcopAlux), which indicates rapid activation of *copA* promoter. *CopA* is an ATPase responsible for the transport of Cu ions between cytosol and periplasm of *E. coli* (Rensing and Grass, 2003) and early activation of *copA* promoter during exposure to nano-CuO indicates that dissolved Cu ions entered bacterial cell very rapidly. Interestingly, the response pattern of Cu-ion biosensor to all studied Cu formulations during the 2–8-h incubation time remained similar (Fig. 2A–C). This suggested that the intracellular level of Cu (from CuSO₄ but also from both CuO formulations) was maintained constant. Despite that, the ROS biosensor was induced only after 5-h of exposure (Fig. 2D and E). Given the *E. coli*'s capability for rapid gene induction, it is highly probable that the level of intracellular ROS produced during the first hours of

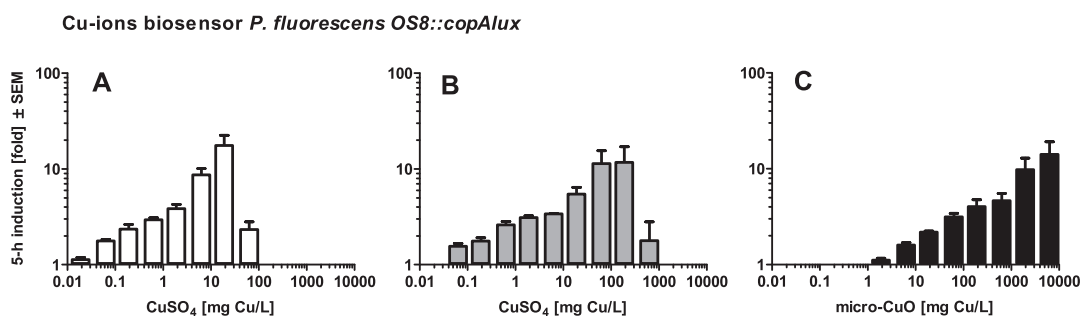
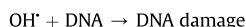
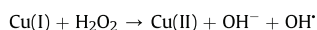
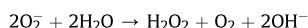
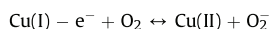


Fig. 6. Induction of bioluminescence in *Pseudomonas fluorescens* Cu-ion biosensor to CuSO₄ (A), nano-CuO (B) and micro-CuO (C) after 5 h of exposure. Concentrations are presented on Cu basis (mg Cu/L). Mean of 3 individual experiments ± standard error of the mean is shown.

exposure was not sufficient to activate bacterial ROS defence system. This is not surprising because the studied nominal concentration of nano-CuO was relatively low (6.35 mg Cu/L). For comparison, Karlsson et al. (2008) detected ROS at 80 mg/L nano-CuO but not at 40 mg/L nano-CuO in mammalian cell cultures, whereas both nano-CuO concentrations were already very toxic to the cells (about 90% cytotoxicity). These facts may indicate that at least during the early exposure (till 2 h), the intracellular ROS was probably not the primary cause of the toxicity of studied Cu formulations. For example, it was recently shown that in *E. coli* Cu ions have an acute mechanism of toxicity that does not involve ROS and act through the inhibition of enzymes involved in the synthesis of branched-chain aminoacids (Macomber and Imlay, 2009).

The accumulation of intracellular ROS after prolonged exposure to low sub-toxic concentrations of Cu formulations may be explained by Cu ion compartmentalization in the bacterial cell and Cu chemistry. It has been previously shown that ROS are produced during reoxidation reaction of Cu(I) to Cu(II) in the following Cu recycling redox system (essentially as in Hoshino et al., 1999; Macomber et al., 2007):



As in the case of Gram-negative bacteria the main pool of intracellular Cu ions is located in the periplasm (Outten et al., 2001), the ROS are mainly produced and get concentrated in the periplasm and do not reach the cytosolic targets (Macomber et al., 2007). The high level accumulation of ROS in the periplasm may however lead to their leakage into the cytosol where they turn on the ROS defence systems, including *katG*. Reoxidation of Cu(I) to Cu(II) generates ROS in the following order: first the superoxide anion is produced and then hydrogen peroxide and hydroxyl radicals will appear (Hoshino et al., 1999). This order of ROS is in accordance with our biosensor results: our previous results have shown that superoxide anions-sensing *sodA*-based luminescent *E. coli* K12::*soxRSsodAlux* was activated by nano-CuO after 2 h of induction (Ivask et al., 2010) but the peroxide-sensing strain K12::*katGlux* in the current study was induced only after 5 h of induction (Fig. 2). Finally, the DNA-damage sensor responded to nano-CuO only after 8-h exposure. Seemingly, the observed DNA-damaging effects were secondary and transient (e.g., due to the RecA-dependent efficient repair of DNA) as CuSO₄ has been classified not mutagenic in the bacterial reversed mutation (Ames) assay according to various available Material Safety Data Sheets (Merck, 2010). Analogously, Macomber et al. (2007) showed that copper ions induced the superoxide dismutase and catalase but did not catalyse significant oxidative DNA damage in *E. coli*.

Based on the previous studies on Cu ion chemistry and time-dependent activation of our biosensor suite, we assume that Cu ions dissolved from nano-CuO are the key factor triggering a series of downstream adverse effects. We suggest a following hypothetical cascade of events: the internalised Cu ions are mainly stored in the periplasm (Outten et al., 2001), where they first induce the production of superoxide anions (Hoshino et al., 1999). Superoxide anions leach into the cytosol, where they activate superoxide-dismutase gene *sodA*. Intracellular SodA and other superoxide dismutases convert superoxide to H₂O₂ that triggers the activation of catalases, e.g., *KatG*. Finally, cytosolic H₂O₂ induces Fe-dependent production of hydroxyl radicals via Fenton reaction (Imlay et al.,

1988) which leads to the unspecific oxidation of various biomolecules including DNA, which activates ssDNA-inducible gene *recA*. Similar sub-toxic cellular responses such as increased activity of catalase, superoxide dismutase and overexpression of Rad51 (RecA homologue in mammals) were also shown in human lung epithelial cells *in vitro* after 24-h incubation with 50 mg/L nano-CuO (Ahamed et al., 2010). DNA damage in response to nano-CuO was also observed in mammalian cells (Midander et al., 2009) and in various plants (Nelson et al., 2012). Thus, our results are coherent with the existing data and to our best knowledge, show for the first time that (i) nano-CuO induces the bacterial ROS and DNA damage defence systems already at very low sub-toxic levels and (ii) these early adverse effects are triggered by dissolved Cu ions. Our results on solubility-dependent toxicity of nano-CuO can be possibly extended to some other unicellular organisms that (i) have no endocytosis and (ii) are *a priori* protected against the nanoparticles entry by the cell wall. However, the described mechanism is most probably not relevant for the most eukaryotic cells capable to internalize the nano-sized particles.

4. Conclusions

As CuO nanoparticles showed adverse effects to bacteria already at very low concentrations and these effects were triggered by the solubilized copper ions, we suggest that dissolution of CuO nanoparticles should be addressed also on Material Safety Data Sheets. For example, the MSDS for 50 nm CuO preparation at Sigma–Aldrich website (reference number 544868) provides no indication on dissolution of these nanoparticles.

Finally, with some refinement, such as choosing/constructing the metal-sensing bacterial strains, depending on the type of metallic NPs analysed, the testing strategy applied in this study is also applicable for the high throughput profiling of (eco)toxicological properties of other (metallic) NPs.

Acknowledgements

This study was supported by projects SF0222601Bs03, ETF6974 and ETF8561, ESF and FP7 project NanoValid (contract No 263147). Prof. Shimshon Belkin is acknowledged for the plasmid pDEW201.

Appendix A. Supplementary material

Supplementary material associated with this article can be found, in the online version, at doi:10.1016/j.envpol.2012.05.009.

References

- Ahamed, M., Siddiqui, M.A., Akhtar, M.J., Ahmad, I., Pant, A.B., Alhadlaq, H.A., 2010. Genotoxic potential of copper oxide nanoparticles in human lung epithelial cells. *Biochem. Biophys. Res. Commun.* 396, 578–583.
- Ahn, J.M., Mitchell, R.J., Gu, M.B., 2004. Detection and classification of oxidative damaging stresses using recombinant bioluminescent bacteria harboring *sodA::pqi::* and *katG::luxCDABE* fusions. *Enzyme Microb. Technol.* 35, 540–544.
- Aruoja, V., Dubourguier, H.C., Kasemets, K., Kahru, A., 2009. Toxicity of nanoparticles of CuO, ZnO and TiO₂ to microalgae *Pseudokirchneriella subcapitata*. *Sci. Total Environ.* 407, 1461–1468.
- Baek, Y.W., An, Y.J., 2011. Microbial toxicity of metal oxide nanoparticles (CuO, NiO, ZnO, and Sb₂O₃) to *Escherichia coli*, *Bacillus subtilis* and *Streptococcus aureus*. *Sci. Total Environ.* 409, 1603–1608.
- Belkin, S., Smulski, D.R., Vollmer, A.C., Van Dyk, T.K., LaRossa, R.A., 1996. Oxidative stress detection with *Escherichia coli* harboring a *katG::lux* fusion. *Appl. Microbiol. Biotechnol.* 62, 2252–2256.
- Blinova, I., Ivask, A., Heinlaan, M., Mortimer, M., Kahru, A., 2010. Ecotoxicity of nanoparticles of CuO and ZnO in natural water. *Environ. Pollut.* 158, 41–47.
- Cioffi, N., Torsi, L., Ditaranto, N., Tantillo, G., Ghibelli, L., Sabbatini, L., Blev-Zacheo, T., D'Alessio, M., Zamboni, P.G., Traversa, E., 2005. Copper nanoparticle/polymer composites with antifungal and bacteriostatic properties. *Chem. Mater.* 17, 5255–5262.

- Davidov, Y., Rozen, R., Smulski, D.R., Van Dyk, T.K., Vollmer, A.C., Elsemore, D.A., LaRossa, R.A., Belkin, S., 2000. Improved bacterial SOS promoter: lux fusions for genotoxicity detection. *Mutat. Res.* 46, 97–107.
- Ebrahimi-Bajestan, E., Niazmand, H., Duangthongsuk, W., Wongwises, S., 2011. Numerical investigation of effective parameters in convective heat transfer of nanofluids flowing under a laminar flow regime. *Int. J. Heat Mass Transfer* 54, 4376–4388.
- European Chemicals Bureau, 2006. Manual of Decisions (MoD) to Directive 67/548/EEC, Amendment 92/93.
- Fahmy, B., Cormier, S.A., 2009. Copper oxide nanoparticles induce oxidative stress and cytotoxicity in airway epithelial cells. *Toxicol. In Vitro* 23, 1365–1371.
- Gabbay, J., Borkow, G., Mishal, J., Magen, E., Zatzoff, R., Shemer-Avni, Y., 2006. Copper oxide impregnated textiles with potent biocidal activities. *J. Ind. Textil.* 35, 323–335.
- Gou, N., Onnis-Hayden, A., Gu, A.Z., 2010. Mechanistic toxicity assessment of nanomaterials by whole-cell-array stress genes expression analysis. *Environ. Sci. Technol.* 44, 5964–5970.
- Griffitt, R.J., Weil, R., Hyndman, K.A., Denslow, N.D., Powers, K., Taylor, D., Barber, D.S., 2007. Exposure to copper nanoparticles causes gill injury and acute lethality in zebrafish (*Danio rerio*). *Environ. Sci. Technol.* 41, 8178–8186.
- Heinlaan, H., Ivask, A., Blinova, I., Dubouguier, H.C., Kahru, A., 2008. Toxicity of nanosized and bulk ZnO, CuO and TiO₂ to bacteria *Vibrio fischeri* and crustaceans *Daphnia magna* and *Thamnocephalus paltryus*. *Chemosphere* 71, 1308–1316.
- Hoshino, N., Kimura, T., Yamaji, A., Ando, T., 1999. Damage to the cytoplasmic membrane of *Escherichia coli* by catechin-copper (II) complexes. *Free Radic. Biol. Med.* 27, 1245–1250.
- Hwang, E.T., Lee, J.H., Chae, Y.J., Kim, Y.S., Kim, B.C., Sang, B.I., Gu, M.B., 2008. Analysis of the toxic mode of action of silver nanoparticles using stress-specific bioluminescent bacteria. *Small* 4, 746–750.
- Iijima, M., Sato, N., Tsukada, M., Kamiya, H., 2007. Dispersion behavior of barium titanate nanoparticles prepared by using various polycarboxylic dispersants. *J. Am. Ceram. Soc.* 90, 2741–2746.
- Imlay, J.A., Chin, S.M., Linn, S., 1988. Toxic DNA damage by hydrogen peroxide through the Fenton reaction *in vivo* and *in vitro*. *Science* 240, 640–642.
- Ivask, A., Bondarenko, O., Jephthina, N., Kahru, A., 2010. Profiling of the reactive oxygen species-related ecotoxicity of CuO, ZnO, TiO₂, silver and fullerene nanoparticles using a set of recombinant luminescent *Escherichia coli* strains: differentiating the impact of particles and solubilised metals. *Anal. Bioanal. Chem.* 398, 701–716.
- Ivask, A., Rõlova, T., Kahru, A., 2009. A suite of recombinant luminescent bacterial strains for the quantification of bioavailable heavy metals and toxicity testing. *BMC Biotechnol.* 9, 41.
- Kahru, A., Dubouguier, H.C., 2010. From ecotoxicology to nanoecotoxicology. *Toxicology* 269, 105–119.
- Karlsson, H.L., Cronholm, P., Gustafsson, J., Möller, L., 2008. Copper oxide nanoparticles are highly toxic: a comparison between metal oxide nanoparticles and carbon nanotubes. *Chem. Res. Toxicol.* 21, 1726–1732.
- LaRossa, R.A., Smulski, D.R., Van Dyk, T.K., 1995. Interaction of lead nitrate and cadmium chloride with *Escherichia coli* K-12 and *Salmonella typhimurium* global regulatory mutants. *J. Ind. Microbiol.* 14, 252–258.
- Lee, H.J., Gu, M.B., 2003. Construction of a *sodA::luxCDABE* fusion *Escherichia coli*: comparison with a katG fusion strain through their responses to oxidative stresses. *Appl. Microbiol. Biotechnol.* 60, 577–580.
- Leedjäv, A., Ivask, A., Virta, M., Kahru, A., 2006. Analysis of bioavailable phenols from natural samples by recombinant luminescent bacterial sensors. *Chemosphere* 64, 1910–1919.
- Macomber, L., Rensing, C., Imlay, J.A., 2007. Intracellular copper does not catalyze the formation of oxidative DNA damage in *Escherichia coli*. *J. Bacteriol.* 189, 1616–1626.
- Macomber, L., Imlay, J.A., 2009. The iron-sulfur clusters of dehydratases are primary intracellular targets of copper toxicity. *Proc. Natl. Acad. Sci. U. S. A.* 106, 8344–8349.
- Merck, 2010. Safety Data Sheet According to Regulation (EC) No. 1907/2006. http://www.alsglobal.eu/docs/eng_20100526_msd_suso4_en.pdf.
- Midander, K., Cronholm, P., Karlsson, H.L., Elihn, K., Möller, L., Leygraf, C., Wallinder, I.O., 2009. Surface characteristics, copper release, and toxicity of nano- and micrometer-sized copper and copper(II) oxide particles: a cross-disciplinary study. *Small* 5, 389–399.
- Mitchell, R.J., Gu, M.B., 2004. An *Escherichia coli* biosensor capable of detecting both genotoxic and oxidative damage. *Appl. Microbiol. Biotechnol.* 64, 46–52.
- Nel, A., Xia, T., Mädlar, L., Li, N., 2006. Toxic potential of materials at the nanolevel. *Science* 311, 622–662.
- Nelson, B.C., Atha, D., Wang, H., Petersen, E.J., Cleveland, D., Holbrook, R.D., Jaruga, P., Dizdaroğlu, M., Xing, B., 2012. Copper oxide nanoparticle mediated DNA damage in terrestrial plant models. *Environ. Sci. Technol.* 46, 1819–1827.
- Outten, F.W., Huffman, D.L., Hale, J.A., O'Halloran, T.V., 2001. The independent *cue* and *cus* systems confer copper tolerance during aerobic and anaerobic growth in *Escherichia coli*. *J. Biol. Chem.* 276, 30670–30677.
- Ren, G., Hu, D., Cheng, E.W.C., Vargas-Reus, M.A., Reip, P., Allaker, R.P., 2009. Characterisation of copper oxide nanoparticles for antimicrobial applications. *Int. J. Antimicrob. Agents* 33, 587–590.
- Rensing, C., Grass, G., 2003. *Escherichia coli* mechanisms of copper homeostasis in a changing environment. *FEMS Microbiol. Rev.* 27, 197–215.
- Rensing, C., Maier, M., 2003. Issues underlying use of biosensors to measure metal bioavailability. *Ecotoxicol. Environ. Saf.* 56, 140–147.
- Ruparelia, J.P., Chatterjee, A.K., Duttgupta, S.P., Mukherji, S., 2008. Strain specificity in antimicrobial activity of silver and copper nanoparticles. *Acta Biomater.* 4, 707–716.
- Sambrook, J., Fritsch, E.F., Maniatis, T., 1989. *Molecular Cloning. A Laboratory Manual*. Cold Spring Harbour Laboratory Press, New York.
- Thomas, K.V., Brooks, S., 2010. The environmental fate and effects of antifouling paint biocides. *Biofouling* 26, 73–88.
- Vollmer, A.C., Belkin, S., Smulski, D.R., Van Dyk, T.K., LaRossa, R.A., 1997. Detection of DNA damage by use of *Escherichia coli* carrying *recA::lux*, *uvrA::lux* or *alkA::lux* reporter plasmids. *Appl. Env. Microbiol.* 63, 2566–2571.
- Wu, B., Huang, R., Sahu, M., Feng, X., Biswas, P., Tang, Y.J., 2010. Bacterial responses to Cu-doped TiO₂ nanoparticles. *Sci. Total Environ.* 408, 1755–1758.

Supplementary data for:

Sub-toxic effects of CuO nanoparticles on bacteria: kinetics, role of Cu ions and possible mechanisms of action

by *Olesja Bondarenko*^{a,b,*}, *Angela Ivask*^a, *Aleksandr Käkinen*^{a,c}, *Anne Kahru*^{a,*}

^a Laboratory of Molecular Genetics, National Institute of Chemical Physics and Biophysics,
Akadeemia tee 23, Tallinn 12618, Estonia

^b Department of Gene Technology, Tallinn University of Technology, Akadeemia tee 15, Tallinn,
12618, Estonia

^c Department of Chemical and Materials Technology, Tallinn University of Technology,
Ehitajate tee 5, Tallinn 19086, Estonia

Contains the description of construction of reactive oxygen species and DNA damage-inducible biosensors and 1 Figure.

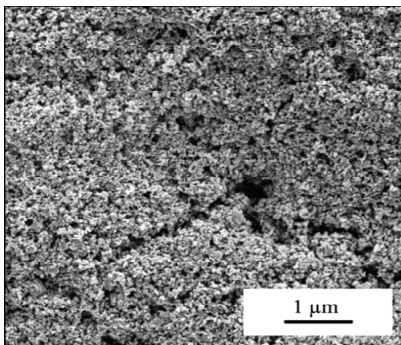
Construction of reactive oxygen species (ROS) and DNA damage-inducible biosensors

The ROS-inducible strain *E. coli* K12::katGlux was constructed by amplifying the 283-bp *katG* promoter from the genomic DNA of *E. coli* K12 (primers: 5' TATACCTAGGAATGAG GCGGGAAA ATAAGGT 3' and 5' TTAAGGATCCCATCAATGTGCTCCCCACTA 3'), digesting the amplified DNA with *Bam*HI and *Avr*II, and ligating it into *Bam*HI–*Avr*II-digested plasmid pSLlux, in front of the *luxCDABE* genes. The resulting plasmid was digested with *Avr*II and *Nhe*I and the fragment containing *katG* promoter and *luxCDABE* was gel-purified, Klenow-treated and inserted into *Stu*I site of pTCRKn (transposon-carrying suicide plasmid, Ivask et al., 2009). Tn5 mini-transposon mutagenesis method (De Lorenzo and Timmis, 1994) was used to create a single chromosomal insertion of the *katG* promoter-*luxCDABE* fusion into *E. coli* K12 chromosome. *E. coli* MC1061(pDEWrecAlux) was constructed by inserting the 164-bp *recA* promoter (amplified from the genomic DNA of *E. coli* K12 with primers 5' ATATGAATTCCATGCCGGGTAATACCGGATA3' and 5' AATTGGATCCACCGTGATG-CGGTGCGTCGTC 3') into the *Eco*RI-*Bam*HI site in front of the *luxCDABE* genes of plasmid pDEW201 (LaRossa et al., 1998).

De Lorenzo, V., Timmis, K.N., 1994. Analysis and construction of stable phenotypes in gram-negative bacteria with Tn5- and Tn10-derived minitransposons. *Methods Enzymol.* 235, 386–405.

LaRossa, A., Van Dyk, T., Rosson, R.A., 1998. *Bioluminescence Methods and Protocols: Photorhabdus luminescens luxCDABE Promoter Probe Vectors*, vol. 102. Humana Press Inc., pp. 85–90.

A: nano-CuO



B: micro-CuO

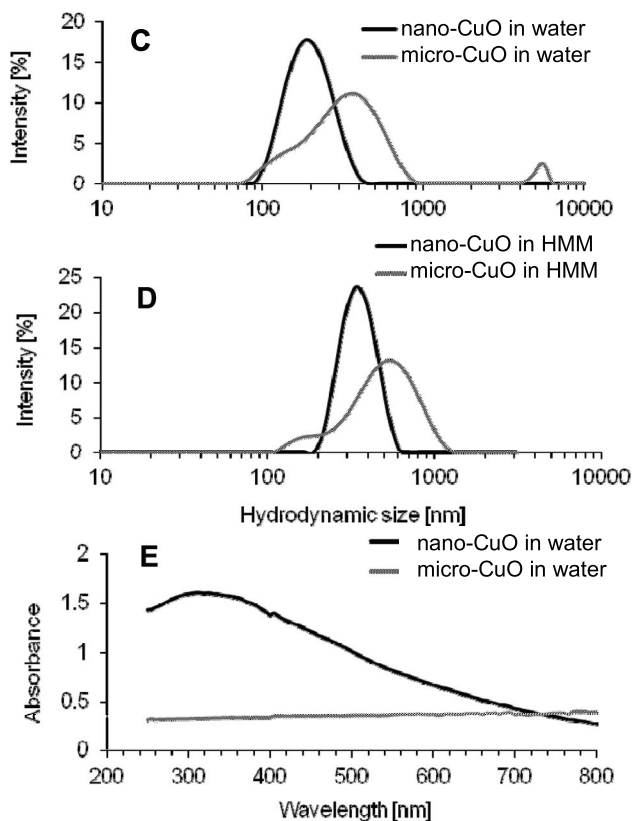
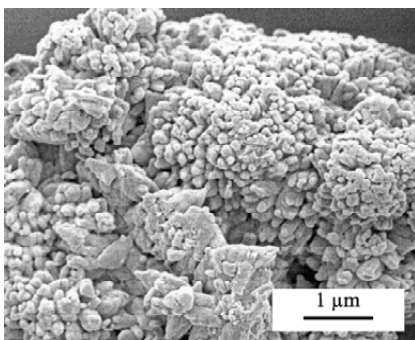


Fig. S1. A-B: SEM images of nano-CuO and micro-CuO (20 000x magnification). C-D: Hydrodynamic diameter of nano-CuO (6.35 mg Cu/L) and micro-CuO (635 mg Cu/L) in deionised water (C) and heavy metal MOPS medium (D). E: UV-Visible absorption spectra of nano-CuO (63.5 mg Cu/L) and micro-CuO (6350 mg Cu/L).

PUBLICATION III

Bondarenko O, Ivask A, **Käkinen A**, Kurvet I, Kahru A (2013). Particle-cell contact enhances antibacterial activity of silver nanoparticles. PLoS ONE, 8(5), e64060

Particle-Cell Contact Enhances Antibacterial Activity of Silver Nanoparticles

Olesja Bondarenko^{1*}, Angela Ivask¹, Aleksandr K  inen^{1,2}, Imbi Kurvet¹, Anne Kahru¹

1 Laboratory of Environmental Toxicology, National Institute of Chemical Physics and Biophysics, Tallinn, Estonia, **2** Department of Chemical and Materials Technology, Tallinn University of Technology, Tallinn, Estonia

Abstract

Background: It is generally accepted that antibacterial properties of Ag nanoparticles (AgNPs) are dictated by their dissolved fraction. However, dissolution-based concept alone does not fully explain the toxic potency of nanoparticulate silver compared to silver ions.

Methodology/Principal Findings: Herein, we demonstrated that the direct contact between bacterial cell and AgNPs' surface enhanced the toxicity of nanosilver. More specifically, cell-NP contact increased the cellular uptake of particle-associated Ag ions – the single and ultimate cause of toxicity. To prove that, we evaluated the toxicity of three different AgNPs (uncoated, PVP-coated and protein-coated) to six bacterial strains: Gram-negative *Escherichia coli*, *Pseudomonas fluorescens*, *P. putida* and *P. aeruginosa* and Gram-positive *Bacillus subtilis* and *Staphylococcus aureus*. While the toxicity of AgNO₃ to these bacteria varied only slightly (the 4-h EC₅₀ ranged from 0.3 to 1.2 mg Ag/l), the 4-h EC₅₀ values of protein-coated AgNPs for various bacterial strains differed remarkably, from 0.35 to 46 mg Ag/l. By systematically comparing the intracellular and extracellular free Ag⁺ liberated from AgNPs, we demonstrated that not only extracellular dissolution in the bacterial test environment but also additional dissolution taking place at the particle-cell interface played an essential role in antibacterial action of AgNPs. The role of the NP-cell contact in dictating the antibacterial activity of Ag-NPs was additionally proven by the following observations: (i) separation of bacterial cells from AgNPs by particle-impermeable membrane (cut-off 20 kDa, ~4 nm) significantly reduced the toxicity of AgNPs and (ii) *P. aeruginosa* cells which tended to attach onto AgNPs, exhibited the highest sensitivity to all forms of nanoparticulate Ag.

Conclusions/Significance: Our findings provide new insights into the mode of antibacterial action of nanosilver and explain some discrepancies in this field, showing that "Ag-ion" and "particle-specific" mechanisms are not controversial but, rather, are two faces of the same coin.

Citation: Bondarenko O, Ivask A, K  inen A, Kurvet I, Kahru A (2013) Particle-Cell Contact Enhances Antibacterial Activity of Silver Nanoparticles. PLoS ONE 8(5): e64060. doi:10.1371/journal.pone.0064060

Editor: Yang Gan, Harbin Institute of Technology, China

Received: January 14, 2013; **Accepted:** April 8, 2013; **Published:** May 30, 2013

Copyright:   2013 Bondarenko et al. This is an open-access article distributed under the terms of the Creative Commons Attribution License, which permits unrestricted use, distribution, and reproduction in any medium, provided the original author and source are credited.

Funding: This research was supported by the Estonian target funding project SF0690063s08, ETF8561 and ETF9347 grants, European Social Fund and EU 7th Framework Programme under grant agreement no. 263147 (NanoValid). The funders had no role in study design, data collection and analysis, decision to publish, or preparation of the manuscript.

Competing Interests: The authors have declared that no competing interests exist.

* E-mail: olesja.bondarenko@kbfi.ee

Introduction

Ag nanoparticles (AgNPs) are the first commercialized NPs that are nowadays used as broad-spectrum antimicrobials in over 300 consumer products including cosmetics, clothing, detergents, dietary supplements, water filters, electronics and children's toys [1], [2]. Actually, colloidal silver, e.g., protein-stabilized nanosized Ag particles, has been used for numerous medical purposes already since the late 19th century [3], [4]. To date, approximately 500 tons of nanosilver is produced annually and there is a high risk for environmental pollution [5] due to its leaching from the nanosilver-containing consumer products as well as through industrial waste streams, mainly *via* waste and sewage treatment plants [6], [7], [8]. Currently, most of the studies on nanosilver toxicity to bacteria focus on a laboratory model bacterium *Escherichia coli* and on human pathogens such as *Staphylococcus aureus* and *Pseudomonas aeruginosa*. Remarkably less information is

available for environmentally relevant bacterial species such as *Pseudomonas putida* and *P. fluorescens* (Figure S1).

Despite of numerous publications, the antimicrobial mechanism of AgNPs is still under debate. It is generally acknowledged that the size and the specific surface area affect the antibacterial activity of AgNPs [9], [10]. More specifically, recent publications have revealed that the toxicity of AgNPs to *E. coli* is proportional to the relative surface area of silver oxide monolayers, which dissolve and release Ag ions upon contact with water [11]. Accordingly, AgNPs lacking oxidized surfaces (and thus, not dissolving) proved not toxic to bacterial cells, suggesting that the toxicity of AgNPs is ultimately dictated by released Ag ions [12], [13].

In contrast, numerous studies have found that Ag⁺ concentrations released from AgNPs into the soluble phase during toxicity assays were too low to explain the observed antibacterial effects [14], [15], [16], [17], [18], [19]. As a rule, in these assays the dissolution of AgNPs was quantified by atomic absorption spectroscopy (AAS) or inductively coupled plasma spectrometry

(ICP) after the separation of nanoparticulate Ag by ultracentrifugation or ultrafiltration. The toxicity of residual soluble Ag in the supernatant/filtrate was further compared with the toxicity of Ag ion applied as a soluble salt. Such an experimental setup assumes that Ag ions are equally distributed outside of bacteria (i.e., in the test medium) and inside the bacterial cells and that the bioavailability of Ag ions to bacterial cells from the surface of AgNPs and from the aqueous phase is similar.

Hereby we hypothesized that AgNPs, even if not toxic *per se*, may serve as efficient carriers of toxic Ag ions. Using a suite of six Gram-positive and Gram-negative bacterial strains, three types on AgNPs with different coatings and three different techniques to determine the dissolution of these AgNPs, we demonstrated the significance of the direct contact between bacterium and NPs' surface. We showed for the first time and quantitatively that the intracellular bioavailable fraction and hence, toxicity of Ag ions from AgNPs could not be always predicted from the conventional studies that measure extracellular dissolution. Rather, the intracellular concentration of silver ions inside the bacterial cells – the ultimate determinant of AgNPs toxicity – was dictated by both, extracellular dissolution of AgNPs and additional dissolution at bio-nano interface. Thus, our results aim to resolve the main controversy behind the Ag ion-related toxicity mechanism of silver nanoparticles.

Materials and Methods

Chemicals and Nanoparticles

All the purchased chemicals were at least of analytical grade. AgNO₃ was from J.T.Baker, uncoated AgNPs (nAg, primary size 30–100 nm) were from Sigma-Aldrich (CAS number 7440-22-4), protein (casein)-coated colloidal AgNPs (nAg-Col, primary size 5–30 nm; [20]) were from Laboratorios Argenol S. L. (batch N° 297). The manufacturer-provided characteristics of nAg-Col were verified: (i) molecular weight of the casein coating was confirmed using UPLC size exclusion chromatography, which identified homogeneous a 5 kDa protein and (ii) the concentration of casein coating was verified using Pierce BCA Protein Assay Kit (Thermo Scientific) (data not shown). Polyvinylpyrrolidone-coated AgNPs (nAg-PVP, primary size 8–11 nm) were synthesized and characterized as described in [21].

The stock solutions of all Ag formulations (1 000 mg Ag/l, 20 ml) were prepared in distilled (DI) water (pH = 5.8) and further stored in the dark at +4°C. The stock solutions of nAg and nAg-PVP were homogenized using ultrasonic probe (40 W, 3 minutes; 450 Ultrasonifier, Branson Ultrasonics Corporation, USA) once after preparation.

The primary particles of AgNPs were visualized by transmission electron microscopy (TEM, SUMY-SELMi, EM-125) and the particle size was measured using ImageJ software. Size distribution of AgNPs (Figure S2) was calculated based on 65 particles. Hydrodynamic size (at ζ -average) and ζ -potential of AgNPs were measured at a concentration of 100 mg/l immediately after AgNPs' dispersion in DI water and in the bacterial growth medium using Malvern Zetasizer (Nano-ZS, Malvern Instruments, UK).

Quantification of Dissolved Silver

The dissolution of AgNPs in DI water as well in the bacterial growth medium was measured using three different techniques that enable to determine the extracellular free Ag⁺, extracellular dissolved Ag and intracellular Ag⁺. **Extracellular free Ag⁺** was measured from the suspensions of AgNPs with Ag-ion selective electrode (Ag-ISE) (Van London-pHoenix Company). **Extracel-**

lular dissolved Ag was determined from the supernatants that were obtained after ultracentrifugation of AgNPs' suspensions at 390 000 g for 60 minutes. According to the calculations, under these conditions all AgNPs and Ag-protein complexes with the molecular mass above 5 kDa should settle [22]. The supernatants were analyzed by atomic absorption spectroscopy (AAS) in a certified laboratory of Tallinn University of Technology, Estonia, applying the standard EVS-EN ISO/IEC 17025:2005. **Intracellular Ag⁺** from AgNPs was quantified with recombinant bioluminescent *Escherichia coli* MC1061 (pSLcueR/pDNPcopAlux) Ag-biosensor [23] as described below.

Bacterial Growth Inhibition Assay

For the growth inhibition assay bacteria (Gram-negative *Escherichia coli* MC1061, *Pseudomonas fluorescens* OS8, *P. putida* KT2440, *P. aeruginosa* DS10-129 and Gram-positive *Bacillus subtilis* BR151 and *Staphylococcus aureus* RN2440; Table S1) were cultivated overnight on a shaker (200 rpm, 30°C) in 3 ml of modified (NaCl-free) LB medium (10 g tryptone and 5 g yeast extract *per* liter, pH = 7). NaCl was not added to the medium to avoid the formation of insoluble AgCl. Before the test, bacterial culture was diluted in NaCl-free LB medium to OD₆₀₀ = 0.05 corresponding to approximately 10⁶ cells/ml. Bacterial growth inhibition assay was conducted on transparent sterile 96-well Cliniplates (Thermo Labsystems). Briefly, 100 μ l of the dilution of AgNPs or AgNO₃ (from 0.01 to 100 mg Ag/l) in DI water (sample) or pure DI water (control) was pipetted onto the wells. Then, 100 μ l of bacterial culture in NaCl-free LB medium was added. The test plates were incubated on a plate shaker (Heidolph Titramax 1000, 350 rpm) at 30°C for 4 hours. Absorbance of the bacterial cultures at 600 nm (OD₆₀₀) was measured in 1 h intervals with Multiskan plate reader (Thermo Scientific). The bacterial growth inhibition (INH%) was calculated as follows:

$$INH\% = 100 - \frac{(OD_{600 \text{ sample}} \times 100)}{OD_{600 \text{ control}}}$$

In the end of the growth inhibition assay, 3 μ l of each sample was removed and plated onto LB agar plates to assess the viability of the cells. The plates were incubated at 30°C for 24 h and the minimum bactericidal concentration (MBC) was characterized as the lowest concentration of Ag compound where no colonies were observed, i.e., the concentration that resulted in irreversible inhibition of the bacterial growth.

To study the role of the direct particle-cell contact in the antibacterial effects of AgNPs, additional experiments where bacteria were separated from AgNPs by 20 kDa (~4 nm, [24]) dialysis membrane (Slide-A-Lyzer MINI Dialysis Device, 20K MWCO, Thermo Scientific) were performed. In this case, 400 μ l of bacterial suspension was pipetted onto the wells of 48-well transparent cell culture plates (nontreated polystyrene, BD Falcon). Then, polypropylene cups with the dialysis membrane on the bottom were inserted into the wells and 400 μ l of AgNPs/AgNO₃ (sample) or DI water (control) were pipetted into the cups. Bacteria were grown at 30°C, 750 rpm for 4 hours and OD₆₀₀ was measured.

Quantification of Intracellular Silver Ions

Quantification of intracellular Ag ions was performed using recombinant biosensor bacteria *Escherichia coli* MC1061 (pSLcueR/pDNPcopAlux). The response of this recombinant *E. coli* to intracellular Ag ions is mediated *via* CueR activator protein and its regulated *copA* promoter that is fused to the biolumines-

cence encoding genes. Therefore, in the sub-toxic region, the presence of intracellular Ag ions leads to the increase of bioluminescence of these recombinant bacteria in a dose-dependent manner [23].

The preparation of test bacteria and the procedure of the biosensor assay was analogous to the bacterial growth inhibition assay with the following exceptions: (i) the growth medium of bioluminescent Ag-biosensor *E. coli* MC1061 (pSLcueR/pDNPco-pAlux) was supplemented with 100 µg/l ampicillin and 10 µg/l tetracycline during overnight cultivation to maintain the recombinant plasmids and (ii) the assay was conducted on white 96-well Cliniplates with transparent bottom that allowed the determination of both, luminescence and optical density in parallel. Multiskan plate reader (Thermo Scientific) was used for optical density and Orion II plate luminometer (Berthold Detection Systems) for the bioluminescence measurement. Briefly, 100 µl of bacterial suspension was exposed to 100 µl of 0.01–100 mg Ag/l dilutions of AgNO₃ or AgNPs in DI water (sample) or DI water (background) at 30°C for 4 hours. Dose-response curves of the Ag-biosensor were obtained by plotting the applied concentrations of Ag against the bioluminescence of Ag-biosensor (as fold induction) in respective samples. Fold induction was calculated as follows:

$$\text{Induction(fold)} = \frac{BL_{\text{sample}}}{BL_{\text{background}}}$$

where BL_{sample} is the bioluminescence of Ag-biosensor in the sample and $BL_{\text{background}}$ is the background bioluminescence. Intracellular Ag was determined by using the log-log linear regression equations derived from the linear region of the dose-response curves of Ag-biosensor to AgNO₃ and AgNPs, whereas AgNO₃ was considered 100% bioavailable and was used as a standard (Figure S3).

Assessment of Cell-Nanoparticles Interaction

Bacterial suspensions were cultivated overnight on a shaker (200 rpm, 30°C) in 3 ml of NaCl-free LB medium. Then, the bacterial cultures were diluted in NaCl-free LB medium to OD₆₀₀ = 0.4. 700 µl of diluted bacterial suspension was added to 700 µl of 20 mg Ag/l nAg-Col in DI water (final concentration of nAg-Col in the test 10 mg Ag/l) and immediately centrifuged at 4 000 g for 5 minutes. 1 ml of obtained supernatants was used to measure the UV-visible (UV-Vis) wavelength absorption spectra with a Thermo Multiskan Spectrum (Thermo Electron Corporation, Finland). As a control, the spectrum of 10 mg/l collargol in half-strength NaCl-free LB medium centrifuged at 4 000 g for 5 minutes was analyzed.

Statistical Analysis

All experiments were performed in at least three biological replicates and the data were expressed as mean ± standard deviation. To define statistically significant differences, the data were analyzed either with one way analysis of variance ANOVA or with unpaired two-tailed *t*-test assuming equal variances at *p* < 0.01.

Results

Characteristics of Silver Nanoparticles

The main rationale behind the selection of Ag nanoparticles for this study was their different surface modification. While the Sigma-Aldrich Ag nanoparticles (nAg) had no coating, collargol (nAg-Col) particles were coated with protein (casein) and the nAg-PVP AgNPs had polyvinylpyrrolidone coating (Table 1). All the

used AgNPs were spherical (Figure 1A) and had negative ζ-potential (Table 1). Collargol formed the most stable dispersion in the test medium used for bacterial growth inhibition assays (half-strength NaCl-free LB). The average hydrodynamic diameter, D_h , of nAg-Col particles was 53 nm and the preparation was relatively monodisperse (pdi 0.2). The efficient dispersion of nAg-Col was most likely due to the steric hindrance and electrostatic repulsion between the casein molecules coating these Ag particles. Compared to nAg-Col, the hydrodynamic size of nAg-PVP was larger (D_h in the test media = 139 nm, pdi 0.2). This was most probably due to the thick PVP coating and almost neutral surface charge of these particles (Table 1). Both coated AgNPs did not aggregate in the test medium during the test, whereas uncoated nAg formed large aggregates (D_h = 269 nm, pdi = 0.7), which settled and formed visible macroscopic silver after 4-h incubation (Figure 1B).

The dissolution rates of AgNPs in both DI water and in the test medium were in the following order: nAg-PVP > nAg-Col > nAg, showing that nAg that formed large aggregates was the least soluble (Table 1). However, despite of its bigger hydrodynamic size, nAg-PVP dissolved better than nAg-Col, indicating that in addition to size, dissolution of AgNPs was also determined by the type of coating. Interestingly, chemical analysis (AAS) revealed that the dissolution rate of all AgNPs was higher in DI water than in test medium (Table 1). Also, according to AAS analysis no additional dissolution of AgNPs in test medium took place during 4 h (insets in Figure S4). At the same time, when 0-h and 4-h UV-Vis spectra of AgNPs in test medium were compared, a decrease in absorption peak height that reveals particle dissolution was observed (Figure S4). Altogether these results indicated a ligand-enhanced dissolution of AgNPs in test medium, whereas the released Ag ions remained bound to the ligands.

Different Bacterial Strains Exhibit Similar Dose-Response to AgNO₃ but not to Silver Nanoparticles

The growth inhibition curves of the three studied AgNPs and AgNO₃ to six Gram-positive and Gram-negative bacteria and the respective 4-h EC₅₀ values are shown in Figure S5 and Figure 2, respectively. As a rule, both coated AgNPs inhibited bacterial growth at concentrations below 20 mg Ag/l (Figure 2) and at somewhat higher concentrations were bactericidal, i.e., inhibited bacterial growth irreversibly (Table S2). Uncoated nAg, however, had no growth inhibitory effect at tested concentrations except towards *P. aeruginosa* (Figure S5). Altogether, the antibacterial efficiency of AgNPs followed the order nAg-PVP > nAg-Col > nAg, showing a clear positive correlation with their dissolution rates. Notably, the correlation between antibacterial efficiency of AgNPs and their size was less evident, because nAg-PVP NPs with the larger hydrodynamic size were mostly more toxic to bacteria than nAg-Col (Figure 2).

The shapes of the dose-response curves of all bacterial strains to AgNO₃ (Figure S5) as well as the corresponding 4-h EC₅₀ values (Figure 2) were similar revealing similar mechanism of toxicity of ionic Ag. Indeed, the difference between the EC₅₀ values of AgNO₃ to various bacterial strains was only 4-fold: the lowest EC₅₀ value was measured for *P. putida* (0.3 mg Ag/l) and the highest for *S. aureus* (1.2 mg Ag/l). However, the shapes of the dose-response curves of various bacterial strains to AgNPs were remarkably different (Figure S5). Especially interesting was the high toxicity of all forms of nanoparticulate Ag to human pathogen *P. aeruginosa*. Even marginally dissolving uncoated Ag inhibited the growth of *P. aeruginosa* (4-h EC₅₀ = 11.8 mg Ag/l), but had no effect on other bacterial strains in the concentration range tested (Figure S5). Furthermore, the 4-h EC₅₀ value of protein-coated nAg-Col for *P. aeruginosa* was 0.35 mg Ag/l, which was

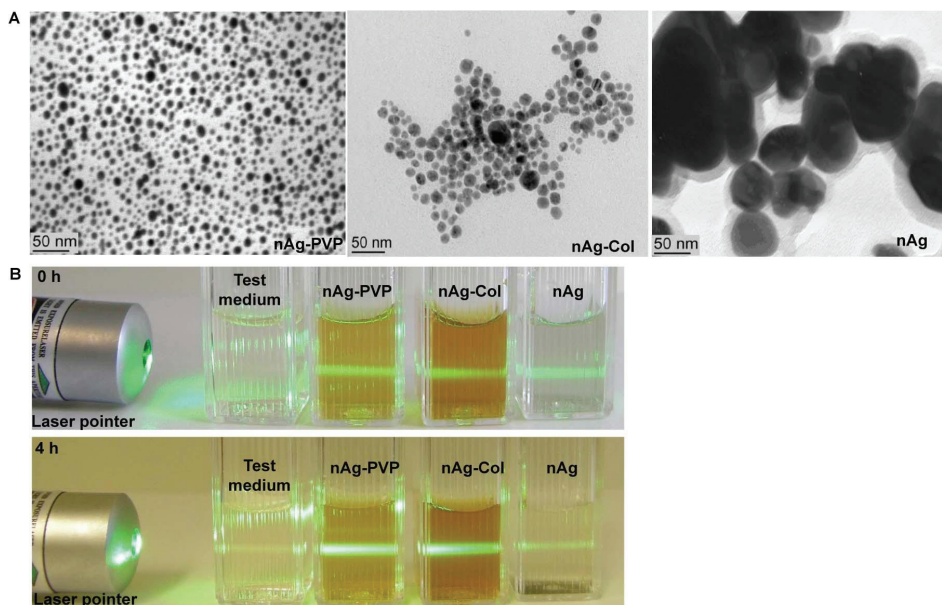


Figure 1. Characterization of silver nanoparticles. A: Transmission electron microscopy images of AgNPs. TEM image of collargol is reprinted from [21] with the permission of Springer. B: Stability of 10 mg/l nanoparticles suspensions in test medium (half-strength NaCl-free LB medium). After 0-h incubation (upper panel), all AgNPs suspensions scattered light upon the illumination by the laser pointer, indicating the presence of particles. After 4-h incubation (lower panel), the light scattering from uncoated nAg was negligible (comparable to that of the test medium with no AgNPs added) and settling of the particles was observed. doi:10.1371/journal.pone.0064060.g001

comparable to ionic Ag and should indicate 100% solubility of nAg-Col (Figure 2), although the chemical analysis showed that the dissolution rate of nAg-Col was just 2.6% (Table 1). Notably, the high sensitivity to nAg-Col was characteristic only to *P. aeruginosa*; the 4-h EC_{50} of nAg-Col to e.g., *S. aureus* was 46 mg Ag/l, being as much as 130-fold higher than the value for *P. aeruginosa*.

As the dose-response of various bacteria to $AgNO_3$ was similar but different to AgNPs, we proposed that either (i) the toxicity of

AgNPs was determined not only by Ag ions, (ii) each bacterial strain had different influence on dissolution of AgNPs or (iii) each bacterial strain modulated differently the uptake of Ag ions dissolved from AgNPs.

Table 1. Characterization of silver nanoparticles (AgNPs) used in the current study.

	nAg	nAg-Col	nAg-PVP
Coating	uncoated	casein (30%) ¹	polyvinylpyrrolidone (71%) ¹
Average primary size², nm	85.7 ± 29.3	14.6 ± 4.7	10.5 ± 4.3
D_n³ in DI water, nm	89 (pdi ⁴ = 0.6)	44 (pdi = 0.2)	122 (pdi = 0.2)
D_n in test medium⁵, nm	269 (pdi = 0.7)	53 (pdi = 0.2)	139 (pdi = 0.2)
ζ-potential in test medium, mV	−25.5	−26.1	−4.5
Dissolution⁶ in DI water, %	0.82	7.6	36.5
Dissolution⁶ in test medium, %	0.48	2.6	4.4
Source/Reference	Sigma-Aldrich	Laboratorios Argenol	[21]

¹Mass fraction of the coating material, analyzed by thermogravimetry [21];

²Measured from TEM micrographs using ImageJ software (n = 65);

³Hydrodynamic size, measured by dynamic light scattering (DLS) immediately after dispersion of silver nanoparticles;

⁴Pdi states for polydispersity index;

⁵Test medium states for half-strength NaCl-free LB;

⁶Analyzed by atomic absorption spectroscopy from supernatants of ultracentrifuged (390 000 g × 60 min) 10 mg/l AgNPs' suspensions after 4-h incubation at 30 °C.

doi:10.1371/journal.pone.0064060.t001

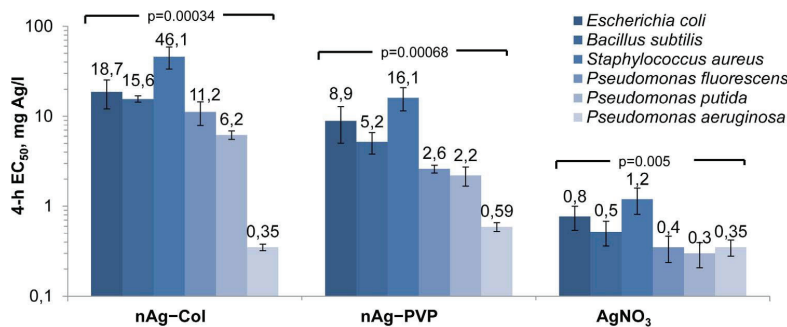


Figure 2. 4-h EC₅₀ values (endpoint: growth inhibition; note the logarithmic scale) for different silver formulations and toxicity to bacteria. nAg-PVP states for PVP-coated AgNPs and nAg-Col for collargol. Concentrations are nominal. Data represent the average \pm SD (n = 3), p-values denote statistically significant differences between different bacteria (ANOVA). doi:10.1371/journal.pone.0064060.g002

Toxicity of Silver Nanoparticles to *Escherichia coli* is a Function of Intracellular Ag Ions

First, the effect of Ag ions in toxicity of AgNPs was quantified. For that a recombinant Ag ion-responding biosensor bacterium *E. coli* MC1061 (pSLcucR/pDNPcpoAlux) was used. As the bioluminescent response of this bacterium is triggered only by Cu and Ag ions [23], its bioluminescence in our test conditions was proportional to intracellular Ag ions.

The dose-response curves of *E. coli* MC1061 (pSLcucR/pDNPcpoAlux) to different Ag formulations are shown in Figure 3A. As expected, the Ag-biosensor was most sensitive to AgNO₃. Among AgNPs, *E. coli* MC1061 (pSLcucR/pDNPcpoAlux) was most sensitive to nAg-PVP, followed by nAg-Col and nAg. The linear region of the sub-toxic part of the dose-response curves (Figure 3A) was used to quantify the intracellular Ag more precisely, revealing that $8.0 \pm 1.1\%$ of nAg-PVP, $4.0 \pm 0.4\%$ of nAg-Col and $0.6 \pm 0.2\%$ of nAg were transformed into intracellular Ag ions. When the nominal *E. coli* 4-h EC₅₀ values of Ag formulations (from Figure 2) were re-calculated on the basis of intracellular Ag ions, the resulting 4-h EC₅₀ values of both coated AgNPs were very close to that of AgNO₃: EC₅₀ (mg Ag/l) for nAg-Col was 0.74, for nAg-PVP 0.71 and for AgNO₃ 0.77 (Figure 3B). As the Ag-biosensor *E. coli* MC1061 (pSLcucR/pDNPcpoAlux) is induced only by intracellular Ag ions and the toxicity of AgNPs measured using *E. coli* growth inhibition assay integrates all the possible toxic effects of AgNPs (i.e., caused by dissolution, production of reactive oxygen species, lipid peroxidation, membrane damage etc.), it was evident that the toxicity of AgNPs was fully determined by intracellular Ag ions.

Particle-Cell Contact Enhances Antibacterial Efficiency of Silver Nanoparticles

As the toxicity of AgNPs was mediated *via* intracellular Ag ions (Figure 3) but was orders of magnitude different to different bacterial strains (Figure 2), it was evident that intracellular bioavailability of Ag ions liberated from AgNPs was bacterial strain-specific. We proposed two hypotheses to explain this phenomenon: (i) either each bacterial strain differently modulated the extracellular dissolution of AgNPs *via* bacterial exudates (organic acids, peptides, biosurfactants) or (ii) the cellular uptake of Ag ions *via* cell-NP interaction was different in different bacterial strains. We studied these two hypotheses using *E. coli* cells as an example. For that, we incubated AgNPs with (biotic dissolution) or

without (abiotic dissolution) bacterial culture (Figure 4). To test the first hypothesis, we separated the dissolved Ag by ultracentrifugation and compared the biotic and abiotic dissolution rates of AgNPs by quantifying the extracellular dissolved Ag and extracellular free Ag⁺ in the supernatant using AAS and Ag ion-selective electrode, respectively. To test the second hypothesis, we exposed *E. coli* MC1061 (pSLcucR/pDNPcpoAlux) Ag-biosensor either to AgNPs' suspensions or to ultracentrifuged supernatants of these suspensions and quantified the internalized Ag ions. Thus, in the former experimental setup *E. coli* cells were in the direct contact with AgNPs and in the latter case, *E. coli* was exposed to the soluble fraction of AgNPs, allowing to estimate the role of cell-NP contact on intracellular Ag ions (Figure 4).

The results from AAS revealed that all AgNPs dissolved slightly more in the presence of bacteria than in abiotic conditions, but this effect was not statistically significant (n = 3, $p > 0.05$) (Figure 5, grey bars). The results obtained using Ag-ISE showed also that compared to abiotic conditions no additional free Ag ions appeared in the test medium when AgNPs were incubated with bacterial cells (Figure 5 A and B, white bars). In both, biotic and abiotic conditions, the extracellular fraction of dissolved Ag determined with AAS exceeded the fraction determined with Ag-ISE about twice. This difference was expected, because Ag-ISE determines only free Ag ions but AAS determines also the complexes of Ag ions with the low-molecular-weight (<5 kDa) components of the test medium that were too small to settle during ultracentrifugation.

While no additional extracellular dissolution of AgNPs was detected in biotic exposure conditions, there was a significantly increased uptake of Ag ions *via* cell-NP interaction. Specifically, in case of direct contact between AgNPs and *E. coli* MC1061 (pSLcucR/pDNPcpoAlux) (i.e., biotic conditions) the biosensor cells internalized about 3 times more Ag ions than were internalized when the biosensor was exposed to ultracentrifuged supernatants of AgNPs (Figure 5A versus 5B, blue bars). This result reveals the importance of direct contact of AgNPs with bacterial cells and demonstrates that the extracellular concentration of Ag ions in the test medium may underestimate the effective intracellular concentrations and hence, antibacterial potency of Ag ions from AgNPs.

To further demonstrate that the intimate surface contact of AgNPs with bacterial cells increases the internalization of particle-associated Ag ions and, therefore, the effective toxicity of AgNPs, comparative growth inhibition assays were carried out with *E. coli*

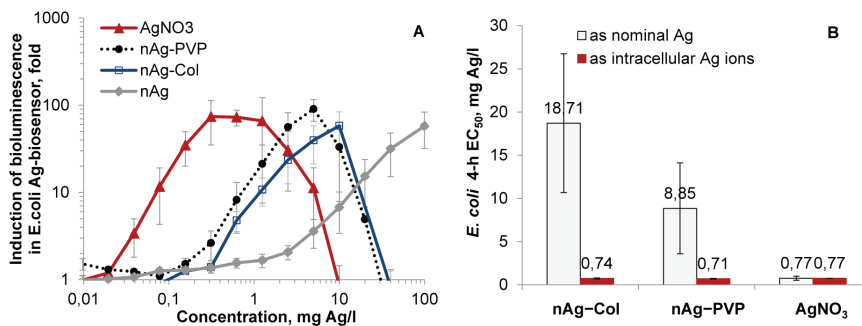


Figure 3. Response of *Escherichia coli* MC1061 to silver formulations. A: Dose-dependent induction of bioluminescence of Ag-biosensor *E. coli* MC1061 (pSLcueR/pDNPcopAlux) in response to silver formulations. The bioluminescence was measured after 4-h exposure (30°C, half-strength NaCl-free LB medium). The decreased bioluminescence at higher concentrations refers to the toxicity. Concentrations are nominal. B: Toxicity (4-h EC₅₀) of silver nanoparticles and AgNO₃ to *E. coli* MC1061. EC₅₀ values based on nominal concentrations (open columns) are from Figure 2; EC₅₀ values based on intracellular Ag ions (red columns) are re-calculated from Figure 3A. Data represent the average \pm SD (n=3). doi:10.1371/journal.pone.0064060.g003

and *P. aeruginosa* cells either directly exposed to nAg-Col particles or separated from the nanoparticles by a particle-proof dialysis membrane (cut-off 20 kDa~4 nm; Figure S6). When *E. coli* cells were in direct contact with AgNPs, the 4-h EC₅₀ value for nAg-Col was around 10 mg/l (Figure 6A). However, when nAg-Col was separated by a membrane, the toxic effect was not observed even at 200 mg/l (Figure 6A, red line) i.e., there was a >20-fold reduction in toxicity. Similarly, membrane-separated nAg-Col did not exhibit any toxic effects to *P. aeruginosa* (Figure 6B). Interestingly, the optical density of *P. aeruginosa* culture was lower in the presence of the dialysis membrane: when the OD₆₀₀ values without the membrane were around 0.35 then in the presence of the membrane the maximum OD₆₀₀ was only 0.2 (Figure 6B). This was most probably because *P. aeruginosa* cells tended to attach to the dialysis membrane immediately after the contact (data not shown).

In the experimental setup used to separate nAg-Col by the dialysis membrane, we did not establish equilibrium for Ag ions between the membrane-separated phases beforehand, because it would have caused additional dissolution of nAg-Col complicating the interpretation of the results. Therefore, most likely there was an unequal distribution of Ag ions between the two membrane-separated phases. To evaluate the efficiency of Ag ions' diffusion through the membrane during the 4-hour test, bacteria were also exposed to AgNO₃ either directly or through a dialysis membrane. Without the dialysis membrane, the complete inhibition of *E. coli* growth after 4 hours of incubation was observed at 1.25 mg Ag/l of AgNO₃. However, when the bacteria were exposed to AgNO₃ through a membrane, 20 mg Ag/l of AgNO₃ was required to inhibit bacterial growth (Figure 6C, D). Thus, the dialysis membrane caused 16-fold reduction in toxicity of AgNO₃. Taking this into account we estimated that if the toxicity of nAg-Col would have been mediated only by the extracellularly dissolved Ag ions, the membrane-separated nAg-Col should have inhibited *P. aeruginosa* and *E. coli* growth starting from 80 or 160 mg/l, respectively. However, this was not the case (Figures 6A, B), additionally confirming that in the absence of direct contact with Ag-particles the effective intracellular concentration of Ag ions in bacterial cells was lower.

Pseudomonas aeruginosa Cells Co-precipitate with Collargol

Since the toxicity of AgNPs was apparently mediated by the cell-NP contact, which depends on specific surface properties of each bacterium, the potential of different bacterial strains to attach to the surface of AgNPs was studied. For that, all the six test bacteria were mixed with nAg-Col, immediately settled by centrifugation and UV-Vis spectra of the obtained supernatants were measured. The plasmon absorption band near 400 nm that is proportional to the concentration of metallic nanosized Ag [25] enabled to estimate the fraction of nAg-Col which remained unadsorbed to bacterial cells. Before the experiment we verified that the addition of bacterial culture to nAg-Col suspension had no effect on the specific plasmon resonance peak of the nanoparticles (Figure S7). While no co-precipitation of AgNPs with *E. coli*, *B. subtilis*, *S. aureus*, *P. fluorescens* and *P. putida* cells was observed (the UV-Vis absorption spectra before and after centrifugation were similar), there was a significant co-precipitation of nAg-Col and *P. aeruginosa* cells (Figure 7). According to the peak of UV-Vis spectrum, $9.2 \pm 2.6\%$ of nAg-Col was readily sorbed to the cell surface and co-precipitated with *P. aeruginosa* cells during the centrifugation. This observation suggests that *P. aeruginosa* cells had higher affinity to AgNPs than the other tested bacterial strains. We assume that the adhesion of *P. aeruginosa* cells to nAg-Col particles was responsible for the high antibacterial potency of nAg-Col particles towards this pathogenic bacterium (Figure 2).

Discussion

It is generally acknowledged that the toxicity of AgNPs depends on the release of Ag⁺ ions, which interact with -SH groups of membrane-bound enzymes and proteins, uncoupling the respiratory chain of bacteria [26], [27] and disrupting bacterial cell membranes [28]. This hypothesis implies that the toxic effects of nanosilver are proportional to the activity of free Ag ions released from AgNPs into extracellular solution, assuming the equal distribution of Ag⁺ on the surface of nanoparticles, in the solution and inside bacterial cell. This explanation of the toxicity does not consider the impact of direct interaction of AgNPs with bacterial cells.

In this study we characterized three differently coated AgNPs and quantified their effects on the growth and viability of six

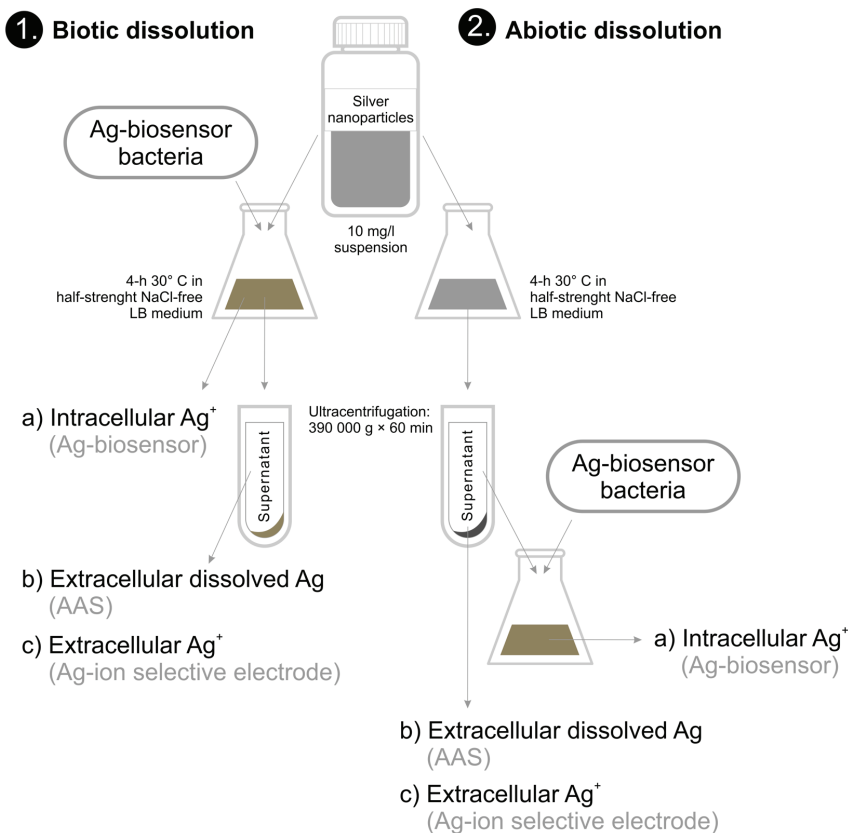


Figure 4. Schematic representation of the experiment to study dissolution of AgNPs. Intracellular Ag ions, extracellular dissolved Ag and extracellular Ag ions were quantified in **biotic** (left) as well **abiotic** (right) conditions. Ag-biosensor *E. coli* MC1061(pSLcueR/pDNPcopAlux) was exposed either to the 10 mg/l suspensions of AgNPs (biotic dissolution) or to the supernatants obtained after ultracentrifugation (390 000 g×60 min) of the respective AgNPs' suspensions (abiotic dissolution). Intracellular Ag ions were quantified as a function of increase of bioluminescence Ag-biosensor *E. coli* MC1061(pSLcueR/pDNPcopAlux), extracellular dissolved Ag was measured by atomic absorption spectroscopy (AAS) and extracellular Ag ions by ion-selective electrode (Ag-ISE). doi:10.1371/journal.pone.0064060.g004

bacterial strains. To measure Ag dissolved from AgNPs, we used three different techniques that enabled to distinguish between the fractions of extracellular dissolved Ag, extracellular free Ag ions and intracellular Ag ions.

The sensitivity of all the six used bacterial strains towards AgNO₃ was relatively similar. The difference between the most and the least susceptible bacterial strain (*P. putida* and *S. aureus*, respectively) was only 4-fold. At the same time there was 130-fold difference between the toxicity of protein-coated nAg-Col to different bacterial strains (*P. aeruginosa* vs. *S. aureus*, Figure 2). It was evident that Ag dissolved from AgNPs played a strong antibacterial role as the dissolution rate of AgNPs (Table 1) correlated well with their toxicity to bacteria (Figure 2). However, the **extracellular** dissolution alone did not explain the orders of magnitude difference in toxicity of AgNPs to different bacterial strains. At the same time, the toxicity of AgNPs to *E. coli* MC1061 was fully predicted by **intracellular** effective fraction of Ag ions (Figure 3) determined by Ag-biosensor *E. coli* MC1061 (pSLcueR/pDNPcopAlux). Further, the results of Ag-biosensor revealed that 3–4

times more Ag ions were internalized by *E. coli* cells upon direct contact with nanoparticles compared to the particle-free supernatants of respective ultracentrifuged suspensions (Figure 5). These results showed that intracellular Ag ion is the single and ultimate cause of the antibacterial action of studied AgNPs and that the concentrations of the former depended mainly on two factors: extracellular dissolution (Table 1) and cell-NP contact (Figures 5–7).

There are plenty of data showing that AgNPs are more toxic to bacterial cells than dissolved silver released from these NPs [16], [29], [30]. In the literature, additional particle-attributed toxicity is usually explained by the production of reactive oxygen species (ROS) by the particle surface and/or mechanical damage of bacterial cell membranes [10], [31]. At the same time it has been clearly shown that AgNPs that lacked oxidized surfaces (and therefore were not dissolving) proved also not toxic to bacteria [12], [13], excluding the involvement of ROS and cell membrane damage by particles *per se*. These seemingly contradicting results can be explained by additional dissolution of AgNPs in the close

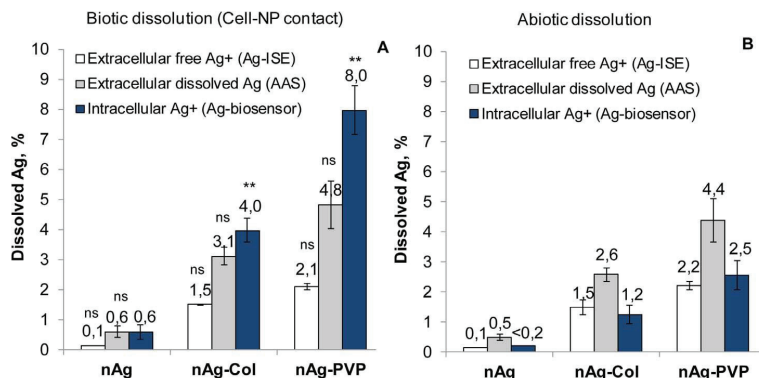


Figure 5. Dissolved, free and intracellular concentrations of Ag in biotic and abiotic conditions. A: Dissolved, free and intracellular Ag after 4-h direct cell-NP contact. Intracellular Ag⁺ was quantified from bioluminescent response of *E. coli* MC1061 (pSLcueR/pDNPcopAlux) to AgNPs suspension. Extracellular dissolved Ag was measured by atomic absorption spectroscopy (AAS) and free Ag⁺ was measured by Ag-ion-selective electrode (Ag-ISE) from the test medium after settling of NPs and bacterial cells by ultracentrifugation at 390 000 g for 1 hour. B: Dissolved, free and intracellular Ag in abiotic conditions. Extracellular dissolved Ag (AAS), extracellular free Ag⁺ (Ag-ISE) and intracellular Ag⁺ (Ag-biosensor *E. coli* MC1061 (pSLcueR/pDNPcopAlux)) were measured from the test medium after settling of NPs by ultracentrifugation at 390 000 g for 1 hour. Data represent the average \pm SD (n=3). **p<0.01, ns – not significant (p>0.05) compared to abiotic dissolution according to two-tailed unpaired t-test. doi:10.1371/journal.pone.0064060.g005

vicinity of bacterial cell envelope upon cell-NP interaction. The importance of cell-NP contact has been also suggested and discussed previously [32], [33], [34]. Using *E. coli*, McQuillan et al. [18] noticed that Ag⁺ from AgNPs induced 2–3-fold up-regulation of Ag⁺-response genes *copA*, *cueO* and *cusA* compared to AgNO₃ and referred to this effect as “nanoparticle-enhanced silver ion

stress”. Recently, Taglietti et al. [35] suggested that overall bactericidal effect of glutathione-coated nAg to *E. coli* and *S. aureus* depended on two factors: the release of Ag ions from the NPs referred to by authors as “long-distance mechanism” and the nanomechanical damage of bacterial membranes (“short-distance mechanism”). Hereby, we complement these studies and show

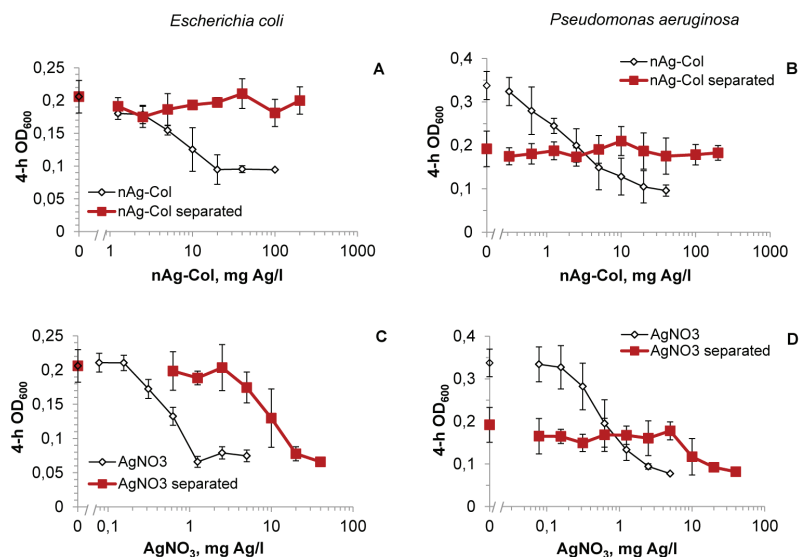


Figure 6. Bacterial growth after 4-h exposure to collargol directly and through the dialysis membrane. *Escherichia coli* MC1061 (A, C) and *Pseudomonas aeruginosa* D510-129 (B, D) upon exposure to collargol (nAg-Col; A, B) after 4 h in half-strength NaCl-free LB at 30°C in the direct contact with nanoparticles (rectangle) or being separated from particles by 20 kDa (4 nm) cut-off membrane (diamond). AgNO₃ was handled analogously to collargol and was used as a control (C, D). Data represent the average \pm SD (n=4). doi:10.1371/journal.pone.0064060.g006

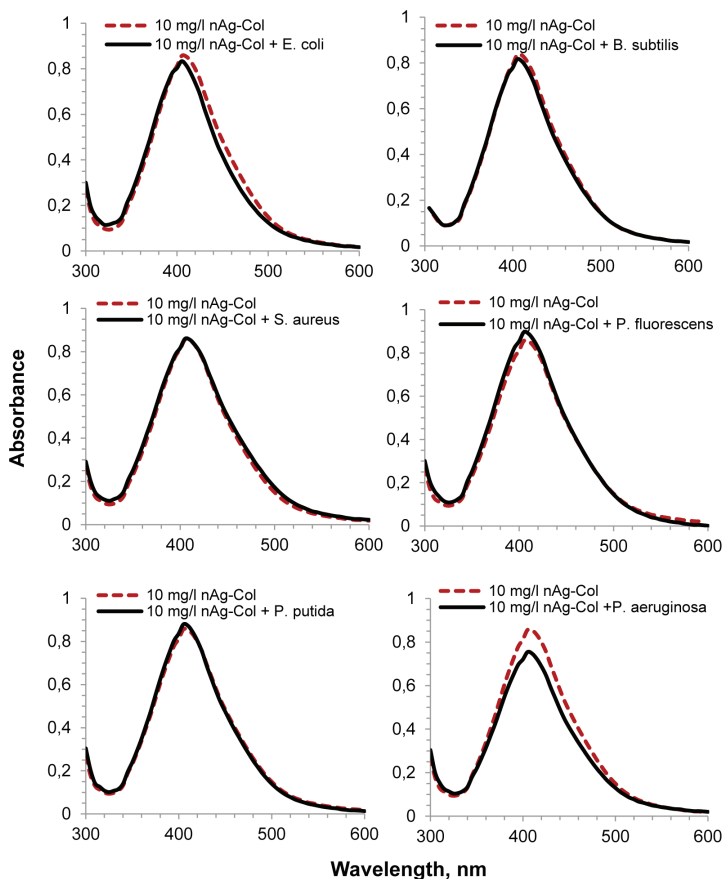


Figure 7. UV-visible absorption spectra of nAg-Col suspensions (10 mg Ag/l) with or without bacteria. UV-Vis spectra of AgNPs in half-strength NaCl-free LB medium without bacterial cells (dashed red line) or after exposure of bacterial cells to nAg-Col (solid line). Before measurement, bacterial cells and cell-associated nanoparticles were removed by centrifugation at 4 000 g for 5 minutes. The difference between dashed and continuous lines shows the co-precipitation of nAg-Col particles with bacterial cells. The representative figures from the three independent experiments are shown.

doi:10.1371/journal.pone.0064060.g007

that both, “long-distance” and “short-distance” effects of AgNPs are in fact the action of Ag ions. It should be pointed out that the release and adverse effects of “long-distance Ag ions” (extracellular dissolution) are well-known and can be easily quantified using AAS or ICP. In contrast, the contribution of “short-distance Ag ions” (dissolution at cell-NP interface) to the toxicity is a complex process that is often overlooked and is rather reported in terms of secondary effects such as damage to bacterial cell wall.

The enhanced toxicity of particle-associated Ag^+ through the cell-NP interaction assumingly involves the release of silver ions in the close proximity of bacterial outer surface and also possible cellular internalization of AgNPs. In the aqueous environment, the surface of most nanoparticles is electrically charged and therefore, may attract counter-ions [32], [36], [37]. Most of the nanoparticles as well as AgNPs used in our study encounter negative charge (measured as ζ -potential, Table 1) in aqueous media [37]. Thus, they have the potency to attract counter-ions e.g., Ag^+ and

H^+ cations into their diffuse layer, e.g., by chemisorption [38]. Upon direct contact with negatively charged bacterial cells (Table S3), the increased concentration of both, Ag^+ and H^+ ions on the particle surface would cause additional damage to bacterial cell membranes, because of the higher local concentration of Ag ions and higher local dissolution rate of AgNPs upon low pH. It is well known that Ag ions destabilize the membranes of both Gram-positive and Gram-negative bacteria [14], [28], [39]. Such local intensive influx and damaging action of Ag ions from AgNPs may create pits in bacterial cells walls, disrupting cellular integrity, facilitating the internalization of AgNPs [18], [31], [40] and causing a myriad of secondary effects such as Ag^+ -triggered accumulation of intracellular ROS and damage of vital biomolecules. High toxicity of all forms of nanoparticulate silver (Figure 2), especially collargol, to *P. aeruginosa* supports this hypothesis, as *P. aeruginosa* adhered to nAg-Col stronger than the rest of the tested bacterial species (Figure 7). The attachment of

microbes to a surface is also an initial phase of the biofilm formation [41]. *P. aeruginosa* strains tend to form biofilms in immunocompromised hosts and in human implants, exhibiting increased tolerance to antibiotics in biofilm state [42]. On the basis of our results we suggest that nanoparticulate silver may be especially efficient in inhibiting initial cell attachment and thus, retarding the formation of bacterial biofilms as was already shown empirically for *Pseudomonas aeruginosa* PAO1 [43].

All the above indicate that the net antibacterial effect of the studied silver depends exclusively on the effective concentration of silver ions inside the bacterial cells, which is determined by two main factors (i) extracellular dissolution of AgNPs and (ii) dissolution of AgNPs on particle-cell interface. Notably, as only a limited number of spherical AgNPs were utilized in this study, further research may be needed to understand whether the cell-NP interaction is also responsible for the shape-dependent [15], surface charge dependent [44] or surface-defect and crystallinity-dependent [45] toxicity of AgNPs.

Taken together, this paper is one of the first to provide quantitative evidence on the role of cell-NP contact in the toxicity of AgNPs and to demonstrate that enhanced “particle-specific” toxicity debated in the literature is manifested *via* increased intracellular effective concentration of Ag ions – the ultimate cause of toxicity of AgNPs. The exact physico-chemical and cellular mechanisms underlying this phenomenon remain, however, still hypothetical and need further research.

Supporting Information

Figure S1 Number and share of articles on silver nanoparticles for six bacterial species in ISI WoS. Keywords used for the search and respective number of retrieved papers were as follows: ‘silver nanoparticles’ and ‘*Escherichia coli*’ (1162 papers); ‘silver nanoparticles’ and ‘*Staphylococcus aureus*’ (554 papers); ‘silver nanoparticles’ and ‘*Pseudomonas aeruginosa*’ (184 papers); ‘silver nanoparticles’ and ‘*Bacillus subtilis*’ (114 papers); ‘silver nanoparticles’ and ‘*Pseudomonas putida*’ (11 papers); ‘silver nanoparticles’ and ‘*Pseudomonas fluorescens*’ (10 papers). Total: 2035 papers. Search made: 06.12.2012. (DOCX)

Figure S2 Primary size distribution of silver nanoparticles. A: PVP-coated nAg-PVP, B: protein-coated nAg-Col and C: uncoated nAg. Sizes of the silver nanoparticles were measured from TEM micrographs (Figure 1); altogether 65 particles were measured. (DOCX)

Figure S3 Response of Ag-biosensor to silver formulations. Representative calibration curves of Ag-biosensor *Escherichia coli* MC1061 (pSLuciferase/pDNPCopAlux) for AgNO₃ (A–C), nAg-PVP (A), nAg-Col (B) and nAg (C) are shown. The lines represent the calibration plots for the linear regression between log(C)–log(indBL), whereas C is concentration of Ag (mg/l) in the samples and indBL is a fold induction of bioluminescence in Ag-biosensor in response to intracellular Ag. Linear range of the regression and regression equations are shown. Intracellular Ag was determined by using the linear regression equation for AgNO₃, which was considered 100% bioavailable and was used as a standard. Calculations were performed at BL = 10. An example for quantification of intracellular dissolution of nAg-PVP is given below:

$$\text{Log}(C_{\text{AgNO}_3}; \text{indBL}) = \frac{1 - 2,7069}{1,5256} = -1,119$$

$$C_{\text{AgNO}_3} = 10 \wedge -1,119 = 0,076 \text{ (mg Ag/l)}$$

$$\text{Log}(C_{\text{nAgPVP}}; \text{indBL}) = \frac{1 - 1,1395}{1,3274} = -0,105$$

$$C_{\text{nAgPVP}} = 10 \wedge -0,128 = 0,785 \text{ (mg Ag/l)}$$

$$\text{Intracellular Ag from nAgPVP} = \frac{0,076}{0,785} \times 100\% = 9,7\%$$

(DOCX)

Figure S4 Ultraviolet - visible (UV-Vis) wavelength absorption spectra for silver nanoparticles. UV-Vis spectra for 10 mg/l nAg-Col suspension (A) and 10 mg/l nAg-PVP suspension (B) immediately after dispersion in the test medium (half-strength NaCl-free LB) (solid line) and after 4-h incubation (dashed green line) are shown. The UV-Vis measurement could not be conducted for the uncoated nAg NPs due to their quick sedimentation. The plasmon absorption peak at 405 nm is proportional to the concentration of metallic nanosized Ag and the decrease of this peak indicates dissolution of AgNPs. The absence of shift of plasmon absorption peak indicates that AgNPs do not aggregate. Insets in the Figure S4 indicate dissolution of AgNPs measured by atomic absorption spectroscopy (AAS) from the ultracentrifuged (390 000 g for 60 minutes) supernatants of AgNPs. During 4-h incubation, AgNPs dissolved but released Ag ions were complexed by the components of test medium that settled during ultracentrifugation. (DOCX)

Figure S5 Growth inhibition of bacterial strains by silver nanoparticles. Growth inhibition of *Escherichia coli* (A), *Bacillus subtilis* (B), *Staphylococcus aureus* (C), *Pseudomonas fluorescens* (D), *Pseudomonas putida* (E) and *Pseudomonas aeruginosa* (F) by uncoated Ag nanoparticles (nAg; triangle), collargol (nAg-Col; rectangle), PVP-coated Ag nanoparticles (nAg-PVP; cross) or AgNO₃ (diamond) after 4-h incubation in half-strength NaCl-free LB medium at 30°C. The representative figures from three biological replicates are shown. (DOCX)

Figure S6 Setup of the dialysis membrane test. Bacterial cells were separated from AgNPs or AgNO₃ by 20 kDa (about 4 nm) dialysis membrane (Slide-A-Lyzer MINI Dialysis Device, 20K MWCO, Thermo Scientific). 400 µl of bacterial suspension was pipetted into the wells, polypropylene cups with the dialysis membrane on the bottom were inserted into the wells and 400 µl of AgNPs, AgNO₃ or DI water (control) was pipetted into the cups. During the optical density measurements the cups were removed. (DOCX)

Figure S7 UV-visible absorption spectra of nAg-Col suspensions (10 mg Ag/l) with or without bacteria. UV-Vis spectra of AgNPs in half-strength NaCl-free LB medium without bacterial cells (dashed red line) or after exposure of nAg-Col to bacterial cells (solid line). No separation of particles and/or bacterial cells was done before the measurement. The experiment is a control for Figure 7 to exclude the interference of bacterial cells with the measurements of UV-Vis absorption spectra of nAg-

Col. Addition of bacterial culture had no significant effect on the UV-Vis spectra of nAg-Col. (DOCX)

Table S1 Characteristics of the bacterial strains used in this study. (DOCX)

Table S2 Minimum bactericidal concentration (MBC mg Ag/l) of silver nanoparticles and AgNO₃ to six bacterial strains. nAg states for uncoated AgNPs, nAg-PVP for PVP-coated AgNPs and nAg-Col for collargol. Bacteria were incubated with different concentrations of Ag-compounds in half-strength NaCl-free LB medium at 30°C for 4 h. Then, 3 µl of the test sample was pipetted onto agarized LB plates, incubated at 30°C for 24 h and visually inspected for the growth. The lowest tested concentration that completely inhibited the visible growth of bacteria was designated as a MBC. (DOCX)

References

- Marambio-Jones C, Hoek E (2010) A review of the antibacterial effects of silver nanoparticles and potential implications for human health and the environment. *J Nanopart Res* 12: 1531–1551.
- Cerkez I, Kocer HB, Worley SD, Broughton RM, Huang TS (2012) Multifunctional cotton fabric: Antimicrobial and durable press. *J Appl Polym Sci* 124: 4230–4238.
- Fung MC, Bowen D (1996) Silver products for medical indications: risk-benefit assessment. *J Toxicol Clin Toxicol* 34: 119–126.
- Nowack B, Krug HF, Height M (2011) 120 Years of nanosilver history: implications for policy makers. *Environ Sci Technol* 45: 1177–1183.
- Kahru A, Ivask A (2013) Mapping the Dawn of Nanocotoxicological Research. *Acc Chem Res* 46: 823–833.
- Cleveland D, Long SE, Pennington PL, Cooper E, Fulton MH, et al. (2012) Pilot estuarine mesocosm study on the environmental fate of silver nanoparticles leached from consumer products. *Sci Total Environ* 421–422: 267–272.
- Mueller NC, Nowack B (2008) Exposure modeling of engineered nanoparticles in the environment. *Environ Sci Technol* 42: 4447–4453.
- Wijnhoven SWP, Peijnenburg WJGM, Herberts CA, Hagens WI, Oomen AG, et al. (2009) Nano-silver – a review of available data and knowledge gaps in human and environmental risk assessment. *Nanotoxicology* 3: 109–138.
- Panaček A, Kvítek L, Prucek R, Kolář M, Večeřová R, et al. (2006) Silver colloid nanoparticles: synthesis, characterization, and their antibacterial activity. *J Phys Chem B* 110: 16248–16253.
- Choi O, Hu Z (2008) Size dependent and reactive oxygen species related nanosilver toxicity to nitrifying bacteria. *Environ Sci Technol* 42: 4583–4588.
- Sotiriou GA, Meyer A, Knijnenburg JTN, Panke S, Pratsinis SE (2012) Quantifying the origin of released Ag⁺ ions from nanosilver. *Langmuir* 28: 15929–15936.
- Lok CN, Ho CM, Chen R, He QY, Yu WY, et al. (2007) Silver nanoparticles: partial oxidation and antibacterial activities. *J Biol Inorg Chem* 12: 527–534.
- Xiu ZM, Zhang QB, Puppala HL, Colvin VL, Alvarez PJ (2012) Negligible particle-specific antibacterial activity of silver nanoparticles. *Nano Lett* 12: 4271–4275.
- Lok CN, Ho CM, Chen R, He QY, Yu WY, et al. (2006) Proteomic analysis of the mode of antibacterial action of silver nanoparticles. *J Proteome Res* 5: 916–924.
- Pal S, Tak YK, Song JM (2007) Does the antibacterial activity of silver nanoparticles depend on the shape of the nanoparticle? A study of the gram-negative bacterium *Escherichia coli*. *Appl Environ Microbiol* 73: 1712–1720.
- Jin X, Li M, Wang J, Marambio-Jones C, Peng F, et al. (2010) High-throughput screening of silver nanoparticle stability and bacterial inactivation in aquatic media: influence of specific ions. *Environ Sci Technol* 44: 7321–7328.
- Gunawan C, Teoh W, Marquis C, Lifa J, Amal R (2009) Reversible antimicrobial photoswitching in nanosilver. *Small* 5: 341–344.
- McQuillan JS, Infante GH, Stokes E, Shaw AM (2012) Silver nanoparticle enhanced silver ion stress response in *Escherichia coli* K12. *Nanotoxicology* 6: 857–866.
- Ivask A, George S, Bondarenko O, Kahru A (2012) Metal-containing nano-antimicrobials: differentiating the impact of solubilized metals and particles. In: *Nano-antimicrobials: Progress and Prospects*, Cioffi N, Rai M, editors. Springer. pp. 253–290.
- Bogdanichkova NE, Dulin MN, Vasilevskaya EI, Kalinkin AV (1992) Stabilization of silver clusters by matrices of various chemical nature. *React Kinet Catal L* 48: 475–481.
- Blinova I, Niskanen J, Kajankari P, Kanaribik L, Käkinen A, et al. (2012) Toxicity of two types of silver nanoparticles to aquatic crustaceans *Daphnia magna* and *Thamnocephalus platyurus*. *Environ Sci Pollut Res* 1–8.
- Tsao TM, Wang MK, Huang PM (2009) Automated ultrafiltration device for efficient collection of environmental nanoparticles from aqueous suspensions. *Soil Sci Soc Am J* 73: 1808–1816.
- Ivask A, Rõlova T, Kahru A (2009) A suite of recombinant luminescent bacterial strains for the quantification of bioavailable heavy metals and toxicity testing. *BMC Biotech* 9: 41.
- Erickson H (2009) Size and shape of protein molecules at the nanometer level determined by sedimentation, gel filtration, and electron microscopy. *Biol Proced Online* 11: 32–51.
- Zook JM, Long SE, Cleveland D, Geronimo CLA, MacCuspie RI (2011) Measuring silver nanoparticle dissolution in complex biological and environmental matrices using UV–visible absorbance. *Anal Bioanal Chem* 401: 1993–2002.
- Bragg PD, Rainnie DJ (1974) The effect of silver ions on the respiratory chains of *Escherichia coli*. *Can J Microbiol* 20: 883–889.
- Holt KB, Bard AJ (2005) Interaction of silver (I) ions with the respiratory chain of *Escherichia coli*: an electrochemical and scanning electrochemical microscopy study of the antimicrobial mechanism of micromolar Ag⁺. *Biochemistry* 44: 13214–13223.
- Feng QL, Wu J, Chen GQ, Cui FZ, Kim TN, et al. (2000) A mechanistic study of the antibacterial effect of silver ions on *Escherichia coli* and *Staphylococcus aureus*. *J Biomed Mater Res* 52: 662–668.
- Fabrega J, Fawcett SR, Renshaw JC, Lead JR (2009) Silver nanoparticle impact on bacterial growth: effect of pH, concentration, and organic matter. *Environ Sci Technol* 43: 7285–7290.
- Sotiriou GA, Pratsinis SE (2010) Antibacterial activity of nanosilver ions and particles. *Environ Sci Technol* 44: 5649–5654.
- Morones JR, Elechiguerra JL, Camacho A, Holt K, Kouri JB, et al. (2005) The bactericidal effect of silver nanoparticles. *Nanotechnology* 16: 2346–2353.
- Neal AL (2008) What can be inferred from bacterium–nanoparticle interactions about the potential consequences of environmental exposure to nanoparticles? *Ecotoxicology* 17: 362–371.
- Dallas P, Sharma V, Zboril R (2011) Silver polymeric nanocomposites as advanced antimicrobial agents: classification, synthetic paths, applications, and perspectives. *Adv Colloid Interface Sci* 166: 119–135.
- Stefan M, Hritcu L, Mihasan M, Pricop D, Gostin I, et al. (2011) Enhanced antibacterial effect of silver nanoparticles obtained by electrochemical synthesis in poly(amide-hydroxyurethane) media. *J Mater Sci Mater Med* 22: 789–796.
- Taglietti A, Diaz Fernandez Y, Amato E, Cucu L, Dacarro G, et al. (2012) Antibacterial activity of glutathione-coated silver nanoparticles against Gram positive and Gram negative bacteria. *Langmuir* 28: 8140–8148.
- O'Reilly JP, Butts CP, F'anso IA, Shaw AM (2005) Interfacial pH at an isolated silica–water surface. *J Am Chem Soc* 127: 1632–1633.
- Nel AE, Madler L, Velegol D, Xia T, Hoek EMV, et al. (2009) Understanding biophysicochemical interactions at the nano-bio interface. *Nat Mater* 8: 543–557.
- Henglein A (1998) Colloidal silver nanoparticles: photochemical preparation and interaction with O₂, CCl₄, and some metal ions. *Chem Mater* 10: 444–450.
- Li W-R, Xie X-B, Shi Q-S, Zeng H-Y, Ou-Yang Y-S, et al. (2010) Antibacterial activity and mechanism of silver nanoparticles on *Escherichia coli*. *Appl Microbiol Biotechnol* 85: 1115–1122.

Table S3 ζ-potential of bacterial cells in half-strength NaCl-free LB medium. (DOCX)

Acknowledgments

Prof. Damjana Drobne (University of Ljubljana) is acknowledged for the TEM image of collargol. Dr. Villem Aruoja is acknowledged for the language editing. Dr. Pattanathu Rahman (Teesside University) is acknowledged for the *P. aeruginosa* strain, Dr. Martin Romantschuk (University of Helsinki) for the *P. fluorescens* strain, Prof. Matti Karp (Tampere University of Technology) and Dr. Marko Virta (University of Helsinki) for the *E. coli*, *B. subtilis* and *S. aureus* strains. Mr. Heiki Vija and Mr. Ilja Makarenkov are acknowledged for the technical help.

Author Contributions

Conceived and designed the experiments: OB A. Kahru AI. Performed the experiments: OB AKäkinen IK. Analyzed the data: OB A. Kahru AI A. Käkinen IK. Wrote the paper: OB A. Kahru AI. Final approval of the manuscript: OB A. Kahru AI A. Käkinen IK.

40. Sondi I, Salopek-Sondi B (2004) Silver nanoparticles as antimicrobial agent: a case study on *E. coli* as a model for Gram-negative bacteria. *J Colloid Interface Sci* 275: 177–182.
41. Dunne WM (2002) Bacterial adhesion: seen any good biofilm lately? *Clin Microbiol Rev* 15: 155–166.
42. Hutchison ML, Govan JRW (1999) Pathogenicity of microbes associated with cystic fibrosis. *Microbes Infect* 1: 1005–1014.
43. Dror-Ehre A, Adin A, Mamane H (2012) Control of membrane biofouling by silver nanoparticles using *Pseudomonas aeruginosa* as a model bacterium. *Desalin Water Treat* 48: 130–137.
44. El Badawy A, Silva R, Morris B, Scheckel K, Suidan M, et al. (2011) Surface charge-dependent toxicity of silver nanoparticles. *Environ Sci Technol* 45: 283–287.
45. George S, Lin S, Ji Z, Thomas C, Li L, et al. (2012) Surface defects on plate-shaped silver nanoparticles contribute to its hazard potential in a fish gill cell line and zebrafish embryos. *ACS Nano* 6: 3745–3759.

Supporting Information

Particle-Cell Contact Enhances Antibacterial Activity of Silver Nanoparticles

Olesja Bondarenko, Angela Ivask, Aleksandr Käkinen, Imbi Kurvet, Anne Kahru

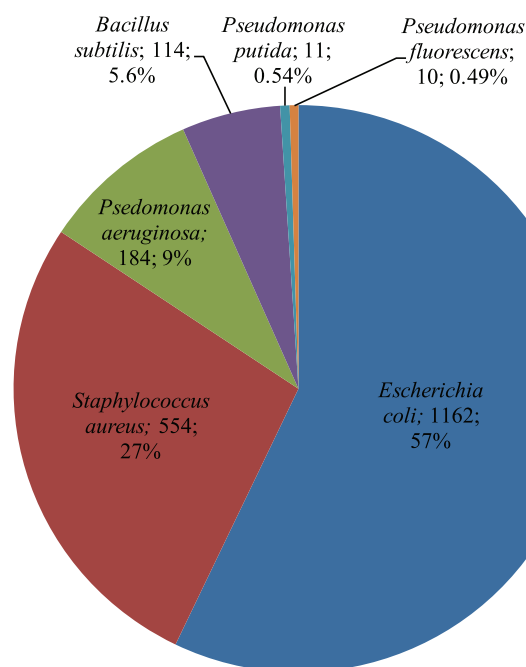


Figure S1 Number and share of articles on silver nanoparticles for six bacterial species in ISI WoS. Keywords used for the search and respective number of retrieved papers were as follows: ‘silver nanoparticles’ and ‘*Escherichia coli*’ (1162 papers); ‘silver nanoparticles’ and ‘*Staphylococcus aureus*’ (554 papers), ‘silver nanoparticles’ and ‘*Pseudomonas aeruginosa*’ (184 papers); ‘silver nanoparticles’ and ‘*Bacillus subtilis*’ (114 papers); ‘silver nanoparticles’ and ‘*Pseudomonas putida*’ (11 papers); ‘silver nanoparticles’ and ‘*Pseudomonas fluorescens*’ (10 papers). Total: 2035 papers. Search made: 06.12.2012.

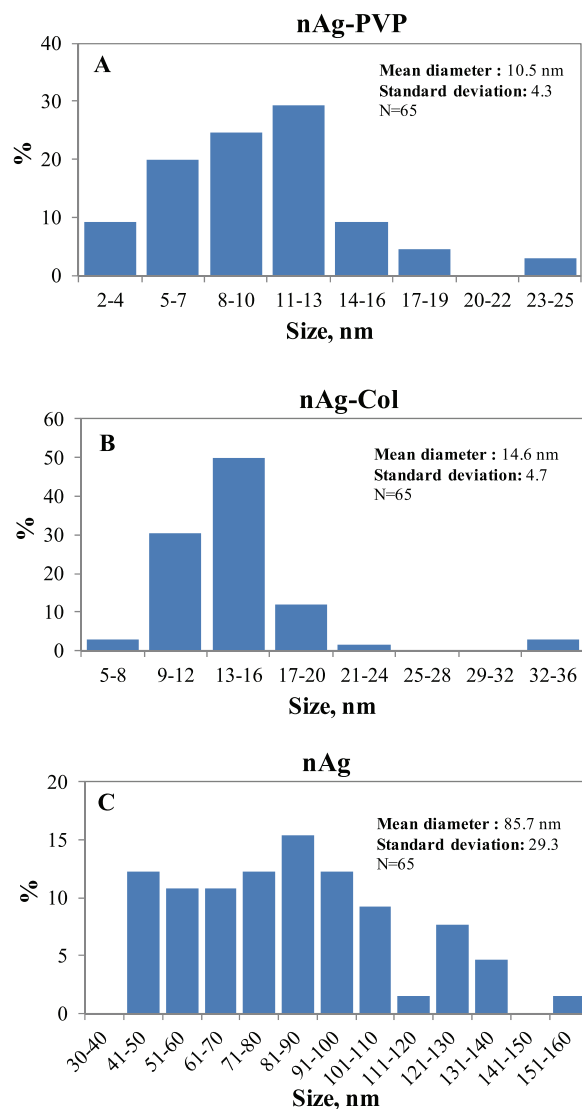


Figure S2 Primary size distribution of silver nanoparticles. A: PVP-coated nAg-PVP, B: protein-coated nAg-Col and C: uncoated nAg. Sizes of the silver nanoparticles were measured from TEM micrographs (Figure 1); altogether 65 particles were measured.

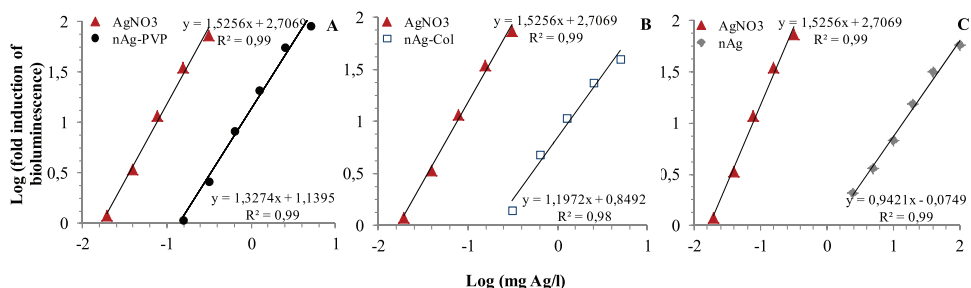


Figure S3 Response of Ag-biosensor to silver formulations. Representative calibration curves of Ag-biosensor *Escherichia coli* MC1061 (pSLcueR/pDNPCopAlux) for AgNO₃ (A–C), nAg-PVP (A), nAg-Col (B) and nAg (C) are shown. The lines represent the calibration plots for the linear regression between log(C)–log(indBL), whereas C is concentration of Ag (mg/l) in the samples and indBL is a fold induction of bioluminescence in Ag-biosensor in response to intracellular Ag. Linear range of the regression and regression equations are shown. Intracellular Ag was determined by using the linear regression equation for AgNO₃, which was considered 100% bioavailable and was used as a standard. Calculations were performed at BL = 10. An example for quantification of intracellular dissolution of nAg-PVP is given below:

$$\text{Log}(C_{\text{AgNO}_3}; \text{indBL} = 10) = \frac{1 - 2,7069}{1,5256} = -1,119$$

$$C_{\text{AgNO}_3} = 10 \wedge -1,119 = 0,076 \text{ (mg Ag/l)}$$

$$\text{Log}(C_{\text{nAgPVP}}; \text{indBL} = 10) = \frac{1 - 1,1395}{1,3274} = -0,105$$

$$C_{\text{nAgPVP}} = 10 \wedge -0,128 = 0,785 \text{ (mg Ag/l)}$$

$$\text{Intracellular Ag from nAgPVP} = \frac{0,076}{0,785} \times 100\% = 9,7\%$$

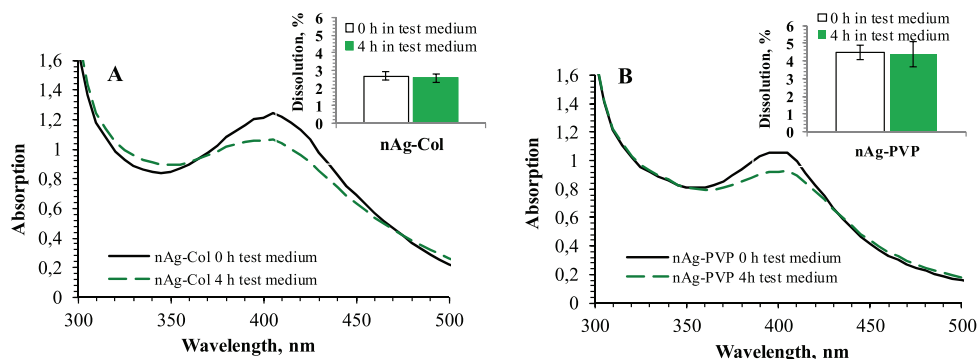


Figure S4 Ultraviolet - visible (UV-Vis) wavelength absorption spectra for silver nanoparticles. UV-Vis spectra for 10 mg/l nAg-Col suspension (A) and 10 mg/l nAg-PVP suspension (B) immediately after dispersion in the test medium (half-strength NaCl-free LB) (solid line) and after 4-h incubation (dashed green line) are shown. The UV-Vis measurement could not be conducted for the uncoated nAg NPs due to their quick sedimentation. The plasmon absorption peak at 405 nm is proportional to the concentration of metallic nanosized Ag and the decrease of this peak indicates dissolution of AgNPs. The absence of shift of plasmon absorption peak indicates that AgNPs do not aggregate. Insets in the Figure S4 indicate dissolution of AgNPs measured by atomic absorption spectroscopy (AAS) from the ultracentrifuged (390 000 g for 60 minutes) supernatants of AgNPs. During 4-h incubation, AgNPs dissolved but released Ag ions were complexed by the components of test medium that settled during ultracentrifugation.

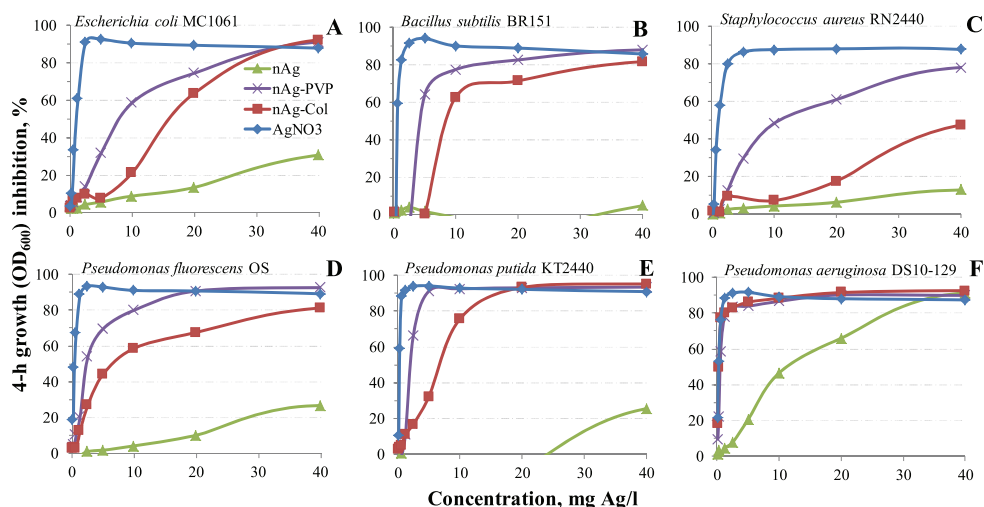


Figure S5 Growth inhibition of bacterial strains by silver nanoparticles. Growth inhibition of *Escherichia coli* (A), *Bacillus subtilis* (B), *Staphylococcus aureus* (C), *Pseudomonas fluorescens* (D), *Pseudomonas putida* (E) and *Pseudomonas aeruginosa* (F) by uncoated Ag nanoparticles (nAg; triangle), collargol (nAg-Col; rectangle), PVP-coated Ag nanoparticles (nAg-PVP; cross) or AgNO₃ (diamond) after 4-h incubation in half-strength NaCl-free LB medium at 30°C. The representative figures from three biological replicates are shown.

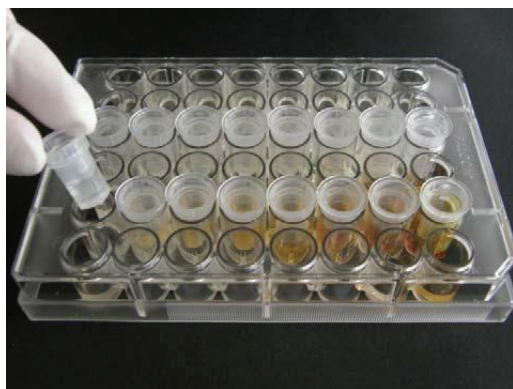


Figure S6 Setup of the dialysis membrane test. Bacterial cells were separated from AgNPs or AgNO₃ by 20 kDa (about 4 nm) dialysis membrane (Slide-A-Lyzer MINI Dialysis Device, 20K MWCO, Thermo Scientific). 400 μ l of bacterial suspension was pipetted into the wells, polypropylene cups with the dialysis membrane on the bottom were inserted into the wells and

400 μ l of AgNPs, AgNO₃ or DI water (control) was pipetted into the cups. During the optical density measurements the cups were removed.

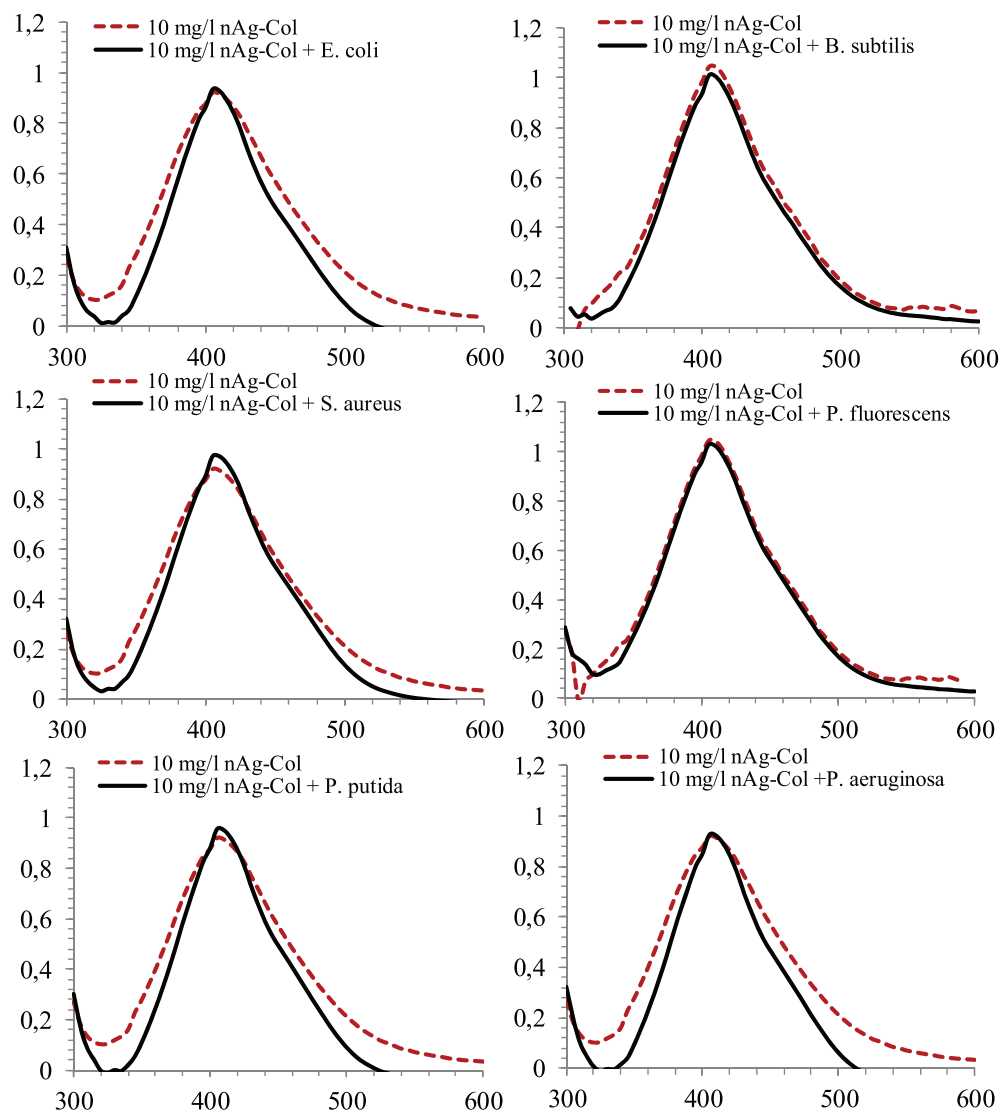


Figure S7 UV-visible absorption spectra of nAg-Col suspensions (10 mg Ag/l) with or without bacteria. UV-Vis spectra of AgNPs in half-strength NaCl-free LB medium without bacterial cells (dashed red line) or after exposure of nAg-Col to bacterial cells (solid line). No separation of

particles and/or bacterial cells was done before the measurement. The experiment is a control for [Figure 7](#) to exclude the interference of bacterial cells with the measurements of UV-Vis absorption spectra of nAg-Col. Addition of bacterial culture had no significant effect on the UV-Vis spectra of nAg-Col.

Table S1 Characteristics of the bacterial strains used in this study.

Bacterial strain	Genotype or description	Reference
<i>Escherichia coli</i> MC1061	<i>araD139 Δ(ara, leu)7697 ΔlacX74 galU galK hsdR2 strA mcrA mcrB1</i>	¹ Casadaban and Cohen, 1980
<i>Bacillus subtilis</i> BR151	<i>trpC2 lys-3 metB10</i>	² Young et al., 1969
<i>Staphylococcus aureus</i> RN4220	<i>rsbU- agr-</i>	³ Kreiswirth et al., 1983
<i>Pseudomonas fluorescens</i> OS8	Rifampicin ^r , isolated from toluates-contaminated soil	⁴ Sarand et al., 2000
<i>Pseudomonas putida</i> KT2440	<i>rmo- mod+</i>	⁵ Bagdasarian et al., 1981
<i>Pseudomonas aeruginosa</i> DS10-129	Ampicillin ^r , kanamycin ^r , isolated from diesel-contaminated site	⁶ Rahman et al., 2000

¹ Casadaban MJ, Cohen SN (1980) Analysis of gene control signals by DNA fusion and cloning in *Escherichia coli*. J Mol Biol 138: 179–207.

² Young FE, Smith C, Reilly BE (1969) Chromosomal location of genes regulating resistance to bacteriophage in *Bacillus subtilis*. J Bacteriol 98: 1087–1097.

³ Kreiswirth BN, Lofdahl S, Betley MJ, O'Reilly M, Schlievert PM et al. (1983) The toxic shock syndrome exotoxin structural gene is not detectably transmitted by a prophage. Nature. 305: 709–712.

⁴ Sarand I, Haario H, Jorgenson KS, Romantschuk M (2000) Effect of inoculation of a TOL plasmid containing mycorrhizosphere bacterium on development of Scots pine seedlings, their mycorrhizosphere and the microbial flora in m-toluene-amended soil. FEMS Microbiol Ecol 31: 127–141.

⁵ Bagdasarian M, Lurz R, Ruckert B, Franklin FC, Bagdasarian MM et al. (1981) Specific-purpose plasmid cloning vectors. II. Broad host range, high copy number, RSF1010-derived vectors, and a host-vector system for gene cloning in *Pseudomonas*. Gene 16: 237–247.

⁶ Rahman KSM, Rahman TJ, Lakshmanaperumalsamy P, Marchant R, Banat IM (2002) Emulsification potential of bacterial isolates with a range of hydrocarbon substrates. Acta Biotechnol 23: 335–345.

Table S2 Minimum bactericidal concentration (MBC mg Ag/l) of silver nanoparticles and AgNO₃ to six bacterial strains. nAg states for uncoated AgNPs, nAg-PVP for PVP-coated AgNPs and nAg-Col for collargol. Bacteria were incubated with different concentrations of Ag-compounds in half-strength NaCl-free LB medium at 30°C for 4 h. Then, 3 µl of the test sample was pipetted onto agarized LB plates, incubated at 30°C for 24 h and visually inspected for the growth. The lowest tested concentration that completely inhibited the visible growth of bacteria was designated as a MBC.

Bacterial strain	Gram	4-h minimum bactericidal concentration (MBC), mg Ag/l			
		nAg	nAg-Col	nAg-PVP	AgNO ₃
<i>Escherichia coli</i> MC1061	G–	>100	40	40	5
<i>Bacillus subtilis</i> BR151	G+	>100	40	20	5
<i>Staphylococcus aureus</i> RN2440	G+	>100	100	>100	40
<i>Pseudomonas fluorescens</i> OS8	G–	>100	100	40	5
<i>Pseudomonas putida</i> KT2440	G–	>100	40	40	5
<i>Pseudomonas aeruginosa</i> DS10-129	G–	100	5	20	5

Table S3. ζ-potential of bacterial cells in half-strength NaCl-free LB medium.

Bacterial strain	ζ-potential
<i>Escherichia coli</i> MC1061	-32,9
<i>Bacillus subtilis</i> BR151	-35,2
<i>Staphylococcus aureus</i> RN2440	-14,0
<i>Pseudomonas fluorescens</i> OS8	-8,4
<i>Pseudomonas putida</i> KT2440	-9,1
<i>Pseudomonas aeruginosa</i> DS10-129	-23,9

PUBLICATION IV

Käkinen A, Ding F, Chen P, Mortimer M, Kahru A and Ke PC (2013). Interaction of firefly luciferase and silver nanoparticles and its impact on enzyme activity. *Nanotechnology*, 24(34):345101

Interaction of firefly luciferase and silver nanoparticles and its impact on enzyme activity

Aleksandr Käkinen^{1,2}, Feng Ding³, Pengyu Chen^{4,5}, Monika Mortimer¹, Anne Kahru¹ and Pu Chun Ke⁴

¹ Laboratory of Environmental Toxicology, National Institute of Chemical Physics and Biophysics, Akadeemia tee 23, Tallinn 12618, Estonia

² Department of Chemical and Materials Technology, Tallinn University of Technology, Ehitajate tee 5, Tallinn 19086, Estonia

³ Structure, Dynamics, and Function of Biomolecules and Molecular Complexes Laboratory, Clemson University, Clemson, SC 29634, USA

⁴ Nano-Biophysics and Soft Matter Laboratory, COMSET, Clemson University, Clemson, SC 29634, USA

⁵ Microsystems Technology and Science Laboratory, University of Michigan, Ann Arbor, MI 48109, USA

E-mail: anne.kahru@kbfi.ee and pcke11@clemson.edu


Received 2 April 2013, in final form 7 July 2013

Published 30 July 2013

Online at stacks.iop.org/Nano/24/345101

Abstract

We report on the dose-dependent inhibition of firefly luciferase activity induced by exposure of the enzyme to 20 nm citrate-coated silver nanoparticles (AgNPs). The inhibition mechanism was examined by characterizing the physicochemical properties and biophysical interactions of the enzyme and the AgNPs. Consistently, binding of the enzyme induced an increase in zeta potential from -22 to 6 mV for the AgNPs, triggered a red-shift of 44 nm in the absorbance peak of the AgNPs, and rendered a 'protein corona' of 20 nm in thickness on the nanoparticle surfaces. However, the secondary structures of the enzyme were only marginally affected upon formation of the protein corona, as verified by circular dichroism spectroscopy measurement and multiscale discrete molecular dynamics simulations. Rather, inductively coupled plasma mass spectrometry measurement revealed a significant ion release from the AgNPs. The released silver ions could readily react with the cysteine residues and N-groups of the enzyme to alter the physicochemical environment of their neighboring catalytic site and subsequently impair the enzymatic activity.

 Online supplementary data available from stacks.iop.org/Nano/24/345101/mmedia

(Some figures may appear in colour only in the online journal)

1. Introduction

The recent advancement of nanotechnology has transformed the landscape of modern science and engineering and, concomitantly, presented many challenges to our understanding of the biological and environmental implications of engineered nanomaterials [1, 2]. From the perspectives of biophysics and physical chemistry the interactions between

nanoparticles and biomolecules involve a description of energy minimization for the thermodynamic system, as well as characterizations of the time evolution and transformation of nanoparticle–biomolecular 'coronas' in changing environments (pH, temperature, salinity, and biomolecular diversity of different origin, abundance, and amphiphilicity) [3–5]. Microscopically and macroscopically such biophysical and biochemical interactions present themselves through the

endpoints of immune responses and toxicological effects on cellular and whole organism levels, yet the strategies employed by the latter fields remain to be fully validated for nanoscale objects that possess a high surface energy and reactivity as well as distinct physicochemical properties that are unavailable to bulk materials [6, 7]. Indeed, a number of studies in the recent past by our lab [8–11] and by others [3, 5, 12–15] have demonstrated the effectiveness and insight of applying the principles and methodologies of physical sciences in addressing the fate of nanoparticles in living systems. Especially on the molecular level these physical studies offer essential information complementary to the results from biological and toxicological approaches. The current study continues such an effort by examining the physicochemical and biophysical phenomena of silver nanoparticles (AgNPs) interacting with firefly luciferase and the manifestation of such interactions in the hindered activity of the enzyme.

Silver nanoparticles are a class of the most produced nanomaterials that have found their major use in antibacterial applications, in addition to their more traditional roles in catalysis and generation of surface plasmon resonance (SPR) for sensing and DNA hybridization [16–20]. The working hypotheses of the antibacterial properties of AgNPs—still much an ongoing debate today—involve the release of silver ions in the extracellular space followed by cell uptake and a cascade of intracellular reactions, direct interactions of AgNPs with cell membranes to compromise the major aspects from protein function to proton gradient and membrane permeability, and cell uptake of AgNPs which triggers the production of reactive oxygen species (ROS) and the intracellular release of silver ions to hinder DNA replication and ATP synthesis [21–24].

Information on the potentially adverse effects of AgNPs on environmentally relevant organisms is emerging [25]. With regard to the effects of AgNPs on enzymatic activities it is generally recognized that the antimicrobial action of AgNPs (and silver ions) proceeds via the inhibition of vital enzymes such as those involved in ATP production, apparently through interactions with the thiol groups of these proteins [26]. For example, Li *et al* reported that the activity of respiratory chain dehydrogenases in *Escherichia coli* was inhibited by AgNPs in a dose-dependent manner [27]. Also, soil exoenzyme activities, especially for urease and dehydrogenases, were influenced by citrate-coated AgNPs [28]. AgNPs also hindered the activity of creatine kinase from rat brain and skeletal muscle *in vitro*, presumably through interactions with the thiol groups of the enzyme [29]. It should be pointed out that ligands and enzymes with thiol groups within mammalian cells like glutathione, thioredoxin, superoxide dismutase, and thioredoxin peroxidase are key components of the cell's antioxidant defense mechanism, which is responsible for neutralizing intracellular ROS largely generated by mitochondrial energy metabolism [30].

Firefly (*Photinus pyralis*) luciferase is a 62 kDa (550 residues) protein that catalyzes the production of light by converting chemical energy into photoenergy. Specifically, this process involves the oxidation of luciferin—the heterocyclic substrate of the enzyme, in the presence of

Mg-ATP and molecular oxygen [31]. This reaction has an unusual kinetics in that luciferase turns over very slowly; after an initial flash of light, the luminescence rapidly decreases to a low level of emission, probably due to product inhibition of the enzyme.

Although the adverse effects of nanomaterials may occur on several levels for biological organizations, enzymes regulate life processes in all cells and are expected to play a pivotal role in evoking biological responses to nanomaterial exposure. In consideration of the mass production of AgNPs and also given the wide use of firefly luciferase as a reporter in a variety of *in vitro* bioassays, AgNPs and firefly luciferase were selected as a model system for our current evaluation of the biological and ecological impact of engineered nanomaterials.

In this study we examine the binding of luciferase with AgNPs and analyze the hindered enzyme activity as a result of the interaction. Specifically, using UV–vis spectrophotometry we characterize the spectral shift of the characteristic SPR of AgNPs induced by their surface coating of the (dielectric) enzyme (sections 2.3 and 3.2). We confirm the formation of an AgNP–luciferase ‘corona’ [32] using transmission electron microscopy (TEM) (sections 2.4 and 3.2) and illustrate the molecular details of such a process by state-of-the-art multiscale discrete molecular dynamics (DMD) computer simulations [33] (sections 2.8, 3.2, and 3.4). In addition, we analyze changes in the secondary structures of luciferase induced by AgNPs using circular dichroism (CD) spectroscopy (sections 2.5 and 3.2) and corroborate our observations by the simulations (sections 2.8, 3.2, and 3.4). We further characterize silver ion release from AgNPs using inductively coupled plasma mass spectrometry (ICP-MS) (sections 2.6 and 3.2) and attribute hindered enzyme luminescence to the high affinity of silver ions for the sulfhydryl (–SH) groups in the cysteine residues of the luciferase (sections 2.3, 2.7, 3.3, and 3.4). This mechanistic study offers a biophysical and physicochemical basis for facilitating our interpretation of the biological and environmental implications of nanomaterials at the molecular level.

2. Materials and methods

2.1. Materials

Citrate-coated AgNP stock suspensions (Biopure, 20 nm in diameter, 1 mg ml^{−1} in 2 mM citrate, or 0.03 × 10^{−4} M) were purchased from NanoComposix and stored at 4 °C. Citrate is widely used as a capping agent in AgNP synthesis, where the negatively charged, noncovalent citrate coating renders AgNP suspensions stable as a result of electrostatic repulsion. TRIS-acetate buffer of 25 mM, pH 7.8 was used as the test medium. TRIS base, acetic acid, and NaCl (≥99.5% purity) were purchased from J T Baker. The TRIS base was dissolved in Milli-Q water (Nanopure Diamond, Barnstead) and its pH was adjusted to 7.8 with acetic acid. QuantiLum Recombinant Firefly Luciferase (MW 62 000 Da, 13.75 mg ml^{−1} or 2.25 × 10^{−4} M) and the Luciferase Assay System were purchased

from Promega and stored at -80°C and -18°C , respectively. Silver nitrate AgNO_3 ($\geq 99.0\%$ purity), gold (III) chloride AuCl_3 ($\geq 99.99\%$ purity), and D-luciferin were purchased from Sigma Aldrich. The AgNO_3 and AuCl_3 stock solutions (1 mg ml^{-1}) were prepared in Milli-Q water and stored at 4°C . The D-luciferin stock solution (1 mg ml^{-1}) was prepared in the TRIS-acetate buffer and stored at 4°C . All experiments were performed at room temperature (20°C).

2.2. Hydrodynamic size and zeta potential

The average hydrodynamic sizes of luciferase (137.5 mg l^{-1}), AgNPs (10 mg l^{-1}), and AgNP-luciferase mixtures were determined using dynamic light scattering (DLS) (Zetasizer Nano S90, Malvern Instruments). The measurements were carried out in standard polypropylene plastic cuvettes of 1 cm path length. The surface charges of the samples were measured in Milli-Q water to avoid interference of TRIS-acetate buffer on the analytes' potentials, using a Zetasizer Nano ZS (Malvern instruments). Different luciferase concentrations were titrated with the AgNP suspensions. The samples were allowed to stabilize for 2 h at room temperature prior to the zeta potential measurement.

2.3. UV-vis spectrophotometry

The binding of luciferase (13.75 mg l^{-1}) to AgNPs (10 mg l^{-1}) was investigated by measuring the SPR peak ($350\text{--}500\text{ nm}$ wavelength) of the AgNPs using a UV-vis spectrophotometer (Cary 300 Bio, Varian). This measurement was done in Milli-Q water at room temperature using a polypropylene plastic cuvette of 1 cm path length. The binding affinities of luciferase (200 mg l^{-1}), ATP (100 mg l^{-1}), and luciferin (50 mg l^{-1}) for silver ions were investigated using the UV-vis spectrophotometer and quartz cuvettes of 1 cm path length.

2.4. TEM

Direct observation of AgNP-luciferase coronas was performed by TEM (Hitachi H7600). Specifically, AgNPs (1 mg l^{-1}) were incubated with luciferase (13.75 mg l^{-1}) for 2 h , pipetted on a copper grid, and stained with phosphotungstic acid for 10 min prior to imaging. The same procedure was applied to control samples of AgNPs (1 mg l^{-1}) alone. All dilutions were performed in 25 mM TRIS-acetate buffer and stored at room temperature.

2.5. CD spectroscopy

A spectrometer (J-810, Jasco) was used to assess the effects of AgNP binding on the secondary structures of the enzyme. For this purpose, luciferase (13.75 mg l^{-1}) was incubated with AgNPs (1 mg l^{-1}) and silver ions (1 mg l^{-1}) for 2 h at room temperature and the measurement was performed in a quartz cuvette of 1 cm path length between 190 and 300 nm at 1 nm intervals. The selection of this wavelength range

avoided strong absorption and SPR from the AgNPs. The backgrounds of the AgNPs and the silver ions were subtracted accordingly to exclude their interferences with that of the luciferase. Milli-Q water instead of the TRIS buffer was used to minimize interference to the CD signal from the buffer.

2.6. ICP-MS

Silver ion release from citrate-coated AgNPs, upon their incubation with luciferase, was performed using ICP-MS (X Series 2, Thermo Scientific). For this measurement AgNPs (1 mg l^{-1}) and luciferase (13.75 mg l^{-1}) were mixed in TRIS-acetate buffer and incubated at room temperature for 0 , 2 , 4 , 8 , 24 , 48 , and 72 h in polypropylene Eppendorf tubes. At each time point the samples were centrifuged at $12\,100\text{ RCF}$ (MiniSpin, Eppendorf) for 30 min , and the supernatants were collected and stored at -18°C . The effectiveness of centrifugation for the precipitation of AgNPs was confirmed by measuring UV-vis absorbance for the suspensions before and after the procedure. The effect of luciferase concentration (2.74 , 6.85 , 13.75 , 137.5 mg l^{-1}) on ion release from the AgNPs (1 mg l^{-1}) was determined using the procedure described above, for 24 h incubation. Prior to the ICP-MS analysis the samples were thawed and diluted 10 -fold in 2% HNO_3 .

2.7. Luciferase activity assay

The effect of AgNPs on luciferase activity was determined using the Luciferase Assay System (Promega). The assay was first calibrated for the concentrations of luciferase ($10^{-8}\text{--}10^{-17}\text{ M}$) and the AgNPs (0.01 , 0.1 , 1 , 10 , 100 mg l^{-1}). For the study of the inhibitory effect of silver ions, AgNO_3 of 0.002 , 0.02 , 0.2 , 2 , and 20 mg l^{-1} was used and the testing was conducted following the same procedures as for the AgNPs. The concentrations of silver ions were chosen by taking into account that AgNPs released $\sim 20\%$ of their mass to silver ions in 2 h . Luciferase was incubated with AgNPs or AgNO_3 for 2 h at room temperature prior to the measurement. A pre-incubated AgNP-luciferase mixture of $20\text{ }\mu\text{l}$ was added to $100\text{ }\mu\text{l}$ of the Luciferase Assay System and the signal was recorded with a luminometer (Turner BioSystem 20/20n). The luciferase activity assay was also performed in the presence of Na^+ (as NaCl ; 2 , 20 , 200 mg of Na l^{-1}) or Au^{3+} (as AuCl_3 ; $0.002\text{--}200\text{ mg Au l}^{-1}$) to determine the specificity of the observed inhibition. In order to identify if any of the reaction components in the Luciferase Assay System limited luciferase activity, a kinetic study was performed where an extra $20\text{ }\mu\text{l}$ of luciferase, ATP (100 mg l^{-1}), or luciferin (100 mg l^{-1}) was added to the assay after 20 min of reaction and the resulting luminescence was recorded for the next 20 min .

In addition, a rapid kinetics assay was performed for the luminescence reaction (Orion II luminometer, Berthold Technologies). This experiment was conducted at room temperature using 96 -well white polypropylene microplates. A Luciferase Assay System reagent of $100\text{ }\mu\text{l}$ and nanoparticle suspensions or ions of $10\text{ }\mu\text{l}$ ($0.4\text{--}400\text{ mg Ag l}^{-1}$) were

Table 1. Zeta potentials of luciferase–AgNP mixtures at different enzyme concentrations. Prior to the measurements AgNPs of 10 mg l^{-1} were pre-incubated with luciferase of different concentrations for 2 h in Milli-Q water. Data presented are the averages of three samples \pm standard deviations.

Sample	Zeta potential (mV)
137.5 mg l^{-1} luciferase	3.2 ± 0.2
137.5 mg l^{-1} luciferase + 10 mg l^{-1} AgNPs	6.0 ± 0.3
13.8 mg l^{-1} luciferase + 10 mg l^{-1} AgNPs	4.5 ± 0.5
6.8 mg l^{-1} luciferase + 10 mg l^{-1} AgNPs	-5.0 ± 0.8
2.8 mg l^{-1} luciferase + 10 mg l^{-1} AgNPs	-19.3 ± 0.3
10 mg l^{-1} AgNPs	-22.0 ± 0.3

pipetted into each well. Then luciferase of $20 \mu\text{l}$ was automatically dispensed into the microplate wells in the luminometer testing chamber. The luminescence was recorded during the first 10 s at 5 data points s^{-1} .

2.8. Computer simulation of AgNP–luciferase binding

Multiscale DMD simulations [33] were applied to study the interactions between luciferase and AgNPs *in silico*. Specifically, atomistic simulations [34] were used to identify the binding modes between an individual luciferase and a citrate-coated AgNP, and coarse-grained simulations [35] were used to characterize the corona formation between multiple luciferase molecules and one citrate-coated AgNP. DMD is a special type of molecular dynamics simulation algorithm [36], which features high sampling efficiency and has been increasingly used to study biomolecules [37]. A model citrate-coated AgNP of 10 nm in diameter as detailed recently [38] was employed for the current study, where the surface silver atoms of the nanoparticle were mostly hydrophobic without charges and only a small fraction of the surface atoms were positively charged. This approach of using a smaller AgNP in the simulations than in the experiments (20 nm in diameter) significantly reduced the computational cost without compromising much of the physical phenomena under examination. The x-ray crystallography structure of the luciferase from *Photinus pyralis* was used as a reference structure (PDB [39] ID: 1BA3).

3. Results and discussion

3.1. An empirically determined luciferase to AgNP ratio

The mean diameter of AgNPs was $20 \pm 3 \text{ nm}$ as specified by the manufacturer, and the QuantiLum Recombinant Firefly Luciferase (MW 62 000 Da) was $\sim 6 \text{ nm}$ in size. Based on the surface areas and sizes of the AgNPs and the luciferase, the optimized enzyme to nanoparticle ratio of N was calculated as follows:

$$N = \frac{4\pi(R_{\text{Ag}} + R_{\text{Luciferase}})^2}{\pi R_{\text{Luciferase}}^2}, \quad (1)$$

where R_{Ag} and $R_{\text{Luciferase}}$ are the radii of AgNPs and luciferase, respectively. According to this equation, it is estimated that up to 75 luciferase molecules can be adsorbed onto each individual AgNP, equivalent to a concentration ratio of 137.5 mg l^{-1} of luciferase to 10 mg l^{-1} of AgNPs.

3.2. Physicochemical interactions of luciferase and AgNPs

The hydrodynamic size of AgNPs in 25 mM TRIS-acetate buffer (pH 7.8) was measured to be $26.2 \pm 0.1 \text{ nm}$, consistent with the specifications provided by the manufacturer. However, luciferase displayed significant agglomerations in the test medium ($>1 \mu\text{m}$), making it difficult to infer the hydrodynamic size of AgNPs upon luciferase adsorption. Nonetheless, binding of the enzyme to AgNPs was evidenced from the zeta potential measurement through titrating different concentrations of luciferase into the AgNP suspensions (10 mg l^{-1}). As shown in table 1 the AgNPs exhibited a negative surface charge (-22 mV) in Milli-Q water due to their citrate coating. Under the same conditions luciferase alone showed a slightly positive surface charge (3.2 mV) as a net result from its positively and negatively charged domains. With increasing concentrations of luciferase the mixtures of luciferase–AgNPs displayed a steady increase in zeta potential up to 6 mV , suggesting binding of the enzyme and the nanoparticles (and their citrate coating), driven by *van der Waals* forces, electrostatic interactions, dynamic exchanges between the enzyme and citrate for their adsorption onto the nanoparticle surfaces, as well as hydrogen bonding between the citrate and the electronegative moieties of the protein.

The formation of AgNP–luciferase corona was confirmed by a comparison of the UV–vis spectra of AgNPs, luciferase, and their mixture (figure 1(a)). The AgNP–luciferase mixture was stable at 2 h, but showed a 24.7% reduction in absorbance at 20 h due to precipitations over time. A characteristic peak of SPR was identified for AgNPs at 402 nm (blue curve). A red-shift of 44 nm in the extinction peak of AgNPs occurred after their incubation with luciferase, accompanied by a decrease of 14% in the magnitude of the peak value. This phenomenon is consistent with our previous study on the binding of AgNPs with human serum albumin [40], indicating an increased dielectric constant for the AgNPs as a result of protein adsorption/coating and nanoparticle aggregation.

The inset of figure 1(b) shows a TEM micrograph of the control AgNPs, which were well dispersed and were approximately spherical. The size of the AgNPs ranged between 21.4 and 24.8 nm, consistent with the manufacturer's information and our DLS measurement. In the presence of luciferase, a thick layer of optically less dense material was clearly visible surrounding the AgNPs (figure 1(b)). The average diameter of the AgNP–luciferase coronas was

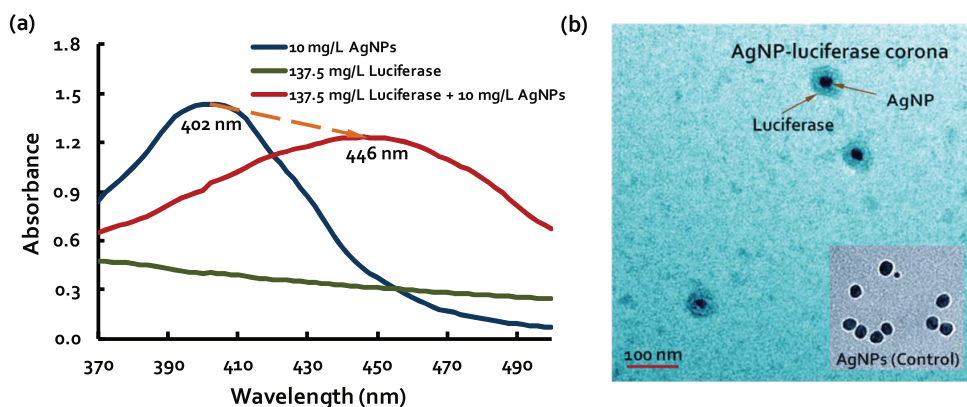


Figure 1. Interactions of AgNPs with luciferase. (a) UV-vis spectra and (b) TEM image. The maroon line in panel (a) describes a spectrum of the AgNP-luciferase mixture and displays a red-shift of 44 nm and a 14% decrease in absorbance value for the SPR peak of AgNPs (blue) as a result of luciferase binding and nanoparticle aggregation. The green line indicates the absorbance of the enzyme. The TEM image (b) shows AgNP-luciferase coronas. Inset in (b): control AgNPs. Scale bar: 100 nm for both the image and the inset.

determined to be ~ 60 nm and the average thickness of the protein layers was ~ 20 nm. This image corroborates the binding of the enzyme with the AgNPs and implies multilayer protein coating of the nanoparticles.

CD spectroscopy was performed to determine the effect of AgNP and silver ion binding on the secondary structures of the luciferase. Our measurement (figure S1 available at stacks.iop.org/Nano/24/345101/mmedia) revealed a decrease of beta sheets from 26% to 22% (or a relative decrease of 15.4%) and a corresponding increase of alpha helices from 20% to 22% (or a relative increase of 10%) after incubating the protein ($500\times$ dilution from stock, i.e., 27.5 mg l^{-1}) with the AgNPs (0.9 mg l^{-1}) in Milli-Q water. Due to the differences in their surface curvatures, the globular luciferase molecules (~ 6 nm) could sense the AgNPs (~ 20 nm) as relatively flat substrates upon their binding. In addition, since the enzyme formed a multilayer coating the protein conformation of the outer layers could be affected by the inner layers without direct contact with the particle surfaces. Consequently, modest conformational changes were induced and the enzyme was later shown in the activity assay and in the computer simulations as only slightly perturbed by the physical adsorption of the nanoparticles. Similar to the trend observed for proteins exposed to AgNPs, silver ions in AgNP suspensions could also alter the protein conformation, as indicated by the CD measurement on luciferase incubated with free silver ions (figure S1, blue line, where beta sheets decreased from 26% to 23% and alpha helices increased from 20% to 21% as derived from the spectrum).

AgNPs released silver ions upon their incubation with the enzyme in aqueous solutions. The released silver ions have been evidenced to be highly reactive to inhibit respiratory enzymes, induce overproduction of ROS, and bind sulfur- and phosphorus-containing molecules to interrupt cell defense systems or deplete intracellular concentrations of such molecules [30]. Indeed, our data showed that AgNPs (1 mg l^{-1}) were completely dissolved during 24 h in the

test medium. In the presence of luciferase our ICP-MS measurement revealed a significantly reduced ion release from the AgNPs over time (figure 2(a)), conceivably due to the blockage by the adsorbed proteins. Specifically, the mixture of luciferase (137.5 mg l^{-1}) and AgNPs (1 mg l^{-1}) showed 15% dissolution of the AgNPs after 4 h and the ion release was terminated after 72 h. For a given AgNP concentration (1 mg l^{-1}) and at 24 h of incubation, when the luciferase concentration was reduced from 137.5 to 2.74 mg l^{-1} the silver ion release was increased from 7 to $641\text{ }\mu\text{g of Ag}^+\text{ l}^{-1}$ (figure 2(b)).

3.3. Luciferase enzymatic activity

A luciferase concentration of 10^{-9} M in the middle of the calibrated linear response curve (data not shown) was chosen for examining the enzymatic activity. Our experiment showed that AgNPs inhibited light producing a reaction catalyzed by the luciferase, mirroring the same tendency found for the reaction with Ag^+ alone (figure 3). The luminescence signals were comparable for AgNPs and Ag^+ of concentrations equivalent to $\sim 20\%$ of the AgNPs in mass, in agreement with the 2 h ion release from AgNPs determined by the ICP-MS experiment (figure 2(a)). This assay suggests that the inhibition of luciferase was largely induced by silver ions while the physical adsorption onto AgNPs and its induced crowding and conformational changes in protein structure only exerted a minor effect on the enzyme function. The latter point was further corroborated by the DMD simulation described in section 3.4.

Additional UV-vis absorbance measurements were conducted to investigate the binding affinities of silver ions for the reaction components ATP, luciferase, and luciferin (figure S2 available at stacks.iop.org/Nano/24/345101/mmedia). Overall Ag^+ showed a higher affinity for luciferase than for ATP or luciferin, judged by the corresponding spectral changes for these ligands. This

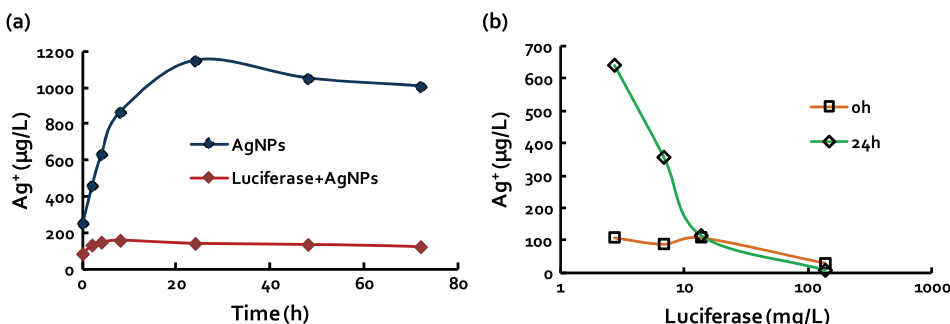


Figure 2. Effects of incubation and luciferase concentration on silver ion release from AgNPs. (a) 1 mg l⁻¹ of AgNP suspension was incubated with and without luciferase (137.5 mg l⁻¹) for 72 h. (b) 1 mg l⁻¹ of AgNP suspension was incubated with luciferase of 2.64–137.5 mg l⁻¹. The concentrations of silver ions are shown for two time points (0 and 24 h). The ion release experiment was performed first by sample centrifugation and supernatant collection. The quality of the samples was controlled by UV-vis and DLS to ensure the absence of nanoparticles after centrifugation. The ICP-MS measurement was then performed with three parallels. The samples had ~20% ions at the ‘zero point’ of measurement immediately after dilutions and centrifugations.

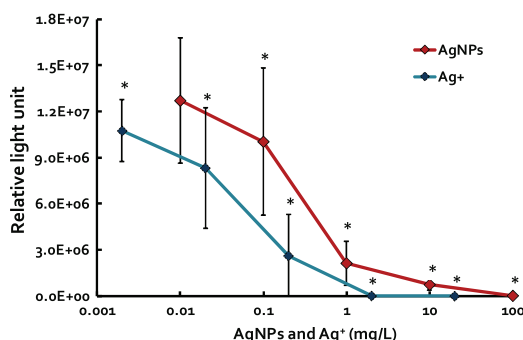


Figure 3. Inhibition of luciferase activity by AgNPs and Ag⁺. Statistically significant differences between the samples and the controls (i.e., when neither AgNPs nor silver ions were applied to the reaction) were determined by the Student *t*-test (asterisk * indicates *p* < 0.05). This experiment was performed using three independent replicates and the average values are presented.

measurement further suggests that the limiting factor in the inhibition of luciferase luminescence was the interaction between the enzyme and silver ions. Consistently, our kinetic study showed a recovery of luminescence intensity upon addition of extra luciferase 1200 s into the reaction (figure 4(a)), while no such recovery was observed for the addition of extra ATP or luciferin (data not shown). Since our assay with Au³⁺ (figure 4(c)) showed a similar but less pronounced inhibition pattern than that observed for Ag⁺, unlike the case with Na⁺ (figure 4(b)), we further attribute the observed luminescence inhibition to the interactions of Ag⁺ or Au³⁺ with the sulphhydryl groups in the cysteine residues of the luciferase. The strengths of such thiol-heavy metal bonds are of the order of 100 kJ mol⁻¹ and are often utilized to render molecular self-assemblies that are stable in a variety of temperatures, solvents, and potentials [41]. *N*-containing functional groups could also complex with

Ag⁺ or Au³⁺. However, the strength of such complexation would be weaker than the disulfide bonds formed between Ag and cysteines. Although the covalent-like thiol–Au bond is slightly stronger than the thiol–Ag bond according to density functional theory calculations [42], the structural stability of the protein and the spatial distribution (and hence differential accessibility) of the cysteine residues (figure 5(a)) should favor their bond formation with the monovalent Ag⁺ over the trivalent Au³⁺, as reflected by a lack of rapid inhibition induced by Au³⁺ (figure S3(c) available at stacks.iop.org/Nano/24/345101/mmedia) and the differential inhibition efficiencies associated with the two types of heavy metals after 2 h of incubation (figure 4(c)). Firefly luciferase possesses four cysteine residues per monomer, all of which are positioned away from the active site (figure 5(a)) with the shortest distance ~1.5 nm. Although it does not appear that a specific cysteine mediates the loss of luciferase activity, complete inactivation of luciferase activity has been demonstrated by the blockage of all four cysteine thiols and the concomitant incorporation of four moles of *N*-acetyl-*N'*-(5-sulfo-1-naphthyl)ethylenediamine (AEDANS) per mole of enzyme [43]. Nonetheless, such interactions between silver ions and cysteine residues ought to alter the enzyme conformation directly or allosterically, modify the local environment (charge, amphiphilicity, and accessibility) of the enzyme active site to impair its interactions with luciferin, ATP, oxygen, and cofactors and further hinder the catalysis of light emission.

3.4. DMD simulation of AgNP–luciferase corona

We first performed all-atom DMD simulations of a luciferase molecule interacting with a citrate-coated AgNP. We started with the apo-structure of luciferase (figure 5(a), left panel) initially positioned away from the AgNP. Independent simulations with different starting configurations suggested that the inter-molecular interactions were dominated by

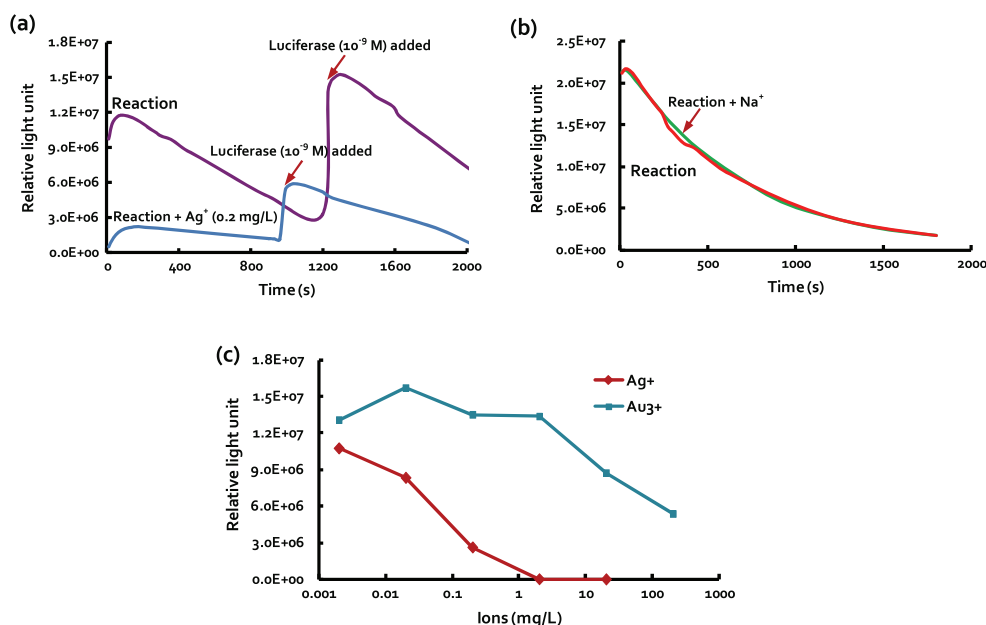


Figure 4. Inhibition of luciferase activity by silver and gold ions. (a) Luminescence kinetics upon addition of extra luciferase after 1200 s of reaction. The addition of luciferase resulted in an increase in luminescence intensity while no such effect was observed for the addition of ATP or luciferin (data not shown). (b) No effect on reaction kinetics was observed with the addition of Na⁺. (c) A comparison of the inhibitory effects of Ag⁺ and Au³⁺ on enzyme activity. Each data curve was averaged over three independent measurements.

electrostatic attraction between the negatively charged luciferase residues and the positively charged domains of the AgNP surface (figure 5(b)). Interestingly, we observed that the luciferase molecule could adopt a holo-like structure with the C-terminal domain packed closely against the N-terminal domain (figure 5(b)) during the simulations, suggesting that two luciferase sub-domains (figure 5(a)) are flexible and that the holo-like structure is thermodynamically stable in the absence of a substrate. Despite the inter-domain flexibility, each of the sub-domains remained native-like upon binding to the AgNP. This observation is consistent with the CD experiment as well as the activity assay where the AgNP-bound luciferase was still active with its bioluminescent function. Although the effect of cysteine–Ag coordination was not studied in our simulations due to the lack of thiol–Ag bond parameterization in our current force field [34], these simulations have excluded the direct role of AgNPs in causing the inhibition of luciferase luminescence.

Based on the specific inter-molecular interactions extracted from multiple all-atom DMD simulations, we built a coarse-grained model of AgNP–luciferase interactions [38]. We performed the coarse-grained DMD simulation of ten luciferase molecules interacting with one citrate-coated AgNP (figure 5(c)). A protein molecule was found to either bind directly to the AgNP or interact with the proteins already bound to the nanoparticle. The direct AgNP–protein contact was a result of the interactions between the nanoparticle and a specific set of the luciferase residues (figure S4 available at stacks.iop.org/Nano/24/345101/mmedia), as determined from

the atomistic simulations. The indirect interaction was due to the non-specific protein–protein attractions (figure 5(c)), which were found important for protein aggregation and association [35]. A three-layer luciferase corona corresponds to an increase of ~20 nm in radius as observed in the TEM experiment (figure 1(b)). Although computationally too expensive to demonstrate, we expect that a multilayer AgNP–luciferase corona would form in the simulation with a significantly longer observation time and a higher stoichiometric ratio of proteins to nanoparticles.

4. Conclusions

In summary, we have investigated the binding of luciferase with citrate-coated AgNPs and established a crucial connection between such physical interactions and their endpoint in the hindered enzyme activity. Although luciferase readily bound to AgNPs through electrostatic interactions, *van der Waals* forces, dynamic exchanges with the citrate, as well as hydrogen bonding to render a protein corona as evidenced by our physicochemical characterizations and state-of-the-art DMD computer simulations, little conformational changes in the enzyme resulted from such direct interactions. Instead, AgNPs readily released silver ions to dose-dependently inhibit the enzymatic activity, on both short (i.e., sub-seconds to seconds) and long (i.e., minutes to hours) timescales. An analogous inhibition pattern was observed for Au³⁺ but not for Na⁺. Conceivably, silver ions were bound to the cysteine residues ~20 Å away from the catalytic site of the protein

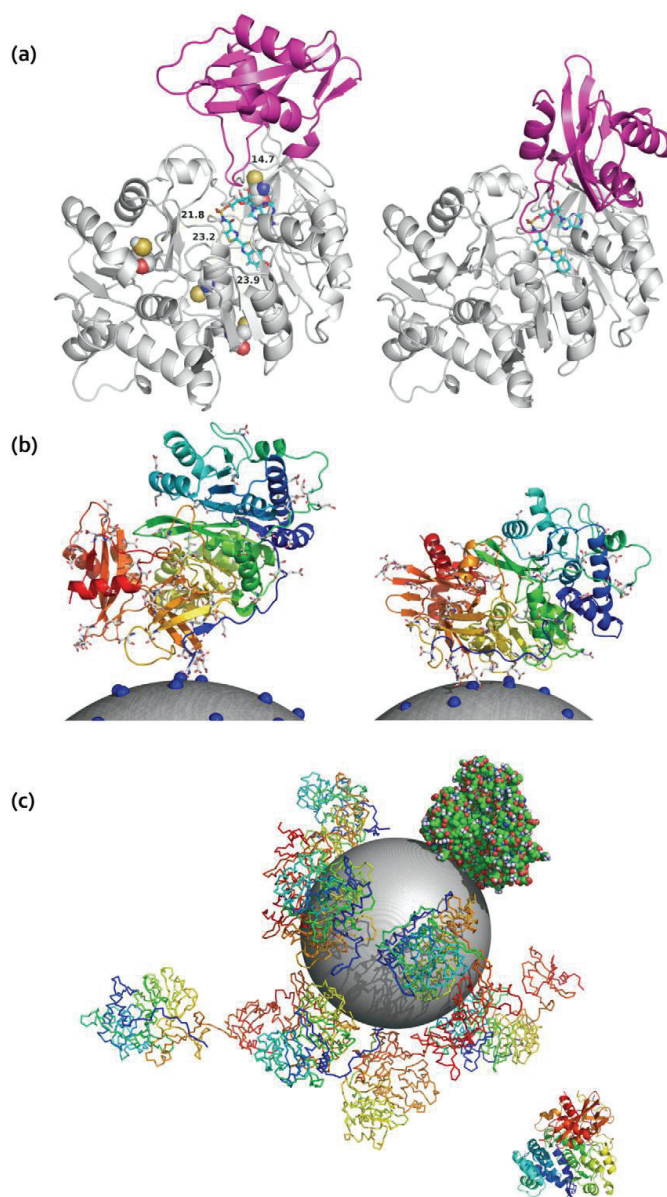


Figure 5. DMD simulation of AgNP–luciferase corona. (a) The apo- (left panel; PDB ID: 1BA3) and holo- (right panel; PDB ID: 2D1S) structure of luciferase. The C-terminal domain (in red) undergoes major conformational changes upon binding to substrates and is packed against the N-terminal domain (in gray) to form a more compact holo-conformation. The distances between the four cysteine residues (as spheres) and a substrate in the active site (as sticks in cyan color) are specified (in Å) for the apo-structure. (b) Two representative AgNP–luciferase binding conformations. The large gray sphere represents the AgNP and the blue spheres denote the surface positive charges of the nanoparticle. The protein is rainbow colored from blue (N-terminal) to red (C-terminal). The negatively charged residues are shown in sticks. (c) A typical snapshot of the coarse-grained simulation of ten luciferase proteins interacting with one AgNP. An AgNP-bound protein is shown in spheres, illustrating its contacts with the nanoparticle, and an incoming protein is illustrated in cartoon representation. The rest of the proteins are shown in backbone-trace representation.

and directly or allosterically altered the conformation and physicochemical environment of the protein to hinder its luminescence reaction. Silver ions could also complex with

the N-groups of the protein, though likely of less impact on protein conformation and function than the thiol–Ag bond. Taken together, this study offers a much needed biophysical

perspective for advancing our understanding of the biological and environmental implications of nanomaterials.

Acknowledgments

This research was supported by NSF grant no. CBET-1232724 to Ke, a graduate mobility grant to Käkinen from the Archimedes Foundation of Estonia, and EU FP7 NanoValid and ETF grant no. 8561 to Kahru and Käkinen. The authors thank Dr William Baldwin for providing the Turner BioSystem luminometer and Dr Brian Powell and Aby Thyparambil for assisting the ICP-MS and CD measurements.

References

- [1] Wiesner M, Lowry G V, Alvarez P, Dionysiou D and Biswas P 2006 *Environ. Sci. Technol.* **40** 4336
- [2] Nel A, Xia T, Madler L and Li N 2006 *Science* **311** 622
- [3] Nel A E, Mädler L, Velegol D, Xia T, Hoek E M, Somasundaran P, Klaessig F, Castranova V and Thompson M 2009 *Nature Mater.* **8** 543
- [4] Ke P C and Lamm M H 2011 *Phys. Chem. Chem. Phys.* **13** 7273
- [5] Xia X R, Monteiro-Riviere N A, Mathur S, Song X, Xiao L, Oldenberg S J, Fadeel B and Riviere J E 2011 *ACS Nano* **5** 9074
- [6] Maynard A D *et al* 2006 *Nature* **444** 267
- [7] Baun A, Hartmann N B, Grieger K and Kusk K O 2008 *Ecotoxicology* **17** 387
- [8] Qiao R, Roberts A P, Mount A S, Klaine S J and Ke P C 2007 *Nano Lett.* **7** 614
- [9] Salonen E, Lin S, Reid M L, Allegood M S, Wang X, Rao A M, Vattulainen I and Ke P C 2008 *Small* **4** 1986
- [10] Ratnikova T A, Govindan P N, Salonen E and Ke P C 2011 *ACS Nano* **5** 6306
- [11] Chen R, Ratnikova T A, Stone M B, Lin S, Lard M, Huang G, Hudson J S and Ke P C 2010 *Small* **6** 612
- [12] Wong-ekkabut J, Baoukina S, Triampo W, Tang I M, Tieleman D P and Monticelli L 2008 *Nature Nanotechnol.* **3** 363
- [13] Barnard A S 2009 *Nature Nanotechnol.* **4** 332
- [14] Kubiak K and Mulheran P A 2009 *J. Phys. Chem. B* **113** 12189
- [15] Hung A, Mwenifumbo S, Mager M, Kuna J J, Stellacci F, Yarovsky I and Stevens M M 2011 *J. Am. Chem. Soc.* **133** 1438
- [16] Jin X, Li M, Wang J, Marambio-Jones C, Peng F, Huang X, Damoiseaux R and Hoek E M V 2010 *Environ. Sci. Technol.* **44** 7321
- [17] Choi O and Hu Z 2008 *Environ. Sci. Technol.* **42** 4583
- [18] Kennedy A, Hull M, Bednar A J, Goss J, Gunter J, Bouldin J, Vikesland P and Steevens J 2010 *Environ. Sci. Technol.* **44** 9571
- [19] Fabrega J, Renshaw J C and Lead J R 2009 *Environ. Sci. Technol.* **43** 9004
- [20] Croteau M-N, Misra S K, Luoma S N and Valsami-Jones E 2011 *Environ. Sci. Technol.* **45** 6600
- [21] Zhang W, Yao Y, Sullivan N and Chen Y 2011 *Environ. Sci. Technol.* **45** 4422
- [22] Sotiriou G A and Pratsinis S E 2010 *Environ. Sci. Technol.* **44** 5649
- [23] Kittler S, Greulich C, Diendorf J, Koller M and Eppler M 2010 *Chem. Mater.* **22** 4548
- [24] Navarro E, Piccapietra F, Wagner B, Marconi F, Kaegi R, Odzak N, Sigg L and Behra R 2008 *Environ. Sci. Technol.* **42** 8959
- [25] Kahru A and Dubourguier H C 2010 *Toxicology* **269** 105
- [26] Louie A Y and Meade T J 1999 *Chem. Rev.* **99** 2711
- [27] Li W R, Xie X B, Shi Q S, Zeng H Y, Ou-Yang Y S and Chen Y B 2010 *Appl. Microbiol. Biotechnol.* **85** 1115
- [28] Shin Y J, Kwak J I and An Y J 2012 *Chemosphere* **88** 524
- [29] Paula M M S, Costa C S, Baldin M C, Scaini G, Rezin G T, Segala K, Andrade V M, Franco C V and Streck E L 2009 *J. Braz. Chem. Soc.* **20** 1556
- [30] Chen X and Schluesener H J 2008 *Toxicol. Lett.* **176** 1
- [31] Conti E, Franks N P and Brick P 1996 *Structure* **4** 287
- [32] Cedervall T, Lynch I, Lindman S, Berggard T, Thulin E, Nilsson H, Dawson K A and Linse S 2007 *Proc. Natl Acad. Sci. USA* **104** 2050
- [33] Ding F, Furukawa Y, Nukina N and Dokholyan N V 2012 *J. Mol. Biol.* **421** 548
- [34] Ding F, Tsao D, Nie H and Dokholyan N V 2008 *Structure* **16** 1010
- [35] Ding F, Dokholyan N V, Buldyrev S V, Stanley H E and Shakhnovich E I 2002 *J. Mol. Biol.* **324** 851
- [36] Rapaport D C 1997 *The Art of Molecular Dynamics Simulation* (Cambridge: Cambridge University Press)
- [37] Ding F and Dokholyan N V 2012 Discrete molecular dynamics simulation of biomolecules *Computational Modeling of Biological Systems: From Molecules to Pathways* ed N V Dokholyan (Berlin: Springer) pp 57–74
- [38] Ding F, Radic S, Chen R, Chen P, Geitner N K, Brown J M and Ke P C 2013 Direct observation of a silver nanoparticle-ubiquitin corona formation *Nanoscale* *at press*
- [39] Berman H M, Westbrook J, Feng Z, Gilliland G, Bhat T N, Weissig H, Shindyalov I N and Bourne P E 2000 *Nucl. Acids Res.* **28** 235
- [40] Chen R, Choudhary P, Schurr R N, Bhattacharya P, Brown J M and Ke P C 2012 *Appl. Phys. Lett.* **100** 013703
- [41] Weisbecker C S, Merritt M V and Whitesides G M 1996 *Langmuir* **12** 3763
- [42] Kacprzak K A, Lopez-Acevedo O, Hakkinen H and Gronbeck H 2010 *J. Phys. Chem. C* **114** 13571
- [43] Branchini B R, Magyar R A, Murtiashaw M H, Magnasco N, Hinz L K and Stroh J G 1997 *Arch. Biochem. Biophys.* **340** 52

Supporting Information

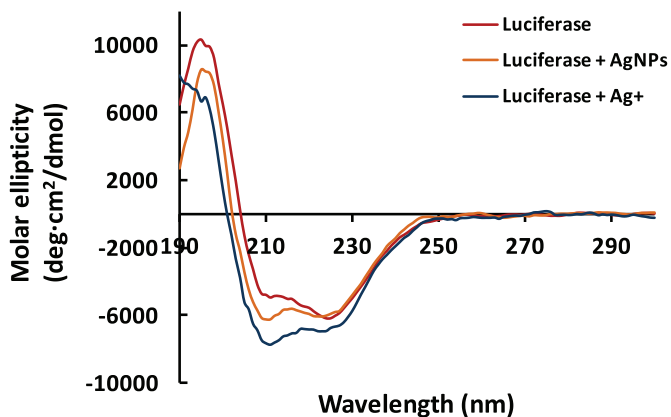


Figure S1. CD spectra of Luciferase (maroon line), Luciferase with AgNPs (amber line) and Luciferase with silver ions (blue line). The readout values of the luciferase ellipticity (θ , in mdeg) were converted to a standard unit of deg·cm²/dmol ($[\theta]$) using equation $[\theta] = (\theta \times M_0)/(10000 \times C_{\text{soln}} \times L)$, where M_0 is the mean residue molecular weight (118 g/mol), C_{soln} is the protein concentration in solution (in g/mL), and L is the path length through the buffer (1 cm).

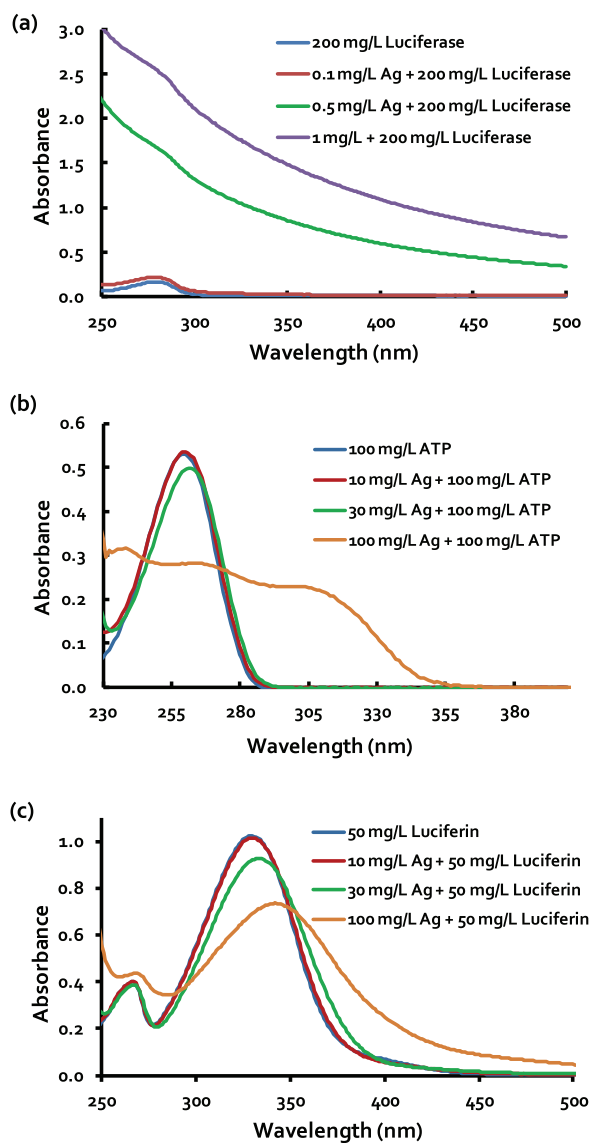


Figure S2. Binding of silver ions with (a) luciferase, (b) ATP, and (c) luciferin. The silver ions showed a significantly higher affinity for luciferase (0.5 mg Ag⁺/L) than for ATP and luciferin (>30 mg Ag⁺/L).

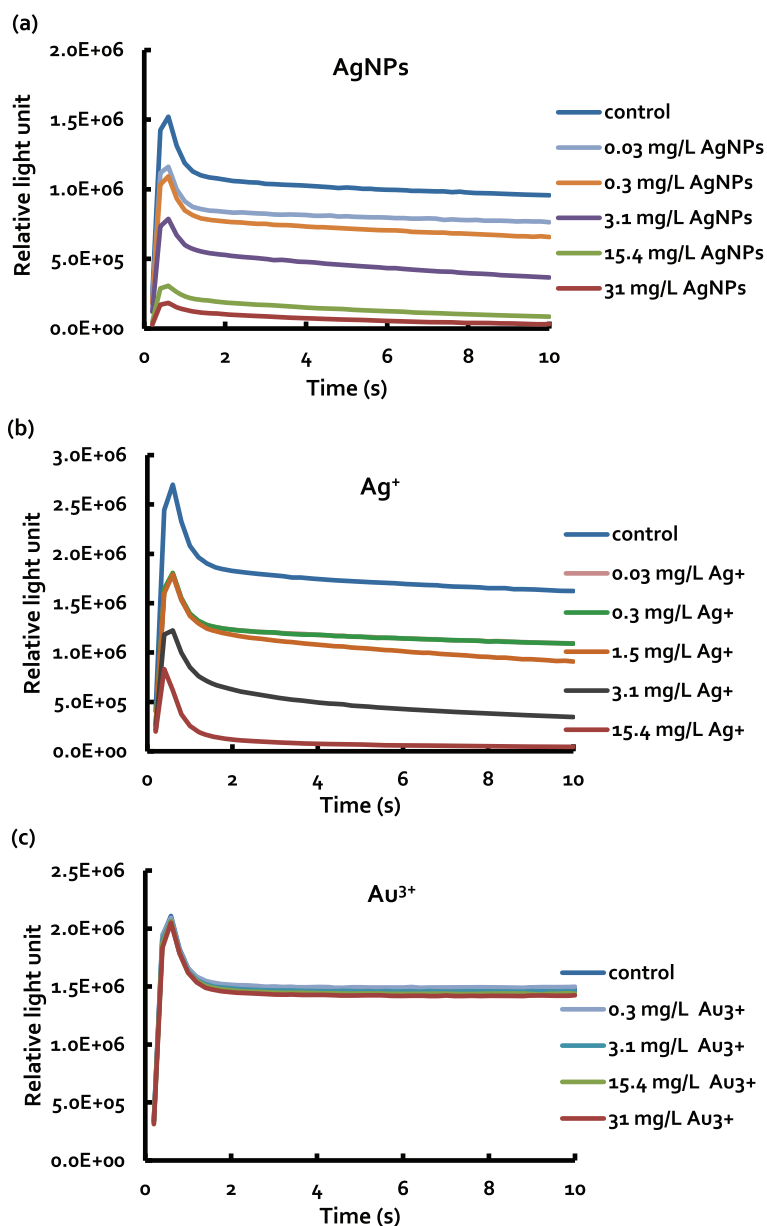


Figure S3. Rapid kinetics of luciferase bioluminescence: effects of (a) AgNPs, (b) Ag⁺, and (c) Au³⁺ on enzyme activity. The kinetics showed rapid initial flashes at 0.6 s and

concentration-dependent inhibition of the luminescence already within the first 1-10 s of incubation with AgNPs or Ag^+ (up to 31 mg Ag/L). In contrast, no such rapid inhibition was observed for Au^{3+} (up to 31 mg/L).

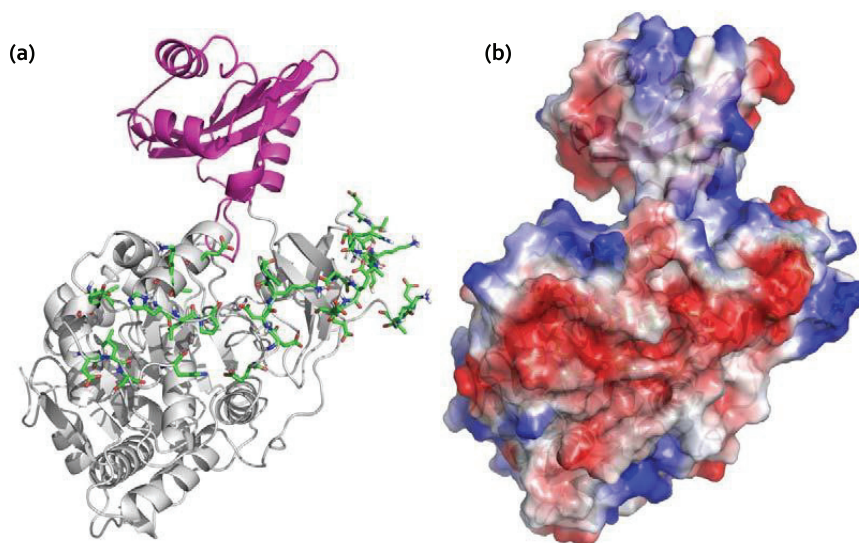


Figure S4. Binding residues and surface electrostatic potentials of firefly luciferase. (a) The AgNP-binding residues determined from all-atom DMD simulations are shown in sticks. All the AgNP-binding residues are located in the N-terminal domain (in gray). (b) The surface electrostatic potentials computed using PyMol (www.pymol.org), where regions with negative potentials are shown in red and those with positive potentials are illustrated in blue. The AgNP-binding residues form a large patch with low electrostatic potentials.

CURRICULUM VITAE

1. Personal data

Name Aleksandr Käkinen
 Date and place of birth 15.05.1987 Narva-Jõesuu
 E-mail address aleksandr.kakinen@kbfi.ee

2. Education

Educational institution	Graduation year	Education (field of study/degree)
Tallinn University of Technology	2010-...	Chemical and Materials Technology, doctoral studies
Tallinn University of Technology	2010	Environmental and Chemical Technology, M. Sc.
University of Tartu	2008	Chemistry, B. Sc.

3. Language competence/skills (fluent, average, basic skills)

Language	Level
Estonian	fluent
Russian	fluent
English	average

4. Special courses

Period	Educational or other organisation
17.09-17.12.2013	Laboratory work in the Clemson University (SC, USA) in Nanomaterials Research Laboratory (group leader Prof. Apparao M. Rao). Role of defects in the physiological fate of carbon nanomaterials.
21.08-21.12.2012	Laboratory work in the Clemson University (SC, USA) in Nano-Biophysics and Soft Matter Laboratory (group leader Prof. Pu-Chun Ke). Hindered Firefly Luciferase Activity upon Silver Nanoparticles Exposure.
4-6.01. 2012	Nano Winter Training School: The synthesis, characterisation, ecotoxicity, hazard and risk assessment of engineered nanoparticles (University of Plymouth, UK).

4-25.02.2011	Laboratory work in the University of Helsinki (Finland) in Laboratory of Polymer Chemistry (group leader Prof. Heikki Tenhu; supervisor Dr. V. Aseyev). Static and dynamic light scattering theoretical studying and practical using.
2011-...	Graduate school „Functional Materials and Processes“ (University of Tartu and Tallinn University of Technology)

5. Professional employment

Period	Organisation	Position
2008-...	National Institute of Chemical Physics and Biophysics, The Laboratory of Environmental Toxicology	engineer and MSc-PhD student

6. Defended theses

M. Sc. thesis: The mobility and bioavailability of heavy metals in the oil shale combustion fly ashes of Narva power plants and surrounding topsoils. Tallinn University of Technology, 2007. Supervisor: O. Bondarenko, M. Trapido, A. Kahru.

7. Publications

1. Klauson D, Budarnaja O, Stepanova K, Krichevskaya M, Dedova T, K  inen A, Preis S (2014). Selective performance of sol-gel synthesised titanium dioxide photocatalysts in aqueous oxidation of various-type organic pollutants. *Kinetics and Catalysis*, 55(1), 47 - 55.
2. K  inen A, Ding F, Chen P, Mortimer M, Kahru A and Ke PC. (2013). Interaction of firefly luciferase and silver nanoparticles and its impact on enzyme activity. *Nanotechnology*, 24 (345101).
3. Klauson D, Pilnik-Sudareva J, Pronina N, Budarnaja O, Krichevskaya M, K  inen A, Juganson K, Preis S. (2013). Aqueous photocatalytic oxidation of prednisolone. *Central European Journal of Chemistry*, 11(10), 1620 - 1633.
4. Radic S, Geitner NK, Podila R, K  inen A, Chen P, Ke PC, Ding F. (2013). Competitive binding of natural amphiphiles with graphene derivatives. *Scientific Reports*, 3, 2273.
5. Bondarenko O, Ivask A, K  inen A, Kurvet I, Kahru A. (2013). Particle-cell contact enhances antibacterial activity of silver nanoparticles. *PLoS ONE*, 8(5), e64060.

6. Blinova I, Niskanen J, Kajankari P, Kanarbik L, Käkkinen A, Tenhu H, Penttinen OP, Kahru A. (2013). Toxicity of two types of silver nanoparticles to aquatic crustaceans *Daphnia magna* and *Thamnocephalus platyurus*. *Environmental Science and Pollution Research*, 20(5), 3456 - 3463.
7. Blinova I, Bitjukova L, Kasemets K, Ivask A, Käkkinen A, Kurvet I, Bondarenko, O, Kanarbik L, Sihtmäe M, Aruoja V, Schvede H, Kahru A. (2012). Environmental hazard of oil shale combustion fly ash. *Journal of Hazardous Materials*, 229,230, 192 - 200.
8. Bondarenko O, Ivask A, Käkkinen A, Kahru A. (2012). Sub-toxic effects of CuO nanoparticles on bacteria: Kinetics, role of Cu ions and possible mechanisms of action. *Environmental Pollution*, 169, 81 – 8.
9. Käkkinen A, Bondarenko O, Ivask A, Kahru A. (2011). The effect of composition of different ecotoxicological test media on free and bioavailable copper from CuSO₄ and CuO nanoparticles: comparative evidence from a Cu-Selective electrode and a Cu-biosensor . *Sensors*, 11(11), 10502 - 10521.
10. Kahru A, Bondarenko O, Kajankari P, Käkkinen A, Ivask A, Kasemets K, Mortimer M, Blinova I. (2011). Bioavailability and toxicity of copper oxide and silver nanoparticles to bacteria, yeasts, crustaceans and protozoa. *Toxicology Letters*, 205, S284 - S285.

ELULOOKIRJELDUS

1. Isikuandmed

Ees- ja perekonnanimi Aleksandr Käkinen
Sünniaeg ja -koht 15.05.1987 Narva-Jõesuu
Kodakondsus Eesti
E-posti aadress aleksandr.kakinen@kbfi.ee

2. Hariduskäik

Õppeasutus (nimetus lõpetamise ajal)	Lõpetamise aeg	Haridus (eriala/kraad)
Tallinna Tehnikaülikool	2010-...	Keemia- ja materjali- tehnoloogia, doktoriõpe
Tallinna Tehnikaülikool	2010	Keemia- ja keskkonna- kaitse tehnoloogia, magistrikraad
Tartu Ülikool	2008	Keemia, bakalaureu- sekraad

3. Keelteoskus (alg-, kesk- või kõrgtase)

Keel	Tase
Eesti keel	kõrgtase
Vene keel	kõrgtase
Inglise keel	kesktase

4. Täiendusõpe

Õppimise aeg	Täiendusõppe korraldaja nimetus
17.09.-17.12.2013	Välispraktikum Clemsoni Ülikoolis, USA, Nanomaterials Research Laboratory (juht Prof. Apparao M. Rao). Teema: Süsiniknanotorude defektide mõju proteiini adsorptsioonile.
21.08.-21.12.2012	Välispraktikum Clemsoni Ülikoolis, USA, Nano-Biophysics and Soft Matter Laboratory (juht Prof. Pu-Chun Ke). Teema: Hõbeda (Ag) nanoosakeste ja ensüümide interaktsioonide uurimine.

5.-6.01.2012	Kursus "Nanoosakeste süntees, iseloomustamine, ökotoksikoloogia ja riskihindamine" (Plymouth Ülikool, Inglismaa).
14.02-25.02.2011	Välispraktikum Helsinki Ülikoolis, Soome, Polümeeri-de Keemia Labor (Juht Prof. Heikki Tenhu, Juhendaja Vladimir Aseyev). Valguse hajutamise meetodi füüsikalise-keemilise põhimõtte õppimine ja praktiline kasutamine.
2011-...	Doktorikool „Funktsionaalsed materjalid ja tehnoloogiad“ (Tartu Ülikool ja Tallinna Tehnikaülikool).

5. Teenistuskäik

Töötamise aeg	Tööandja nimetus	Ametikoht
2008-...	Keemilise ja Bioloogilise Füüsika Instituut, Keskkonnatoksikoloogia Laboratoorium	insener ja magistrant/doktorant

6. Kaitstud lõputööd

Magistritöö: Raskmetallide liikuvus ja biosaadavus Narva elektrijaamade lendtuhkades ning neist mõjustatud pinnastes, Tallinna Tehnikaülikool, 2010. Juhendajad: O. Bondarenko, M. Trapido, A. Kahru.

7. Publikatsioonid eelretsenseeritud ajakirjades

1. Klauson D, Budarnaja O, Stepanova K, Krichevskaya M, Dedova T, Käkinen A, Preis S (2014). Selective performance of sol-gel synthesised titanium dioxide photocatalysts in aqueous oxidation of various-type organic pollutants. *Kinetics and Catalysis*, 55(1), 47 - 55.
2. Käkinen A, Ding F, Chen P, Mortimer M, Kahru A and Ke PC. (2013). Interaction of firefly luciferase and silver nanoparticles and its impact on enzyme activity. *Nanotechnology*, 24 (345101).
3. Klauson D, Pilnik-Sudareva J, Pronina N, Budarnaja O, Krichevskaya M, Käkinen A, Juganson K, Preis S. (2013). Aqueous photocatalytic oxidation of prednisolone. *Central European Journal of Chemistry*, 11(10), 1620 - 1633.
4. Radic S, Geitner NK, Podila R, Käkinen A, Chen P, Ke PC, Ding F. (2013). Competitive binding of natural amphiphiles with graphene derivatives. *Scientific Reports*, 3, 2273.

5. Bondarenko O, Ivask A, K  inen A, Kurvet I, Kahru A. (2013). Particle-cell contact enhances antibacterial activity of silver nanoparticles. PLoS ONE, 8(5), e64060.
6. Blinova I, Niskanen J, Kajankari P, Kanarbik L, K  inen A, Tenhu H, Penttinen OP, Kahru A. (2013). Toxicity of two types of silver nanoparticles to aquatic crustaceans *Daphnia magna* and *Thamnocephalus platyurus*. Environmental Science and Pollution Research, 20(5), 3456 - 3463.
7. Blinova I, Bitukova L, Kasemets K, Ivask A, K  inen A, Kurvet I, Bondarenko, O, Kanarbik L, Sihtm  e M, Aruoja V, Schvede H, Kahru A. (2012). Environmental hazard of oil shale combustion fly ash. Journal of Hazardous Materials, 229,230, 192 - 200.
8. Bondarenko O, Ivask A, K  inen A, Kahru A. (2012). Sub-toxic effects of CuO nanoparticles on bacteria: Kinetics, role of Cu ions and possible mechanisms of action. Environmental Pollution, 169, 81 – 8.
9. K  inen A, Bondarenko O, Ivask A, Kahru A. (2011). The effect of composition of different ecotoxicological test media on free and bioavailable copper from CuSO₄ and CuO nanoparticles: comparative evidence from a Cu-Selective electrode and a Cu-biosensor . Sensors, 11(11), 10502 - 10521.
10. Kahru A, Bondarenko O, Kajankari P, K  inen A, Ivask A, Kasemets K, Mortimer M, Blinova I. (2011). Bioavailability and toxicity of copper oxide and silver nanoparticles to bacteria, yeasts, crustaceans and protozoa. Toxicology Letters, 205, S284 - S285.

**DISSERTATIONS DEFENDED AT
TALLINN UNIVERSITY OF TECHNOLOGY ON
CHEMISTRY AND CHEMICAL ENGINEERING**

1. **Endel Piiraja**. Oxidation and Destruction of Polyethylene. 1993.
2. **Meili Rei**. Lihatehnoloogia teaduslikud alused. Fundamentals of Food Technology. 1995.
3. **Meeme Põldme**. Phase Transformations in Hydrothermal Sintering Processing of Phosphate Rock. 1995.
4. **Kaia Tõnsuaadu**. Thermophosphates from Kovdor and Siilinjärvi Apatites. 1995.
5. **Anu Hamburg**. The Influence of Food Processing and Storage on the N-Nitrosamines Formation and Content in Some Estonian Foodstuffs. 1995.
6. **Ruth Kuldvee**. Computerized Sampling in Ion Chromatography and in Capillary Electrophoresis. 1999.
7. **Külliki Varvas**. Enzymatic Oxidation of Arachidonic Acid in the Coral *Gersemia fruticosa*. 1999.
8. **Marina Kudrjašova**. Application of Factor Analysis to Thermochromatography and Promotion Studies. 2000.
9. **Viia Lepane**. Characterization of Aquatic Humic Substances by Size Exclusion Chromatography and Capillary Electrophoresis. 2001.
10. **Andres Trikkel**. Estonian Calcareous Rocks and Oil Shale Ash as Sorbents for SO₂. 2001.
11. **Marina Kritševskaja**. Photocatalytic Oxidation of Organic Pollutants in Aqueous and Gaseous Phases. 2003.
12. **Inna Kamenev**. Aerobic Bio-Oxidation with Ozonation in Recalcitrant Wastewater Treatment. 2003.
13. **Janek Reinik**. Methods for Purification of Xylidine-Polluted Water. 2003.
14. **Andres Krumme**. Crystallisation Behaviour of High Density Polyethylene Blends with Bimodal Molar Mass Distribution. 2003.
15. **Anna Goi**. Advanced Oxidation Processes for Water Purification and Soil Remediation. 2005.
16. **Pille Meier**. Influence of Aqueous Solutions of Organic Substances on Structure and Properties of Pinewood (*Pinus sylvestris*). 2007.
17. **Kristjan Kruusement**. Water Conversion of Oil Shales and Biomass. 2007.

18. **Niina Kulik.** The Application of Fenton-Based Processes for Wastewater and Soil Treatment. 2008.
19. **Raul Järviste.** The Study of the Changes of Diesel Fuel Properties a its Long Term Storage. 2008.
20. **Mai Uibu.** Abatement of CO₂ Emissions in Estonian Oil Shale-Based Power Production. 2008.
21. **Valeri Gorkunov.** Calcium-Aluminothermal Production of Niobium and Utilization of Wastes. 2008.
22. **Elina Portjanskaja.** Photocatalytic Oxidation of Natural Polymers in Aqueous Solutions. 2009.
23. **Karin Reinhold.** Workplace Assessment: Determination of Hazards Profile using a Flexible Risk Assessment Method. 2009.
24. **Natalja Savest.** Solvent Swelling of Estonian Oil Shales: Low Temperature Thermochemical Conversion Caused Changes in Swelling. 2010.
25. **Triin Märtson.** Methodology and Equipment for Optical Studies of Fast Crystallizing Polymers. 2010.
26. **Deniss Klauson.** Aqueous Photocatalytic Oxidation of Non-Biodegradable Pollutants. 2010.
27. **Oliver Järvik.** Intensification of Activated Sludge Process – the Impact of Ozone and Activated Carbon. 2011.
28. **Triinu Poltimäe.** Thermal Analysis of Crystallization Behaviour of Polyethylene Copolymers and Their Blends. 2011.
29. **Mariliis Sihtmäe.** (Eco)toxicological Information on REACH-Relevant Chemicals: Contribution of Alternative Methods to *in vivo* Approaches. 2011.
30. **Olga Velts.** Oil Shale Ash as a Source of Calcium for Calcium Carbonate: Process Feasibility, Mechanism and Modeling. 2011.
31. **Svetlana Jõks.** Gas-Phase Photocatalytic Oxidation of Organic Air Pollutants. 2012.
32. **Aleksandr Dulov.** Advanced Oxidation Processes for the Treatment of Water and Wastewater Contaminated with Refractory Organic Compounds. 2012.
33. **Aleksei Zaidentsal.** Investigation of Estonian Oil Shale Thermo-bituminization in Open and Closed System. 2012.